Energy efficiency improvement of Li-ion battery packs via balancing techniques

PhD Student: IOSU AIZPURU LARRAÑAGA

Supervisors: JOSU IMANOL GALARZA IBARRONDO

ANDER GOIKOETXEA ARANA

Mondragon Goi Eskola Politeknikoa

University of Mondragon

Arrasate-Mondragon (Gipuzkoa), July 2015

ESKERRAK-ACKNOWLEDGMENTS

Lehenik eta behin Jose María Canalesi eskerrak eman nahiko nizkioke. Bera izan da tesi hau egiteko aukera eman didana eta azken urteetan asko ikasi eta ziur oraindik askoz gehiago ikasiko dudala berarengandik. Unai Iraolataz bereziki gogoratuko nahiko nuke, badira 12 bat urte elkarrekin gaudela; ikasi, proiektua, lana eta tesia egiten. Mila esker emandako laguntzagatik eta nire tesian egindako lan bikainarengatik. Ander Goikoetxeari ere eskerrak azken momentuan nire tesi zuzendari orde lanak hartzearren.

"Orona gela"-ko lagunek aipamen berezia merezi dute. Nola ez gogoratu bereziki Unaitxo eta Aritzez, barre edarrak egin ditugu tesi garaian, beti edozertarako prest egon zarete. Baita ere eskerrak Eneko, Iratxo, Txejo eta Eduri, tesiaren azken txanpa zuen laguntzarekin askoz errazagoa izan da. Aipamen berezia merezia dute Orona gelatik igaro diren bekario eta proiektugile desberdinek, beraiekin lana egiteko aukera bikaina izan dut: Iker, Mikel, David, Lorea eta Iñigo. Espero zuek ere niregatik ikasteko aukera izan izana.

Departamentuko beste kideei ere eskerrak. Departamentu honetan dagoen giroa ez dut uste beste inon aurkitzerik dagoenik. Miloi bat esker zuri Ibon, zure gabe departamentu hau ez litzateke aurrera joango, mila esker nire tesian egindako lanagatik eta beti laguntzeko prest egoteagatik.

I would like to express my gratitude to EIGSI in La Rochelle, and specially to Mr. Andre Mieze. Thank you very much for all your advice and great discussions about energy storage systems. Thank you also to my "Erasmus" friends (Gerard, Elias, etc,), great time with you in La Rochelle ;).

I would like to thank the members of the jury for coming to the PhD defence event and for giving me their point of view of the developed work.

-

Nire lagunena zer esan. Gerra edarra edukitzen dugu beti elektroniko eta mekanikoen artean…jejejejeje…hala ere tesi lanetik deskonektatzen ikaragarri lagundu nauzue. Beti edukiko dut gogoan ostiraletako lehenengo zerbeza hori, kristonak zerate!!

Nire gurasoei eskerrik handienak. Mila esker benetan eman didazuen aukeragatik. Beti zaudete laguntzeko prest eta bizitzan gauzak aurrera ateratzen erakutsi didazue. Zuena da dudarik gabe tesi honen zatirik handiena.

Azkenik zu Aitzi! Mila esker emandako denagatik. Azken aldian batez ere, garai gogorrak izan dira eta zu beti egon zara bertan edozertarako prest. Bion artean errazagoa izan da hau dena.

Eskerrik asko guztioi.

Iosu Aizpuru Larrañaga.

TESIAREN LABURPENA

Mundu mailako energia kontsumoa igotzen ari denez, araudi energetiko berriak sortzen ari dira erregai fosilen kontsumoa murritzeko, energia berriztagarriak ezartzeko eta efizientzia energetikoa handitzeko. Energia berriztagarrien ezartzea eta beraien erabilpena sare elektrikoan, asko hobetzen da metatze sistemen laguntzarekin. Metatze sistemek energia batzen dute kontsumo txikiko uneetan energia txertatuz sare elektrikora kontsumo handiko aldiuneetan, sare elektrikoaren efizientzia eta egonkortasuna hobetuz.

Tesi lana litio ioizko metatze sistemen energia efizientzia hobetzean datza. Litio ioizko metatze sistemak litio zelden serie konekzioak dira. Seriean konektatuko sistema hauen efizientzia hobetzeko beharrezkoa da sistema orekatzaileak erabiltzea zelden artean sortutako desberdintasunak konpentsatzeko. Tesi hau zelden arteko desoreken analisian eta desoreka hauek konpentsatzeko beharrezkoak diren oreka sistemen diseinuan zentratzen da. Oreka sistema aktibo konpetitiboen diseinua, oreka sistema pasiboekin lehiatzeko da tesiaren lan inguru nagusienetakoa.

Funtsezko hitzak: *Energia metaketa, Li-ion, oreka sistema aktiboak, BMS.*

THESIS ABSTRACT

Due to worldwide energy consumption increase, different energy strategies are growing in order to reduce fossil fuel consumption, increase renewable energy impact and increase energy efficiency. Renewable energy impact in the electric grid is increased by combination with energy storage systems. Energy storage systems storage energy during low consumption periods and insert energy during high power demand time. The efficiency and the stability of the electric grid are improved.

The thesis work is focused on the energy improvement of Li-ion based energy storage systems. To improve the energy of series connected Li-ion energy storage system balancing systems are required. The thesis deals with the analysis of unbalancing processes in series connected Li-ion cells and the balancing system design to improve the Li-ion battery pack energetic behavior. The search of a low complexity active balancing system to compete against the passive balancing system is one of the most important research lines.

Keywords: *Energy storage systems, Li-ion, active balancing system, BMS.*

RESUMEN DE LA TESIS

La creciente demanda energética mundial, está generando la implantación de directrices en busca de una disminución de consumo de combustibles fósiles, aumento de la inserción de renovables y mejora de la eficiencia energética. La inserción de renovables y su uso en la red eléctrica mejora al combinarlo con sistemas de almacenamiento. Los sistemas de almacenamiento permiten almacenar la energía durante momentos de bajo consumo y entregarla en picos de consumo, mejorando la eficiencia y la estabilidad de la red eléctrica.

El trabajo de tesis se centra en la mejora de la eficiencia energética de sistemas de almacenamiento basados en litio-ion. Los sistemas de almacenamiento de litio se componen de conexiones serie de celdas de litio. Para mejorar la eficiencia de estos sistemas conectados en serie es necesario el uso de sistemas de equilibrado para compensar los desequilibrios de las celdas y mejorar la eficiencia total del pack de baterías. Esta tesis se centra en el análisis de los desequilibrios de sistemas de Li-ion y la compensación de los desequilibrios mediante sistemas de equilibrado. La búsqueda de un sistema de equilibrado activo competitivo para competir con el sistema de equilibrado pasivo es una de las principales líneas de trabajo.

Palabras clave: *Sistemas de almacenamiento energético, Li-ion, equilibrado activo, BMS.*

TABLE OF CONTENTS

GLOSSARY OF VARIABLES AND ABBREVIATIONS

GENERAL BATTERY NOMENCLATURE

Q_{Nom}	[Ah]	Nominal cell capacity
Q	[Ah]	Instantaneous cell capacity
E	[Wh]	Instantaneous cell capacity
Q_{Max}	[Ah]	Maximum cell capacity
Q_{SD}	[%]	Self discharge capacity loss
R_{in}	[Ω]	Internal resistance
T_{amb}	[ºC]	Ambient or working temperature
T_C	[ºC]	Cell temperature
SOC	[%]	State of Charge. Instantaneous charge respect to maximum cell capacity
SOH	[%]	State of Health
C-rate	[ ]	Current rate respect to nominal capacity

ABBREVIATIONS

AB	...	Active Balancing
NB	...	No balancing
BP	...	Battery Pack
Cb	...	Cell balancing
LCO	...	Lithium Cobalt Oxide technology
LFP	...	Lithium Iron Phosphate technology
LMO	...	Lithium Manganese Spinel technology
LTO	...	Lithium Titanate technology
Mb	...	Module balancing
NCA	...	Lithium Nickel Cobalt Aluminium technology
NMC	...	Lithium Nickel Manganese Cobalt technology
PB	...	Passive Balancing
SOA	...	Safe Operation Area

MAIN VARIABLES

INDEXES FOR VARIABLES

i	i^{th} cell inside a module
j	j^{th} module inside a battery pack
W	Denotes weak cell or module
S	Denotes strong cells or modules
D	Discharge process (for battery energetic issues)
C	Charge process (for battery energetic issues)
Loss	Power loss (For balancing system analysis)
T	Total, for total power calculation in balancing systems

VARIABLES

D_C	[ ]	Critical duty cycle
I_{BP}	[A]	Battery pack current
I_C	[A]	Cell current
I_M	[A]	Module current
I_{Cb}	[A]	Intramodule balancing current through a cell
I_{Mb}	[A]	Intermodule balancing current through a module
V_{BP}	[V]	Battery pack voltage
V_C	[V]	Cell voltage
V_M	[V]	Module voltage
P_{Cb}	[W]	Intramodule balancing system power
η_{Cb}	[%]	Intramodule balancing system efficiency
P_{Mb}	[W]	Intermodule balancing system power
η_{Mb}	[%]	Intermodule balancing system effiviency
W_{BP}	[Wh]	Battery energy
W_{SB}	[Wh]	Battery standby lost energy
η_{BP}	[%]	Battery efficiency
W^*_{BP}	[Wh]	Battery energy from the point of view of the customer
η^*_{BP}	[%]	Battery efficiency from the point of view of the customer
T_{BS}	[ºC]	Balancing system maximum temperature
T_{Max}	[ºC]	Maximum temperature of a cell in a battery pack
ΔT	[ºC]	Maximum temperature dispersion between cells in a battery pack
$C_€$	[€]	Balancing system cost

Chapter 1

INTRODUCTION

The energy consumption is growing during last decades day-to-day. The main energy supplies based on oil fuels are controlled by a few countries which represent a very big energetic dependency for the consumer countries respect to the producer countries. Over the last decades continental, country and regional politics are making great emphasis in key factors as energy efficiency, renewable energies and CO_2 emission reduction. Energy storage systems have a big impact on this work.

This chapter introduces the thesis work "Energy efficiency improvement of Li-ion battery packs via balancing techniques" with a brief description of the actual context and the framework of the thesis. The objectives of the thesis will be focused on the problematic and deficiency of actual context energy and efficiency issues. After that, the outline of the thesis will present the general structure of the presented work. Finally the scientific contributions of the thesis work and the publications presented in international conferences and journals will be enumerated.

1.1 Framework of the thesis

Over the last decades a worldwide awareness about energy consumption, energy efficiency and the climate change is growing.

Fuel and fossil energy requirement of worldwide economy, makes a dependency relationship with producer countries and their tariffs. The obsolete electric grids and old energy management strategies decrease grid energy efficiency, due to power losses during energy transportation. On the other hand, CO_2 emissions have contributed to the global warming and the climate change effect.

To deal with these problems, there are some strategic plans presented in Table 1.1 for continental, country and regional levels to change the existing energy situation.

Energy research has been a fundamental axis in the Basque industrial politic and competitiveness during last 30 years. *Energibasque* (Basque country's industrial and technological development strategy) is focused in some plans and strategies that compose his reference objectives and follows same directions as European and state strategies.

The Basque Government *3E2020* Energy Plan is framed inside "Plan de Ciencia, Tecnología e Innovación" *PCTI* directives. Inside *Energibasque* there are six energetic issues that are especially attractive for the Basque industrial market and development. *Energibasque* has 3 main objectives for the Basque Country energetic sector until year 2020:

- Consolidate Basque energetic **driving enterprises** as technological referent in their energetic sectors.
- Develop business activity in **emerging energy sectors.**

Table 1.1 Worldwide continental, state and regional energy strategic plans

Region	Strategic plan	Message/Function
USA	20x10	Fossil fuel consumption reduction, renewable energy insertion and energy efficiency increase
Europe	20-20-20	
Spain	20-20-10d	
Euskadi	3E2020	

Table 1.2 Strategic energy sectors selector from *EnergiBasque* for the Basque energy market positioning. Impact factors: Low ○, Medium ◐, High ●. *Source: EnergiBasque 2012*

	Market appealing			**Basque Country position**		
Energy sectors	Market size	Market growth	Market insertion	Driving enterprises	Coverage value chain	Technology positioning
Wind energy	●	◐	○	●	◐	●
Thermal solar energy	○	●	●	●	◐	●
Marine	○	◐	●	◐	◐	◐
Electric grid	●	◐	●	●	●	●
Energy storage	○	●	◐	◐	○	◐
Electric transport	○	●	◐	●	◐	◐

- From investments in *3E2020*, generate **new energy opportunities and markets** for Basque enterprises.

Inside *Energibasque* strategy there are six energetic sectors that are especially attractive for the Basque industrial Market and development which are presented in Table 1.2. Wind energy and electric grid sectors are well known markets where Basque energy driving enterprises are head positioned, as Iberdrola and Gamesa. Even if the market is still small it is expected that the market growth for thermal solar energy, energy storage and electric transportation will be huge, with good positioned Basque enterprises specially in thermal solar energy and electric transport. Marine energy is also attractive due to easy market insertion process.

To accomplish with 3E2020 objectives, electricity is the key factor to join all energy sectors, and energy storage is the "enabling technology" to help in this issue Fig 1.1.

Energy storage systems can increase the insertion of renewable energies in the electric grid generation [1]. Energy storage systems permit to improve the grid performance and functionality by next characteristics [2]:

- Integration of **distributed generation** energy systems.
- **Grid balance**. Compensation between **valley** hours and **power peak** hours consumption.

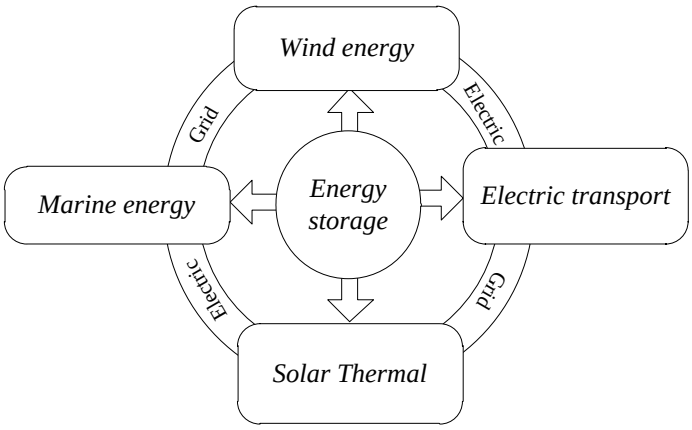

Fig 1.1 *Energibasque* policy strategy. Main interest energy sectors, with electricity as the key factor and energy storage as the "enabling technology". *Source: EnergyBasque 2012*

- **Grid stability**. Regulation under sags, swells and interruptions.
- Management of energy demand, with **smart grids** and **electric mobility**.
- **Improvement** of **conventional energy** generation efficiency and functionality.
- Availability of direct integration into new concept **DC grids.**

Energy storage systems are distinguished by their physical way to storage the energy [3]. Fig 1.2 divides energy storage systems by the physical characteristics in mechanical, electrical, thermal and chemical.

Mechanical storage systems store the energy in a potential or a kinetic way. Hydroelectric energy and hydro pumps are the most common potential energy examples, being the biggest energy storage systems. Flywheels are the kinetic energy storage system of reference. They are high efficient and fast energy storage systems.

Electrical energy storage systems store the energy in electrostatic way as capacitors and ultracaps, or in magnetic currents as presented in superconducting energy storage.

Thermal energy storage stores energy directly in thermal heat. The thermal energy is used to heat buildings, water, etc.

Chemical energy storage is the group with more different technologies. Thermochemical energy storage, although promising, is a very new technology and it is not really used. Inside the electrochemical group batteries and fuel cells are used. Fuel

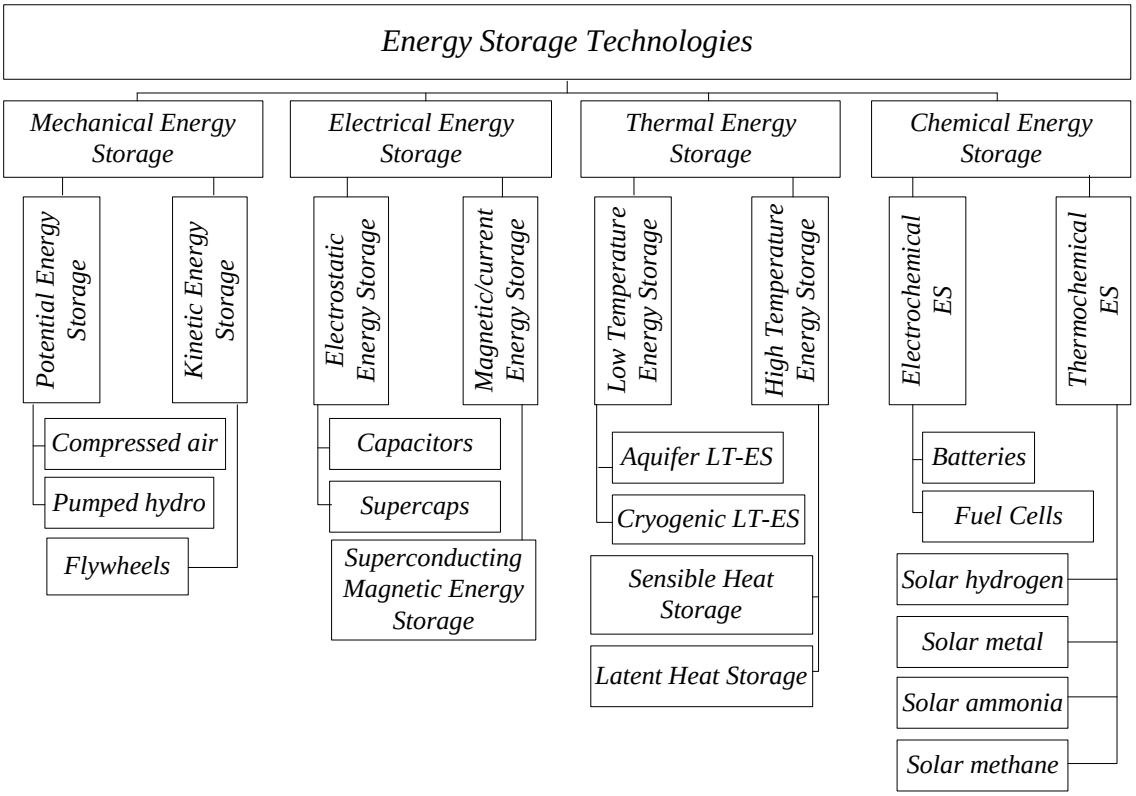

Fig 1.2 Energy storage systems classification. Mechanical, electrical thermal and chemical [3]

cells convert hydrogen based storage in electricity, and batteries convert previously inserted energy stored chemically in new electric energy, with a high efficiency.

Batteries are one of the most heterogeneous energy storage system groups, with main characteristic differences regarding energy and power specifications:

- **Energy:** Specific energy (Wh/Kg) and volumetric energy density (Wh/L).
- **Power:** Specific power (W/Kg) and volumetric power density (W/L).

There is not a single battery that could meet all the applications. For energy storage systems ragone plots define the working region of an specific battery technology [4]–[7].

Fig 1.3 presents main battery technologies ragone plot. Electrostatic systems are presented to overview that they are limited to high power low energy applications as supercaps, EDLCs or Li-caps. Flow batteries and Sodium Sulfur NaS batteries are taking great interest for big stationary energy storage applications. NaNiCL or *Zebra* batteries are high temperature batteries that are a promising technology for electric

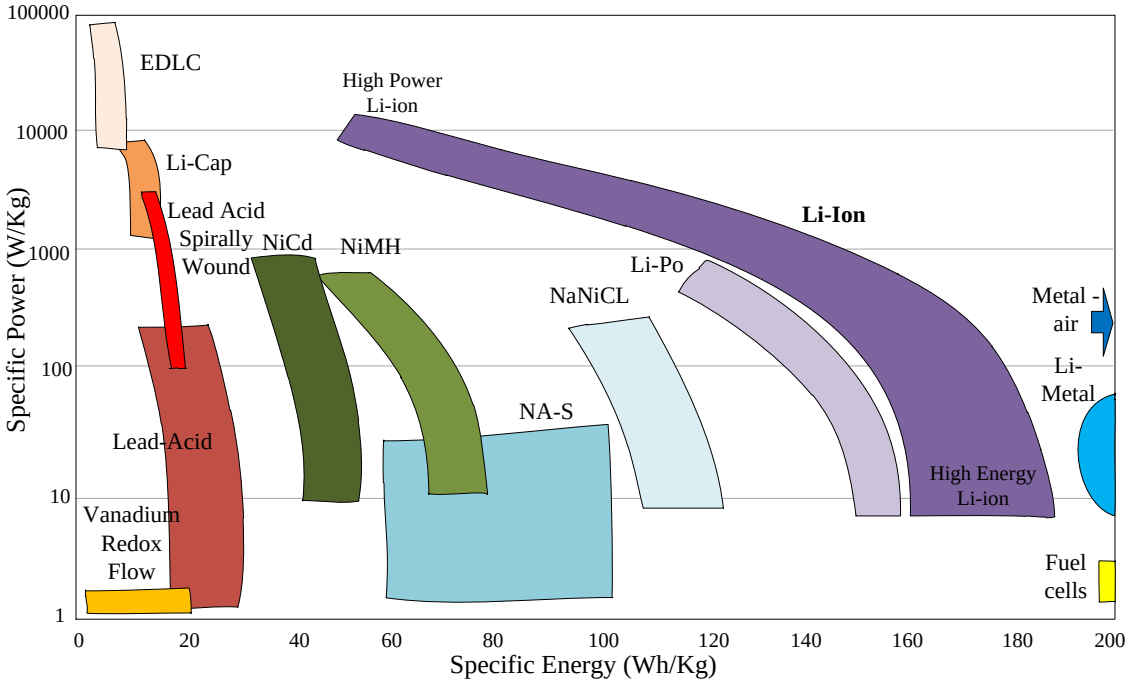

Fig 1.3 Ragone plot of main battery energy storage technologies for gravimetric (Kg) characteristics. Analysis resume from [4]–[7].

mobility and stationary energy storage. Fuel cells are high specific energy systems with the disadvantage of the hydrogen production problem. Li-Metal and Metal-air technologies are future promising technologies with very high specific energy. Metal-air theoretical energy density ~11000 Wh/kg is near gasoline. LiS batteries are entering nowadays the market but metal air rechargeable batteries are far away of commerciality.

The most used technologies for different applications are lead-acid, nickel based and li-ion technologies are compared in Table 1.3. Lead-acid batteries are the most used technology. Their biggest advantage is that they are very cheap. However, they present low energy density, high temperature dependency and low capacity in high current rate applications. Spirally wound technology leads with higher current rates. Nickel based technologies as NiCd and NiMH, have bigger energy density than lead acid batteries. They also present high discharge rate capacity. However, they present high self-discharge rates and memory effect. NiMH has become more popular as doubles NiCd energy density, and overcomes Cadmium toxicity problem.

Li-ion chemistry is the most promising and versatile battery technology. Li-ion cells present a wide operation zone, with high power cells and high energy cells

Table 1.3 Main characteristics of principle battery technologies. Lead, acid, Nickel based and Li-ion [4], [8]

Characteristic	Lead acid	Ni-Cd	Ni-MH	Li-ion
Energy density[Wh/kg]	20-30	40-60	60-80	40-180
Cycle life	200-300	1500	300-500	400-2000
Self-discharge [%/month]	5	20	30-50	1-10
Charge-discharge efficiency 1C [%]	50%	70-90	66	>90
Maintenance	30-60 days	30-60 days	3-6 months	free
Overcharge Tolerance	High	Moderate	Low	Very low
Voltage [V]	2	1,25	1,25	3,3
Commercial use since	1970	1950	1990	1991

depending on the application. **This versatility, high power-energy density and long life time presents lithium-ion chemistry as the reference battery technology for nowadays battery storage applications.**

1.2 Objectives

The main objective of the PhD thesis and the origin of this work is expressed by:

Energy and efficiency improvement of an energy storage system based on Lithium-ion technology.

The accomplishment of this objective could be done by 3 different research lines or works:

- Energy storage converter: Design of the output converter of a battery pack to maximize the energy taking into account the battery pack technology characteristics.
- **Balancing system**: Design of the balancing system for maximizing the energy and improving the life span of the battery pack.
- Mechanical design: Improvement of the lay out of the battery pack to expand its specifications and life span.

During this PhD, the research work will be focused on the balancing system design of a series connected Li-ion battery pack for power applications. The unbalancing behaviour of a battery pack and the requirement of a correct balancing system regarding to the improvement of the energy and the efficiency are taken as the central point of the research project. To achieve this main objective other sub objectives are listed below:

- Lithium-ion battery pack unbalancing analysis, obtaining knowledge about the main unbalancing effects and causes in series connected cells.
- Study and analysis of different balancing systems, regarding main parameters and functionalities.
- Balancing systems modelling with special emphasis in energy transfer calculation between weak and strong cells.
- A balancing system design methodology, for correct balancing design depending on the application requirements.

1.3 Outline of the Thesis

This document is divided in seven different chapters presenting the scientific work done during the thesis period. **Chapter 1** INTRODUCTION presents the framework of the Thesis introducing worldwide situation of energy policies making emphasis in the importance of energy storage systems. The objectives are focused on the improvement of the efficiency of Li-ion based energy storage systems, working in the design of balancing systems for series connected devices. The thesis work distribution, the scientific contributions and the publications are enumerated.

In **Chapter 2** STATE OF THE ART the situation about Li-ion battery packs is evaluated. Li-ion battery packs are a combination of series-parallel connections of single cells and more complex modules. Main structures presented in literature are enumerated. Series connection of Li-ion cells presents an unbalancing effect between cells. Literature description in unbalancing effects and causes of Li-ion cells is evaluated. After evaluating unbalancing behaviour of Li-ion cells, balancing systems analysis is presented. The conclusions of the STATE OF THE ART present the weakness found in the literature and the principal basis and reason of the thesis work.

Chapter 3 LFP SERIES CONNECTED UNBALANCING EFFECTS AND CAUSES presents a novel methodology to cycle and evaluate Li-ion series connected cells. The research work is focused in cycle behaviour and rest analysis of battery packs. A conference contribution is presented [PAPER C1].

During **Chapter 4** SERIES CONNECTED ENERGY STORAGE MODULAR BALANCING SYSTEMS balancing system modelling is performed. Battery pack balancing is focused in efficient active balancing, dividing the balancing problem into intramodule (inside module) and intermodule (between modules) balancing systems. The modelling is performed to obtain balancing current equations between weak and strong cells, taking into account system efficiency. [PAPER J2] is submitted to an International Transaction.

Chapter 5 METHODOLOGY FOR BALANCING SYSTEM DESIGN presents a methodology to design a battery balancing system. The methodology gives different

design processes to completely define a balancing system for a battery pack divided in m number of modules. The methodology is implemented for different active and passive balancing systems. [PAPER C2] is presented in an international conference to prove the methodology in the design of a passive balancing system.

In **Chapter 6** EVALUATION OF ACTIVE BALANCING SYSTEMS active balancing systems behaviour is evaluated. An extensive comparison is made versus passive balancing system to prove viability (performance, cost, etc) of active balancing systems. Life span improvement on the battery pack due to balancing systems is also presented. The research work has contributed with 2 international transaction publications presented in [PAPER J1] and [PAPER J3].

Finally in **Chapter 7** CONCLUSIONS AND FUTURE WORK main conclusions of the Thesis work and future research lines are presented in detail.

Annex A and **Annex B** present auxiliary documents to help understanding the thesis document work. **Annex A** presents main modelling and power analysis techniques used during the thesis work. **Annex B** focuses on the specific modelling equations for the balancing systems designed. **Annex C** presents some assemblies carried out during the thesis work.

1.4 Scientific Contributions

This research work presents a detailed study about Li-ion technology unbalances and the balancing system design procedure. During the PhD work different scientific contributions present solutions and improvements for literature weakness and lack of information.

- A methodology to analyse the unbalancing effect in series connected Li-ion cells is presented. Lack of information is presented in literature focused on unbalancing of series connected cells. The methodology presents different parameters impact in the unbalancing cause and effects of series connected Li-ion cells. The methodology considers cycling and standby behaviour of series connected cells under different *physical* (temperature), *chemical* (SOC) and *human process* (C-rate, measurement system, etc) parameters.
- A complete analysis is presented regarding single switch open loop active balancing systems. Special effort is made to reduce the complexity of a series connected balancing system, minimizing control complexity and number of elements. The balancing problem is reduced by dividing the battery pack in different *modules*, designing *intramodule* balancing systems and *intermodule* balancing systems. The analysis process is finished by a methodology where balancing systems are designed based on single cell tests and in general knowledge.
- A new comparison pattern is presented to compare balancing systems regarding energetic, temperature and cost issues. Special interest is focused on comparison between passive balancing and single switch active balancing systems.
- A new balancing system topology is presented where a mixed intramodule and intermodule balancing system is designed for 16S1P, which could be extrapolated to high number of series connected large battery packs.

1.5 Publications

CONFERENCES

[PAPER C1] Aizpuru, I.; Iraola, U.; Canales, J.M.; Unamuno, E.; Gil, I., "Battery pack tests to detect unbalancing effects in series connected Li-ion cells," Clean Electrical Power (ICCEP), 2013 International Conference on , vol., no., pp.99,106, 11-13 June 2013.

[PAPER C2] Aizpuru, I.; Iraola, U.; Canales, J.M.; Echeverria, M.; Gil, I., "Passive balancing design for Li-ion battery packs based on single cell experimental tests for a CCCV charging mode," Clean Electrical Power (ICCEP), 2013 International Conference on , vol., no., pp.93,98, 11-13 June 2013.

[PAPER C3] Iraola, U.; Aizpuru, I.; Canales, J.M.; Etxeberria, A.; Gil, I., "Methodology for thermal modelling of lithium-ion batteries," Industrial Electronics Society, IECON 2013 - 39th Annual Conference of the IEEE , vol., no., pp.6752,6757, 10-13 Nov. 2013.

[PAPER C4] Unamuno, E.; Gorrotxategi, L.; Aizpuru, I.; Iraola, U.; Fernandez, I.; Gil, I., "Li-ion battery modeling optimization based on Electrical Impedance Spectroscopy measurements," Power Electronics, Electrical Drives, Automation and Motion (SPEEDAM), 2014 International Symposium on , vol., no., pp.154,160, 18-20 June 2014.

JOURNALS

[PAPER J1] Iraola, U., Aizpuru, I., Gorrotxategi, L., Segade, J. M. C., Larrazabal, A. E., & Gil, I. (2014). Influence of Voltage Balancing on the Temperature Distribution of a Li-Ion Battery Module. Energy Conversion, IEEE Transactions on. doi:10.1109/TEC.2014.2366375.

[PAPER J2] Aizpuru, I., Iraola, U., Canales, J.M., Goikoetxea, A., "Single Switch Active Balancing Systems for Series Connected Energy Storage Systems" Energy Conversion, IEEE Transactions on **(SUBMITTED).**

[PAPER J3] Aizpuru, I., Iraola, U., Canales, J.M., Goikoetxea, A., "Comparative Study and Evaluation of Passive Balancing Against Single Switch Active Balancing Systems for Energy Storage Systems" Energy Conversion, IEEE Transactions on **(SUBMITTED).**

Chapter 2

STATE OF THE ART

During this chapter State of the Art references, guidelines and publications will be analysed related to Li-ion technology. Main industrial guidelines and most relevant scientific papers regarding to Li-ion series connected battery packs.

First headline presents Li-ion battery pack composition, main structures and configurations. Different battery architectures and main drawbacks and problems of battery packs will be presented. The second part presents literature investigations about unbalancing effects in Li-ion cells, specially focused on unbalancing effects in series/parallel connected battery packs. After understanding unbalancing processes a balancing system literature resume will be presented paying attention to the most promising technologies.

Main conclusions and weaknesses of the State of the Art will be the guideline and target for the Thesis work.

2.1 Li-ion battery packs

Li-ion battery packs are series-parallel connection of modules/cells. A module is a combination of series-parallel connection of cells made to decrease battery construction complexity. The battery pack construction is influenced by energy/power dimensioning (cell type, total energy, cycle life, etc), volume/mass issues (Electric vehicle insertion, etc) or behaviour improvement (thermal management, etc). Due to natural unsafe behaviour of Li-ion technology a Battery Management System BMS has to preserve the battery pack under safe working conditions.

2.1.1 Li-ion technology

Lithium presents optimum characteristics to act as an energy storage usage metal. It disposes some physical characteristics to be a solid candidate for different energy storage applications.

- **High potential electrode** (High energy, high voltage).
- **Light material** (High power/energy density).
- **High electric conductivity** (Low resistivity, high power).

The lithium electrode potential is much higher than lead Pb or nickel Ni electrodes Table 2.1. Lithium is much lighter than other common metals as copper Cu and aluminium Al, and also has lower resistivity than those materials.

Li-ion cells are divided in primary and secondary cells. Primary cells could only be discharged, while secondary cells are reversible and main focus of the thesis work.

A Li-ion secondary cell is a complex system composed of different subsystems where Lithium is used as the transfer material Fig 2.1.

Table 2.1 Lithium metal potential properties for energy storage applications.

Characteristic	Lithium	Others	Advantage
Electrode potential	-3,04 V	Pb 1,69, Ni -0,24	High power
Lightness	0.53 g/cm3	Al 2,7, Cu 9	High density
Electric conductivity	108 mΩ/cm	Al 379, Cu 596	Low resistivity

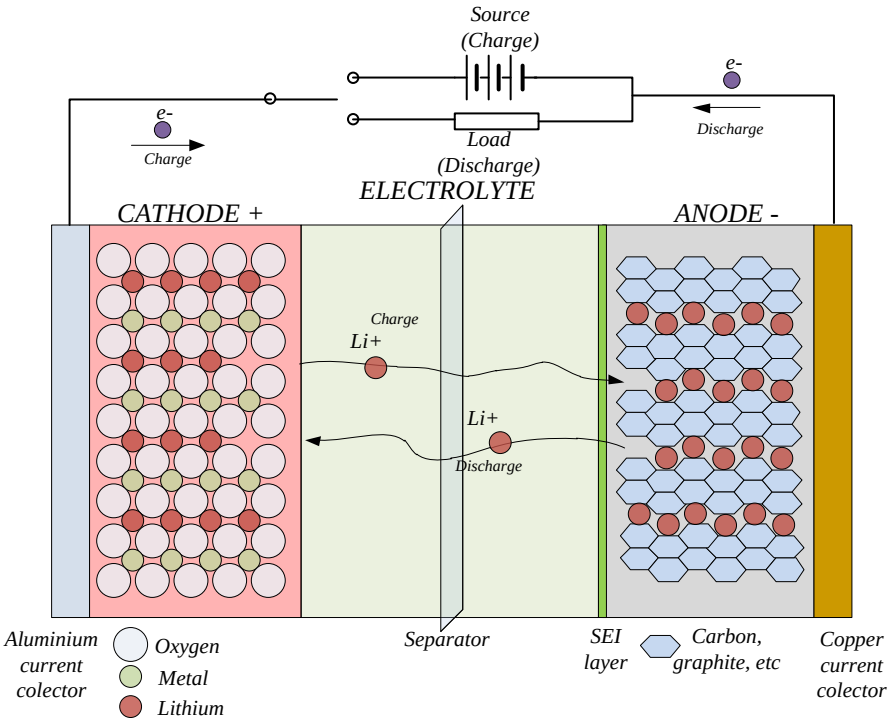

Fig 2.1 Li-ion secondary cell chemical reaction scheme. Source [6]

The Li-ion cell is composed of 3 main components. Two electrodes (anode and cathode) and an electrolyte. The cathode is composed typically by a mixture between Lithium, oxygen and a metal, and it is commonly known as the positive electrode. The anode or negative electrode is a typically carbon-graphite based compound where the lithium can be intercalated, although new titanate and silicon based anodes are entering the market. The electrolyte is the ionic medium where the Lithium ions flow between electrodes, making a barrier for electron flow.

Secondary items of the Li-ion as the SEI layer which is made up as barrier between the electrolyte and the anode during first charge/discharge process, although Li-ion cell power capacity is decreased. The current collectors (aluminium cathode and copper anode) are responsible for the interconnection with the external circuit.

Li-ion technology establishes the intercalation process as its chemical operation behaviour. During charge an energy source is connected between both electrodes. The Li-ions flow through the electrolyte from the cathode to the anode, and the electrons flow through the external current path to stabilize the chemical reaction. During discharge a load connects electrically the anode and the cathode. The Li-ions inserted in

the anode during charge, flow through the electrolyte to the cathode and the electrons go through the electric pad to equal the chemical reaction. Anode and cathode chemical reactions during charge and discharge are presented in (2.1) and (2.2) for the $LiCoO_2$ technology.

$$\mathbf{CATHODE(-)}\quad LiCoO_2 \underset{\text{discharge}}{\overset{\text{charge}}{\Leftrightarrow}} Li_{1-x}CoO_2 + nLi^+ + ne^- \tag{2.1}$$

$$\mathbf{ANODE(-)}\quad nLi^+ + ne^- + C \underset{\text{discharge}}{\overset{\text{charge}}{\Leftrightarrow}} Li_yC \tag{2.2}$$

Li-ion cells are typically denominated by their cathode mixture material, except the lithium titanate technology. Table 2.2 presents main characteristics of different Li-ion compositions regarding their nominal voltage, specific energy and cycle life for a review in 2012 [10] and based on 2011 technological information [9]. A comparison of 6 main Li-ion chemistries is resumed from [11] where cost, performance, life span, specific energy and specific power are compared in Fig 2.2.

Lithium-cobalt LCO was one of the first Li-ion technologies. It is widely used for high energy applications as cell phones. However their high cost and unsafety produced a change in the cathode design to improve safety via thermal stability by Nickel Cobalt

Table 2.2 Different Li-ion chemistry potential properties for energy and power applications. Real source [9] and journal article [10].

Chemistry	Abrev.	Nominal Voltage [V]	Specific energy [Wh/Kg]	Cycle life []	Applications
Lithium Cobalt	LCO	3,6-3,7	175-240	>500	Energy
Nickel Cobalt Aluminium	NCA	3,6-3,7	175-240	>500	Safety, high power and energy
Nickel Manganese Cobalt	NMC	3,6-3,7	100-240	>500	Safety, high power and energy
Lithium Manganese Spinel	LMO	3,7-3,8	100-150	>500	High power
Lithium Iron Phospate	LFP	3,3	60-110	>1000	Safety, high power
Lithium Titanate	LTO	2,3	70	>4000	Cycle life, low temp. performance, safe

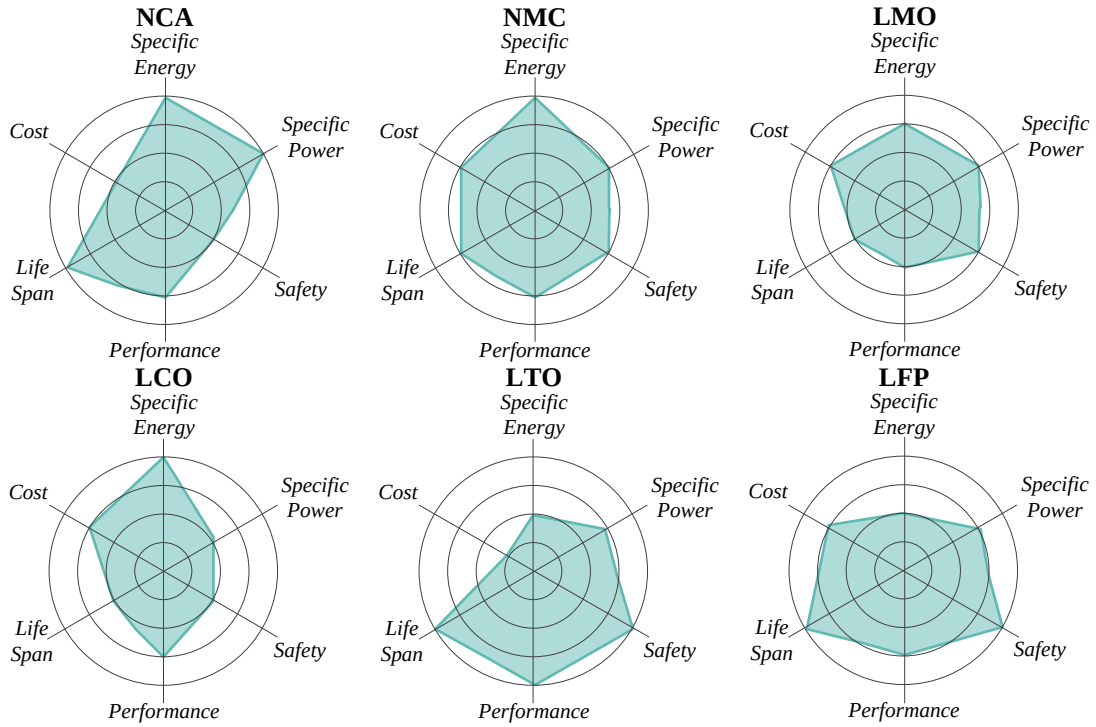

Fig 2.2 Li-ion chemical technology main characteristics: Cost, specific energy, specific power, safety, performance and life span. Source [11].

Aluminium NCA and Nickel Manganese Cobalt NMC cathodes. NCA and NMC improve safety compared to LCO, maintaining high energy properties and they also improve low power specifications of LCO cells. The small amount of Cobalt presented in nature leads to design a manganese based cathode. The Lithium manganese dioxide spinel LMO presents lower cost, higher safety but lower energy density than Cobalt based cathodes, also the performance of the chemistry is not very good. The low performance of LMO chemistry was increased by changing the graphite anode by a titanate based anode creating the Lithium titanate cell LTO. LTO presents excellent life span (>4000 cycles), performance and safety. However the titanate anode material decreases nominal cell voltage decreasing the specific energy of the cell. In order to avoid toxic elements in the cathode an alternative cathode technology of Lithium Iron Phospate LFP was developed first in Texas University (1996) with very good safety performance, cycle life >1000 and low cost, although it has lower energy density than previous presented Cobalt based chemistries. LFP is becoming one of the most promising technologies where safety is an important issue as in electric vehicles.

Table 2.3 General guide of Safe Operating Area SOA of different Li-ion chemistries. Voltage, current and temperature limits [9].

Chemistry	Voltage [V]		Current Rate [ ]		Working Temperature [ºC]	
	Min	*Max*	*Continuous*	*Pulse*	*Charge*	*Discharge*
LCO	2,5	4,2	2-3C	5C	0-45	-20-60
NCA	2,5	4,2	2-3C	5C	0-45	-20-60
NMC	2,5	4,2	2-3C (Energy) >30C (Power)	>5C (Energy) >30C (Power)	0-45	-20-60
LMO	2,5	4,2	>30C	>100C	0-45	-30-60
LFP	2	3,6	10-125C	Up to 250C	0-45	-30-60
LTO	1,5	2,8	10C	20C	-20-45	-30-60

Li-ion technology presents a wide variety of chemistries. The main difference between Li-ion cells is if the cell is made for **energy** or **power** applications. Typically, Cobalt based technologies are used for energy applications, due to their higher specific energy. NMC technology is well suited for power and energy applications and LMO, LFP and LTO are better suited for power applications.

Inside different applications safety is one of the most critical issues in Li-ion cells. Li-ion technology can produce fire or explosion due to operation outside the Safe Operation Area SOA. The 3 main variables where the battery has to be limited are **voltage, current** and **temperature**. Different Li-ion chemistries have different working SOAs as presented in Table 2.3.

Voltage profiles of Li-ion chemistries differ in flatness and sharpness. Cobalt based chemistries and LMO have sharper voltage curves, with nearly constant slope. LFP and LTO chemistries have flatter voltage curves, nearly constant between 20% and 80% capacity [12], [13] as presented in Fig 2.3 a). The cell overcharge could generate metallic lithium platting, solvent co-intercalation or gas evolution and cracking formation with the consecutive capacity fade. On the other hand overdischarge generates a power fade due to current collector corrosion also enhancing other aging mechanisms [14].

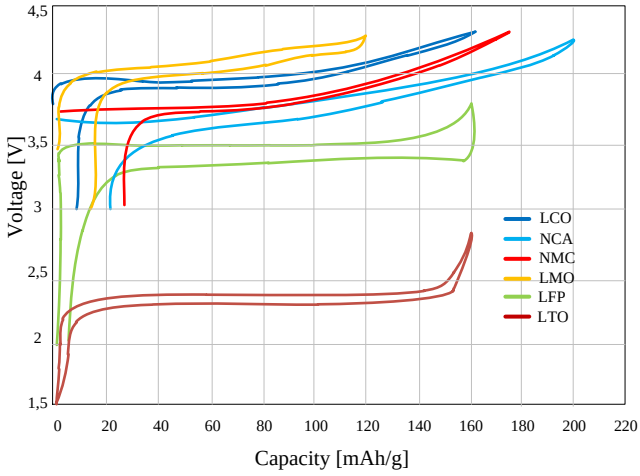

a)

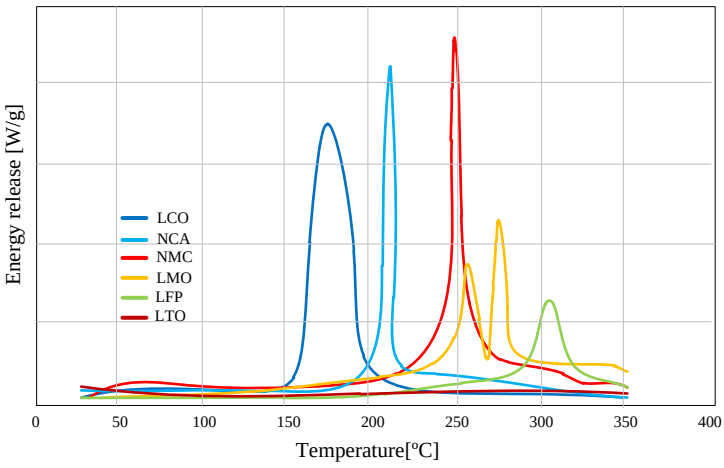

b)

Fig 2.3 Li-ion chemistries voltage and thermal behavior resume a) Voltage charge discharge profiles respect to gravimetric capacity[12], [13] b) Thermal runaway energy release chart [13], [16], [17].

Current rate is limited in Li-ion chemistry. Excessive current rate could generate a power fade due to anode porosity change, or a capacity fade due to lithium platting or contact loss of active material [15]. Although these loss mechanisms are not a security hazard, high current rates could generate excessive power losses inside the cell generating a big increase in internal cell temperature.

Temperature presents the biggest security hazard in Li-ion chemistry. Exceeding working temperature bounds presented in Table 2.3 could generate electrolyte decomposition, decrease of accessible surface in the anode or decomposition of the binder [14], provoking a capacity or power fade. Low temperatures could generate metallic plating and could be lethal for the aging of the cell if it is charged at low

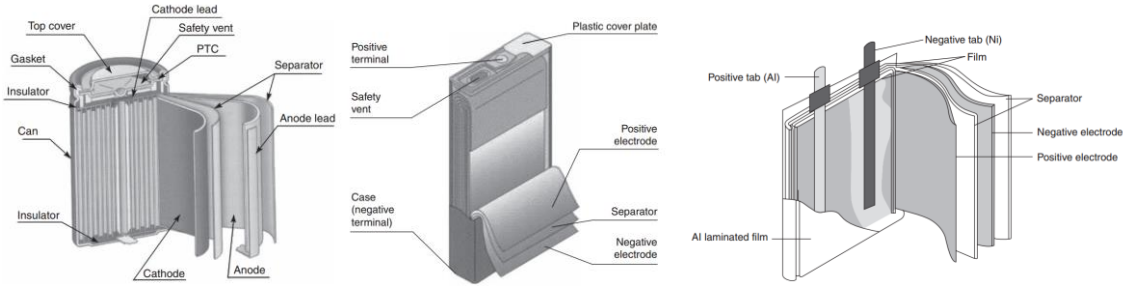

a) **b)** **c)**

Fig 2.4 Li-ion chemistry format cells [9]. a) Wounded spiral cylindrical cell b) Wounded prismatic cell. c) Pouch cell.

temperatures (below 0ºC). However the critical temperature issue is the thermal runaway which can cause, fire or explosion in the Li-ion cell [17]. In Fig 2.3b) could be seen that Cobalt based technologies (LCO, NMC and NCA) present lower runaway temperatures with higher energy releases, being less secure chemistries. LMO presents an improvement in security compared to Cobalt based chemistries increasing the thermal runaway temperature above 250 ºC. LFP technology has been a breakthrough in safety issues, due to high thermal runaway temperature 300 ºC and extreme low energy release. LTO presents the maximum security, specially due to the anode change from graphite to cathode. It presents no energy release over 300ºC (even 700 ºC is claimed [13]). It also presents an exceptional security mechanism for short circuits in the electrolyte, because on the contrary to graphite based anodes LTO anodes are made with not conducting materials.

Li-ion cells are presented in 3 different formats Fig 2.4. Cylindrical cells are widely used in low capacity applications. Cylindrical cells are wounded in a metallic case. They present good mechanical and thermal behaviour, with possibility of PTC temperature switch and pressure vent as security options. Main drawbacks are low space utilization and the difficulty of thermal heat exchange with heat sinks. Prismatic cells are the biggest capacity format Li-ion cells (>1000 Ah). They have a rigid case (plastic or metal) and could be wounded or stacked. They present good thermal and mechanical stability, with high space utilization for a battery pack assembly. Finally pouch cells assembly are the highest energy density cells. They are mechanically weak and easy to construct, although the assembly difficulty is high in a battery pack.

Table 2.4 Main characteristics of Li-ion cells formats: Bad ○, Good ◔, Very Good ◕, Excellent ●.

Characteristic	Cylindrical	Prismatic	Pouch
Energy density	◔	◕	●
Mechanical stability	◕	◔	○
Thermal behaviour	◔	◕	○
Space utilization	○	◕	●
Production cost*	◕	◔	●
Resistance against pressure	◕	◔	○
Assembly	○	◕	○
Terminals connection	Thread, contact	Thread, screw	Tab

There is not a Li-ion cell, regarding chemistry, performance, format, etc suitable for all the applications, so each application needs a good analysis before selecting the most appropriate Li-ion cell. Table 2.4 presents the main basic characteristics in order to select a Li-ion cell format.

2.1.2 Battery pack composition

A battery pack is a series-parallel combination of modules or cells. A module is typically a series connection of single or paralleled cells. The battery pack is a m n system of m modules and n cells in each module. The two typical configurations are m·n m modules in parallel of n series connected cells or m modules in series with n series connected cells as presented in Fig 2.5.

Low power Li-ion portable solutions use a single cell (mobile phones, music players, etc) or a low number of series connected cells as laptops, etc. For high power applications, high current is required. High current applications produce power losses

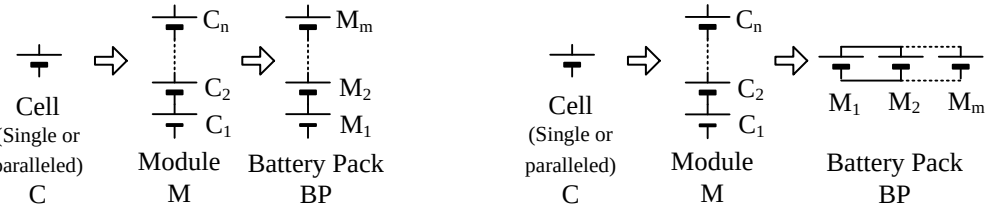

Fig 2.5 Battery pack electrical composition typical structures. a) m·n series-series battery pack. Module: n series cells. Battery pack: m series modules b) m·n parallel-series battery pack. Module: n series cells. Battery pack: m parallel modules

Table 2.5 Resume of main energy storage applications for series connected Li-ion battery packs

Application	Power/Energy [W/Wh]	Voltage [V]	Cells in series
Laptop	20/60	14-15	3-4
Small power tools (drill,etc)	6-100/18-72	7-18	3-5
Lead acid battery substitution	6k-50k/600-5k	12-24-48	4-8-15
Small electric mobility (e-bike, etc)	1k-2k/300-500	48	12-15
HEV	25k-50k/1k-4,4k	70-200	20-60
EV	10k-100k/10k-50k	100-600	30-200
Grid energy storage	1M-5M/250k-1M	>1000	>300

due to joule effect. Joule losses are generated in the internal impedance of the cells, the current collectors, current cables, etc. To decrease the losses of the whole system the voltage of the whole battery pack is increased. To increase the battery pack voltage the cells are connected in series leading to series connected arrays from 3-4 cells in laptops to hundreds of cells for huge energy storage systems as presented in Table 2.5.

Series connection of cells and modules presents a high engineering problem when the number of series connected cells is high. The mechanical distribution of high number of cells and the interconnection between different modules is complicated and could be space dependent, for example in an EV. Series connection of high number of cells introduces a bigger effect in unbalancing behaviour of series connected cells. If the number of series connected cells is increased the probability of deviation or unbalance between 2 series connected cells is enhanced. The complexity of the battery packs is decreased by modularity. Modular battery packs permit to control independently the cells inside the module. The modularity also permits for the industrial partner the opportunity to own a wide variety of different battery packs starting for one module

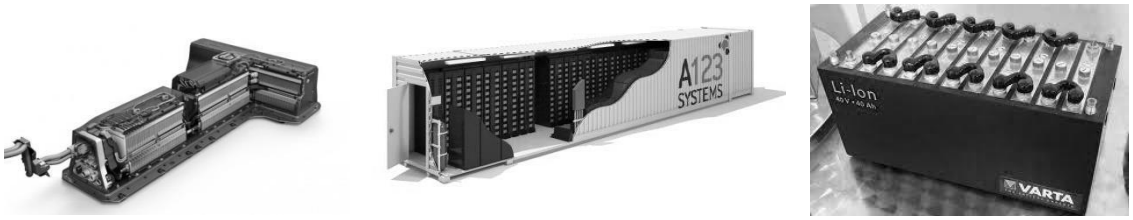

a) **b)** **c)**

Fig 2.6 Li-ion power battery packs. a) EV battery pack (Chevy Volt). b) Grid energy storage battery system (A123). c) General purpose battery pack (Varta)

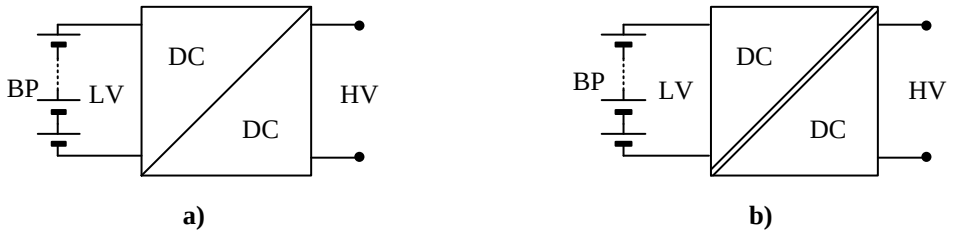

Fig 2.7 HV DC connection point from LV side battery pack using a full power DC-DC converter system as interface. Block diagram presentation a) Non isolated DC-DC converter [18] b) Isolated DC-DC converter [19], [20].

battery pack to several module series/parallel connected battery packs. The complexity of the battery pack increases from a simple module Fig 2.6 c) to a big battery pack Fig 2.6 a) as presented in an EV or the maximum complexity of a huge battery pack Fig 2.6 b) used for high energy grid storage systems.

To reduce the complexity of series connection modules or cells a full power DC-DC converter could be introduced as an interface between the battery pack and the DC connection point. The advantages are the possibility to use low voltage battery packs [18], an isolation option with isolated DC-DC converters [19], [20] and the control of current and voltage in the HV connection point or the LV battery side [21] Fig 2.8.

For high power applications the configuration presented in Fig 2.8 needs a full power DC-DC converter to give the application power. To decrease the power rate of the DC-DC converter, partial power converters are connected to lower energy batteries making a modular system. The outputs of partial power systems could be connected in series for HV loads [23] or in parallel for LV heavy loads [22]. The most flexible design is a modular partial power converter where the inputs and outputs can be connected in

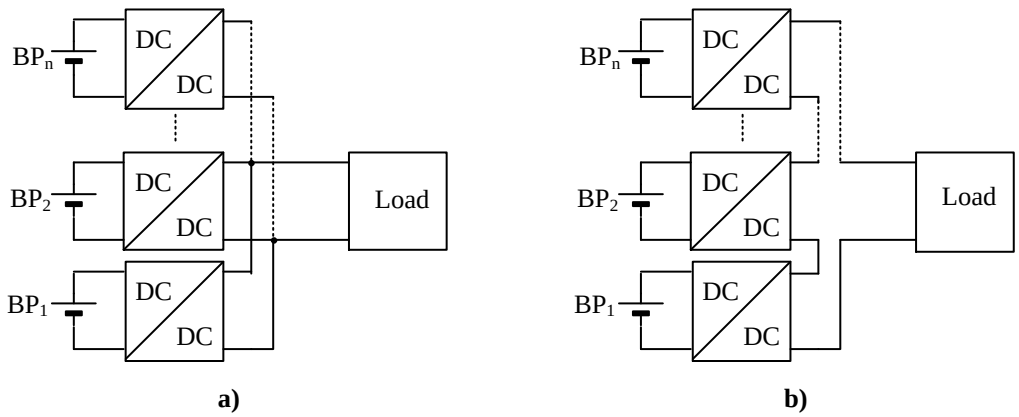

Fig 2.8 LV battery pack connection system based on partial power DC-DC converters a) Output ports connected in parallel for LV heavy loads [22]. b) Output ports connected in series for HV loads [23].

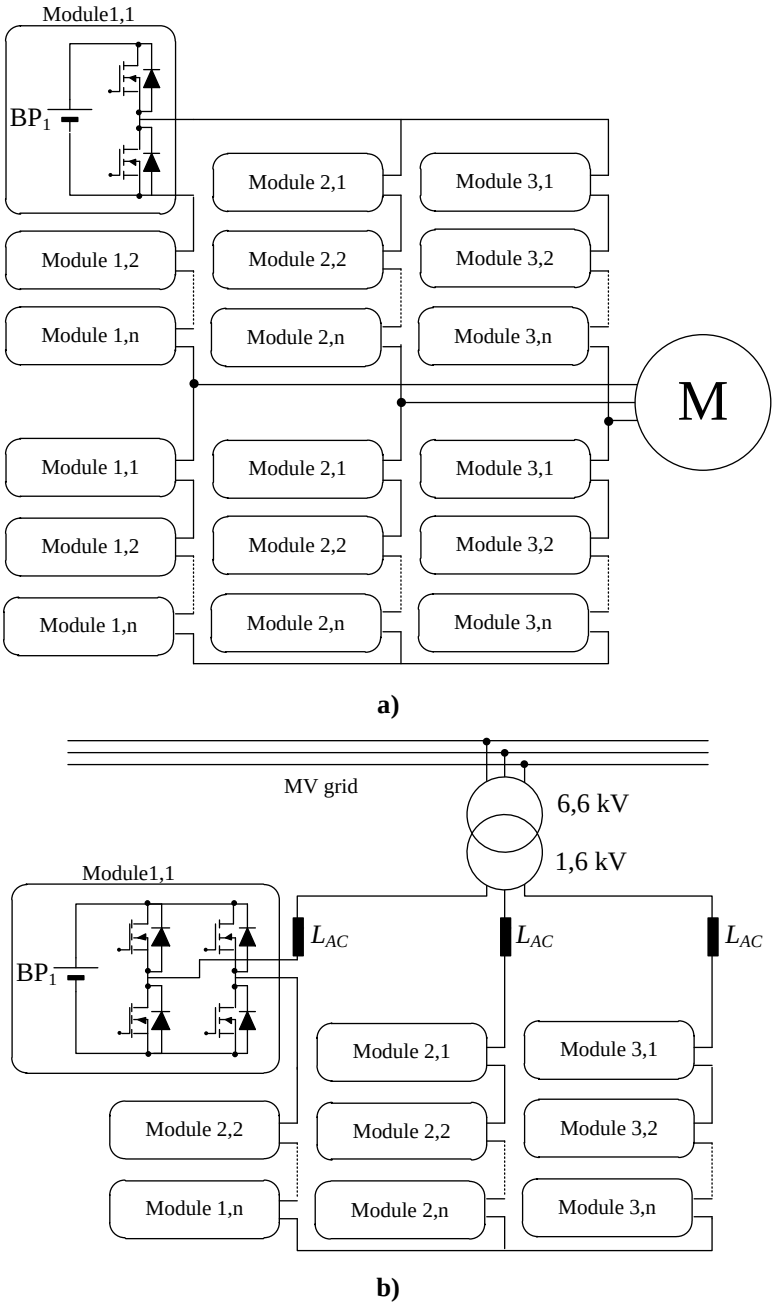

Fig 2.9 Multilevel connection of modular converter with battery packs as energy storage systems a) Half-bridge converter for traction applications [29] b) Full-bridge converter for grid stability applications [30].

parallel or series depending on the application characteristics [24]–[27]. These topologies present the key factor for distributed generation and micro grid market insertion [28].

The battery pack modularity and the partial power converter systems permit to connect directly to the application using multilevel topologies. The HV connection side is not connected to a DC bus, converting the DC-DC converter to a DC-AC converter as

Table 2.6 Main battery pack connection configurations resume for HV configurations. Advantages and main drawbacks.

Connection type	Advantages	Disadvantages
Series connection of cells and modules for HV	•No converter need •Direct connect of battery pack.	•High complexity battery pack.
Full power DC-DC converter with LV battery pack	•LV battery pack. •Control of output HV voltage.	•Total power DC-DC converter need. •DC-DC converter specific.
Partial power DC-DC converters with LV battery packs/modules	•LV battery pack. •Modularity. •Series/parallel connection option.	•Cost. •Control complexity.
Partial power converters for application direct connect	•Direct application connection. •LV battery pack. •Modularity.	•Cost. •Control complexity.

half bridge or full-bridge topology. Each battery pack is a DC bus for the power converter. Applications for power traction [29] and grid stability [30] as FACTs are the most popular systems.

The differences between each connection configuration for a battery pack are presented in Table 2.6.

2.1.3 Battery Management System BMS

The natural unsafety behaviour of Li-ion technology forces the use of a Battery Management System BMS for the security, inspection and control of the Li-ion battery pack.

During subchapter **2.1.1 Li-ion technology** main Li-ion characteristics are presented. BMS has two main objectives for a Li-ion battery pack.

- **Safety:** Guarantee the security of the Li-ion battery pack under different environments.
- **Energy:** Maximize the total energy of the battery pack during the whole cycle life.

Security issues are the most important part of a BMS in Li-ion technologies. Special effort is needed when human interaction is presented as in EVs or cell phones. Besides security issue, human interaction application Li-ion failures also present a big

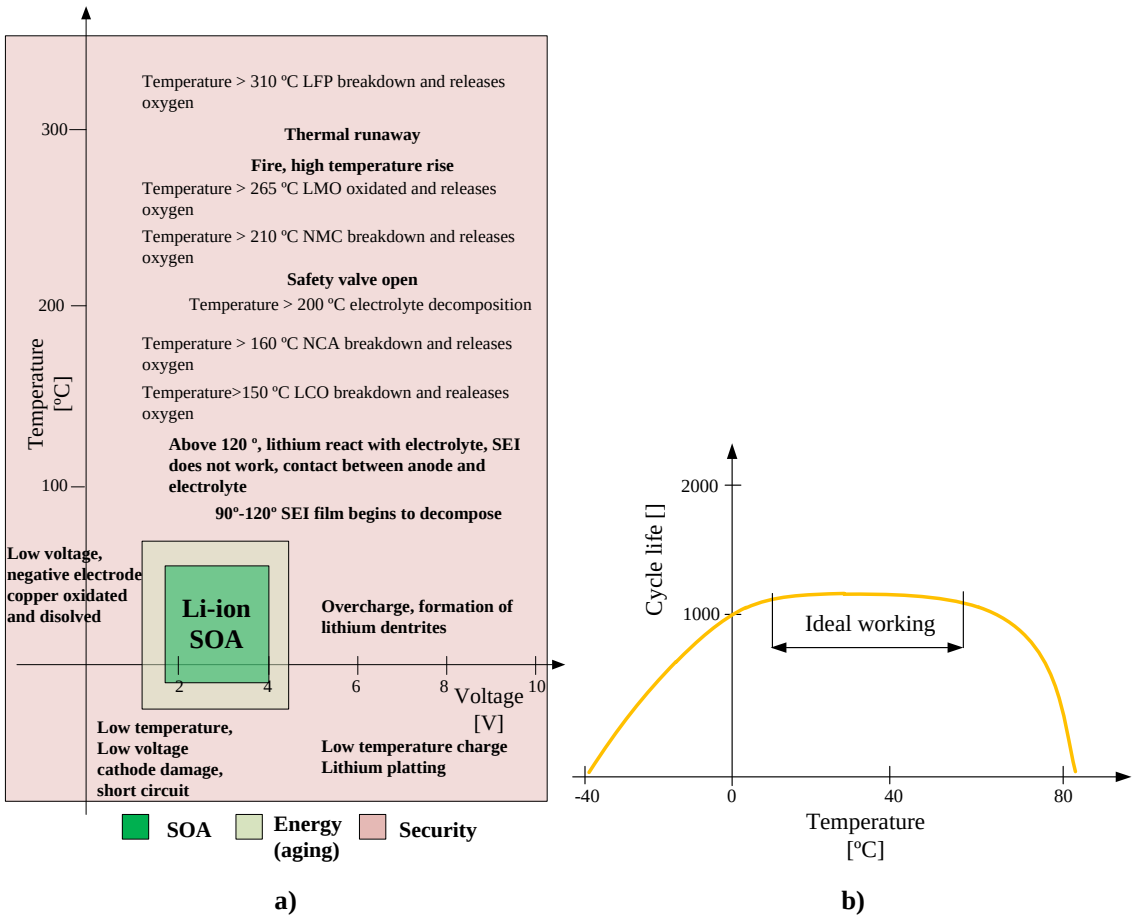

Fig 2.10 BMS safety and energy requirement issues. a) SOA of Li-ion technology for a voltage vs. temperature chart [31]. b) Cycle life improvement vs. operating temperature [16].

risk for Li-ion technology settlement. Li-ion failures appear in press decreasing Li-ion market impact. Voltage, current and temperature limits present the SOA of the Li-ion technology as presented in subchapter 2.1.1. Li-ion current rate generates a temperature increase so current limits are related with temperature limits. Main security risks and Li-ion cell voltage and temperature internal limits are presented in Fig 2.10 a) [31]. Outside the SOA (SOA) an external zone (Energy (aging)) where aging mechanisms are accelerated is presented. The biggest risk area (Safety) is mainly related with high working temperatures, where thermal runaway and fire are the biggest security hazards.

Related with cycle life improvement, and total energy improvement during the battery life, an ideal working temperature zone is presented in Fig 2.10 b). Low temperatures and high temperatures decrease dramatically cycle life. However, working

in a narrow temperature working zone could also increase the thermal management effort, increasing the energy consumption of the whole system[16].

To maintain the battery under SOA and maximize the energy during the cycle life the BMS has 3 main functions: **measure, act, inform** as presented in Fig 2.11.

Li-ion cell parameter measurement presents two type of measurements. Direct measurements are physical measurements of instantaneous battery variables, typically voltage, current and temperature. The direct measurements are critical parameters for battery safe operation. Indirect measurements permit to obtain other parameters by estimation functions. SOC and SOH are the most important estimated parameters to know battery working state. Temperature could also be estimated by a thermal model of the Li-ion battery pack.

After measurement the BMS acts to modify the battery pack parameters. If a security hazard is detected from voltage, current or temperature over limits the battery pack could be disconnected via a power relay or a solid state switch. To improve the energy behaviour of the battery pack a balancing system is controlled to balance the energy of the consecutive series connected cells. The cycle life of the battery pack could be also improved by the control of a Thermal Management System TMS by the BMS.

Optionally the BMS could be connected to an information system. The BMS could datalog battery variables, could also interface with human or control systems, or could be part of a more complex system interconnecting the BMS with the charger, the Electronic Control Unit ECU, etc.

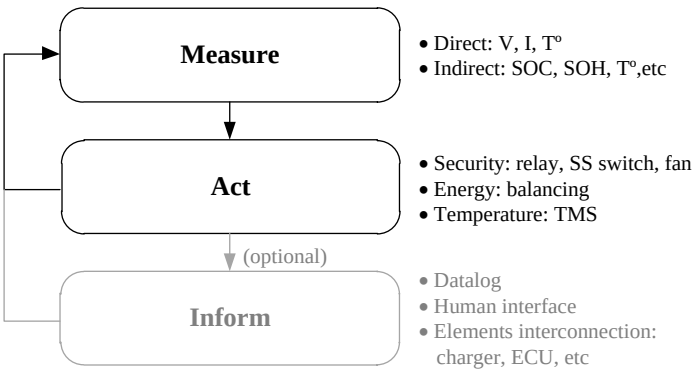

Fig 2.11 BMS working chart. Measure, act and optionally inform.

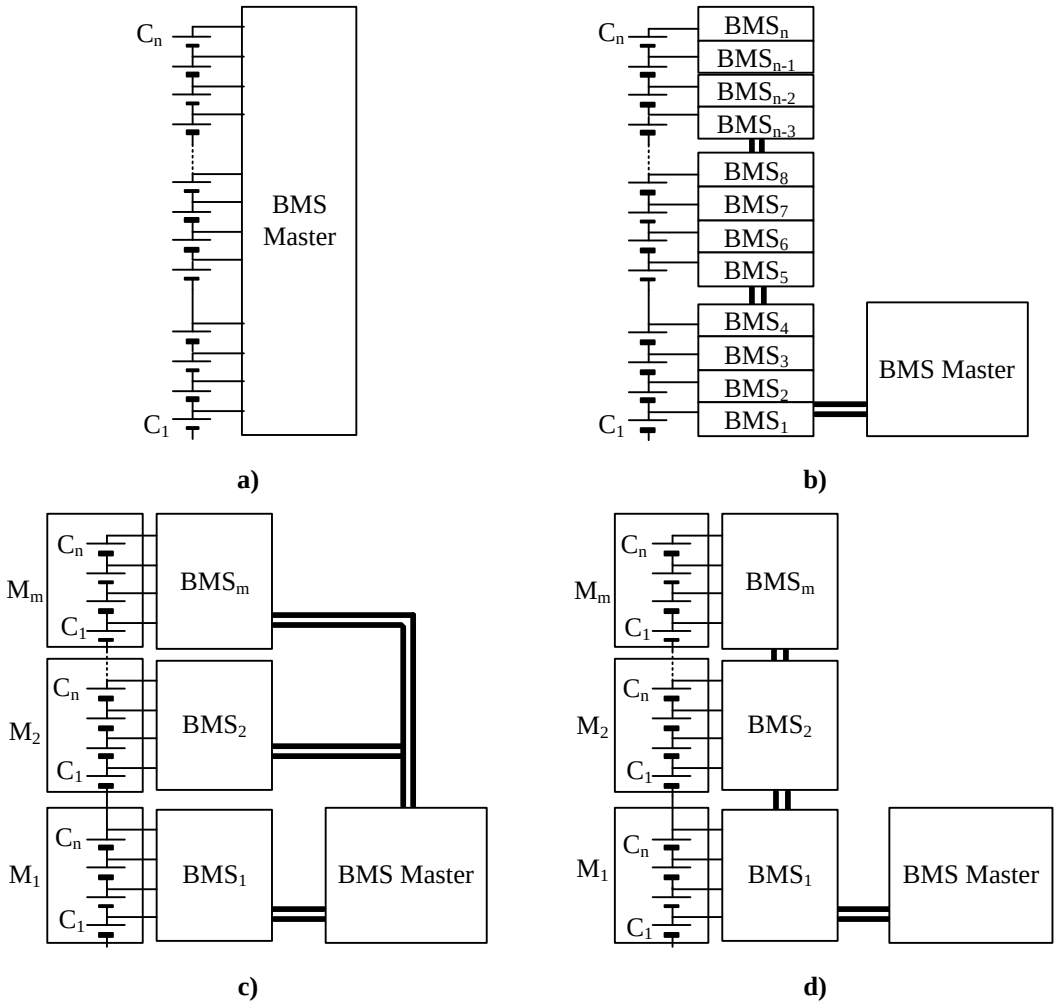

Fig 2.12 BMS different arrangement configurations a) Centralized master BMS with direct measurements b) Distributed slave BMS per single cell c) Modular slave BMS distribution with parallel communication. d) Modular slave BMS distribution with series communication.

When the dimension of a battery pack and the number of series connected cells increase the BMS complexity also increases. The analysis of Li-ion cells is work for the master BMS, which captures all the variables of the complete system and acts after analysing all the different variables. The measurement of the variables could be centralized by the master BMS, measuring directly the Li-ion cells variables Fig 2.12 a) or distributing slave BMSs to measure Li-ion variables and transferring the information to the master BMS Fig 2.12 b). When the number of cells is high in a battery pack, the measurement BMS are distributed in modules, reducing the number of slave BMS slave systems. The BMSs are connected in parallel Fig 2.12 c) or in series (daisy chain) Fig 2.12 d) to communicate with the master BMS.

Table 2.7 Main commercial available ICs for distributed modular BMS configuration.

Manufacturer	Reference	Max. Cells per module (n)	Max. modules per battery pack (m)	Communication
TI	Bq76pl536	6	32	SPI daisy chain
Maxim	MAX11068	12	31	I2C, SMbus
LT	LTC6804-1	12	>10	SPI serial
LT	LTC6804-2	12	>10	SPI parallel
Intersil	ISL78600	12	14	SPI serial
Atmel	ATA6870	12	96	SPI serial

To decrease the complexity of modular BMS design new Integrated Circuits ICs permit to measure and act in battery modules, communicating with the master BMS by an isolated communication BUS for information exchange Table 2.7. The BMS ICs permit to measure, balance and insert communication in a single chip reducing the size and the PCB complexity of the module BMS.

2.2 Lithium-ion unbalancing causes and effects

Unbalancing effects and causes in Li-ion cells are a sum of environmental and manufacturing process differences that generate dispersion between two identical cells. Under a battery pack of series/parallel connected cells unbalancing effects produce a decrease in the whole battery pack performance. The unbalancing causes generate subsequent unbalancing effects in the battery pack.

2.2.1 Unbalancing causes

Li-ion unbalancing causes are divided in 3 main affection groups where manufacturing process dispersions are dependent on the Li-ion cell manufacturer, and the environmental and human interface interactions, are application dependent.

- **Manufacturing process dispersion**: Assembly process non-repeatability and chemical composition mismatch.
- **Environmental variables mismatch**: Temperature deviations.
- **External circuitry connection:** BMS interaction, as voltage measurement or balancing system connection.

Li-ion manufacturing process exhibit differences due to non-controlled variables during manufacturing process. Starting from the manufacturing of the electrodes (mixing the materials, coating, etc), continuing with the assembly of the cell (filling, packing, welding, etc) and finishing with the formation and the final quality check [32], there are little variations that produce mismatch between cells manufactured in the same process.

The **variations in manufacturing processes** present 3 main parameter dispersions in Li-ion cells, capacity dispersion ΔQ_{Max}, self discharge differences ΔQ_{SD}, and variations in the internal resistance ΔR_{in}. The capacity dispersion ΔQ_{Max} between new cells depends on material and construction mismatches. The capacity of the Li-ion manufacturer cells presents a deviation between cell capacity Q_{Max} and nominal capacity Q_{Nom} Fig 2.13 a) and also between same batch cells ΔQ_{Max}. In the manufacturing of a battery pack is necessary to assemble matched cells with nearly equal capacities Q_{Max}. A maximum dispersion of $\pm \Delta Q_{Max}$=2,5 % is necessary [33].

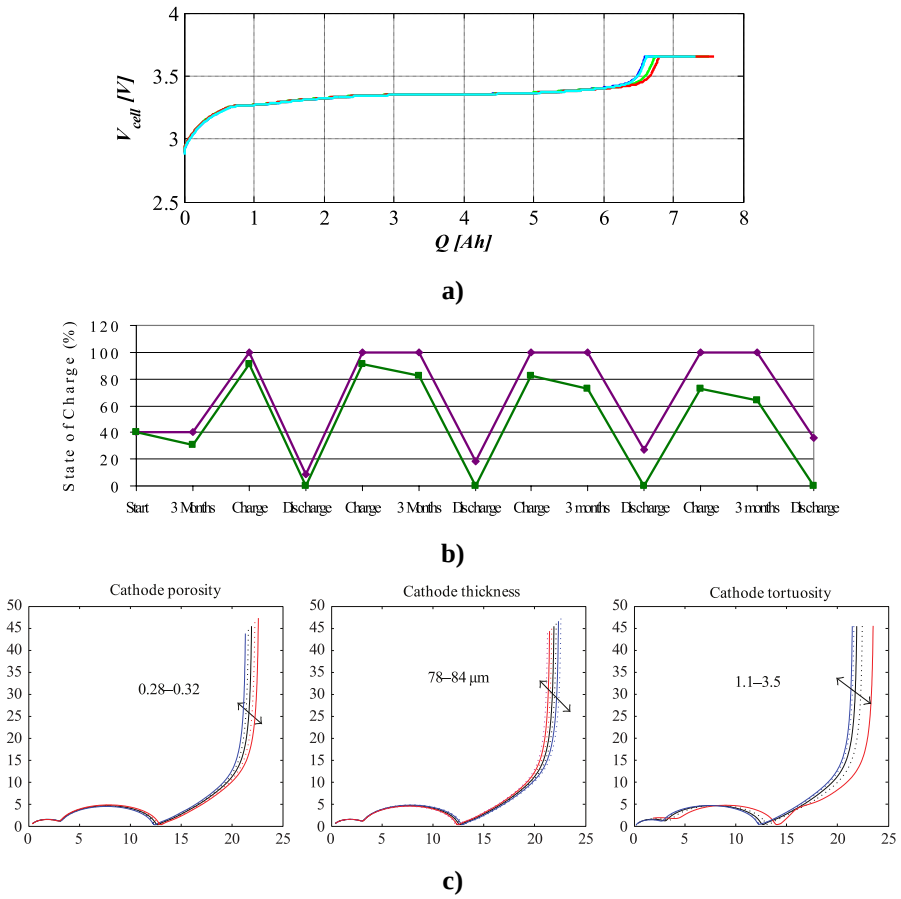

Fig 2.13 Manufacturing process dispersion contributions to battery Li-ion cell unbalance. a) Li-ion charge process dispersion for 4 cells Q_{Nom}=6,5 Ah. ΔQ_{Max} and Q_{Max} variations appreciable in new cells b) ΔQ_{SD} effect for 3 month rest periods [36]. c) cathode impedance change due to porosity, thickness and tortuosity changes in material [37].

Capacity self discharge Q_{SD} of Li-ion cells is a leakage capacity loss due to storage of Li-ion cells Fig 2.13 b). Q_{SD} is directly related to SEI formation and thickness, although phase transformation from Li rich regions to Li poor regions could change the Q_{SD} [34]. Q_{SD} of Li-ion cells is also related with poor isolation of package, reactions between electrodes and electrolyte, partial dissolution of the electrode's active material or even by a rise of internal pressure generating a gain on the cell leakage behaviour [35]. Q_{SD} of Li-ion cells is around 5% during first cycles and decreases to 1-2% per month [33]. Impurities in construction generate dispersion between cell capacities ΔQ_{SD} presenting mismatch behaviour of cells. ΔQ_{SD} influence is negligible in Li-ion cycling applications but could present a problem for standby energy storage applications.

The internal resistance of Li-ion cells R_{in} could be different due to differences in porosity of materials, thickness and tortuosity [37] Fig 2.13 c). Variation in internal resistance ΔR_{in} is specially important in paralleled Li-ion cells [38], where current sharing between two cells is totally dependent on $R_{in.}$

Environmental parameter influence in Li-ion cells is limited to temperature causes. Li-ion cells present high dependency with temperature Fig 2.14. Working or ambient temperature T_{amb} and cell temperature T_C affect directly in all Li-ion cell parameters. A variation in temperature could be generated by a change in ambient temperature or by Li-ion internal heat generation [39]. A dispersion in temperature between cells ΔT_C generates an accelerated dispersion in capacity ΔQ_{Max} [40], [41], ΔQ_{SD} [42] and ΔR_{in} [41], [43], [44].

External circuitry connection presents the last cause of unbalance in Li-ion cells. The unsafe chemical of Li-ion cells needs the connection of measurement systems (BMS voltage measurement as principal) and balancing systems to control the safety and energy of Li-ion cells. Voltage measurement could generate self discharge Q_{SD} increase, from 1-2% to an increase of 3% [33], leading to a 5% self discharge. Variation in leakage current of voltage sensors, due to common mode voltage CM for example, could also generate a dispersion in self discharge ΔQ_{SD}. Balancing circuit also influences in unbalancing causes. Balancing system power losses could generate a temperature dispersion between cells ΔT_C due to hot stops on balancing system PCB, or by Li-ion cell internal heat generation due to balancing currents. Frequency domain influence due to complex internal resistance of Li-ion cell also is influenced by

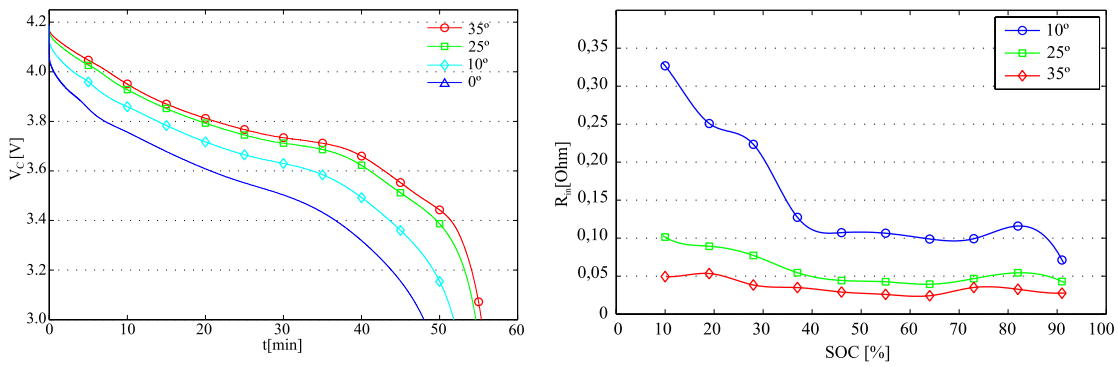

a) **b)**

Fig 2.14 Temperature dependency effect on capacity dispersion ΔQ_{Max} and internal resistance deviation ΔR_{in} for a LiPO Q_{Nom}=1,5Ah cell [41]. a) ΔQ_{Max} for 1 C discharge b) ΔR_{in} for different SOC

frequency component of the balancing current. Balancing current frequency divergences could generate a capacity dispersion ΔQ_{Max} in Li-ion cells [45].

2.2.2 Unbalancing effects

Unbalancing causes presented in previous subchapter generate unbalancing effects between Li-ion cells due to deviations. Unbalancing effects induce battery performance reduction which can be presented in two time domains.

- **Instantaneous:** Unbalancing effects that impact in instantaneous cycling
- **Aging:** Unbalancing effects that generate degradation in Li-ion cells during battery life. The aging mechanisms are divided in **calendar** and **cycle** aging.

The unbalancing effects, both instantaneous and aging, are expressed in two battery performance variables:

- **Capacity:** Variations in capacity Q_{Max} or SOC of Li-ion cells and difference in self discharge ΔQ_{SD} in stationary applications.
- **Power:** Differences in internal resistances ΔRin are main concerning variable.

Instantaneous unbalancing effects are related to battery performance decrease during cycling. Manufacturing process dispersion limit a series connected battery pack. Lower capacity Q_{Max} cells generate a capacity fade and higher internal resistance R_{in} cells generate a power fade. Variations in self discharge ΔQ_{SD} are not significant during cycling. Temperature dispersion between cells ΔT_C generates an increase in performance for high temperature cells ($\uparrow Q_{Max}$-$\downarrow R_{in}$) and a capacity and power fade due to low temperature cells ($\downarrow Q_{Max}$-$\uparrow R_{in}$) [41]. External circuitry voltage measurements does not affect during cycling, however balancing system could generate a big capacity increase during cycling by exploiting the whole battery pack energy [46].

Unbalancing effects presented due to aging mechanisms are divided in calendar aging and cycling aging. Calendar aging is related to self discharge Q_{SD}. High SOC and high T_C cells suffer higher self discharge, decreasing cells calendar life [47]–[51]. During calendar aging reversible losses (recovered after charge) and irreversible losses (irrecoverable, permanent losses) are presented in Li-ion cells. Reversible losses are kept constant [47]. Calendar life effect in power fade is much lower than capacity fade.

Table 2.8 Li-ion performance deviation mechanisms. Instantaneous and aging behaviour performances related to capacity and power characteristics. ↑High, ↓Low

	Causes	Capacity	Power
Instantaneous	Manufact. process	•↑Q_{Max} decrease capacity •ΔQ_{SD} no effect	•High R_{in} decrease
	Temperature	•↑T_C increase capacity, ↓T_C decrease capacity [41]	•↑T_C increase power ↓T_C decrease power [41]
	External	•Voltage measurement no effect •Balancing system increase [46]	•No effect
Aging	Manufact. process	•Consequent overvoltage capacity fade and safety hazard [52] •ΔRin Capacity fade in paralleled cells [38]	•ΔRin dispersion power fade [52]
	Temperature	•↑T_C •Capacity fade [53], [54] •↑ Q_{SD} [47], [51] •Very ↓ TC •Capacity fade [54]	•↑T_C •Resistance increase power fade [54], [53] •Very ↓ TC •Resistance increase [54]
	External	•Voltage measurement ↑ ΔQ_{SD} •Capacity increase due to equal aging •Calendar life improvement •Cycle life improvement	•Balancing system increase Rin depending on frequency [45]

Calendar life Cycle life

Cycling aging due to the manufacturing process mismatch is presented as a safety hazard if a cell is continuously took over voltage limits, primarily presented between series connected cells. The cell presents high capacity fade and security hazard problems [52]. When cells are connected in parallel a difference in ΔR_{in} in 20% could accelerate the capacity fade by a 40 % [38]. High T_C >50ºC present accelerated power and capacity aging during cycling [53] and presents even a capacity and power crank in low number of cycles for very low temperatures <0ºC [55]. The cycle life is decreased above 25ºC, primarily due to instability of SEI [54]. Voltage measurement could increase the self discharge dispersion ΔQ_{SD}, decreasing battery cycle life due to higher Q_{SD} cells. However balancing circuits improves battery life equalizing battery aging and maximizing energy, although it can generate a power fade due to Rin increase [45].

SOC and DOD influence are not presented in previous analysis because they are application dependent parameters. However a more extensive analysis in the effect of LFP batteries will be held in next paragraphs.

LFP cells are highly influenced by temperature, Fig 2.15 , but the influence is different for aging and instantaneous cycling. For instantaneous behavior is better to cycle the LFP in higher temperatures , increasing the capacity and decreasing the internal resistance (power increase) [56]. For cycle aging effect, LFP cells should be cycled between 15ºC and 35ºC [54]. Low temperatures <0ºC suffer high lithium platting during cycling reducing dramatically cycle life [54], [55]. High temperature cycling(>45ºC) reduces cycle life and increases internal resistance [54], [55]. However, a recent research reveal a better performance of a 45ºC cycled cell respect to a 25ºC cycled cell during 600 cycles [56]. High temperature effect in calendar aging of LFP is very severe, with greater impact than SOC effect [47]–[49].The capacity fade for 300 days storage due to temperature differences could go from 12% and 16% for 30ºC and 50ºC respectively [47], or 2% to 40% for 30ºC and 60ºc respectively [49].

SOC accelerates aging respect to calendar life for high SOC values [47]–[49]. Even if the impact on calendar aging is smaller than temperature effect a 90% SOC cell ages 10% compared to 6% aging for a 30%SOC cell, for a storage period of 300 days [47]. For cycle life analysis DOD is more representative than SOC. Main studies indicate that high DOD applications accelerate aging [54]. However there are other studies that indicate that DOD is not representative in cycle life reduction, only cycling time [55]. Other studies indicate that also the initial SOC influences the DOD analysis [57].

Current rate impact is also studied for different aging processes. High current rate charge discharge processes decrease life in LFP cells [54], [55], [57], also accelerating aging due to the increase of cell temperature. The cycle life reduction could be very severe, from 2900 cycles at 1C rate to only 559 cycles at 15C rate [54].

The impact of parameter deviation as capacity dispersion between cells and external circuitry is not studied in literature for LFP cells unbalances.

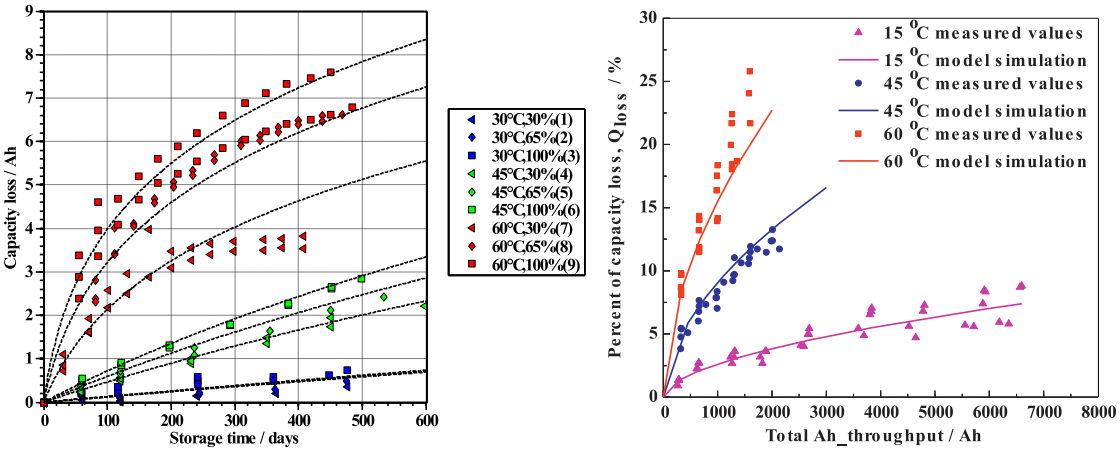

a) **b)**

Fig 2.15 Temperature effect in calendar life and cycle life. a) Calendar life effect due to storage in 15 Ah nominal capacity LFP cells. SOC effect is less severe than temperature effect [49]. Cycle life impact performance of temperature dispersion for a 2,2 Ah LFP cell [55].

2.2.3 Battery pack performance under unbalancing effects

An unbalanced battery pack decreases the battery pack performance due to inefficient use of the battery pack energy. It also accentuates battery pack aging due to different aging procedures inside battery pack cells as presented in previous subchapters.

A battery pack is unbalanced due to SOH and SOC differences between different cells. SOH defines the relation between maximum cell capacity Q_{Max} respect to nominal cell capacity Q_{Nom} (Aging). SOC defines the relation between instantaneous cell capacity Q and maximum cell capacity Q_{Max} (Instantaneous).

$$\begin{aligned} SOH &= \frac{Q_{Max}}{Q_{Nom}} 100 \quad (0 \le SOH) \\ SOC &= \frac{Q}{Q_{Max}} 100 \quad (0 \le SOC \le 100) \end{aligned} \tag{2.3}$$

Unbalancing impact is more influenced in series connected Li-ion cells, than in parallel connected cells. There are 4 possible configurations for series connected Li-ion cells.

- SOH balanced / SOC balanced (Configuration 1).
- SOH balanced / SOC unbalanced (Configuration 2).
- SOH unbalanced / SOC balanced (Configuration 3).

- SOH unbalanced / SOC unbalanced (Configuration 4).

To balance and maximize the energy of a series connected battery pack a balancing system is the key element. The balancing system could balance the battery pack burning the excess energy of the battery pack (passive balancing- charge process) or redistribute the energy of the charged cells to the weak cells (active balancing- charge/discharge process).

The instantaneous capacity of a cell Q and the energy inside a cell W is roughly approximated using (2.3).

$$\begin{aligned} Q &= \frac{SOC}{100} \cdot \frac{SOH}{100} \cdot Q_{Nom} \\ W &= Q \cdot V_{Nom} \end{aligned} \tag{2.4}$$

While the maximum energy W_{Max} that a cell could have is presented when the cell is fully charged to its maximum capacity $Q_{Max,}$ which is dependent on the SOH of the cell

$$\begin{aligned} W_{Max} &= \frac{SOH}{100} \cdot Q_{Nom} \cdot V_{Nom} = Q_{Max} \cdot V_{Nom} \\ W &= Q \cdot V_{Nom} \end{aligned} \tag{2.5}$$

the instantaneous energy of a battery pack W_{BP} is the sum of all the individual energies of the single cells of a battery pack.

$$W_{BP} = \sum_{i=1}^{n} W_i \tag{2.6}$$

The energy of a battery pack is divided in the energy inserted during charge $W_{BP,C}$ and the energy delivered during discharge $W_{BP,D}$. During charge the main objective is to insert the maximum possible energy to the battery pack. If a balancing system is used during charge the battery pack energy is the sum of the maximum energies W_{Max} of the single cells of a battery pack. If a balancing system is not used the charging process is stopped when the battery pack weakest cell is fully charged $W_{Max,W}$ (SOC = 100%). The battery pack charge energy is the sum of the maximum charge of the weak cell $W_{Max,W}$ and the instantaneous energy of the n-1 cells after the charge process.

$$W_{BP,C} = \sum_{i=1}^{n} W_{Max,i} \rightarrow \text{charge balance}$$
$$W_{BP,C} = W_{Max,W} + \sum_{\substack{i=1 \\ i \neq W}}^{n} W_i \rightarrow \text{not balancing} \quad (2.7)$$

During discharge process the energy of the battery pack $W_{BP,D}$ is released. If a battery pack is used without active balancing system the discharge energy of the battery pack is limited to n times the weakest cell energy W_W. If an active balancing system is used the energy of the whole battery pack could be fully used. The total discharge energy would be the sum of all the single cell energies W_n.

$$W_{BP,D} = \sum_{i=1}^{n} W_i \rightarrow \text{discharge balancing}$$
$$W_{BP,D} = nW_W \rightarrow \text{not balancing} \quad (2.8)$$

The 4 battery configurations for series connected cells are analysed under simulated cell characteristics Table 2.9. The battery pack is simulated for a charge process and a consecutive discharge process. The battery pack will be analysed for no balancing connection, charge balancing and charge/discharge active balancing system. The cells connected in series will be divided into n-1 strong cells, and 1 weak cell. The number of series connected cells will be analysed for n=2 and n=16 to evaluate the effect on increasing number of cells. The evaluation of unbalancing performance is analysed under the initial capacity point of

- Cell characteristics: Q_{Nom}: 1 Ah, V_{Nom}: 3 V.
- SOC:
    - Balanced: SOC weak and SOC strong 80%.
    - Unbalanced:
        - a) SOC weak 90% SOC strong 80%.
        - b) SOC weak 80% SOC strong 90%.
- SOH
    - Balanced: SOH weak and SOH strong 100%.
    - Unbalanced: SOH weak 80% SOH strong 100%.

The battery pack performance is evaluated for the energy inserted to the battery pack during charge $W_{BP,C}$ and the consecutive energy obtained during discharge $W_{BP,D}$.

Table 2.9 Battery pack energy analysis for charge $W_{BP,C}$ and consecutive discharge $W_{BP,D}$ for series connected cell battery packs. 2 and 16 series cell connection analysis for different SOC and SOH state V_{Nom}=3V and Q_{Nom}=1 Ah cells. No balancing (No) charge balancing (C) and charge/discharge balancing (C / D) balancing system configuration. Configuration 1: SOC and SOH balanced. Configuration 2: SOC unbalanced SOH balanced. Configuration 3: SOH unbalanced SOC balanced. Configuration 4: SOC: unbalanced SOH unbalanced. Percentage value in grey, energy compared to maximum 100 % for C / D balancing system

		Configuration 1			**Configuration 2-a**		
	Cells	No	C	C / D	No	C	C / D
$W_{BP,C}$	2	6 (100%)	6 (100%)	6 (100%)	5,7 (95%)	6 (100%)	6 (100%)
$W_{BP,D}$		6 (100%)	6 (100%)	6 (100%)	5,4 (90%)	6 (100%)	6 (100%)
$W_{BP,C}$	16	48 (100%)	48 (100%)	48 (100%)	43,5 (90,6%)	48 (100%)	48 (100%)
$W_{BP,D}$		48 (100%)	48 (100%)	48 (100%)	43,2 (90%)	48 (100%)	48 (100%)
		Configuration 2-b			**Configuration 3**		
	Cells	No	No	No	No	C	C / D
$W_{BP,C}$	2	5,7 (100%)	6 (100%)	6 (100%)	5,28 (97,8%)	5,4 (100%)	5,4 (100%)
$W_{BP,D}$		5,4 (100%)	6 (100%)	6 (100%)	4,8 (89%)	4,8 (89%)	5,4 (100%)
$W_{BP,C}$	16	47,7 (99,4%)	48 (100%)	48 (100%)	45,6 (96,2%)	47,4 (100%)	47,4 (100%)
$W_{BP,D}$		43,2 (90%)	48 (100%)	48 (100%)	38,4 (81%)	38,4 (81%)	47,4 (100%)
		Configuration 4-a			**Configuration 4-b**		
	Cells	No	C	C / D	No	C	C / D
$W_{BP,C}$	2	5,04 (93,3%)	5,4 (100%)	5,4 (100%)	5,22 (96,6%)	5,4 (100%)	5,4 (100%)
$W_{BP,D}$		4,8 (89%)	4,8 (89%)	5,4 (100%)	4,44 (82,2%)	4,8 (89%)	5,4 (100%)
$W_{BP,C}$	16	42 (88,6%)	47,4 (100%)	47,4 (100%)	47,22(99,6%)	47,4 (100%)	47,4 (100%)
$W_{BP,D}$		38,4 (81%)	38,4 (81%)	47,4 (100%)	35,52(74,9%)	38,4 (81%)	47,4 (100%)

The battery pack could present 4 different unbalancing configurations, with two different subconfigurations (a-b) for configurations 2 and 4 due to two different SOC unbalance mismatch possibilities between weak and strong cells.

When cells are balanced in SOH and SOC the balancing system does not influence. When a SOC unbalance is presented a charging process balancing system is enough to balance the cells and obtain 100% energy during discharge (Configuration 2-a 2-b). However when an SOH unbalance is presented, only the charge discharge balancing system obtains the whole energy. Even a charging balancing system could be counterproductive, because the battery pack is charged more than without balancing system and the energy obtained is the same (Configuration 4-a). The issue of increasing series connected cells creates a big energy reduction for SOC mismatch without balancing, and even higher for SOH mismatch for a battery pack without balancing system or balancing during charge.

2.3 Energy Storage Balancing Systems

Energy Storage balancing systems permit to maximize the energy of a battery pack, matching the energy between series connected cells. There are different topological reviews about balancing systems [58]–[62]

Permanently connected resistive paths are discarded for energy storage systems, because the energy is wasted unnecessarily. Permanently connected dissipative devices are limited to high dynamic systems like capacitors or low energy ultracaps [63].

Energy storage balancing system topologies are divided in passive and active systems, where the common element is an active switch (relay or semiconductor) for balancing the energy. Passive balancing systems dissipate the excess energy in a power resistor, while active balancing systems redistribute the energy between cells via lossless capacitive and inductive devices. The energy could be transferred between cells or redistributed between one cell and the battery pack Fig 2.16.

2.3.1 Passive balancing systems

Passive balancing systems are the most used balancing systems in industrial applications. The simplicity, cost and reliability are the most important characteristics of passive balancing systems.

An active switch connected with a resistor in series burns the excess energy of the

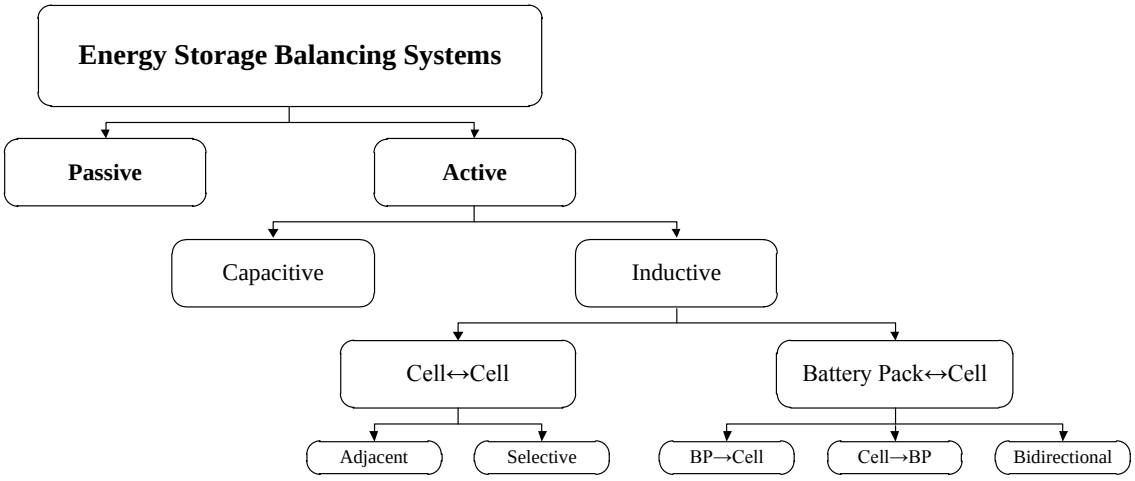

Fig 2.16 Topological overview of energy storage balancing systems.

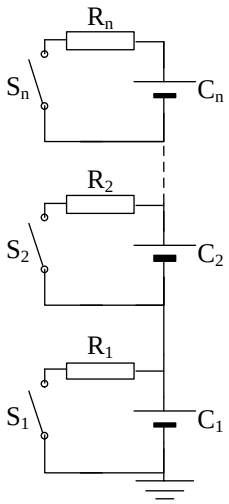

Fig 2.17 Passive balancing system scheme for a n series connected cells battery pack[64].

most charged cell [64]. Due to its dissipative behaviour passive balancing is most used in charging processes, because during discharge only burns energy not contributing to energetic improvement to the series connected energy storage system [65].

2.3.2 Active balancing systems

Active balancing systems redistribute the energy between the series connected cells, by the use of lossless capacitive (capacitors) and inductive (inductors and transformers) devices.

Capacitive balancing systems are mainly based on charging a capacitor by the strongest cell and discharging the energy of the capacitor to the weak cell/s. Single tiered capacitive balancing Fig 2.18 a)is based on consecutive charge exchange between adjacent cells [66]. Capacitors are continuously charged and discharged finally equalizing all the series connected cells. The double tiered capacitive balancing system Fig 2.18 b) is an improvement of the single tired system. A capacitor is placed between n and n-2 cells to increase the balancing speed of the system [67], [68]. If the speed is critical during balancing the flying capacitor capacitive system is the best option Fig 2.18 c), because the selection could be done between two different cells in the battery pack [69].

Capacitive balancing currents are dependant of voltage differences between cells and balancing circuit resistance (switch resistance, PCB path). Due to very small

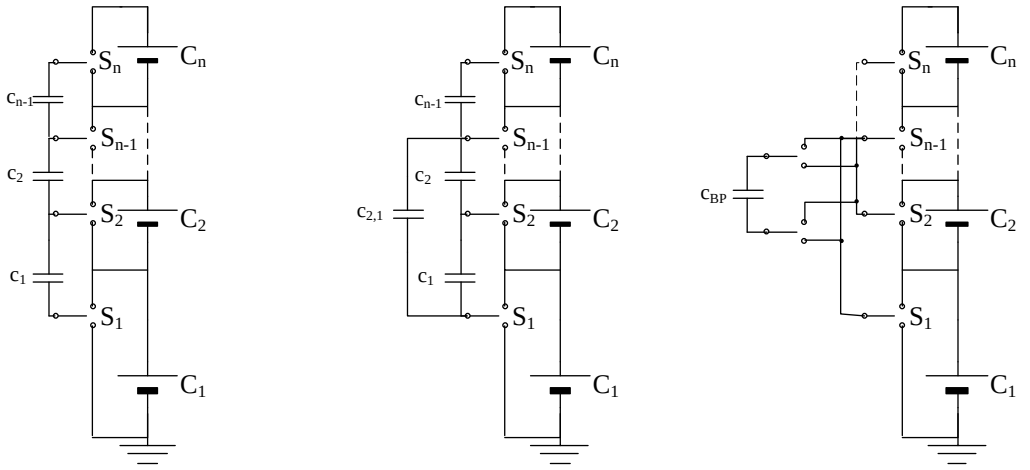

Fig 2.18 Capacitive balancing systems a) Switched capacitor or single tired capacitive balancing system [66]. b) Double tired capacitive balancing system [67], [68]c) Flying capacitor capacitive balancing system [69]

voltage variations of Li-ion cells and specially in LFP chemistry, small balancing currents of C/500 or C/2000 are obtained [62]. Capacitive balancing systems could work with open loop switching control with constant duty cycle gate signals. The number of intelligent switches required is very high and the series connected cells are voltage balanced instead of SOC balanced.

Inductive balancing systems transfer the energy from a voltage source (cell, module or battery pack) converting the energy via a current source (inductor) and inserting again the energy to a voltage source (cell, module or battery pack). The energy transfer is made between single cells or between single cells to higher voltage modules or battery packs.

Cell to cell balancing systems transmit the energy between single cells of a series connected battery system. The energy could be transferred between two different cells transferring the energy from adjacent cell to adjacent cell Fig 2.19 a-1) until the energy is released in the weak cell [70] . This topology requires high number of high frequency switches and the efficiency is low, even though resonant networks could be used to increase efficiency [71] or topological improvements to reduce the switch count [72]. The balancing speed is improved by selective cell balancing [73] Fig 2.19 a-2). The energy is directly transferred from the strong cell to the weak cell. The number of unidirectional or bidirectional switches is very high, specially for high number serialized battery packs.

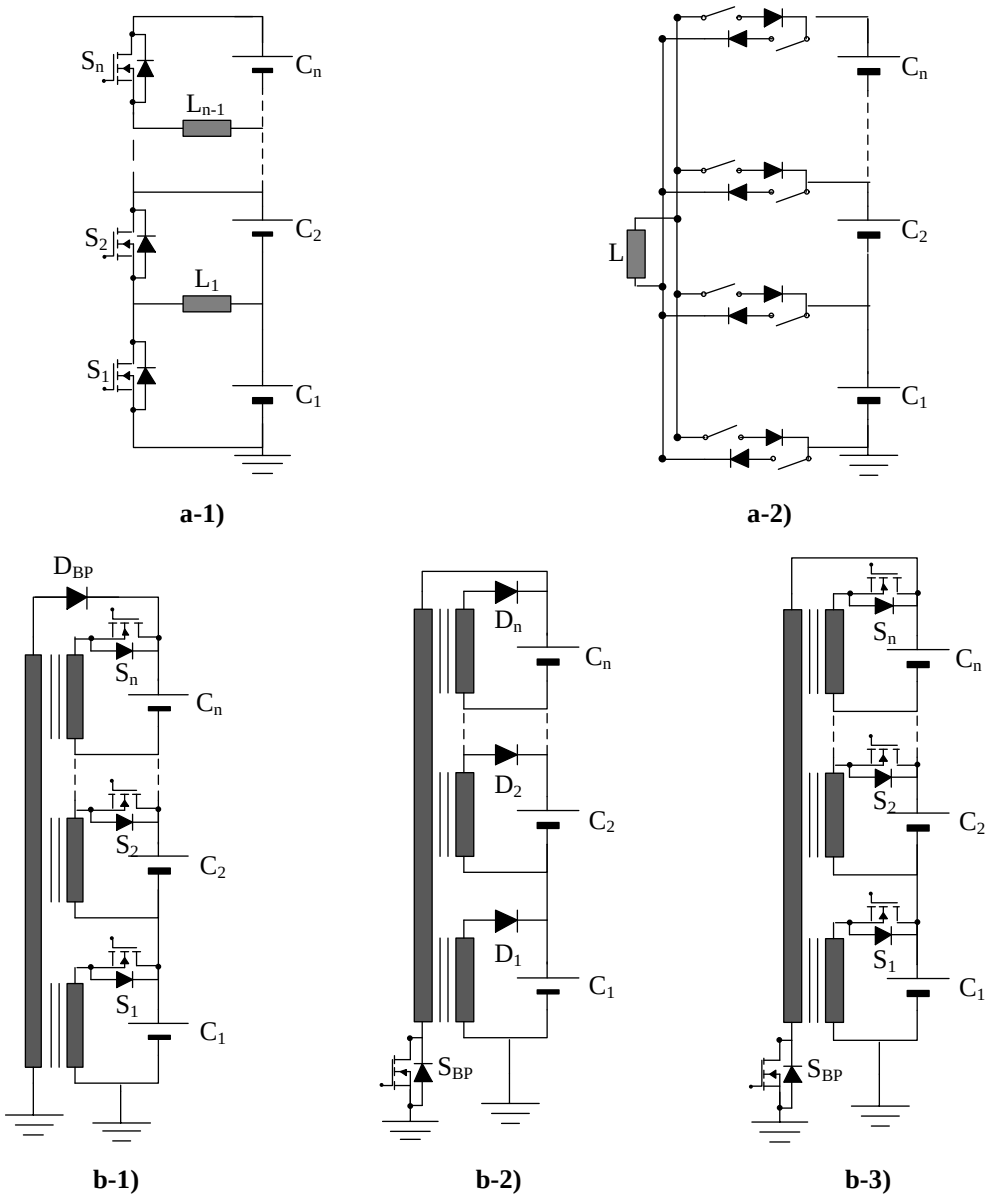

Fig 2.19 Inductive balancing systems a) Cell↔Cell a-1) adjacent cell energy exchange [70] a-2) selective cell energy exchange [73] b) BP↔Cell b-1)Cell→BP balancing system[74]. b-2) BP→Cell balancing system [75] b-3) Bidirectional inductive balancing system [76]

Cell to cell balancing systems offer good SOC balancing behaviour between all the cells of a series connected battery pack. However they are highly complex and have high number of high switching frequency switches, increasing the balancing system cost.

Battery pack ↔ cell balancing systems transfer the energy between a low voltage port (cell) and a high voltage port (module or battery pack, series connected cells). Cell → battery pack systems Fig 2.19 b-1) transfer the energy between the strong cell of a

series connected cell string inserting again the energy to the module or battery pack [74]. The energy transfer is typically made via a transformer to adjust the voltage difference. The configurations could be different changing from a multi-winding transformer [74], independent transformers [77] or a single transformers for all the series connected cells [78].

Battery pack to cell balancing systems obtain the energy from the whole battery pack via one active switch Fig 2.19 b-2) and reinsert the energy to the weaker or weakest cell/s [75]. The configurations could change as the cell to battery systems from multiwinding transformers [75], to independent transformers [59] or one single transformer with high number of cell selection switches [79].

Battery pack↔cell bidirectional balancing systems transfer the energy in both directions [76], having an active switch in the battery pack level and the cell level Fig 2.19 b-3. The typical configurations are multiwinding based transformer [76] or independent DCDC converters for the connection between each cell and the battery pack [46].

Inductive balancing systems permit high current balancing rates. The complexity control and the cost of the balancing system is dependent on the number of active switches. Selective systems present high balancing speeds because the energy is directly transferred between strong and weak cells. The circuit design is complex when high number of cells are involved, specially for multiwinding transformer design.

2.3.3 Single switch active balancing systems

Table 2.10 Main characteristics of active inductive balancing systems.

Topology	Mode	Efficiency	Complexity	Switch count	Speed
Cell↔Cell	Adjacent	Very low	Low	High	Low
	Selective	High	High	Very high	High
BP↔ Cell	BP→Cell	Medium	Low	Low, medium	Medium
	Cell→BP	Medium	Medium	High	Medium
	Bidirectional	High	High	n+1	High

Single switch active balancing systems are a particular topology of battery pack to cell (BP→Cell) balancing systems. The main characteristic is that only one switch is enough to balance all the series connected cells. Series connected cells are voltage balanced, not being possible an SOC based balancing control.

N. Kutkut et al. present the first designs of flyback based single switch converters starting in early 1995 [74], [75], [80]–[82] Fig 2.20 a). A special effort has to be done in the design of the mulwinding transformer where the parasitic deviation between windings could be controlled by the use of coaxial cables [83].

M. Uno et al. present that any input buck-boost (buck, boost or buck-boost) cell that generates a rectangular voltage waveform could be coupled to a voltage multiplier circuit to generate a series connected cell balancing system [84]–[88]. The voltage multiplier circuits are series connection of diode and/or inductors via a capacitor energy exchange in series, avoiding the use of high cost transformers and simplifying modularity Fig 2.20 b). They present single switch buck-boost type converters with a Sepic design [89], diode based voltage multipliers [90] or with resonant networks [91].

2.3.4 Modular balancing systems

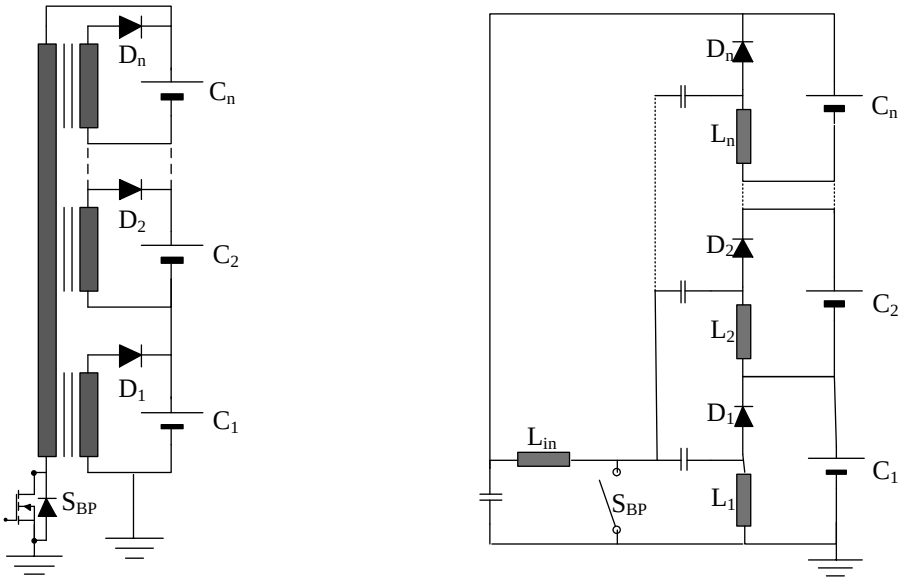

a) **b)**

Fig 2.20 Main single switch active balancing system a) Flyback based systems proposed by N. Kutkut. A multiwing flyback balancing system [80]. b) Buck-boost based balancing system proposed by M. Uno. Multistacked Sepic converter [89]

High number of series connected energy storage cells are connected in high power/energy applications, even several hundreds of cells as for big grid energy storage systems Table 2.5. Balancing of high number of series connected cells is a very complex and difficult issue, while balancing of series connected cells is critical to use all the energy inside the battery pack as presented in Subchapter 2.2.3. Modular balancing systems permit to divide the balancing problem in smaller subsystems simplifying the balancing problem of series connected energy storage devices [92]–[99].

Modular balancing systems balance the whole series connected battery pack balancing the cells inside a module with an intramodule balancing system and balancing between different modules using intermodule balancing systems [95]. A high number series connected cells battery pack could be constructed using intermodule balancing systems and commercially available battery modules (12 V, 24 V and 48 V most common voltages).

The division of the balancing of series connected cells in intramodule balancing systems and in intermodule balancing systems permit to use mixed balancing systems , using best suited balancing system for each situation [100].

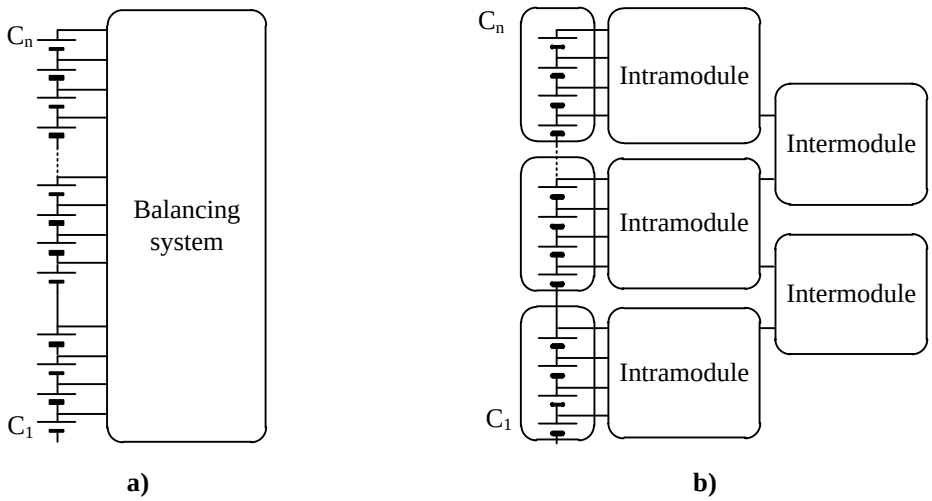

Fig 2.21 Balancing system architecture of high number series connected cells [99]a) Conventional architecture, presented in passive balancing systems b) modular architecture with intramodule and intermodule balancing systems.

2.4 Conclusions of the chapter

Lithium-ion cells are one of the most promising and important technologies regarding energy storage system and energy efficiency. Inside Lithium-ion family, LFP cells are one of the most promising technologies due to their safety characteristics and high power density. This two particular properties present LFP cells as the best option for power applications where human safety is critical as electric mobility. **LFP technology** will be the studied technology during the PhD work.

Li-ion power applications require series connection of cells to decrease conduction power losses, by the reduction of application current stress. High number of series connected battery packs are divided in smaller **modules** to reduce mechanical and electrical design effort. The reduction of design effort to modules permits to use the module for different applications, via parallelization or series connection. The battery pack could be also constructed from commercially available modules where 12 V, 24 V and 48 V are the most common voltage ranges.

Due to natural unsafe behaviour of Li-ion chemistry a Battery Management System **BMS is indispensable** to work with Li-ion technology inside a Safe Operation Area SOA. When high number of cells are connected in series the BMS design is complex. New **commercially available ICs** are a good choice to reduce battery management design difficulty.

Li-ion cells present performance variations due to manufacturing processes, environmental issues and human interaction that are presented in instantaneous and aging unbalancing effects. However there is a **lack of information about unbalancing effects in series connected cells**. Literature works only present performance deviations between single cells. When cells are connected in series unbalancing effects generate great energy and performance reduction of the battery pack. When the number of series connected cells is increased, a balancing system is necessary to maximize the energy, and an **active system is indispensable when a SOH deviation** occurs.

Balancing systems permit to maximize the energy of the battery pack. **Passive balancing system is the most used topology** in the literature and for industrial

applications. In order to compete with passive balancing the most critical parameter is the cost and complexity reduction of the active balancing system. These disadvantages are greatly conditioned by the high number of active switches and converters. **Modular balancing** systems permit to reduce the balancing problem complexity **into intramodule and intermodule** balancing systems. To reduce the cost **single switch balancing systems** could be a great candidate for intramodule balancing systems giving the cost reduction to finally design competitive active balancing systems to dispute with passive balancing systems.

Balancing system design and sizing is not well presented in literature. A **contribution should be done with a methodology for designing balancing systems**, designing the balancing system taken into account the differences between the weak and the strong cell.

The following thesis work will try to fill the weaknesses found in the state of the art.

Chapter 3

LFP SERIES CONNECTED UNBALANCING EFFECTS AND CAUSES

There is a complete lack of information about unbalancing effects and causes in Li-ion series connected battery packs. Even though there are plenty of studies related to single cell level behaviour, there is not information about performance decrease due to unbalancing in series connected Li-ion battery packs.

To understand series connected Li-ion battery packs, concretely LFP, a test methodology is designed to understand battery pack unbalancing effects and causes. The methodology will analyse different parameters referred to cycling behaviour and rest or calendar life behaviour.

Battery cycle tests are performed to evaluate unbalancing of series connected LFP cells under cycling conditions. Different parameters deviation is evaluated to biggest unbalancing impact parameters.

Rest or calendar life tests evaluate stand by unbalancing effect in series connected LFP cells. Variation in SOC between cells and various external circuitry connections are evaluated.

Finally main conclusions, emphasizing main unbalancing contributions are resumed. The methodology and results were presented in [PAPER C1].

3.1 LFP Unbalancing test methodology

A LFP battery pack is a multivariable system composed of series/parallel connection of single cells Fig 3.1. The battery pack unbalances are influenced by manufacturing process, environmental variables and external circuitry connected as the BMS.

However there is a big lack of information about experimental data and performance of series connected battery packs, and for our interest work, LFP series connected battery packs.

To detect the unbalancing effects presented in series connected LFP battery packs and evaluate the influence on total battery performance, a test methodology has been designed to estimate different parameter influence in series connected LFP battery packs. The unbalancing test methodology has been divided in two different test groups.

Cycle tests will evaluate unbalancing effects in series connected cells due to continuous cycling. The battery pack will be tested under different Current rates (C-rate); and temperature or SOC unbalances (ΔSOC, ΔT) will be intentionally generated to assess unbalancing effects during cycling.

Rest tests will evaluate unbalancing effects in series connected cells due to self-discharge mechanisms and external circuitry influence (ΔQ_{SD}).

The test methodology will be implemented in a 4S1P LFP battery pack of 6,5 Ah

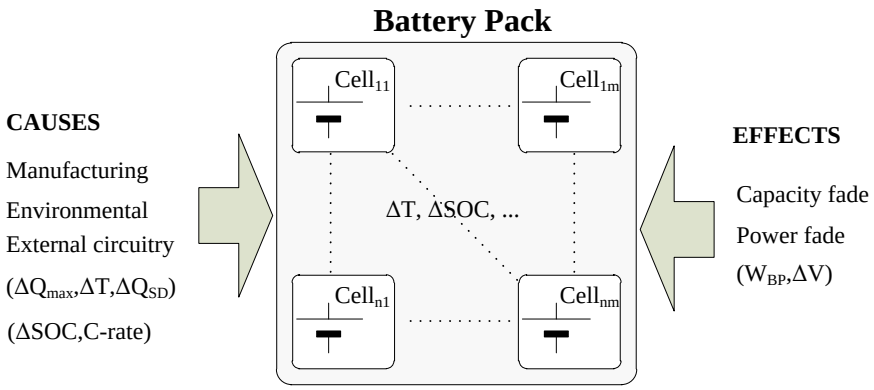

Fig 3.1 Battery pack multivariable system. Schematic representation of the influence of different battery pack parameters for unbalancing effects.

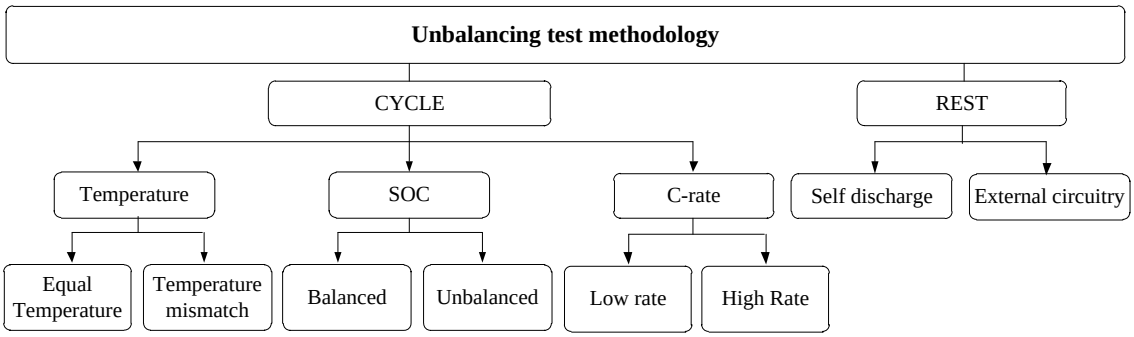

Fig 3.2 Unbalancing test methodology structure to evaluate unbalancing effect influence in series connected LFP battery packs.

nominal capacity Q_{Nom}. The test methodology is performed first, with an initialization process where the series connected cells are started to a concrete initial state, and after a test sequence. The equipment used for the test methodology is described below:

- Basytec XCTS battery tester: 4 channels of a Basytec battery tester are utilized to establish individual initial SOC conditions for 4 LFP single cells (ΔSOC).
- Chroma charge discharge system (C-rate)
    - Chroma 62024P-80-60: Power supply to charge the battery pack.
    - Chroma 63201: Electronic Load to discharge the 4S1P battery pack.
- Acquisition and control system: National Instruments based system:
    - Host: Ni program based to control Chroma power supply and electronic load via series communication.
    - Real Time: Crio 9022 real time controller in a 9114 chassis.
        - NI 9205: 16 DI/32 SE voltage measurement system (Voltage and current).
        - NI 9213: 16 Termocouple measurement system (Temperature measurement)
        - NI 9403: 32 DIO system (security relay control)
- Prebatem temperature chambers: 2 Prebatem 80L temperature chambers to unbalance cell in temperature (ΔT).
- Precision shunt resistors: 1% shunt resistors to measure different current rates with good accuracy for coulomb counting.

3.2 LFP series connected cycle tests.

Battery pack cycle tests will analyse if a series connected LFP battery pack is unbalanced during cycling. 4S1P battery pack has been designed with 6,5 Ah Q_{Nom} capacity. LFP cells under test present prismatic format and are connected in series with an air gap of 2 cm to discard temperature influence on centre situated battery pack cells.

The 4 LFP cells under test are characterized with the Basytec XCTS battery tester to obtain initial maximum capacity Q_{Max} of each cell and the initial unbalancing effect due to manufacturing dispersion effect in capacity deviation ΔQ_{Max} Table 3.1. 0,317 Ah dispersion, or 4,9% respect to Q_{Nom} is presented. All the cells present higher capacities than nominal capacity.

Before assembled in series the 4 cells are charged with CC of C/2 until 3,65V, and after a CV charge is done until the currents goes under C/20. (CCCV charging mode). The cells are charged at constant 25 ºC. After charging process, a ΔSOC is inserted if necessary to generate an unbalancing effect.

The cycle test is defined with the next specifications and presented in Fig 3.3.

- CC discharge until one cell reaches 2V.(DISCHARGE)
- 1 h rest period after discharge. (REST D)
- CC charge until one cell reaches 3,65 V. (CHARGE)
- 1h rest period after charge. (REST C)

The cycle test is repeated during 50 complete cycles to evaluate different battery parameters. The parameters under evaluation during cycle tests are:

- Coulombimetric behaviour: Capacity inserted to the battery pack during charge $Q_{BP,C}$ and obtained during discharge $Q_{BP,D}$. The capacity measurement is extensively used in literature for single cells.

Table 3.1 Initial maximum capacity and capacity dispersion of LFP cells under test. 1C discharge test after CCCV charge. Manufacturing deviation effect. Percentage respect to 6,5 Ah nominal capacity

$Q_{Max,1}$	$Q_{Max,2}$	$Q_{Max,3}$	$Q_{Max,4}$	ΔQ_{Max}	Mean Q
7,273	7,51	7,59	7,314	0,317	7,42
112%	115%	117%	112%	4,9%	114%

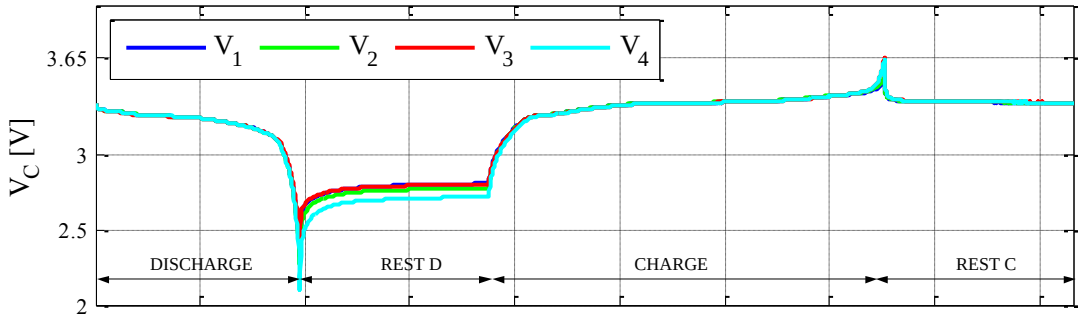

Fig 3.3 LFP series connected unbalancing cycle test. Full cycle description.

- Energetic behaviour: Energy inserted to the battery pack during charge $W_{BP,C}$ and obtained during discharge $W_{BP,D}$. Even if energetic behaviour is not utilized in literature is presented more important than coulombimetric because gives the real energetic parameter of the battery pack taking into account the LFP technology voltage profile.
- Unbalancing effect in voltage: Maximum voltage dispersion during charge $\Delta V_{Max,C}$ and discharge $\Delta V_{Max,D}$ are measured between 4S1P cells. The maximum voltage dispersions appear during charge and discharge final process. Voltage dispersion will be evaluated to discard hypothesis described in [101] which says that voltage difference is increased due to consecutive overcharges in one single cell.

The parameters dispersions for the cycle unbalancing tests are presented in Table 3.2. An evaluation of a temperature mismatch ΔT of 5ºC will be evaluated for temperature influence, a ΔSOC dispersion of 3% will give an idea of a battery pack performance under unbalancing effects and different C-rate current tests will evaluate battery pack performance for different power applications.

Table 3.2 Parameter deviation for unbalancing cycle tests. Temperature, SOC and current rate differences for unbalancing tests.

ΔT		**ΔSOC**		**C-rate**	
Balanced	Unbalanced	Balanced	Unbalanced	Low rate	High rate
0ºC	5ºC	0	3%	C/2 Charge 1C Discharge	3,5C Charge 7C Discharge

3.2.1 Balanced series connected cells

The 4S1P battery pack is tested under balanced situation and low current rate regimen. The mean discharge capacity of the battery pack $Q_{BP,D,AV}$ is 6,92 Ah giving nearly 100% coulombimetric efficiency between charge and discharge. The mean discharge energy $W_{BP,D,AV}$ is 88,5044 Wh with nearly 4 Wh constant losses between charge and discharge process during the whole 50 cycles. The maximum voltage deviation ΔV_{Max} is given in discharge with a maximum dispersion of $AV_{Max,D}$ between 0,3 V and 0,4 V. The voltage dispersion does not increase during cycling as expected and presented in literature [101].

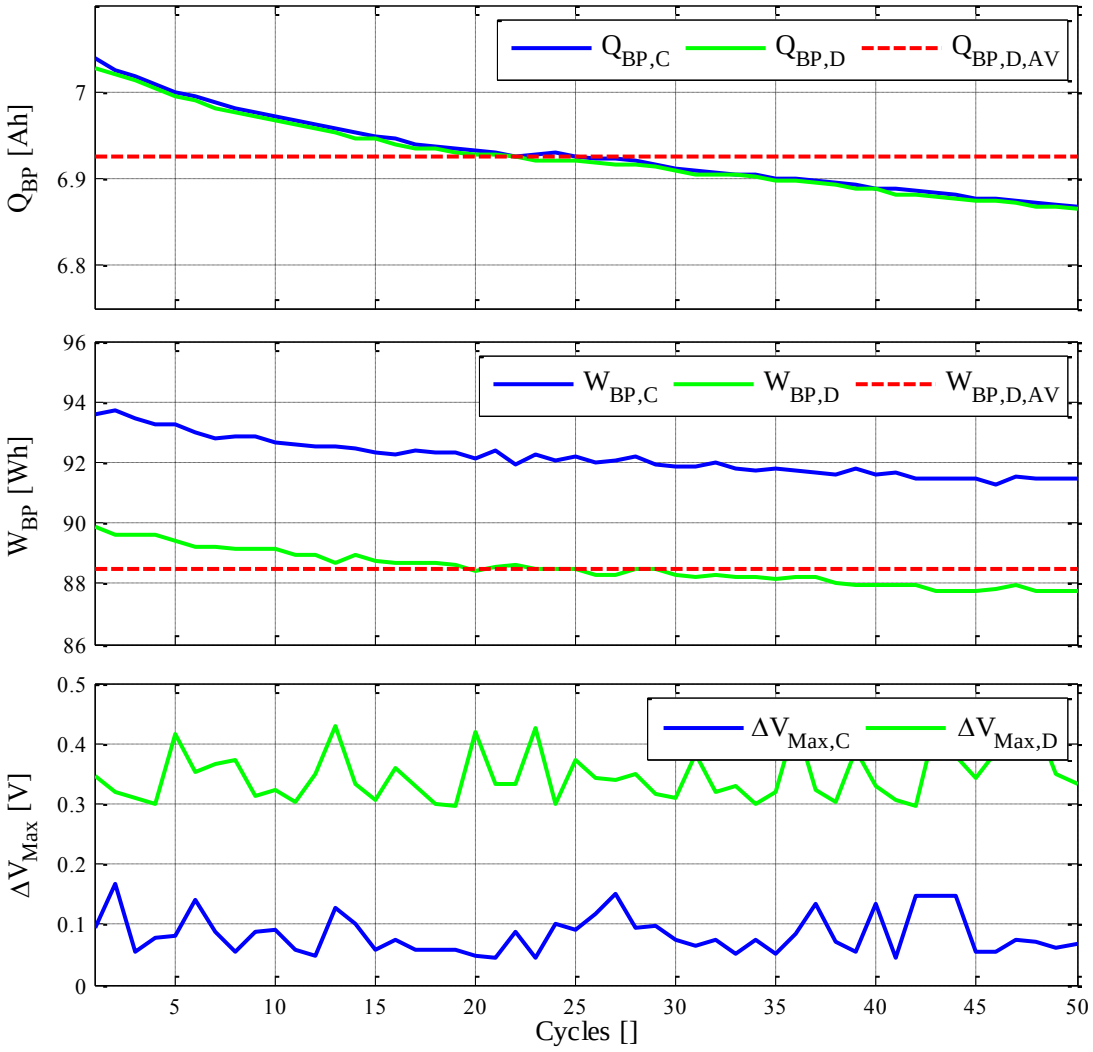

Fig 3.4 Balanced cells under low current rate tests. Top: Battery pack capacity Q_{BP}. Middle: Battery pack energy W_{BP}. Bottom: Voltage unbalance between series connected cells ΔV_{Max}.

3.2.2 Temperature unbalance effect ΔT

3 cells are inserted in a temperature chamber to 30ºC and a single cell is held to 25ºC in the second temperature chamber. The cells are SOC balanced and cycled in low rate condition. The mean discharge capacity $Q_{BP,D,AV}$ and the mean discharge energy $W_{BP,D,AV}$ are 6,66 Ah and 85,18 Wh respectively, decreasing the total energy obtained respect to balanced condition. The maximum voltage dispersion $\Delta V_{Max,D}$ decreases compared to balanced situation ($\Delta V_{Max,D}$ from 0,3-0,4 to 0,1-0,2), even the critical parameter of voltage dispersion during 50 cycles is kept constant, presenting that no voltage deviation is presented due to cycling, even if a temperature unbalanced is presented in the battery pack.

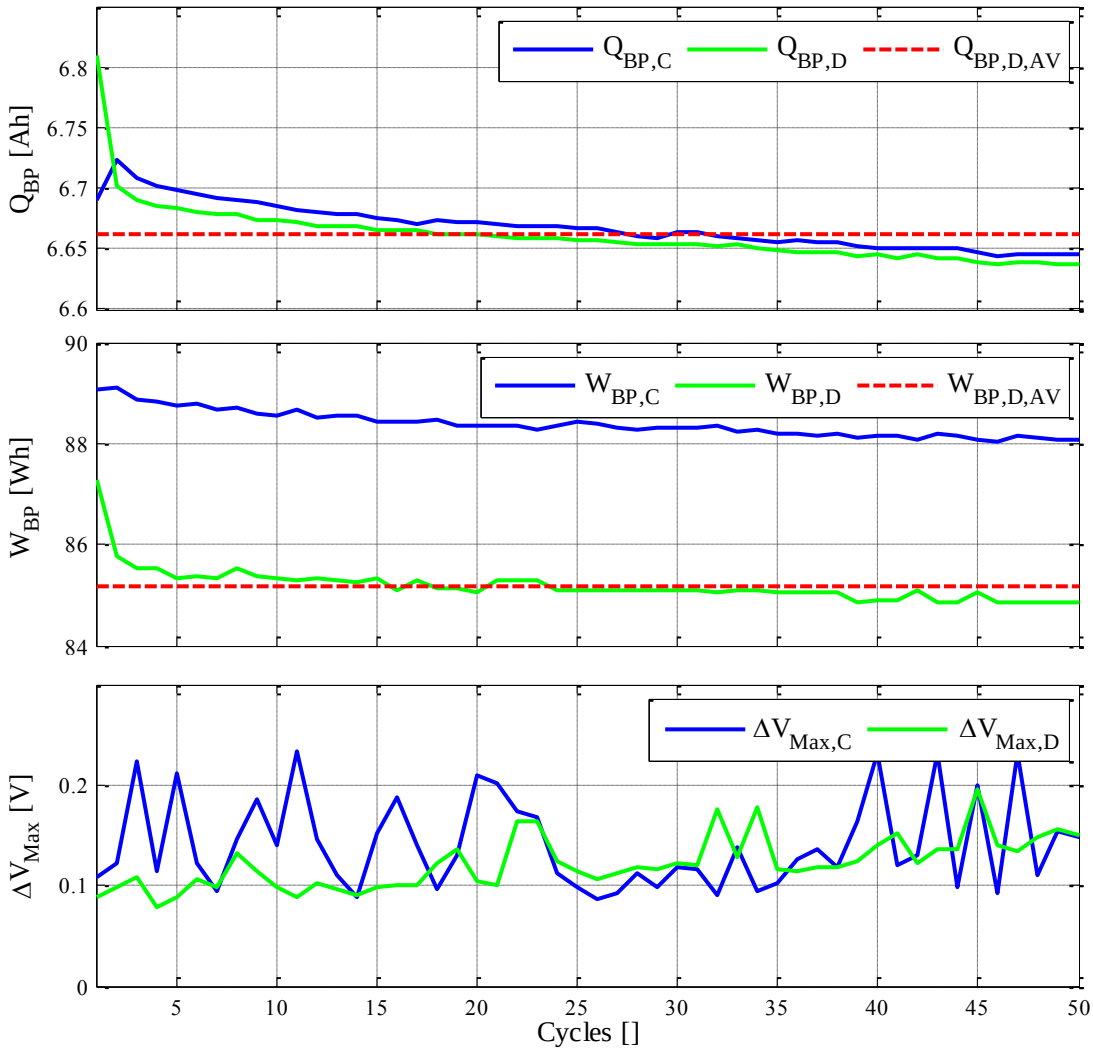

Fig 3.5 5 ºC temperature unbalance (3 cells 30ºC one cell 25ºC) results for a Low current rate test. Top: Battery pack capacity Q_{BP}. Middle: Battery pack energy W_{BP}. Bottom: Voltage unbalance between series connected cells ΔV_{Max}.

3.2.3 SOC unbalance effect ΔSOC

A SOC unbalance of 3% is inserted to 1 cell of the 4S1P battery pack. The mean discharge capacity $Q_{BP,D,AV}$ is 6,64 Ah and the mean discharge energy is $W_{BP,D,AV}$ 81,20 Wh. The energetic efficiency is kept with ≈4 Wh losses between charge and discharge as temperature unbalance and balanced situation. The energetic efficiency is only dependant on the current rates during charge and discharge. The voltage difference $\Delta V_{Max,D}$ is highly increased respect to both previous cases to 0,6 V during discharge. However the voltage dispersion during the continuous 50 cycles is kept nearly constant, non-increasing the voltage dispersion.

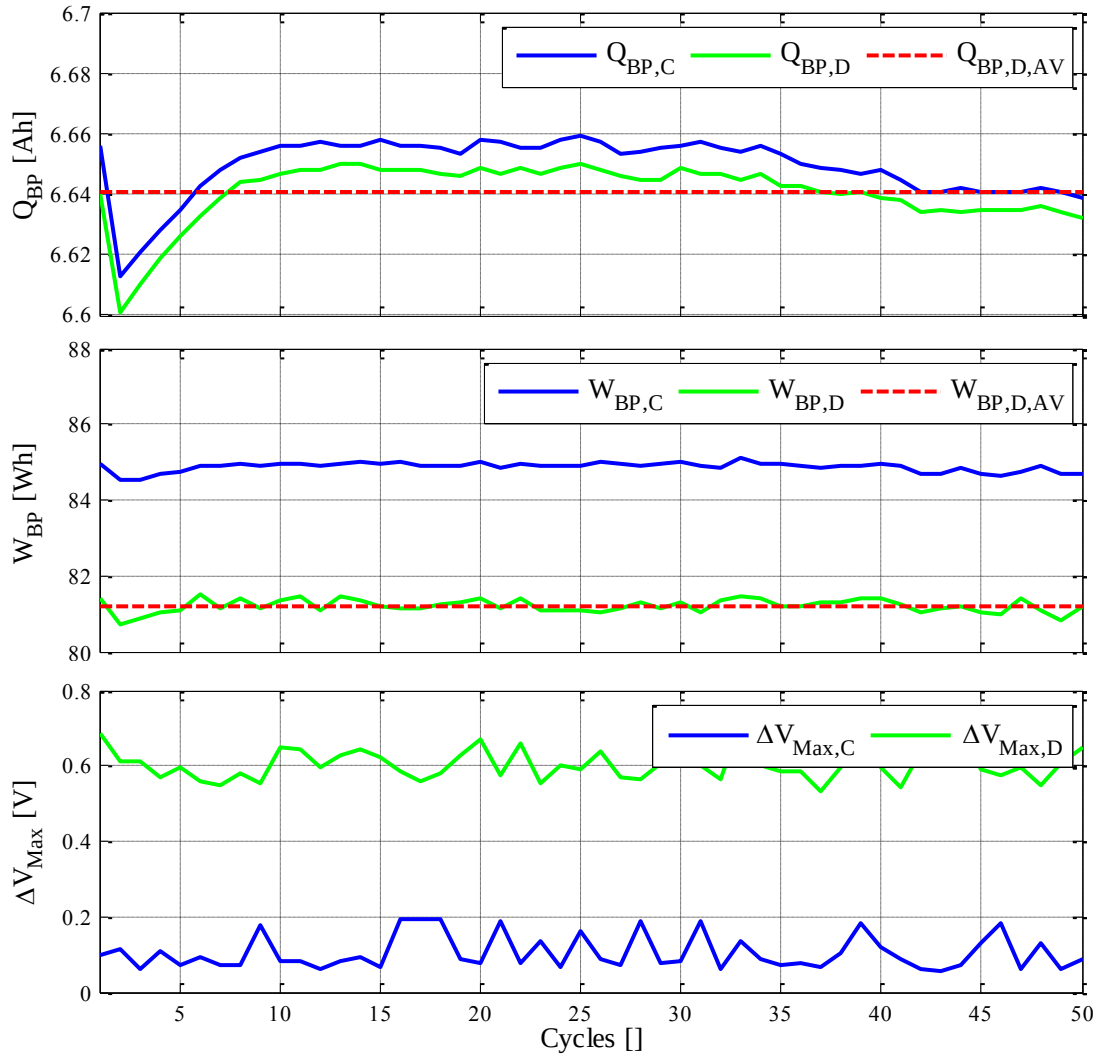

Fig 3.6 3% SOC unbalance (3 cells 30ºC one cell 25ºC) results for a Low current rate test. Top: Battery pack capacity Q_{BP}. Middle: Battery pack energy W_{BP}. Bottom: Voltage unbalance between series connected cells ΔV_{Max}.

3.2.4 High current rate effect

The 4S1P battery pack is tested under high charge and discharge current rates as specified in Table 3.2. The mean capacity and energy during discharge are highly decreased due to high current rates (7 times higher than low current rate cycle). $Q_{BP,D,AV}$ is 4,71 Ah and the $W_{BP,D,AV}$ is 53,65, with an energetic efficiency decrease of ≈8 Wh from charge process to discharge process. The voltage deviation is low ($\Delta V_{Max,D}$ ≈0,1 V)because the low SOC region is not reached due to high current rate. The temperature of the cells reach 38 ºC during discharge process, however it can be seen in Fig 3.7 that the voltage dispersion is not increased during the 50 cycles period.

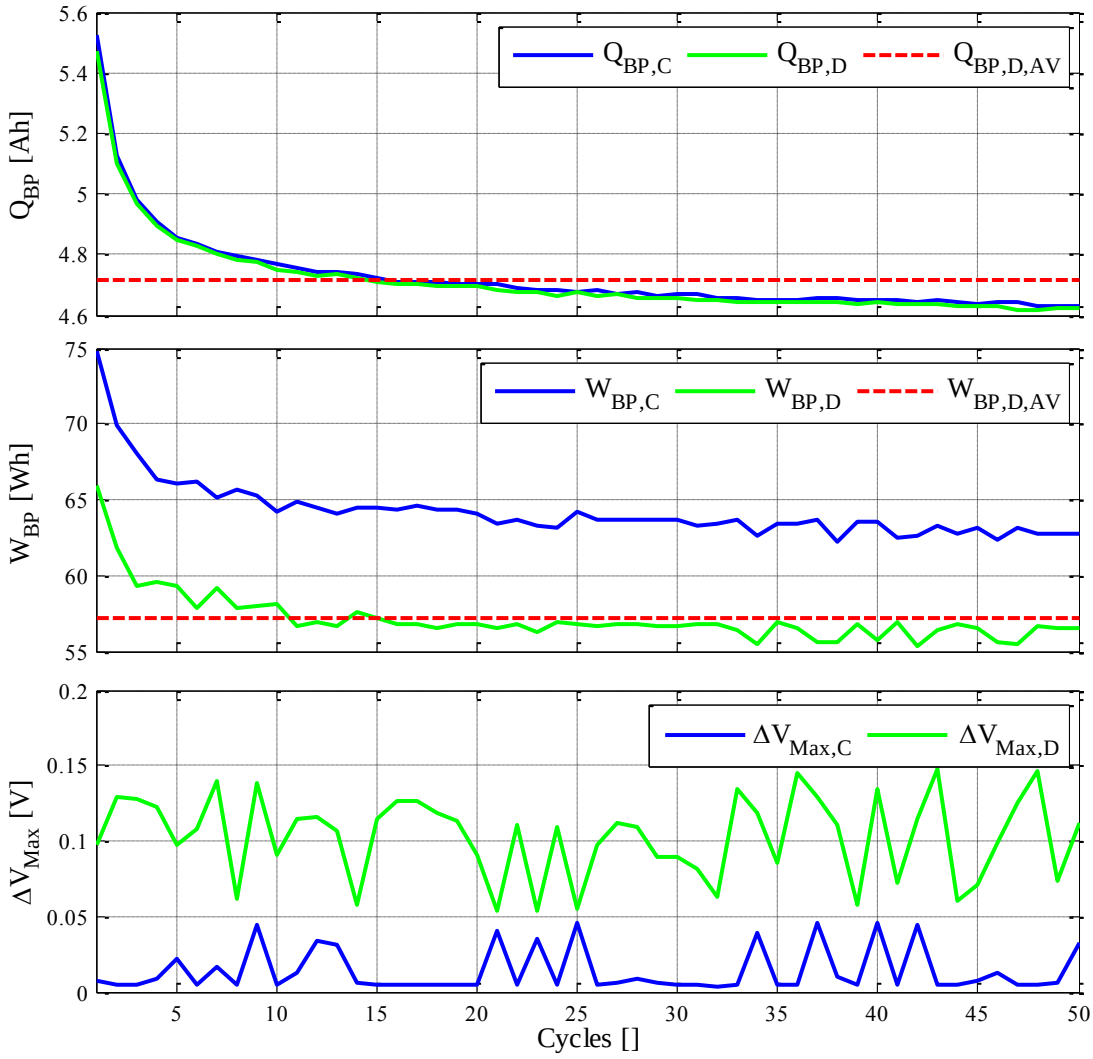

Fig 3.7 Balanced cells under high current rate tests (7xLow rate). Top: Battery pack capacity Q_{BP}. Middle: Battery pack energy W_{BP}. Bottom: Voltage unbalance between series connected cells ΔV_{Max}.

3.2.5 High cycle number test influence

To ensure the independence of voltage dispersion due to cycling the high rate cycle presented in 3.2.4 has been repeated during 150 cycles. High rate cycling is chosen because high rate cycles will increase the temperature of the cells and could lead to a higher unbalancing influence. However, Fig 3.8 presents that no voltage unbalance ΔV_{Max} dispersion effect is presented due to cycling. It is again illustrated that energy and capacity is decreased due to high rate cycling ($Q_{BP,D,AV}$ = 4,44Ah and the $W_{BP,D,AV}$ = 53,65 Wh) and that energetic losses are ≈8 Wh per charge /discharge cycle.

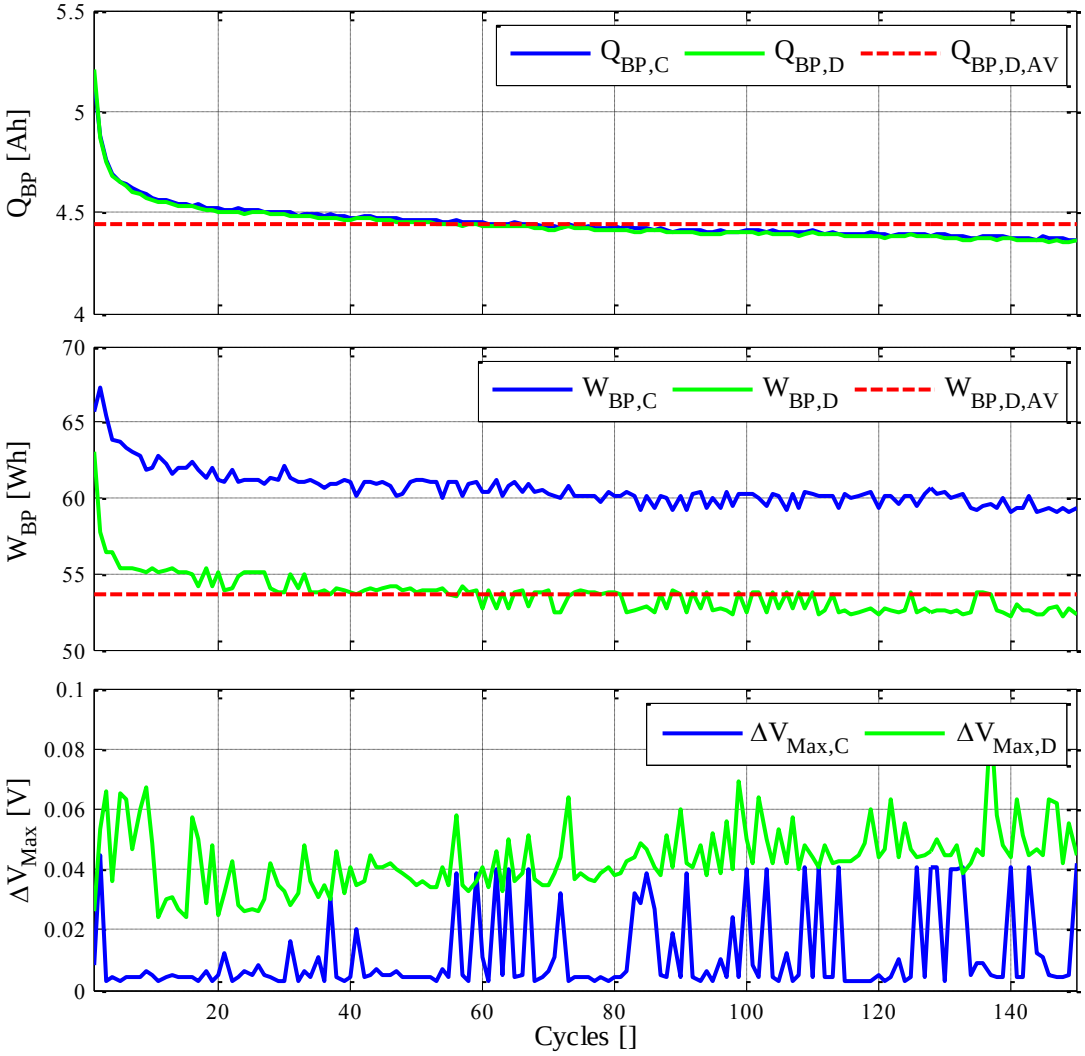

Fig 3.8 Balanced cells under high current rate tests (7xLow rate) for analysis of voltage dispersion for high cycle numbers (150 cycles). Top: Battery pack capacity Q_{BP}. Middle: Battery pack energy W_{BP}. Bottom: Voltage unbalance between series connected cells ΔV_{Max}.

3.3 LFP series connected rest tests

LFP series connected rest tests will evaluate the unbalancing effects produced due to rest periods of battery packs. During rest tests the unbalancing effect due to self-discharge of LFP cells and the influence of external circuitry connected to series connected cells will be evaluated independently. During the rest tests the cells are initially charged to an initial predefined capacity Q, and after that cells are kept in standby situation. After the rest period the cells are fully discharged to evaluate the lost capacity Q_{LOSS} during the rest period. The cells under test will be the same cells as for the cycle tests, LFP cells of Q_{Nom}= 6,5 Ah.

Self-discharge behaviour tests will present the deviation in self-discharge due to different SOC between single cells. The self-discharge behaviour of single cells will give the predicted behaviour of cells and the unbalancing effect under series connection.

Different external circuitries will be connected to evaluate the difference between the natural self-discharge of cells and the influence on capacity loss and unbalancing due to external circuitry connection.

3.3.1 Self-discharge behaviour tests

During self-discharge tests 4 cells are tested individually (not series connected) to evaluate single cell self-discharge. The 4 cells are stored inside a temperature chamber with two different capacities, 2 cells stored to 50% SOC and another 2 cells to 70% SOC. The SOC will be calculated respect to the nominal capacity Q_{NOM} instead of the maximum capacity Q_{Max}.

Table 3.3 Self-discharge capacity loss $Q_{SD}=Q_{LOSS}$ for single cells. SOC 50% and SOC 70%.

Cells	Initial capacity Q [Ah]	Lost capacity per month $Q_{LOSS}=Q_{SD}$ [Ah]	Percentage Q_{LOSS} per month [%]*
1-50%	3,25	0,05	0,76
2-50%	3,25	0,05	0,76
3-70%	4,55	0,1	1,5
4-70%	4,55	0,1	1,5

*Percentage respect to nominal capacity Q_{Nom}=6,5 Ah

Higher SOC cells (3-4 70 % SOC) suffer higher losses or self-discharge $Q_{LOSS}=Q_{SD}$ than lower SOC cells 50% SOC. These tests corroborate literature previously presented results [47]–[49]. There is not dispersion between tested LFP cells for same SOC values. A capacity self-discharge of 0,76% per month for 50% SOC and 1,5% per month for 70% SOC is measured during self-discharge tests. The variation in self-discharge capacity ΔQ_{SD} doubles from 70% to 50%.

The results obtained for single cells permit to suggest that SOC unbalance will lead to a natural balancing effect in series connected cells. High SOC cells will suffer more self-discharge, balancing their capacity to lower SOC cells generating an auto balancing effect in series connected battery packs

3.3.2 External circuitry influence tests

LFP battery packs and all Li-ion technology battery packs need external circuitry first and most important to guarantee safety issues (voltage, temperature, etc. measurement) and second to improve battery life and performance (balancing system, thermal management system, etc). External circuitry adds extra capacity loss Q_{LOSS}, generating bigger capacity losses than single cell self-discharge Q_{SD} ($Q_{LOSS}>Q_{SD}$).

In order to measure the influence of different measurement systems, a 4S1P battery pack with 4 LFP Q_{Nom}=6,5 Ah charged to 50% SOC is built. Each single cell is individually charged to 50% SOC. The capacity loss Q_{LOSS} will be compared with the self-discharge loss of 50% SOC cells presented in previous subchapter.

During the analysis process 4 different systems have been connected to the 4S1P battery pack as presented in Fig 3.9.

- Fig 3.9 a) presents a measurement system based on differential operational amplifiers. The operational amplifiers should have bigger CMRR while number of series connected cells increases. The operational amplifier used during the tests is the INA 210 with an input impedance of 1 MΩ.
- The second configuration in Fig 3.9 b) adds a passive balancing system to the operational amplifier based measurement system. The passive balancing

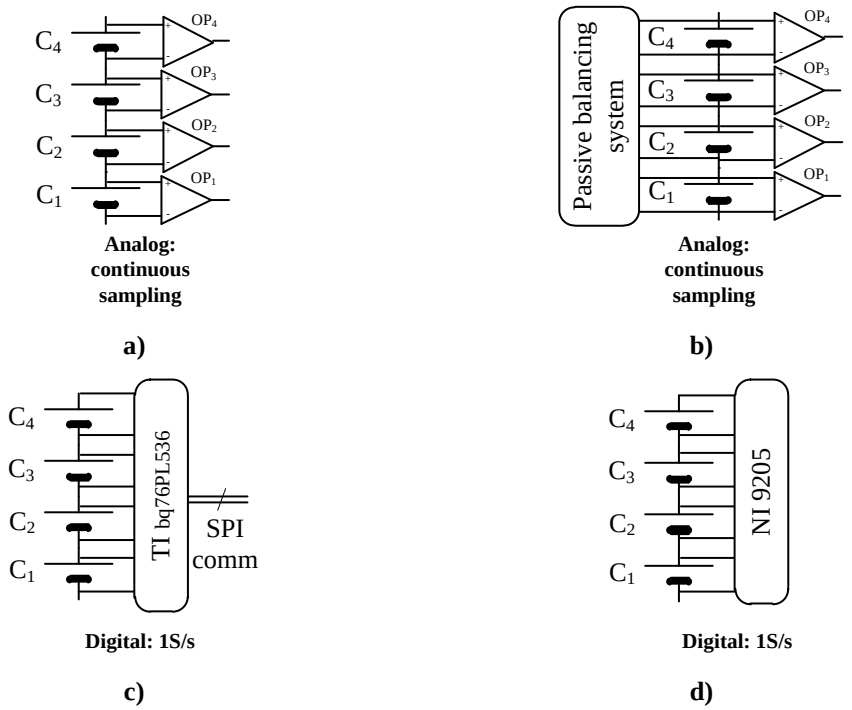

Fig 3.9. External circuitry configurations for unbalancing effect detection. A) INA 210 analog measurement system b) INA 210 analog measurement system with passive balancing system c) TI bq76PL536 BMS specific IC d) NI 9205 voltage measurement module.

system is controlled by an optocoupler that switches a BJT transistor in series with a 120 Ω balancing resistor.

- Configuration presented in Fig 3.9 c) utilizes a commercial IC as BMS. The IC is a Texas Instruments bq76PL536 Li-ion battery monitor and secondary protection IC. The IC is kept in standby and woken up every 1 second to establish a measurement speed of 1 sample per second (1S/s). The IC is communicated by SPI protocol with a main control or display system. The input impedance is 2 MΩ.
- The final configuration presented in Fig 3.9 d) measures the 4S1P cell voltages with a National Instruments NI 9205 voltage measurement module connected to a Real time cRio controller. The measurement speed is set to 1S/s as it is enough for battery applications and as comparison to the Texas Instruments IC. The input impedance of the cRio is 10 GΩ from Analog input to ground and a maximum input bias current of 100 pA.

During the tests 4S1P battery pack cell voltages are measured during a period of 1 month. After the rest period the battery pack is disassembled and the remaining capacity

Table 3.4 Self-discharge capacity loss $Q_{SD}=Q_{LOSS}$ for single cells. SOC 50% and SOC 70%.

Configuration Fig 3.9	**Maximum capacity loss [Ah] ($Q_{LOSS}/C_{n)}$**	**Minimum capacity loss [Ah] (Q_{LOSS}/C_n)**	**Percentage maximum Q_{LOSS} per month [%]***
a)	$0,36/C_1$	$0,12/C_4$	5,54
b)	$0,37/C_1$	$0,12/C_4$	5,57
c)	$0,22/C_4$	$0,16/C_1$	3,38
d)	0,1	0,1	1,5

*Percentage respect to nominal capacity Q_{Nom}=6,5 Ah

of each cell is measured with the Basytec battery tester to determine which cell of the battery pack suffers bigger capacity loss Q_{LOSS} Table 3.4.

Analog measuring systems based on differential operational amplifiers asses a capacity loss of 0,36 Ah maximum, generating a 5,54 % capacity loss per month in a cell. The highest capacity loss is presented in the lowest situated cell (C_1), with 3 times more capacity loss respect to highest situated cell (C_4) ΔQ_{LOSS}. The passive balancing leakage current does not increase significantly the capacity loss, so the influence is negligible.

Digital measurement systems reduce the capacity loss sustainably compared to analog systems. Bq76PL536 based measurement system generates a capacity loss of 0,22 Ah (3,38 % per month) in cell C_4 (highest situated) and 0,16 Ah in C_1. National Instruments NI 9205 voltage measurement module generates the smaller capacity loss 1,5 % per month and it does not introduce any capacity loss deviation between series connected cells.

3.4 LFP battery packs test results summary

LFP series connected cycle test results are presented in Table 3.5. Cycle tests evaluate energetic issues due to cycling and the most critical parameters to obtain the maximum energy of the battery pack. Unbalancing degradation, by the analysis of voltage dispersion during cycling has been evaluated to analyze if the battery pack is voltage unbalanced due to cycling.

Regarding energetic issues during discharge ($Q_{BP,D,AV}$ and $W_{BP,D,AV}$) the most important parameter is the current rate (C-rate) of the charge/discharge process, reducing the total battery energy more than a 30% respect to a Low rate application(88,5 Wh Low rate 57,15 High rate). A 3% SOC unbalance is much more harmful than a 5ºC mismatch for the battery pack energy.

Maximum voltage variation is given during the final discharge process $\Delta V_{Max,D}$. High current rate applications do not suffer from big voltage differences because they do not reach Low SOC regions where the OCV curve is sharper. SOC mismatch generates the bigger voltage dispersion reaching a maximum voltage difference of 0,722 V during a discharge. However the standard deviation for all the tests is less than 45 mV which denotes that there is not voltage variance or dispersion due to cycling. A 150 cycle test with high current stress has been carries with identical results.

LFP series connected rest tests are focused to evaluate battery capacity loss due to self-discharge Q_{SD} and capacity loss due to external circuitry Q_{LOSS}. The unbalancing

Table 3.5 LFP series connected cycle test results for each test presented in chapter 3.2. $Q_{BP,D,AV}$ and $W_{BP,D,AV}$ values. Maximum discharge voltage difference $\Delta V_{Max,D}$ statistics for the whole test. Maximum diference during cycles (Max). Minimum difference during cycles (Min). Average value during cycles (AV). Standard deviation during cycles (σ).

Tests	**$Q_{BP,D,AV}$ [Ah]**	**$W_{BP,D,AV}$ [Wh]**	**$\Delta V_{Max,D}$ [V]**			
			Max	Min	AV	σ
3.2.1	6,92	88,5	0,435	0,296	0,346	0,042
3.2.2	6,66	85,19	0,195	0,079	0,122	0,025
3.2.3	6,64	81,2	0,722	0,53	0,605	0,044
3.2.4	4,71	57,15	0,148	0,053	0,103	0,027
3.2.5	4,44	53,65	0,09	0,024	0,043	0,0105

Table 3.6 LFP series connected rest test. Self-discharge SD and External circuitry EC effect related to total capacity loss Q_{LOSS} and capacity loss variation ΔQ_{LOSS}

Test	Maximum capacity loss [Ah] ($Q_{LOSS}/C_{n)}$	Minimum capacity loss [Ah] (Q_{LOSS}/C_n)	Percentage maximum Q_{LOSS} per month [%]*	ΔQ_{LOSS} per month [%]*
SD 50%	0,05	0,05	0,76	0
SD 70%	0,1	0,1	1,5	0
EC a)	$0,36/C_1$	$0,12/C_4$	5,54	3,69
EC b)	$0,37/C_1$	$0,12/C_4$	5,57	3,84
EC c)	$0,22/C_4$	$0,16/C_1$	3,38	0,92
EC d)	0,1	0,1	1,5	0

*Percentage respect to nominal capacity Q_{Nom}=6,5 Ah

effect performed in the battery pack due to capacity loss variation ΔQ_{LOSS} is studied which could be a determinant parameter in the unbalancing process of a battery pack (generating voltage variations AV for example). Rest test results are resumed in Table 3.6.

Self-discharge tests evaluate capacity loss of cells due to storage without any external circuitry. The self-discharge loss Q_{SD} is equal to the total capacity loss Q_{LOSS} (Q_{SD}=Q_{LOSS}). 70% cells suffer 2 times more Q_{SD} than 50% cells (1,5 % per month respect to 0,76 % per month). No capacity loss variation ΔQ_{LOSS} is appreciated between different cells ΔQ_{SD}= ΔQ_{LOSS}=0.

External circuitry generates capacity loss increase and capacity loss dispersion between series connected cells. Analog differential operational amplifiers generate the biggest loss (5,54 % per month) and the biggest dispersion ΔQ_{LOSS}= 3,69%. The insertion of a passive balancing system does not influence in the capacity loss. Digital measurement systems generate lower capacity losses. The capacity dispersion is also lower and the NI 9205 measurement system even has not capacity loss variation (ΔQ_{LOSS}= 0).

3.5 Conclusions of the chapter

Due to low information regarding unbalancing effects and causes in series connected LFP cells, a test methodology has been defined to identify unbalancing effects and the influence on LFP battery packs behaviour. To detect unbalancing effects cycling and rest tests have been

The behaviour of the battery pack is evaluated for **energy decrease and the unbalancing generation**. The energy deterioration is evaluated for different parameters with the energy and capacity during discharge ($Q_{BP,D,AV}$ and $W_{BP,D,AV}$) and the capacity losses due to rest periods (Q_{LOSS}). The unbalancing generation is evaluated with the voltage dispersion during cycling ($\Delta V_{Max,D}$) and the capacity loss variation ΔQ_{LOSS} during rest periods.

Battery pack energy decrease during cycling is primarily influenced by high C-rate currents. The energy reduction has to be taken into account for battery pack sizing. An SOC variation of 3% is also more harmful than a 5ºC variation between series connected cells. Good SOC match maximizes the energy of the battery pack. High SOC cells suffer higher Q_{LOSS} than low SOC cells. 70% SOC cells double self-discharge respect to 50% SOC cells (1,5%-0,76% per month respectively). Analog voltage measurement system generate high Q_{LOSS} (Q_{LOSS}>5%), so digital measurement systems should be used with low measurement periods (1S/s or greater) and low consumption

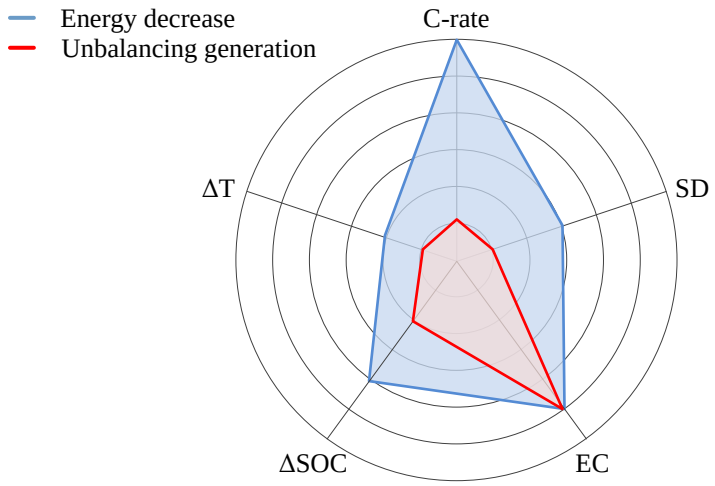

Fig 3.10. Spider chart showing energy decrease influence and unbalancing generation in series connected LFP cells. Current rate (C-rate), temperature mismatch (ΔT), SOC unbalance (ΔSOC), self-discharge (SD) and external circuitry (EC) qualitative influence.

standby and idle modes. Commercial high impedance measurement systems are a good option for laboratory measurements (as National Instruments equipment) and commercial specific BMS ICs are the best candidate for industrial applications for high number series connected battery packs.

No unbalancing is generated due to cycling even if SOC, temperature and current variations are inserted. **LFP cells due not have voltage unbalance due to cycling**. The maximum voltage variation is generated due to SOC unbalance but is kept constant while cycling. During rest periods self-discharge of different cells do not induce variation in capacity loss, however when an external measurement circuit is connected a capacity loss variation is generated, which could induce a voltage variation after time. Analog systems generate a capacity variation bigger than digital systems so should be avoided for LFP series connected cells. Digital sampling systems with speeds lower than 1 second, low standby current consumption and input impedances higher than 2 MΩ (like the bq76PL536 and the NI 9205) are well suited for LFP cells.

Chapter 4

SERIES CONNECTED ENERGY STORAGE MODULAR BALANCING SYSTEMS

Series connected energy storage balancing systems increase complexity with high number of series connected cells. To reduce balancing system complexity modular balancing systems decrease balancing effort dividing the battery pack in different modules.

During the thesis work modular balancing systems are divided in intramodule systems and intermodule systems. Intramodule balancing systems balance the cells inside the module and intermodule balancing systems balance the different modules inside the battery pack. The thesis work is specially focused in low complexity, low component number systems. All the designed balancing systems are prepared to work in open loop mode without the need of a control feedback loop.

During balancing system analysis and design main equations related to balancing current between weak and strong cell/modules are presented, as it is the main parameter to take into account in a balancing system design.

Main conclusions of modular balancing systems are presented. The intramodule balancing system analysis is presented in [PAPER J2].

4.1 Modularity in series connected cells

The complexity of high number series connected cells is decreased by dividing the Battery Pack (BP) in m modules (M) of n cells (C). Each module has an intramodule and an intermodule balancing system as presented in Fig 4.1.

The cells inside a module are balanced by an intramodule balancing system. The balancing system inserts a current $I_{Cb,i}$ to each cell. The modules are balanced by an intermodule balancing system which can be connected in series or parallel. The balancing current inserted to each module is defined by $I_{Mb,j}$.

The total current of a cell $I_{C,i}$ or a module $I_{M,j}$ inside a battery pack is defined by superposition with equations (4.1) and (4.2) respectively.

$$I_{C,i} = I_{BP} + I_{Mb,j} + I_{Cb,i} \quad i=[1,n]\ j=[1,m] \tag{4.1}$$

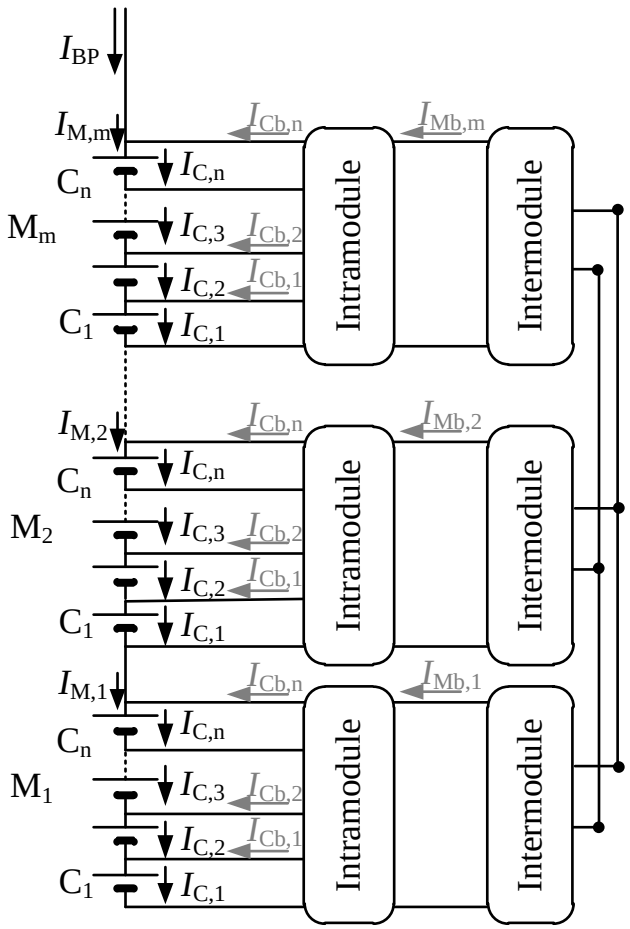

Fig 4.1 Modular representation of a series connected cell battery pack, with modular intramodule balancing systems and intermodule parallel connected balancing systems.

$$I_{M,j} = I_{BP} + I_{Mb,j} \quad j=[1,m] \tag{4.2}$$

To compensate an unbalancing between two cells or modules energy is transferred from the strong (S) cell(s)/module(s) to the weak (W) cell/module.Inside a battery pack one module or cell is considered weak and all the other modules or cells are considered strong. For a balancing system design 3 main parameters are important.

- The balancing current to the weak cell/module ($I_{Cb,W}$ or $I_{Mb,W}$)(positive current).
- The balancing current from the strong cell(s)/module(s) ($I_{Cb,S}$ or $I_{Mb,S}$) (negative current).
- The relation between the balancing current between strong and weak cell(s)/module(s) ($I_{Cb,W}/I_{Cb,S}$ or $I_{Mb,W}/I_{Mb,S}$).

4.2 Ideal/Lossless intramodule model

During this subchapter ideal intramodule balancing system modelling will be presented related to the main balancing current equations and balancing behaviour. Single switch balancing systems present interesting characteristics to be candidates for intramodule balancing systems.

- Low number of components.
- Single active switch.
- Open loop balancing possibility.

The relative low number of components is specially interesting due to the use of single active switch for balancing all the cells inside a module. The balancing procedure could be done with an open loop strategy (switching the single switch with constant duty cycle D=cte). In order to guarantee the open loop control strategy the single switch balancing system should work in Discontinuous Conduction DCM Mode during the full working range (4.3). If the DCM is not guaranteed the balancing system will be destroyed due to continuous increase of the current through the circuit inductors Fig 4.2.

$$\left.\begin{array}{l} T_{ON}+T_1+T_2 = T_S \\ D+D_1+D_2=1 \\ D_2 \geq 0 \end{array}\right\} \text{DCM} \tag{4.3}$$

To guarantee the DCM a discontinuous period time D_2 should be presented. The critical duty cycle D_C is determined by the limit where D_2=0. By keeping D below D_C DCM is guaranteed.

$$\begin{array}{l} D_C = 1 - D_1 \rightarrow D_2 = 0 \\ D \leq D_C \rightarrow \text{DCM guaranteed} \end{array} \tag{4.4}$$

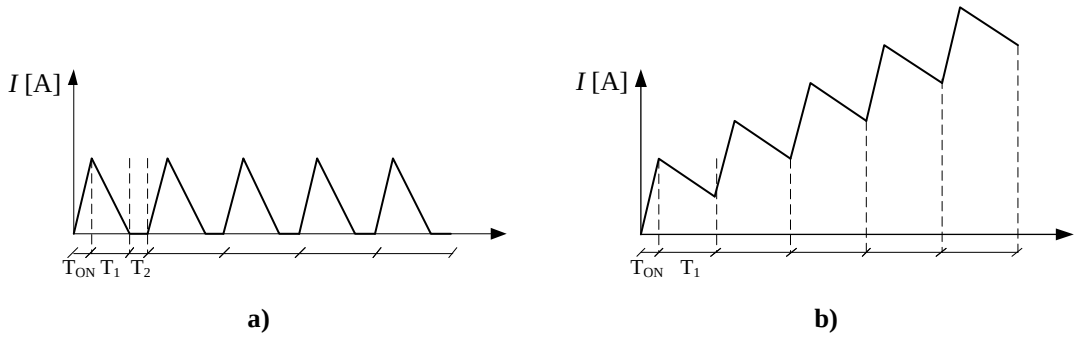

a) **b)**

Fig 4.2 Inductor current representation for explanation of the DCM guarantee requirement under open loop constant duty cycle operation. A) Inductor current controlled under DCM. B) Inductor overcurrent and consequent destroy.

Single switch balancing systems voltage balance the series connected cells naturally. The energy is provided from the most charged cells (strong cells) to the less voltage cell (weak cells). Therefore single switch balancing systems are not suitable for SOC balance strategies. However during the analysis of Chapter 3 it was presented that the SOC unbalance test present the biggest voltage unbalance, so it is generally correlated that a SOC unbalance implies a voltage unbalance. The module voltage V_M in a series connected system is the sum of all the single cells $V_{C,i}$ or equally the sum of the weak cell voltage $V_{C,W}$ and the strong cell voltages $V_{C,S}$.

$$V_M = \sum_{i=1}^{n} V_{C,i} = V_{C,W} + \sum_{\substack{S=1 \\ S \neq W}}^{n} V_{C,S} \tag{4.5}$$

When all the voltages of series connected cells are equal (balanced situation) no balancing current $I_{Cb,n}$ distributed through the cells. However when a voltage deviation is presented (unbalanced situation), the weakest cell receives current from the strong cells.

$$\begin{aligned} &V_{C,1} = V_{C,2} = ... = V_{C,n} \qquad I_{Cb,i} = 0 \quad \text{(balanced)} \quad i = [1,n] \\ &V_{C,W} < V_{C,S} \qquad\qquad\quad I_{Cb,W} > 0 \quad I_{Cb,S} < 0 \quad \text{(unbalanced)} \end{aligned} \tag{4.6}$$

The study of different balancing systems will be held under unbalanced situation. The single switch topologies under study are 3 flyback based systems and 3 buck-boost balancing designs.

- Single core Flyback 4.2.1.
- Multiple core parallel connected Flyback 4.2.2.

Table 4.1 Main characteristics of single switch active balancing topologies for intramodule balancing design. DCM control, number of switches (S) diodes (D) capacitors (Cap) inductors (L), transformers (T), balancing speed and modularity comparison.

Topology	Control [2]	S	D	Cap	L	T	Speed	Modularity
4.2.1	O.L	1	n	_	_	1[1]	High	No
4.2.2	O.L	1	n	_	_	n	High	High
4.2.3	O.L	1	n	_	_	n	Low	Total (except switch)
4.2.4	O.L	1	n	n	n+1	_	High	High
4.2.5	O.L	1	n	n	n+1	_	High	High
4.2.6	O.L	1	n	n+1	n+1	1	High	High

[1] Multiwinding single core transformer.

[2] O.L: Open loop control guaranteeing DCM.

- Multiple core series connected Flyback 4.2.3.
- Multi stacked Sepic 4.2.4.
- Multi stacked Zeta 4.2.5.
- Multi stacked isolated Cuk 4.2.6.

Main characteristics of single switch intramodule balancing systems are presented in Table 4.1. During following subchapters main characteristics of each balancing system regarding advantages and disadvantages are presented. 4 main design parameters will be presented for each balancing system.

- Critical duty cycle D_C to guarantee open loop control.
- Weak cell balancing current $I_{Cb,W}$.
- Strong cells balancing current $I_{Cb,S}$.
- Relation between weak and strong cell current $I_{Cb,W}/I_{Cb,S}$.

Modelling and design process is described in detail in **Annex A** and **Annex B**

4.2.1 Single core Flyback

The converter presented in Fig 4.3 is a single switch flyback converter where one

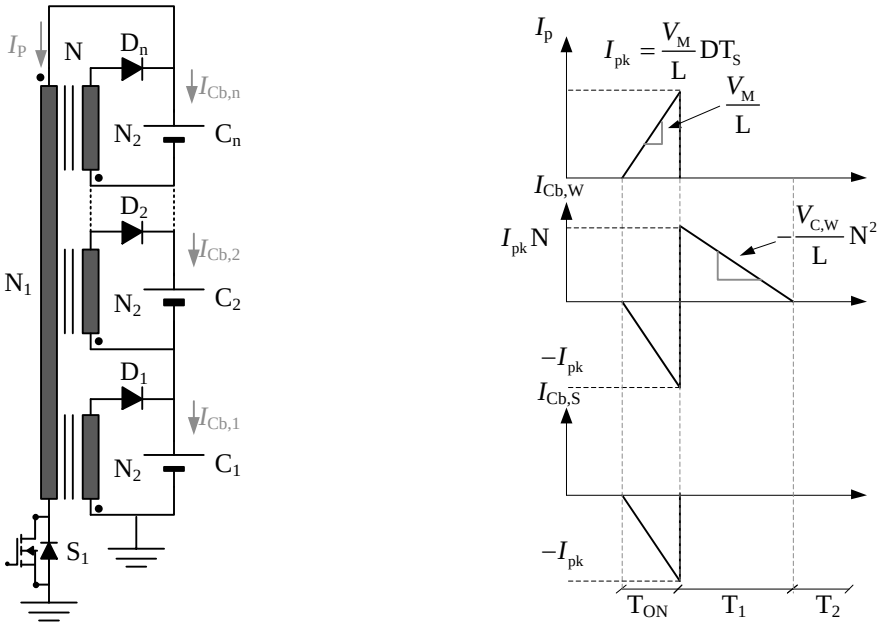

a) **b)**

Fig 4.3. Single core Flyback balancing system. a) n cell module balancing system circuit scheme. b) Main current waveforms for primary current I_P weak cell balancing current $I_{Cb,W}$ and strong cell balancing current $I_{Cb,S}$.

primary and n cell secondaries are wounded in a single magnetic core. The energy is inserted from all the module V_M to the primary inductance L during T_{ON} period. During OFF period only the weak cell secondary is polarized.

The advantage is that only a single core is necessary to balance all the cells inside the module. However a good transformer design is necessary not to have deviations between different windings. Coaxial cable based windings [82] or the use of commercial multiwinding transformers reduce deviations. Main disadvantages are that it is not modular if one more cell is inserted in the module and that a high number of series cells increase the design complexity.

The critical duty cycle D_C where the DCM limit is guaranteed is defined in (4.7) where the transformer turns ratio N gives a freedom degree.

$$D_C = \frac{N V_{C,W}}{V_M + N V_{C,W}} \tag{4.7}$$

The weak and strong cell balancing currents $I_{Cb,W}$ and $I_{Cb,S}$ are highly dependent on the magnetizing inductor L and the module voltage V_M as defined in (4.8) and (4.9). It is relevant that all strong cells give the same current, even if they have different voltage levels. The relation between currents (4.10) is dependent on the division between the module voltage and the weak cell voltage. Higher number of series connected cells gives bigger current relations between weak and strong cell balancing currents.

$$I_{Cb,W} = \frac{V_M D^2 T_s}{2L}\left(\frac{V_M}{V_{C,W}} - 1\right) \tag{4.8}$$

$$I_{Cb,S} = -\frac{V_M D^2 T_s}{2L} \tag{4.9}$$

$$\left|\frac{I_{Cb,W}}{I_{Cb,S}}\right| = \left(\frac{V_M}{V_{C,W}} - 1\right) \tag{4.10}$$

4.2.2 Multiple core parallel connected Flyback

The multiple core parallel connected Flyback controls n independent transformers in parallel with a single switch Fig 4.4. During switch on period TON the n paralleled transformers are magnetized, so all the cells of the module give n times the magnetizing

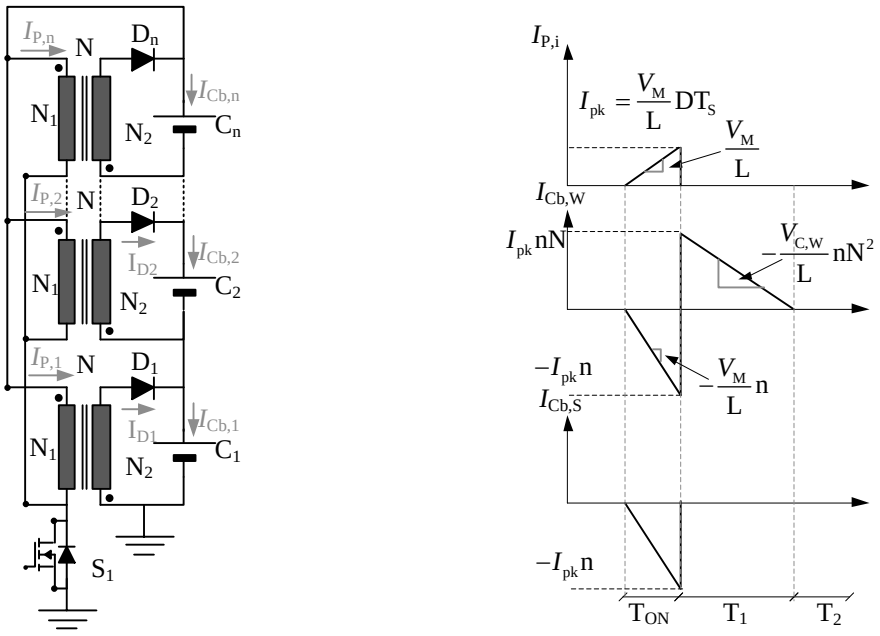

Fig 4.4. Multiple core parallel connected Flyback balancing system. a) n cell module balancing system circuit scheme. b) Main current waveforms for primary transformer currents $I_{P,i}$ weak cell balancing current $I_{Cb,W}$ and strong cell balancing current $I_{Cb,S}$.

current of a single transformer. When the switch is turned off the energy stored in all the transformers is released through the weak cell transformer, so all the other transformers transfer the energy to the weak cell through the weak cell primary.

The main advantage is the modularity that provides the use of independent magnetic cores and the insertion of all the energy to the weak cell during off time as with the single core Flyback balancing system, increasing the balancing speed. The main disadvantage is the increased current in the cells due to parallel connection of the transformers, therefore increasing the power losses.

The D_C is defined equal to single core Flyback balancing system, with equal dependencies on module voltage and weak cell voltage, and turn ratio N freedom degree.

$$D_C = \frac{N V_{C,W}}{V_M + N V_{C,W}} \tag{4.11}$$

The weak and strong balancing currents are dependent on the number of cells with a relation between balancing currents equal to single core Flyback. The strong cell balancing currents are all equal and only dependant on the T_{ON} period energy release.

$$I_{\mathrm{Cb,W}} = \frac{V_{\mathrm{M}} \mathrm{D}^2 \mathrm{T_s} \mathrm{n}}{2\mathrm{L_n}} \left(\frac{V_{\mathrm{M}}}{V_{\mathrm{C,W}}} - 1 \right) \tag{4.12}$$

$$I_{\mathrm{Cb,S}} = -\frac{V_{\mathrm{M}} \mathrm{D}^2 \mathrm{T_s} \mathrm{n}}{2\mathrm{L_n}} \tag{4.13}$$

$$\left| \frac{I_{\mathrm{Cb,W}}}{I_{\mathrm{Cb,S}}} \right| = \left(\frac{V_{\mathrm{M}}}{V_{\mathrm{C,W}}} - 1 \right) \tag{4.14}$$

4.2.3 Multiple core series connected Flyback

The multiple core series connected flyback connects n independent magnetic cores in series to a single active switch as presented in Fig 4.5. The n series magnetizing inductors L are energy charged during T_{ON}. During Off the energy is released to all the cells, not only to the weak cell, making the balancing system not selective. However, the weak cell continues receiving more energy balancing the module.

The main advantage of the system is the modularity, only changing the active while more cells are inserted in series. The biggest drawback is the low balancing speed because the balancing procedure is not selective.

The critical duty cycle is typically higher than in previous balancing systems

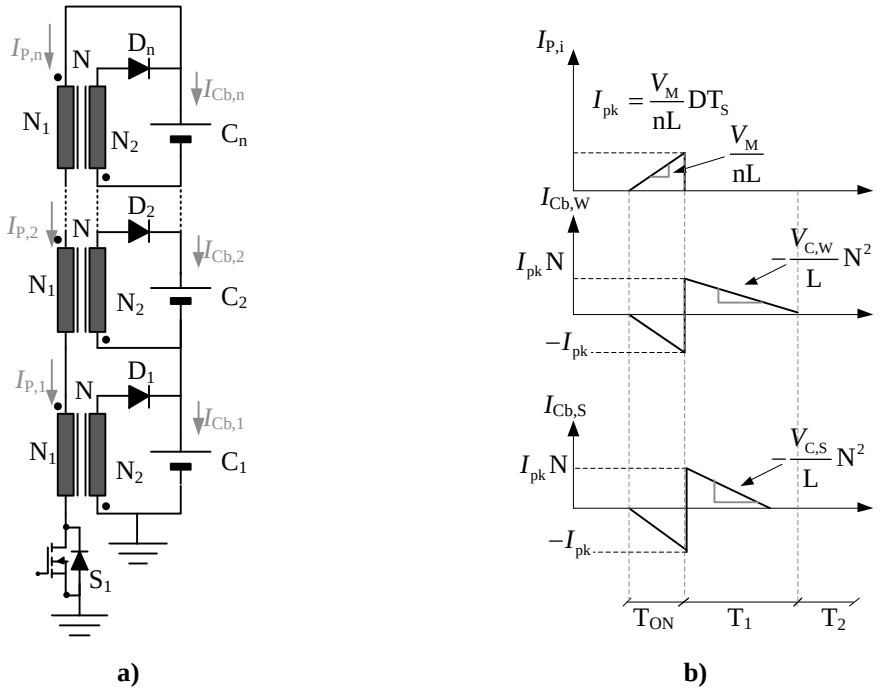

Fig 4.5 Multiple core series connected Flyback balancing system. a) n cell module balancing system circuit scheme. b) Main current waveforms for primary transformer currents $I_{P,i}$ weak cell balancing current $I_{Cb,W}$ and strong cell balancing current $I_{Cb,S}$.

because the V_M term is divided by the number of cells

$$D_C = \frac{N V_{C,W}}{\frac{V_M}{n} + N V_{C,W}} \tag{4.15}$$

The weak and strong balancing currents depend on same equation (4.16), because each cell balancing current $I_{Cb,i}$ only depends on its respective voltage $V_{C,i}$.

$$I_{Cb,i} = \frac{V_M D^2 T_s}{2nL_n}\left(\frac{V_M}{n V_{C,i}} - 1\right) \quad i=[1,n] \quad \begin{matrix} I_{Cb,W} \in V_{C,W} \\ I_{Cb,S} \in V_{C,S} \end{matrix} \tag{4.16}$$

The weak and strong current relation (4.17) is much smaller than in other Flyback configurations, confirming the assumption that the balancing speed of the series connected Flyback is low.

$$\left|\frac{I_{Cb,W}}{I_{Cb,S}}\right| = \frac{\left(\frac{V_M}{n V_{C,W}} - 1\right)}{\left(\frac{V_M}{n V_{C,S}} - 1\right)} \tag{4.17}$$

4.2.4 Multi Stacked Sepic

The multi stacked Sepic balancing system is based on a single input n outputs series configuration Fig 4.6. During T_{ON} the single switch charges the different Lin and Ln inductors of the circuit, while during OFF the weak cell diode is polarized inserting energy to the weak cell, balancing the series connected cells.

The main advantages are the easy modularity of the configuration and the absence of transformer in the design.

Fig 4.6 present the inductor and diode currents ($I_{L,i}$ I_{Lin} $I_{D,i}$) instead of cell balancing currents ($I_{Cb,i}$) due to easier analysis of the system. The balancing currents are obtained by a steady state analysis obtaining the equation (4.18)

$$I_{Cb,i} = I_{D,i} - I_{Lin} \tag{4.18}$$

$I_{D,i}$ for the strong cells is equal to zero because the diodes are never polarized, only $I_{D,W}$ has a positive value, inserting energy to the weak cell. The D_C is dependent on

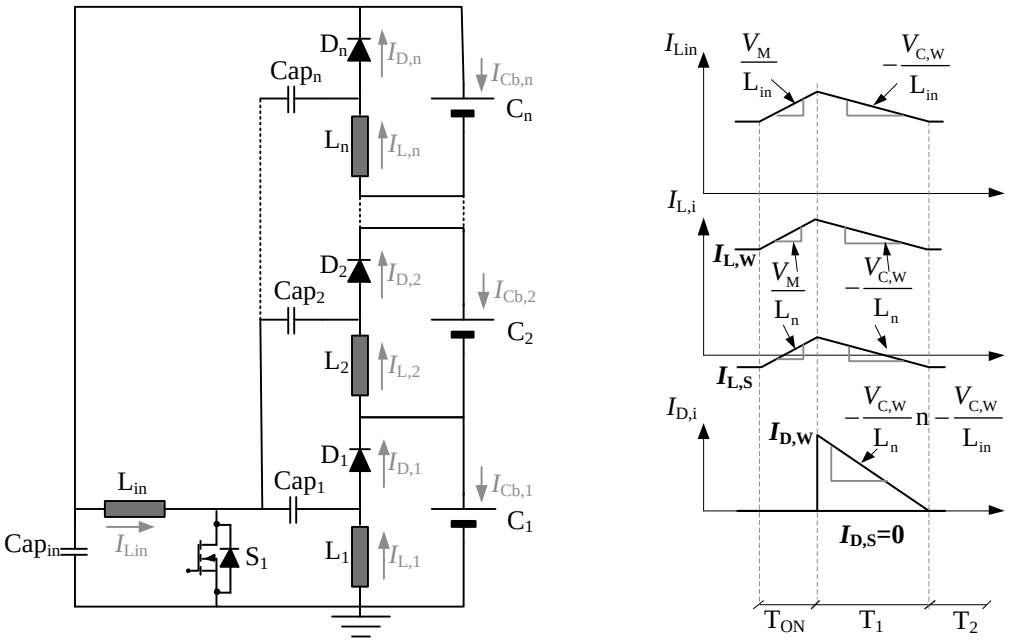

Fig 4.6. Sepic converter based multi stacked balancing system. a) n cell module balancing system circuit scheme. b) Main current waveforms Input inductor current currents I_{Lin} , inductor currents $I_{\mathrm{L,i}}$ with weak $I_{\mathrm{L,W}}$ and strong inductor $I_{\mathrm{L,S}}$ currents and diode currents $I_{\mathrm{D,i}}$ with weak $I_{\mathrm{D,W}}$ and strong diode $I_{\mathrm{D,S}}$ currents presented.

module voltage and weak cell voltage (4.19), which could yield to low duty cycle ratio when high number of cells are connected in series inside a module.

$$\mathrm{D_C}=\frac{V_{\mathrm{C,W}}}{V_{\mathrm{M}}+V_{\mathrm{C,W}}} \tag{4.19}$$

The weak and strong cell balancing currents are defined by equations (4.20) and (4.21) where the module voltage V_{M} and the inductors value ($\mathrm{L_n}$,$\mathrm{L_{in}}$) are the most important impact factors. The relation between the weak and strong balancing current is defined as the single core and multiple core parallel balancing systems ((4.22)=(4.14)=(4.10)) where to increase the balancing relation a higher number of cells or a bigger unbalance is necessary. All the strong cell balancing currents are equal and voltage independent.

$$I_{\mathrm{Cb,W}}=\frac{V_{\mathrm{M}}\mathrm{D}^2\mathrm{T_s}\left(\mathrm{L_n}+\mathrm{nL_{in}}\right)}{2\mathrm{L_nL_{in}}}\left(\frac{V_{\mathrm{M}}}{V_{\mathrm{C,W}}}\text{-}1\right) \tag{4.20}$$

$$I_{\mathrm{Cb,S}}=-\frac{V_{\mathrm{M}}\mathrm{D}^2\mathrm{T_s}\left(\mathrm{L_n}+\mathrm{nL_{in}}\right)}{2\mathrm{L_nL_{in}}} \tag{4.21}$$

$$\left|\frac{I_{\mathrm{Cb,W}}}{I_{\mathrm{Cb,S}}}\right|=\left(\frac{V_{\mathrm{M}}}{V_{\mathrm{C,W}}}\text{-}1\right) \tag{4.22}$$

4.2.5 Multi Stacked Zeta

The multi stacked Zeta converter is a buck-boost configuration as the previous Sepic converter. The difference with the Sepic converter is only visible comparing the instantaneous cell currents. Even if the diode currents or the inductor currents are different the behaviour is equal. The energy is charged in the circuit inductors during T_{ON} and released to the weak cell during off period. Only the weak cell diode is polarized because is the easiest current path of the circuit.

The advantages of modularity and absence of inductors is presented as in the Sepic converter, however as a small drawback could be presented with the high side switch requirement in Zeta configuration.

The D_C equation (4.23) is equal to the Sepic expression. The weak and strong cell current expressions (4.24) and (4.25) and the relation magnitude between currents is also equal to the Sepic converter. The relation magnitude is highly dependent on the weak cell voltage $V_{C,W}$ and the module voltage V_M.

$$D_C = \frac{V_{C,W}}{V_M + V_{C,W}} \tag{4.23}$$

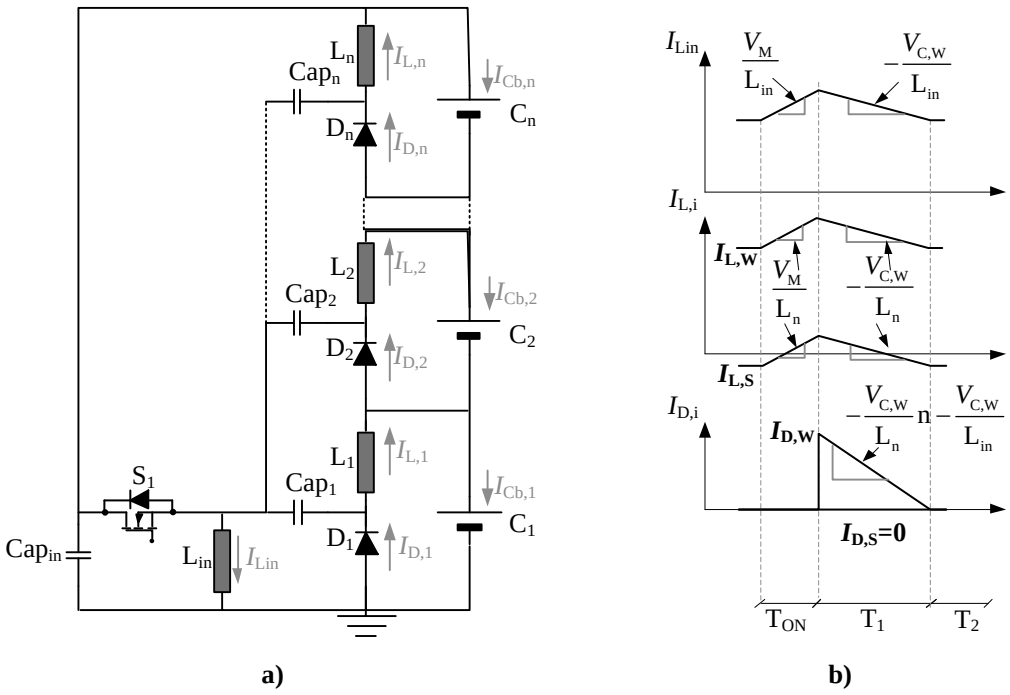

Fig 4.7. Zeta converter based multistacked balancing system. a) n cell module balancing system circuit scheme. b) Main current waveforms Input inductor current currents I_{Lin} , inductor currents $I_{L,i}$ with weak $I_{L,W}$ and strong inductor $I_{L,S}$ currents and diode currents $I_{D,i}$ with weak $I_{D,W}$ and strong diode $I_{D,S}$ currents presented.

$$I_{Cb,W} = \frac{V_M D^2 T_s \left(L_n + nL_{in}\right)}{2nL_n}\left(\frac{V_M}{V_{C,W}} - 1\right) \tag{4.24}$$

$$I_{Cb,S} = -\frac{V_M D^2 T_s \left(L_n + nL_{in}\right)}{2nL_n} \tag{4.25}$$

$$\left|\frac{I_{Cb,W}}{I_{Cb,S}}\right| = \left(\frac{V_M}{V_{C,W}} - 1\right) \tag{4.26}$$

4.2.6 Multi Stacked Isolated Cuk

The multi stacked isolated Cuk is a Cuk configuration with single input and split n stacked outputs, with a transformer to inverse the negative output polarity of the Cuk converter. During T_{ON} the circuit inductors are charged through the module cells while during T_1 energy is released to the weak cell through the respective diode.

The main advantage is the easy modularity as in the Sepic and Zeta configuration. Furthermore the insertion of the transformer gives a freedom degree in the circuit design. The main drawbacks are the need of an extra transformer and the split capacitor Cap_{cuk}.

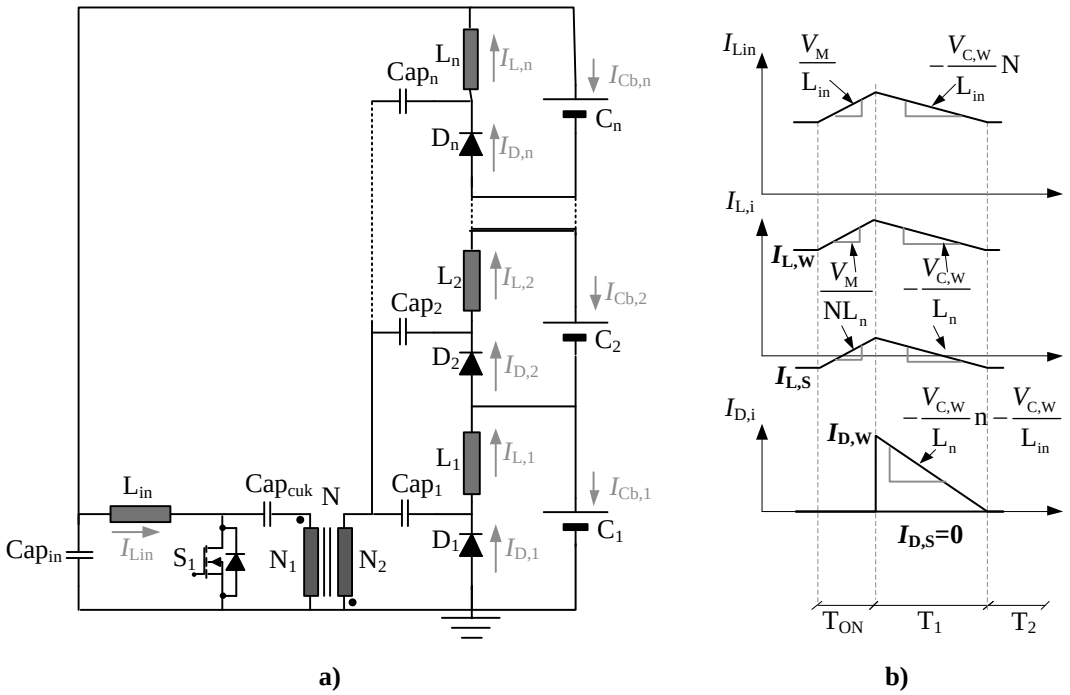

Fig 4.8. Isolated Cuk converter based multistacked balancing system. a) n cell module balancing system circuit scheme. b) Main current waveforms Input inductor current currents I_{Lin} , inductor currents $I_{L,i}$ with weak $I_{L,W}$ and strong inductor $I_{L,S}$ currents and diode currents $I_{D,i}$ with weak $I_{D,W}$ and strong diode $I_{D,S}$ currents presented.

Critical duty cycle D_C is directly dependent on the turn relation of the transformer N (4.27). When high number of cells are connected in series the duty cycle can be adjusted.

$$D_C = \frac{N V_{C,W}}{V_M + V_{C,W}} \tag{4.27}$$

The weak and strong balancing current expressions (4.28) and (4.29)are similar to Sepic and Zeta converter equations, furthermore if the transformer turn relation is unitary the expressions are equal. The strong cells balancing currents are not dependent on their cell voltages, they only depend on V_M.

$$I_{Cb,W} = \frac{V_M D^2 T_s \left(L_n + \frac{nL_{in}}{N^2} \right)}{2N^2 L_n L_{in}} \left(\frac{V_M}{V_{C,W}} - 1 \right) \tag{4.28}$$

$$I_{Cb,S} = - \frac{V_M D^2 T_s \left(L_n + \frac{nL_{in}}{N^2} \right)}{2N^2 L_n L_{in}} \tag{4.29}$$

The relation between weak and strong cell is dependent on the difference between $V_{C,W}$ and V_M. It is clearly seen as in the previous balancing systems that higher the voltage unbalance between cells, higher is the derived current to the weak cell increasing the balancing process speed.

$$\left| \frac{I_{Cb,W}}{I_{Cb,S}} \right| = \left(\frac{V_M}{V_{C,W}} - 1 \right) \tag{4.30}$$

4.3 Intramodule power loss model

Active balancing systems ideally present 100% efficiency lossless behaviour transferring all the balancing power between cells inside the module. However the power losses presented in the converter reduce the efficiency.

If the efficiency is kept >95%, the power losses do not almost affect to the lossless current model presented in chapter 4.2. However in low power systems where high efficiencies are difficult to obtain the power losses should be taken into account to model the converter current.

During this subchapter a different approach is presented where lossless equations are used to determine power losses, but after that are reused to obtain real parameters as presented in Fig 4.9. The parameters under study are presented in

- $I_{Cb,i}$ and $P_{Cb,i}$ lossless ideal current and power of the balancing system.
- $P_{Cb,Loss}$ representing the power losses of the balancing system.
- $I_{CbL,i}$ and $P_{CbL,i}$ which represent the loss modelled current and power of the balancing system.
- The effiency η_{Cb} of the balancing system, which gives the idea of the energy transfer efficiency inside the balancing converter.

After modelling the power losses and recalculating the current and power of the balancing system, the outputs are compared to experimental balancing systems.

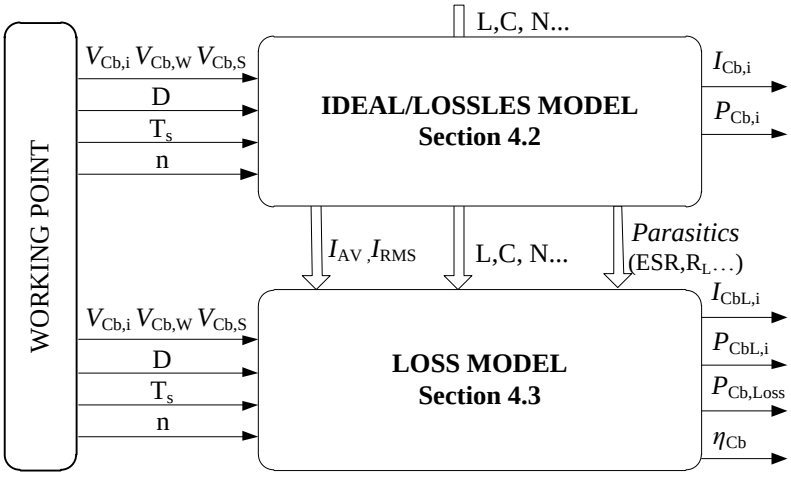

Fig 4.9. Flow chart presentation of the balancing system model strategy. Ideal/lossless model equations feed loss model.

4.3.1 Power loss and efficiency model

Energy transfer in active balancing systems is reduced respect to ideal models due to power losses generated in intramodule balancing systems. DCM behaviour of single switch balancing systems add extra complexity to the power losses analysis primarily because RMS and average AV cannot be assumed equal as CCM operation (4.31).

$$\begin{aligned} I_{\mathrm{AV}} &\approx I_{\mathrm{RMS}} \rightarrow \mathrm{CCM} \\ I_{\mathrm{AV}} &\neq I_{\mathrm{RMS}} \rightarrow \mathrm{DCM} \end{aligned} \tag{4.31}$$

Power losses are calculated with the RMS and AV expressions of each component presented in the circuit. The non-ideal parameters of each component are taken into account for the power loss analysis.

- Power switch: Mosfet $R_{DS,on.}$
- Diodes: Forward Voltage V_D and conduction resistance R_D.
- Capacitors: Equivalent Series Resistance ESR.
- Inductors and transformers: Series resistance R_L.

RMS and AV expression for each component are presented in **Annex B B.1**. Switching losses are neglected due to low impact in DCM and low voltage applications however main basic equations related to switching losses are presented in **Annex A A.2** for future implementation.

The ideal/lossless balancing power transferred to each cell is defined by (4.32).

$$P_{\mathrm{Cb,i}} = V_{\mathrm{C,i}} I_{\mathrm{Cb,i}} \tag{4.32}$$

The total power managed by the ideal balancing system is the sum of the absolute values of the energy transferred by each balancing stage

$$P_{\mathrm{Cb,T}} = \sum_{\mathrm{i=1}}^{\mathrm{n}} V_{\mathrm{C,i}} I_{\mathrm{Cb,i}} \tag{4.33}$$

However the power losses presented in the balancing system reduce the total balancing power exchanged between the cells inside the module to $P_{\mathrm{CbL,T}}$.

$$P_{\mathrm{CbL,T}} = P_{\mathrm{Cb,T}} - P_{\mathrm{Cb,Loss}} \tag{4.34}$$

The efficiency calculation η_{Cb} of the balancing system is not as obvious as a typical single input-single output system as a DCDC converter. The series connected

cells act as the input and the output, redistributing the energy between the weak and strong cells. The efficiency is then calculated respect to the ideal total balancing power $P_{\mathrm{Cb,T}}$ by equation (4.35).

$$\eta_{\mathrm{Cb}} = \frac{P_{\mathrm{CbL,T}}}{P_{\mathrm{Cb,T}}} \cdot 100 = \frac{P_{\mathrm{Cb,T}} - P_{\mathrm{Cb,Loss}}}{P_{\mathrm{Cb,T}}} \cdot 100 \tag{4.35}$$

The power losses of the balancing system are mainly due to redistribution of the energy to the weak cell of the module. The power losses are only contemplated for the weak cell balancing current recalculation, while strong cell currents are kept equal to ideal/lossless model.

$$I_{\mathrm{CbL,W}} = \frac{I_{\mathrm{Cb,W}} V_{\mathrm{C,W}} - P_{\mathrm{Cb,Loss}}}{V_{\mathrm{C,W}}} \quad P_{\mathrm{Cb,Loss}} \xrightarrow{impact} I_{\mathrm{CbL,W}} \tag{4.36}$$

$$I_{\mathrm{CbL,S}} = I_{\mathrm{Cb,S}} \tag{4.37}$$

For the non-selective multiple core series connected flyback the power losses impact to all the cells because during off period all the cells receive balancing current. The weak cell balancing system suffers bigger power losses so the power losses are redistributed proportionally to the ideal balancing current $I_{\mathrm{Cb,i}}$ (4.38)

$$I_{\mathrm{CbL,i}} = \frac{I_{\mathrm{Cb,i}} V_{\mathrm{C,i}} - \dfrac{P_{\mathrm{Cb,Loss}} I_{\mathrm{Cb,i}}}{\sum_{z=1}^{n} \left| I_{\mathrm{Cb,z}} \right|}}{V_{\mathrm{C,i}}} \quad \begin{array}{l} (\text{multiple core series flyback}) \\ P_{\mathrm{Cb,Loss}} \xrightarrow{impact} I_{\mathrm{CbL,i}} \end{array} \tag{4.38}$$

For a balanced situation the model equations are different. The total ideal/lossless balancing power is zero $P_{\mathrm{Cb,T}}$=0 because there is no current under balanced situation. However in a real situation there is a small balancing power to compensate the power losses of the converter. The modelled balancing power $P_{\mathrm{CbL,T}}$ is only used to compensate the power losses $P_{\mathrm{CB,Loss}}$ of the balancing power converter. The efficiency equation (4.35) for unbalanced situation changes because with (4.35) the efficiency will be ∞ (infinite). The analysis under balanced situation is presented by (4.39).

$$\eta_{\mathrm{Cb}} = \frac{P_{\mathrm{CbL,T}} - P_{\mathrm{Cb,Loss}}}{P_{\mathrm{CbL,T}}} \cdot 100 \quad P_{\mathrm{Cb,T}} = 0 \rightarrow \text{balanced} \tag{4.39}$$

4.4 Intramodule balancing system validation

To evaluate the balancing current equations presented in subchapters 4.2 and 4.3, 6 prototypes are designed to compare and validate the ideal and power loss based balancing equations. The prototypes are presented in **Annex C**. The models presented in previous subchapters are compared to real experimental values.

The intramodule balancing systems are designed for a 4 series connected LFP cells module (4S1P). The number of series connected cells is defined as n=4. The definition of the critical duty cycle D_C is made to guarantee the DCM even in the biggest unbalancing situation. The extreme situation is when the weak cell voltage $V_{C,W}$ is 2 V (lowest allowable voltage in LFP), and the 3 strong cells are charged to maximum $V_{C,S}$=3,65 V (highest admissible LFP voltage). The switching frequency is set to 100 kHz (T_S=10 µS), in order to obtain reduced size design. The selective balancing systems weak cell current $I_{Cb,W}$ is set to 400 mA, while the non-selective multiple core series connected flyback $I_{Cb,W}$ is set to 100 mA. The design specifications and the final prototype values are presented in Table 4.2. Detailed design procedure of intramodule balancing systems is defined in subchapter **Annex B B.1** and main balancing equations where presented in subchapter 4.2.

The 6 prototype gate signals are generated with a GW INSTEK AFG-2005 Arbitrary Function Generator. This function generator gives special versatility of full

Table 4.2 Desing and prototype values for 4S1P intramodule balancing systems presented from subchapters 4.2.1 to 4.2.6.Design parameters: n=4 $V_{Cb,W}$=2 V $V_{Cb,S}$=3,65V switching frequency 100 kHz (T_S=10 µS)

Topology	Design					Prototype				
	$I_{Cb,W}$ [mA]	D_C [ ]	L_n[1] [µH]	Lin [µH]	N [ ]	$I_{Cb,W}$ [mA]	D [ ]	L_n[1] [µH]	Lin [µH]	N [ ]
4.2.1	400	0,134	16	_	1	500	0,13	12	_	1
4.2.2	400	0,134	63	_	1	600	0,13	40	_	1
4.2.3	100	0,382	15	_	1	144	0,38	10	_	1
4.2.4	400	0,134	66	427	_	365	0,13	68	470	_
4.2.5	400	0,134	66	427	_	365	0,13	68	470	_
4.2.6	400	0,134	66	427	1	365	0,13	68	470	1

[1] In Flyback design L_n is referred as the transformer magnetizing inductor L.

control of the duty cycle D, 0,01 to 0.99, in a high 100 kHz switching frequency.

The intramodule balancing systems are tested in a test bench where the 4S1P battery pack is simulated. The test bench is based in a power supply and power resistor connected in parallel which simulates the behaviour of a real Li-ion cell. The resistor R_{PS} should be designed to admit the maximum balancing current of the intramodule balancing system. 4 power supplies are connected in series to simulate the 4S1P Li-ion cells module.

The balancing system evaluation is made in 2 steps Fig 4.10 a). During step 1 the balancing current and voltage of each power supply ($I_{PS1,i}$, $V_{PS,i}$) is measured with the balancing system switched off. The power supply feed the parallel connected resistors.

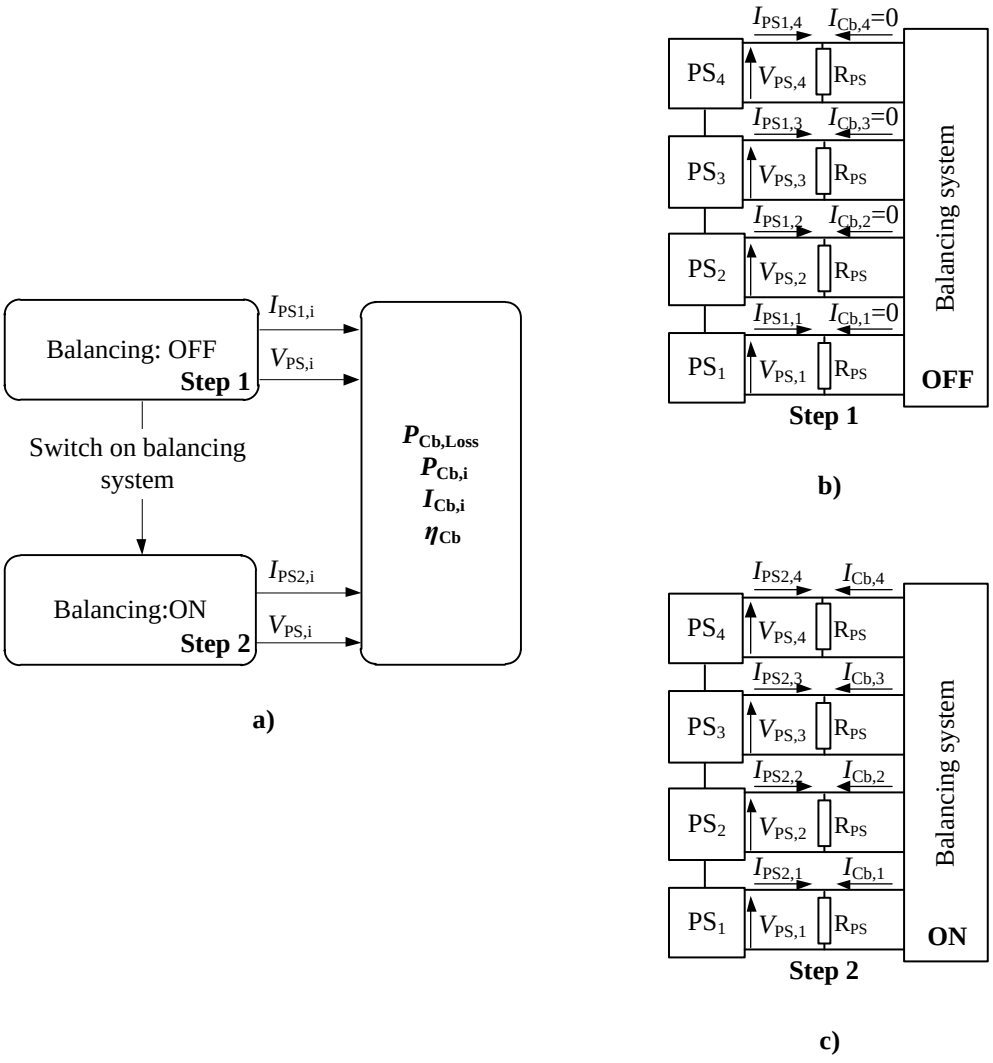

Fig 4.10 Balancing system validation test bench. a) Balancing system variables measurement flow chart in 2 steps. b) Step 1 with balancing system OFF. c) Step 2 with balancing system ON.

In step 2 the balancing system is switched on. The voltage $V_{PS,i}$ of each balancing system is kept constant ($V_{PS,i} = V_{PS1,i} = V_{PS2,i}$) and consequently the current through the resistor R_{PS} is constant (parallel connected). However the current transferred by the power supplies $I_{PS2,i}$ change depending on the voltage of the power supply. Weak power supply (low voltage power supply) reduces the inserted current because strong power supplies (high voltage power supplies) insert more energy to the system. The power supply system behaves equally as an unbalanced series connected Li-ion cell module.

The measurement system for voltage and current measurements can be avoided if a high accuracy power supply is used. During experimental tests two HAMEG HM7042-5 power supplies, with 2 channels each are used. 1 mA current and 10 mV voltage precision is enough accurate with a power precision deviation induced of 10 µW. If a more precise measurement is required higher resolution voltage and current measurement could be connected in the test bench.

During step 1 the balancing current $I_{Cb,i}$ of the balancing system is zero ($I_{Cb,i}$=0). With a constant current path from R_{PS} for step 1 and step 2 $I_{Cb,i}$ can be expressed as

$$I_{Cb,i} = I_{PS1,i} - I_{PS2,i} \tag{4.40}$$

The total balancing power of the system is defined by the sum of the power of each balancing system $P_{Cb,i}$.

$$P_{Cb,T} = \sum_{i=1}^{n} \left| P_{Cb,i} \right| = \sum_{i=1}^{n} \left| V_{PS,i} I_{Cb,i} \right| \qquad \text{n=4 4S1P} \tag{4.41}$$

During step 1 the test bench power supplies only fed the R_{PS} resistor. However in step 2 when the balancing system is switched on the power supplies insert energy for the resistors R_{PS} and the power losses of the balancing system $P_{Cb,Loss}$. The power losses are calculated by

$$P_{Cb,Loss} = \sum_{i=1}^{n} \left| V_{PS,i} I_{PS2,i} \right| - \sum_{i=1}^{n} \left| V_{PS,i} I_{PS1,i} \right| \qquad \text{n=4 4S1P} \tag{4.42}$$

The balancing system efficiency η_{CB} is defined with the total power managed by the system $P_{Cb,T}$ and the total power losses $P_{Cb,Loss}$ as

$$\eta_{Cb} = \frac{P_{Cb,T} - P_{Cb,Loss}}{P_{Cb,T}} \cdot 100 \tag{4.43}$$

The validation analysis will be held under 4 points of view.

- **Unbalancing situation:** The intramodule balancing systems will be tested under different unbalancing situations to demonstrate their balancing characteristics for series connected Li-ion modules.
- **Repeatability of balancing current**: under an unbalancing situation, and the change of the weak cell position, verify that the balancing currents are equal and independent of the situation of the unbalanced cell inside the series connected module.
- **Balanced situation**: The intramodule balancing systems will be tested with the same power supply voltages to demonstrate that the active balancing systems only have to fed up the power losses, so for a balanced case $P_{Cb,T}=P_{Cb,Loss}$.
- **Comparative evaluation of models**: The ideal/lossless and the power loss based models are compared to the experimental results obtained in the test bench.

The first test verifies the correct behaviour of the 6 balancing systems under unbalancing situation and demonstrates that the weak cell (low voltage cell) receives energy from the strong cells (high voltage cells). For this first behaviour validation step, 3 different scenarios are presented.

- Low voltage unbalance: The weak cell voltage is 3,1 V and the strong cell voltages $V_{C,S}$= 3,2 V. This scenario simulates LFP series connected cells in the "flat plateau" of this specific chemistry.
- Medium voltage unbalance: The weak cell voltage $V_{C,W}$= 2 V and the strong cells $V_{C,S}$= 2,5 V. This scenario simulates the cells after the sharp discharge elbow, where higher voltage differences are presented.
- High voltage unbalance: The weak cell voltage is set to the minimum allowable voltage $V_{C,W}$=2 V and the 3 strong cells to 3,65 V. The 3rd scenario permits to evaluate that the critical duty cycle D_C is well defined under the worst case inside a series connected module.

The results are presented in Fig 4.11 where it can be seen that the weak cell balancing current $I_{Cb,W}$ is always bigger than the strong cell balancing current $I_{Cb,S}$.

Furthermore it is also verified that bigger is the unbalancing process higher is the balanced current and higher the relation between $I_{Cb,W}$ and $I_{Cb,S}$ as described in subchapter 4.2.The multiple core series connected flyback is the only balancing system that presents negative values for $I_{Cb,W}$, although it is always bigger than $I_{Cb,S}$.

The repeatability test is hold under a unbalancing situation of a weak cell $V_{C,W}$=2 V and 3 strong cells with $V_{C,S}$= 3 V. The weak cell is placed in different positions from bottom (index 1) to top (index 4).

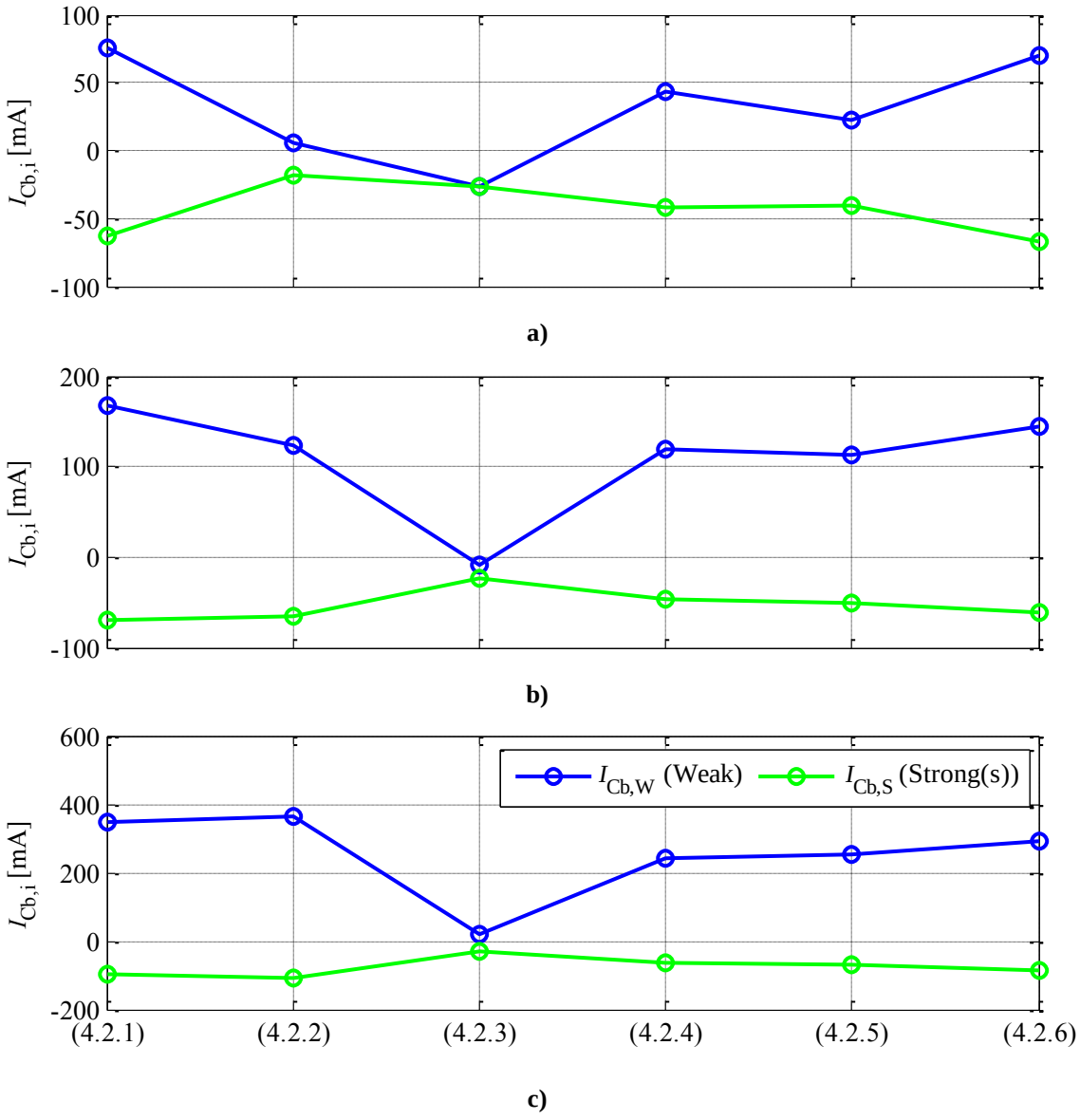

Fig 4.11 Weak cell balancing current $I_{Cb,W}$ and strong cells balancing current $I_{Cb,S}$ under 3 different unbalancing scenarios a) Low unbalancing like LFP plateau $V_{C,W}$= 3,1 V and 3 strong cells $V_{C,S}$=3,2 V. b) Medium unbalance situation, LFP final discharge process simulation $V_{C,W}$ = 2 V and $V_{C,S}$ =2,5 V. c) Extreme unbalance to guarantee DCM in the worst situation $V_{C,W}$ = 2 V and $V_{C,S}$ = 3,65 V.

Table 4.3 Balancing current repeatability test: $V_{C,W}$= 2 V and $V_{C,S}$= 3 V. The index 1 to 4 is referred as 1 bottom cell and 4 top cell of a module. $I_{Cb,W}$ is grade shaded in each test. Average (AV) and standard deviation (σ) of $I_{Cb,W}$ and $I_{Cb,S}$ are presented for each balancing system.

Single core Flyback (4.2.1)					**Multiple core parallel Flyback (4.2.2)**				
$V_{C,W}$	$I_{Cb,1}$ [mA]	$I_{Cb,2}$ [mA]	$I_{Cb,3}$ [mA]	$I_{Cb,4}$ [mA]	$V_{C,W}$	$I_{Cb,1}$ [mA]	$I_{Cb,2}$ [mA]	$I_{Cb,3}$ [mA]	$I_{Cb,4}$ [mA]
1	234	-75	-73	-74	1	232	-86	-101	-95
2	-78	228	-73	-75	2	-107	298	-110	-108
3	-80	-81	241	-79	3	-92	-84	227	-93
4	-78	-79	-77	240	4	-95	-88	-101	242
	$I_{Cb,W}$ [mA]		$I_{Cb,S}$ [mA]			$I_{Cb,W}$ [mA]		$I_{Cb,S}$ [mA]	
	AV	σ	AV	σ		AV	σ	AV	σ
	235,750	6,021	-76,833	2,758		249,750	32,766	-96,667	8,742
Multiple core series Flyback (4.2.3)					**Multi stacked Sepic (4.2.4)**				
$V_{C,W}$	$I_{Cb,1}$ [mA]	$I_{Cb,2}$ [mA]	$I_{Cb,3}$ [mA]	$I_{Cb,4}$ [mA]	$V_{C,W}$	$I_{Cb,1}$ [mA]	$I_{Cb,2}$ [mA]	$I_{Cb,3}$ [mA]	$I_{Cb,4}$ [mA]
1	2	-25	-27	-24	1	170	-32	-47	-50
2	-26	1	-25	-23	2	-60	170	-58	-46
3	-26	-24	1	-23	3	-53	-53	175	-53
4	-25	-24	-24	4	4	-52	-53	-52	169
	$I_{Cb,W}$ [mA]		$I_{Cb,S}$ [mA]			$I_{Cb,W}$ [mA]		$I_{Cb,S}$ [mA]	
	AV	σ	AV	σ		AV	σ	AV	σ
	2,000	1,414	-24,667	1,231		171,000	2,708	-50,750	7,073
Multi stacked Zeta (4.2.5)					**Multi stacked Isolated Cuk (4.2.6)**				
$V_{C,W}$	$I_{Cb,1}$ [mA]	$I_{Cb,2}$ [mA]	$I_{Cb,3}$ [mA]	$I_{Cb,4}$ [mA]	$V_{C,W}$	$I_{Cb,1}$ [mA]	$I_{Cb,2}$ [mA]	$I_{Cb,3}$ [mA]	$I_{Cb,4}$ [mA]
1	175	-58	-60	-59	1	209	-72	-73	-73
2	-59	180	-58	-58	2	-71	209	-73	-73
3	-58	-59	180	-59	3	-80	-73	213	-74
4	-65	-59	-60	177	4	-73	-73	-74	214
	$I_{Cb,W}$ [mA]		$I_{Cb,S}$ [mA]			$I_{Cb,W}$ [mA]		$I_{Cb,S}$ [mA]	
	AV	σ	AV	σ		AV	σ	AV	σ
	178,000	2,449	-59,333	1,923		211,250	2,630	-73,500	2,195

The results of the carried tests are presented in Table 4.3. Good repeatability is presented in the 6 different intramodule balancing systems when the weak cell is placed in different positions inside the battery pack. Buck boost based balancing systems (4.2.4 to 4.2.6) present low standard deviation values between weak and strong cell currents (σ < 3 mA for $I_{Cb,W}$)

To evaluate the behaviour under balanced situation the 4 power supplies are set to $V_{C,i}$=3,65 V. The 3,65 V is set because is the balanced situation where more power losses are generated. Fig 4.12 presents that balancing power $P_{Cb,T}$ and power losses $P_{Cb,Loss}$ are equal for a balanced situation. Equation (4.43) sets that efficiency η_{Cb} is equal to zero. Due to little differences in schematics parasitic or power supply voltages, a small difference appears between $P_{Cb,T}$ and $P_{Cb,Loss}$ giving a slightly bigger efficiency, (always smaller than 5%, so mainly neglectable). Multi stacked Sepic and single core Flyback present low power losses in balanced situation, while multiple core series and parallel connected flybacks have bigger power losses. Parallel connected flyback primarily due to high balancing currents and series connected flyback due to conduction of all the diodes (non-selective behaviour).

The models presented in subchapters 4.2 and 4.3 are compared with the experimental results for a big unbalance effect of $V_{C,W}$= 2 V and 3 strong cells $V_{C,S}$= 3,65V.

Ideal/Lossless modelling does not present power losses and the efficiency of the balancing system η_{Cb} is 100 %. However this situation is not real, and is more critical in

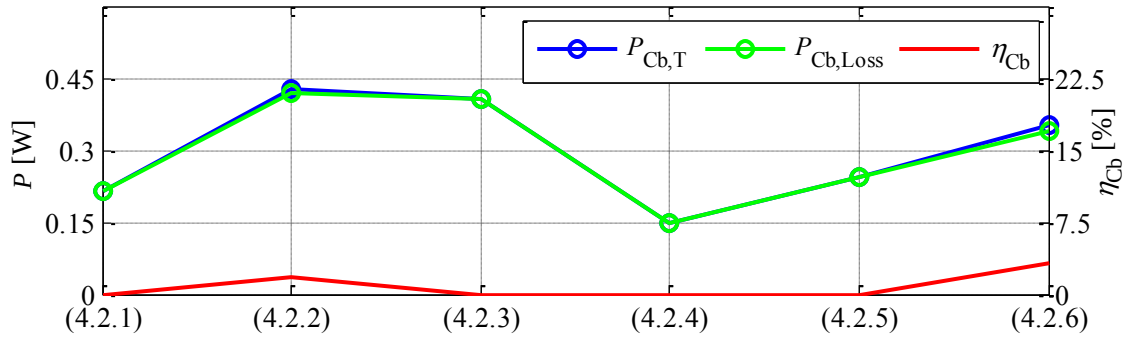

Fig 4.12 Weak cell balancing current $I_{Cb,W}$ and strong cells balancing current $I_{Cb,S}$ under 3 different unbalancing scenarios a) Low unbalancing like LFP plateau $V_{C,W}$= 3,1 V and 3 strong cells $V_{C,S}$=3,2 V. b) Medium unbalance situation, LFP final discharge process simulation $V_{C,W}$ = 2 V and $V_{C,S}$ =2,5 V. c) Extreme unbalance to guarantee DCM in the worst situation $V_{C,W}$ = 2 V and $V_{C,S}$ = 3,65 V.

low power systems where high efficiency is difficult to obtain. Power loss models present good accuracy respect to experimental tests as presented in Fig 4.13. Power losses are calculated with the AV and RMS values calculated for each balancing system element in **Annex B B.1**. Parasitic values (r_L, ESR,etc) of balancing system elements are taken from manufacturer datasheets.

The efficiency of the balancing systems is kept above 75%, except for the multicore series connected flyback where the efficiency is low (<25%) due to low balancing power and high power losses Fig 4.13 b). Fig 4.13 a) presents the power distribution of ideal, power loss modelled and real experimental results. Power loss modelled results distribute the total balancing power $P_{Cb,T}$ of the ideal/lossless model into new balancing power and power losses. The calculation of power losses leads to a recalculation of the balancing currents thanks to equations (4.36) and (4.37). The new

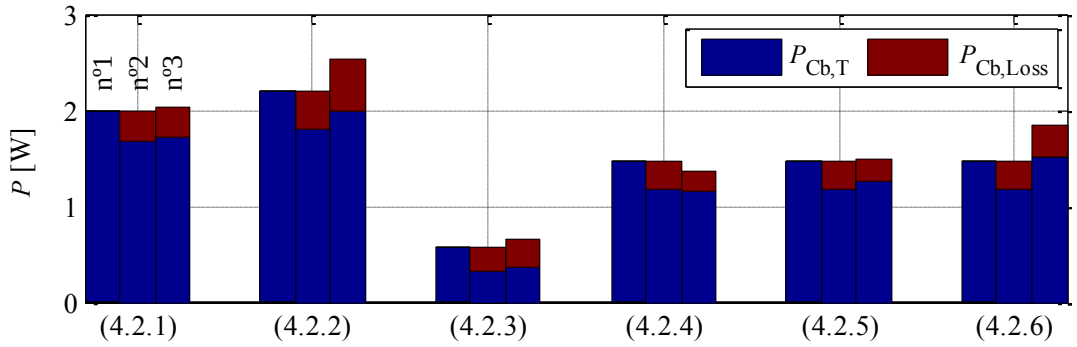

nº1 Ideal nº2 Modelled nº3 Experimental

a)

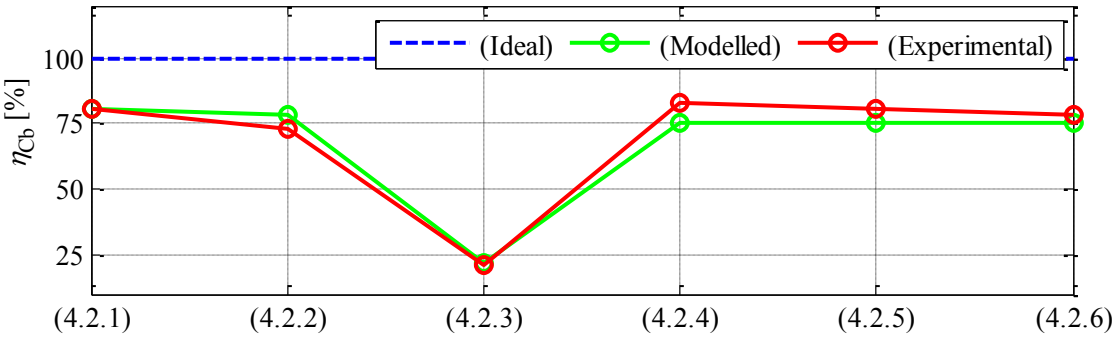

b)

Fig 4.13 Model validation regarding balancing power $P_{Cb,T}$, power losses of the balancing system $P_{Cb,Loss}$ and balancing system efficiency η_{Cb}. for an unbalancing situation of a weak cell voltage $V_{C,W}$ = 2 V and 3 strong cell voltages $V_{C,S}$= 3,65 V. a) Power losses and balancing power distribution for 6 different intramodule systems. Column nº1= ideal/lossless model. Column nº2: Power loss model. Columnnº3: Experimental results. b) Efficiency distribution of ideal/lossless, power loss modelled and experimental tests.

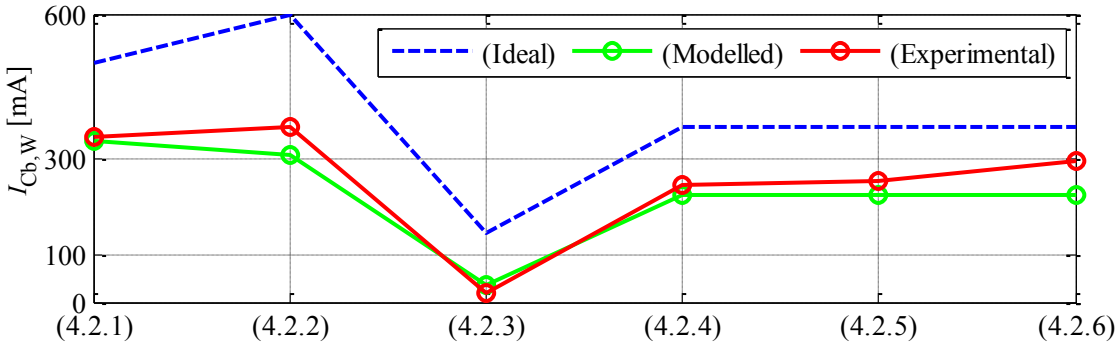

Fig 4.14 Model validation regarding weak cell balancing current. Ideal/lossless model balancing current, power loss modelled estimated current and real experimental current for an unbalancing situation of a weak cell voltage $V_{C,W}$= 2 V and 3 strong cell voltages $V_{C,S}$= 3,65 V.

balancing current approximation is presented in Fig 4.14. ideal modelling gives a good initial point to define the balancing current magnitude of an intramodule balancing system, however is highly different compared to real experimental values. The power loss model gives a better approximation of the weak cell balancing current real magnitude. Main characteristics are summaraized in Table 4.4. Power losses are neglected for simplification of the data table, however could be calculated with equation (4.35) for the modelled case and equation (4.43) for the experimental case. Ideal/lossless model power losses $P_{Cb,Loss}$ are assumed to be zero.

Table 4.4 Data resume for comparison between ideal/lossless, power loss modelled and experimental results of intramodule balancing systems for an unbalancing situation of a weak cell voltage $V_{C,W}$= 2 V and 3 strong cell voltages $V_{C,S}$= 3,65 V.

	$P_{Cb,T}$ [W]			η_{Cb} [%]			$I_{Cb,W}$ [mA]		
Topology	Ideal	Model	Exp.	Ideal	Model	Exp.	Ideal	Model	Exp.
4.2.1	1,997	1,672	1,708	100	80,55	80,78	500	337	345
4.2.2	2,198	1,809	1,991	100	78,54	73,13	600	305	364
4.2.3	0,578	0,324	0,366	100	21,57	20,74	144	37	20
4.2.4	1,461	1,175	1,163	100	75,66	83,24	365	222	242
4.2.5	1,461	1,175	1,256	100	75,66	80,7	365	222	254
4.2.6	1,461	1,174	1,508	100	75,62	77,99	365	222	294

4.5 Ideal/Lossless intermodule model

Intermodule balancing systems balance series connected modules inside a battery pack. During this subchapter ideal modelling equations and balancing system behaviour will be presented. The intermodule balancing system candidates should have next characteristics:

- Open loop balancing behaviour.
- Low complexity.
- Modularity in series connection of modules.
- Isolation.

The intermodule balancing system should guarantee a limited balancing current through the whole working range as was guaranteed by the DCM mode criteria in intramodule systems.

The battery pack voltage V_{BP} is divided into m series connected modules $V_{M,j}$, or the sum of the weak module $V_{M,W}$ and the m-1 strong modules $V_{M,S}$.

$$V_{BP}=\sum_{j=1}^{m} V_{M,j}=V_{M,W}+\sum_{\substack{S=1\\S\neq W}}^{m} V_{M,S} \tag{4.44}$$

The 2 candidates for intermodule balancing systems are a flyback based topology and a full bridge topology presented in Table 4.5. Both topologies present a transformer guarantying the isolation requirement between modules.

- Series connected Flyback (4.5.1).
- Parallel connected Full Bridge (4.5.2).

The series connected flyback presents a single switch per module, although is not selective (current is transferred to all modules), and the voltage of all the battery pack is

Table 4.5 Main characteristics of intermodule balancing system under study. Control, number of switches (S) inductors (L), transformers (T), isolation connection style, selectiveness and modularity behavior.

Topology	Control*	S	L	T	Isolation	Connection	Selective	Modularity
4.5.1	O.L	1	_	1	Yes	Series	No	Partial
4.5.2	O.L	4	1	1	Yes	Parallel	Yes	Total

*O.L=Open Loop

reflected in the switch (not totally modular). The parallel connected full bridge presents 4 switches per module in H-bridge configuration (Half bridge is also possible). Presents total modularity for modules connected in series because is not battery pack voltage dependent.

Main characteristics under analysis are equivalent than for intramodule balancing systems.

- Critical duty cycle D_C to guarantee open loop control.
- Weak module balancing current $I_{Mb,W}$.
- Strong cell balancing current $I_{Mb,S}$.
- Relation between weak and strong modules $I_{Mb,W}/I_{Mb,S}$

Modelling and design process is described in detail in **Annex A** and **Annex B**.

4.5.1 Series connected Flyback

The series connected Flyback based intermodule balancing system is presented in Fig 4.15. Each module is connected to a single switch and a transformer in a flyback configuration. The secondaries of the m connected intermodule systems are connected in series to transmit the energy between the different modules. The energy is inserted

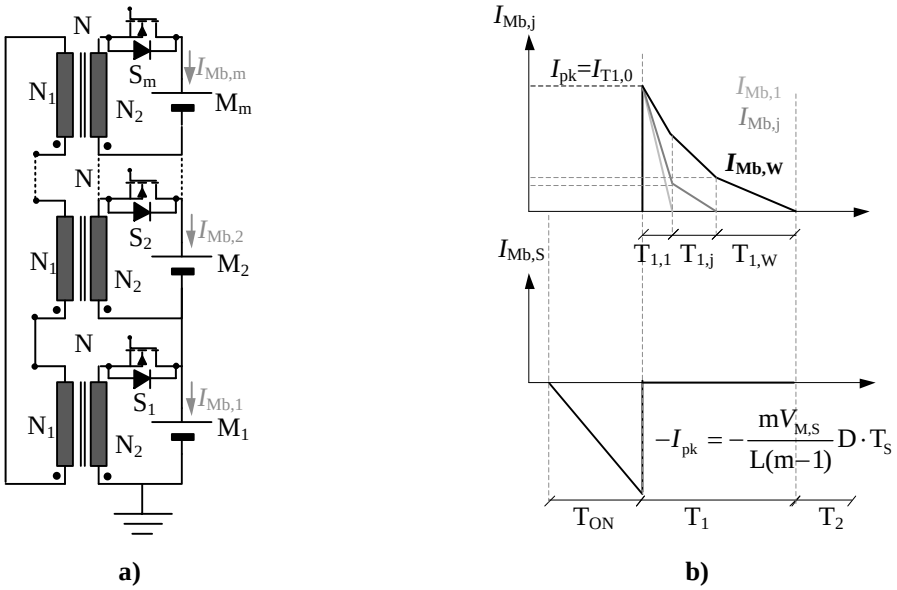

Fig 4.15. Series connected Flyback intermodule balancing system. a) m module battery pack balancing system circuit scheme. b) Main current waveforms for weak module(s) balancing current $I_{Mb,W}$ - $I_{Mb,j}$ and strong module balancing current $I_{Mb,S}$.

during T_{ON} and absorbed from the strong module $I_{Mb,S}$. This configuration permits to absorb the energy from a module that has not the bigger voltage, permitting to use a SOC based control instead of a voltage balance control strategy. During OFF (T_1) the energy is redistributed to all the modules inserting more current $I_{Mb,W}$ to the weak cell module. The redistribution is made via the intrinsic diode of the mosfets to reduce the number of components of the system. The current insertion time is dependent on each module voltage and the current falling slope changes once one module balancing current reaches zero current.

The main advantages are the possibility to select the strong module independent of the voltage and the modularity due to independent magnetic core transformers in each module. The disadvantages are that the battery pack voltage V_{BP} is reflected in the strong module switch, and that the redistribution of the strong module energy is not selective.

The critical duty cycle D_C and the module balancing currents are obtained with an iterative process presented in a flow chart in **Annex B B.2**. This process is made due to balance current slope change during OFF period T_1 in subsequent periods of $T_{1,z}$. where z is the number of series connected modules minus 1 (z=[1,m-1]).

$$T_1 = \sum_{z=1}^{m-1} T_{1,z} \qquad m = \text{number of modules} \tag{4.45}$$

The time periods $T_{1,z}$ are dependent on the initial current value of the module balancing current which is going to zero. However the current value is period dependent $T_{1,z}$ until the weak cell balancing current reaches zero. The initial current in $T_{1,0}$ is equal to I_{pk} as defined in Fig 4.15 b)

$$\begin{aligned} \frac{dI_{Mb,i}}{T_{1,z}} &= -\frac{V_{M,i}}{L} - \frac{V_{BP} - V_{M,S} - \sum_{k=1}^{z-1} V_{M,k}}{zL} \\ I_{Mb,i}\big|_{T_{1,z}} &= I_{Mb,i}\big|_{T_{1,z-1}} + dI_{Mb,i} \cdot T_{1,z} \end{aligned} \tag{4.46}$$

Defining $T_{1,z}$ as the interval when one balancing current reaches zero.

$$T_{1,z} \rightarrow I_{Mb,i}\big|_{T_{1,z-1}} - dI_{Mb,i} \cdot T_{1,z} = 0 \tag{4.47}$$

The strong module balancing current $I_{Mb,S}$ is directly defined by

$$I_{\mathrm{Mb,S}} = \frac{\mathrm{n}\, V_{\mathrm{M,S}} \mathrm{D}^2 \mathrm{T_S}}{(\mathrm{n\text{-}1})\mathrm{L}} \tag{4.48}$$

The critical duty cycle is iteratively calculated as

$$\mathrm{D_C} = 1 - \mathrm{D_1} = 1 - \frac{\mathrm{T_1}}{\mathrm{T_S}} = 1 - \frac{\sum_{z=1}^{m-1} \mathrm{T_{1,z}}}{\mathrm{T_S}} \rightarrow \mathrm{T_2}{=}0, \mathrm{D_2}{=}0 \tag{4.49}$$

4.5.2 Parallel connected Full bridge

The parallel connected Full Bridge or H-bridge presented in Fig 4.16 a) connects each series connected module to an H-bridge. The H-bridge switches an inductor LS connected to a transformer where the secondaries of all transformers are connected in parallel. The switches of each module Sj,1-Sj,4 and Sj,2-Sj,3 are complementary respectively. When the strong module H-bridge is switch on the weak module H-bridges receives the energy through the diodes Fig 4.16 b).

The main advantages of the parallel connected full bridge are the full modularity

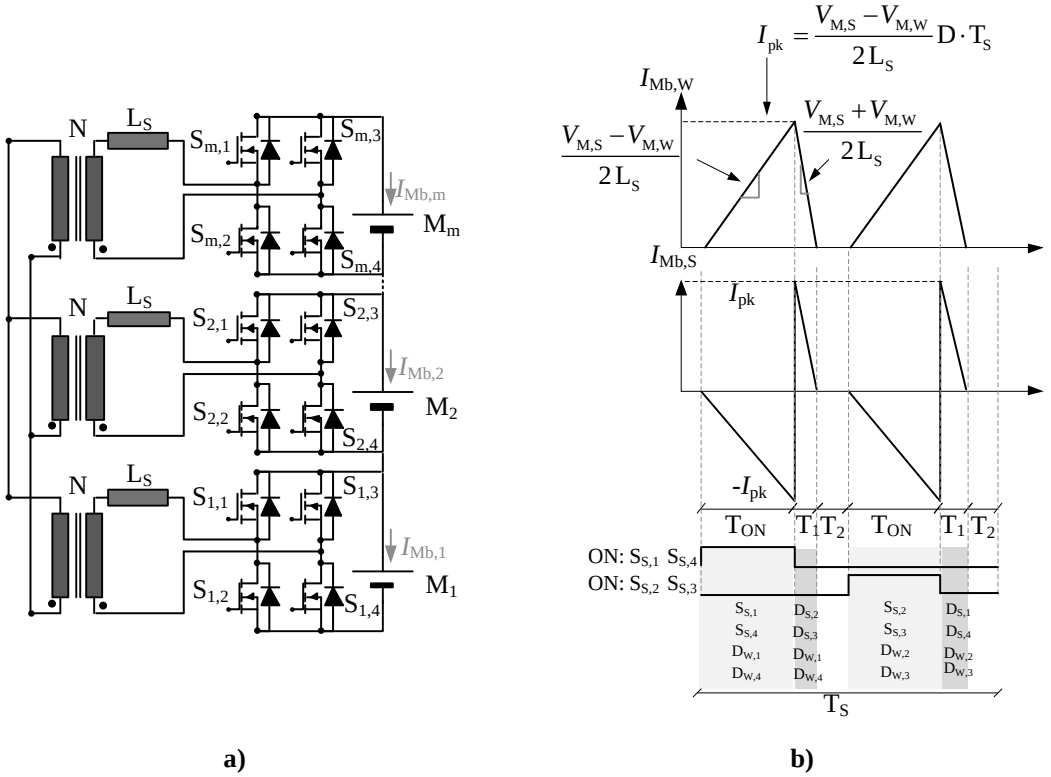

Fig 4.16. Paralell connected Full bridge intermodule balancing system. a) m module battery pack balancing system circuit scheme. b) Main current waveforms for weak module balancing current $I_{\mathrm{Mb,W}}$ and strong module balancing current $I_{\mathrm{Mb,S}}$.

of the system, because is not battery pack voltage V_{BP} dependent. m series modules could be connected without limit (ideal limit=isolation voltage of transformer). The switches control could be made in open loop configuration, with complementary signals between switches. It is also a selective balancing system transferring the energy directly to the weak cell module. The main disadvantage is that the current depends on the difference between weak module $V_{M,W}$ and strong module $V_{M,S}$, which gives low balancing currents with small voltage differences.

The critical duty cycle D_C to guarantee a T_2 period is in (4.50)

$$D_C = \frac{V_{M,S} + V_{M,W}}{4\,V_{M,S}} \tag{4.50}$$

During each period T_S the current is injected twice to the weak module $I_{Mb,W}$. The weak module balancing current $I_{Mb,W}$ and the strong module balancing current are expressed by equations (4.51) and (4.52). The energy transfer between the strong module and the weak module is equal to the two port transformer behaviour (4.53).

$$I_{Mb,W} = \frac{\left(V_{M,S} - V_{M,W}\right) D^2 T_s}{L_S \left(V_{M,S} + V_{M,W}\right)} V_{M,S} \tag{4.51}$$

$$I_{Mb,S} = -\frac{\left(V_{M,S} - V_{M,W}\right) D^2 T_s}{L_S \left(V_{M,S} + V_{M,W}\right)} V_{M,W} \tag{4.52}$$

$$\left|\frac{I_{Mb,W}}{I_{Mb,S}}\right| = \frac{V_{M,S}}{V_{M,W}} \tag{4.53}$$

With the control of the critical duty cycle D_C a period T2 could be guaranteed and reduce the balancing current. However the parallel connected full bridge could be switched in a constant 50% duty cycle ratio. In this configuration the D_C equation (4.50) gives the time period where the switches are conducting current (S_{ON}). Equations (4.51) and (4.52) are valid by substituting the duty cycle D value by the S_{ON}/T_S value. Power transfer equation (4.53) is valid for the constant D=0.5 switching value.

$$S_{ON,1\text{-}4} = S_{ON,2\text{-}3} = \frac{D_C}{T_S} \rightarrow \text{ eq } (4.50) \tag{4.54}$$

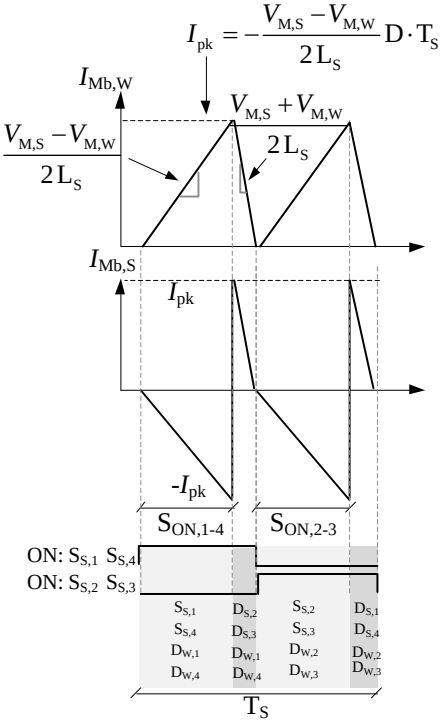

Fig 4.17. Paralell connected Full bridge intermodule balancing system current waveforms for a duty cycle of D=0.5. Main current waveforms for weak module balancing current $I_{Mb,W}$ and strong module balancing current $I_{Mb,S}$.

4.6 Intermodule power loss model

As presented with the intramodule balancing systems active balancing systems are not ideal 100% efficiency systems. When efficiencies lower than 95% are obtained the balancing current waveforms are highly distorted from ideal shape. As contributed during intramodule balancing systems design, an approach will be delivered to recalculate the real balancing currents and obtain more realistic intermodule balancing current values Fig 4.18. The parameters under study are for intermodule balancing systems are presented in next list.

- $I_{Mb,i}$ and $P_{Mb,i}$ lossless ideal current and power of the balancing system.
- $P_{Mb,Loss}$ representing the power losses of the balancing system.
- $I_{MbL,i}$ and $P_{MbL,i}$ which represent the accurate loss modelled current and power of the balancing system.
- The effiency η_{Mb} of the balancing system, which gives the idea of the energy transfer efficiency inside the balancing converter.

The power loss calculation and main current expressions for different balancing system components are presented in **Annex B B.2**.

4.6.1 Power loss and efficiency model

DCM and high current ripple behaviour of intermodule systems require the correct analysis of RMS and AV values of balancing currents in intermodule systems.

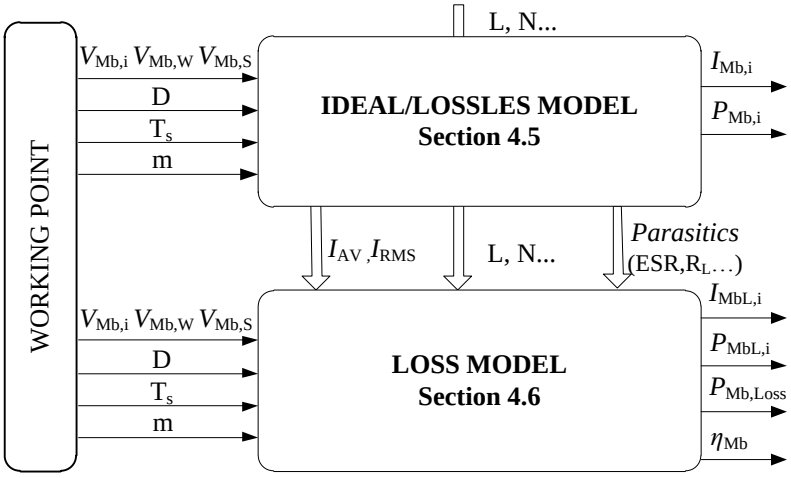

Fig 4.18. Flow chart presentation of the intermodule balancing system model strategy. Ideal/lossless model equations feed loss model.

As presented in (4.31) for intramodule systems RMS are different to AV currents in intermodule systems, complicating the power loss analysis. The non-ideal parameters that influence the balancing system parameters are:

- Power switch: Mosfet $R_{DS,on.}$
- Diodes: Forward Voltage V_D and conduction resistance R_D.
- Inductors and transformers: Series resistance R_L.

RMS and AV expressions are defined in **Annex B B.2** for different components inside the balancing system. The first step is to define the ideal/lossless balancing power for each intermodule balancing system as

$$P_{\mathrm{Mb,j}} = V_{\mathrm{M,j}} I_{\mathrm{Mb,j}} \tag{4.55}$$

With the total balancing power expressed by

$$P_{\mathrm{Mb,T}} = \sum_{\mathrm{j=1}}^{\mathrm{m}} V_{\mathrm{M,j}} I_{\mathrm{Mb,j}} \tag{4.56}$$

The power loss analysis of **Annex A A.2** and the expressions for RMS and AV variables presented in **Annex B B.2** are used to calculate the total power losses of the intermodule balancing system $P_{\mathrm{Mb,Loss}}$. The total real balancing power $P_{\mathrm{MbL,T}}$ is expressed as for intramodule systems by (4.57).

$$P_{\mathrm{MbL,T}} = P_{\mathrm{Mb,T}} - P_{\mathrm{Mb,Loss}} \tag{4.57}$$

The efficiency of the intermodule balancing system is modelled respect to ideal/lossless balancing power by

$$\eta_{\mathrm{Mb}} = \frac{P_{\mathrm{MbL,T}}}{P_{\mathrm{Mb,T}}} = \frac{P_{\mathrm{Mb,T}} - P_{\mathrm{Mb,Loss}}}{P_{\mathrm{Mb,T}}} \tag{4.58}$$

For the series connected flyback intermodule system presented in subchapter 4.5.1 the energy is obtained from the strong module and redistributed to all other modules. The value of the modelled intermodule balancing current $I_{\mathrm{MbL,j}}$ is then obtained by redistributing the power losses, The power losses are redistributed by the impact of each balancing current respect to the total balancing current.

$$I_{\mathrm{MbL,j}} = \frac{I_{\mathrm{Mb,j}} V_{\mathrm{M,j}} - \dfrac{P_{\mathrm{Mb,Loss}} \cdot I_{\mathrm{Mb,j}}}{\sum_{z=1}^{m} \left| I_{\mathrm{Mb},z} \right|}}{V_{\mathrm{M,j}}} \quad \begin{matrix} (\text{series connected Flyback}) \\ P_{\mathrm{Mb,Loss}} \xrightarrow{impact} I_{\mathrm{MbL,j}} \end{matrix} \tag{4.59}$$

The full bridge parallel connected intermodule balancing system only transfers energy between the strong module (ON module) and the weak module (Low voltage module). The power losses are redistributed by the difference between the ideal balancing current $I_{\mathrm{Mb,W}}$ and $I_{\mathrm{Mb,S}}$ as expressed in equations (4.60) and (4.61).

$$I_{\mathrm{MbL,W}} = \frac{I_{\mathrm{Mb,W}} V_{\mathrm{M,W}} - \dfrac{P_{\mathrm{Mb,Loss}} \cdot I_{\mathrm{Mb,W}}}{I_{\mathrm{Mb,W}} + I_{\mathrm{Mb,S}}}}{V_{\mathrm{M,W}}} \tag{4.60}$$

$$I_{\mathrm{MbL,S}} = \frac{I_{\mathrm{Mb,S}} V_{\mathrm{M,S}} - \dfrac{P_{\mathrm{Mb,Loss}} \cdot I_{\mathrm{Mb,S}}}{I_{\mathrm{Mb,W}} + I_{\mathrm{Mb,S}}}}{V_{\mathrm{M,S}}} \tag{4.61}$$

Intermodule balancing systems have active switches in each j module of the battery pack, and can transfer energy between modules even if the modules are balanced. Therefore, the efficiency is not zero as for the intramodule balancing systems equation (4.39).

4.7 Intermodule balancing system validation

In order to evaluate the intermodule balancing equations presented during subchapters 4.5 and 4.6, 2 prototypes of both intermodule balancing systems are designed to compare their behaviour and balancing characteristics. The 2 prototypes are presented in **Annex C C.2**. The 2 prototypes help to evaluate the ideal and power loss based balancing current models.

The intermodule balancing system prototypes are designed for 4 module series connection. Each module is composed by 4 LFP cells connected in series. The intermodule balancing systems are designed for a 16S1P battery pack in a 4 module configuration (m=4 n=4 4Mx4S1P). The critical duty cycle D_C will be defined for the worst unbalance case, where one module is fully discharged (4x2 V= 8 V) and 3 modules are fully charged (4x3,65 V = 14,6 V) The switching frequency is set to 100 kHz to make a compact design. The weak module balancing current $I_{Mb,W}$ has been set to 400 mA for the full bridge parallel design. For the series connected flyback a design restriction has been presented due to high current for available transformers. With the critical duty cycle D_C = 0,62 the maximum current on the transformer is very high for the available 22µH inductance transformer, therefore the duty cycle is limited to D = 0,25 due to the maximum allowable current constraint.

The intermodule balancing system gate signals are generated by the same function generator presented in intramodule systems (GW INSTEK AFG-2005 Arbitrary Function Generator). The experimental power $P_{MB,j}$, current $I_{Mb,j}$ efficiency η_{Mb} and power losses $P_{Mb,Loss}$ are measured by the same test bench used for the intramodule

Table 4.6 Desing and prototype values for 4Mx4S1P intermodule balancing systems presented from subchapters 4.5.1 and 4.5.2.Design parameters: m=4 $V_{Mb,W}$=8 V $V_{Mb,S}$=14,6 V switching frequency 100 kHz (T_S=10 µS)

Topology	Design				Prototype			
	$I_{Mb,W}$ [mA]	D_C [ ]	L_S[1] [µH]	N [ ]	$I_{Mb,W}$ [mA]	D [ ]	L_S[1] [µH]	N [ ]
4.5.1	125	0,25 (0,62)[2]	22	1	125	0,25	22	1
4.5.2	400	0,387	15,95	1	427	0,4	15	1

[1] In Flyback design L_S is referred as the transformer magnetizing inductor L.

[2] Critical duty cycle 0,62 not affordable due to excessive maximum current in transformer

systems (HAMEG HM7042-5 and R_{PS} power resistor in parallel to simulate a battery module system). The parameter measurements are carried out with the same steps as presented in Fig 4.10 and with equations (4.40) to (4.43). The number of cells for the intramodule "n" is substituted by the number of modules "m" for the intermodule systems.

The validation and behavioural analysis of the 2 intermodule balancing systems will be held under 3 points of view.

- **Unbalanced situation:** The intermodule balancing systems will be tested under different unbalancing situations.
- **Balanced test:** The intermodule balancing systems are tested under balanced situation, to see the functionality to absorb current from the strong module even if the modules are voltage balanced.
- **Model comparative evaluation:** The intermodule balancing models will be compared to experimental values obtained in the tests.

The first test will analyse the unbalancing behaviour of the intermodule balancing systems under 4 different scenarios. The weak module or low voltage module will be the module number 1 and the strong module the numbers 2-3-4 (j=[1,4]). The switched module is always the 4th module. The experimental result summary is presented in

Table 4.7 Module balancing current $I_{Mb,j}$ for different unbalance scenarios. The switching module is the number m=4. Low voltage unbalance, nominal voltage unbalance, extreme unbalance and variable unbalance results.

Unbalance scenario	**Topology**	$I_{Mb,j}$			
		$I_{Mb,1} = I_{Mb,W}$ [mA]	$I_{Mb,2}$ [mA]	$I_{Mb,3}$ [mA]	$I_{Mb,4} = I_{Mb,S}$ [mA]
Low voltage unbalance	4.5.1	44	42	42	-165
	4.5.2	11	3	3	-54
Nominal voltage unbalance	4.5.1	57	54	54	-170
	4.5.2	13	4	4	-79
Extreme unbalance	4.5.1	73	60	60	-186
	4.5.2	217	0	0	-209
Variable unbalance	4.5.1	70	68	64	-178
	4.5.2	194	9	1	-205

Table 4.7. 4 different scenarios will be presented for study:

- Low voltage unbalance: The unbalancing will simulate an unbalancing behaviour where all the modules are near complete discharge (cells near 2 V). The weak module $V_{M,W}$= 8V and the strong modules $V_{M,S}$ = 8,4V.
- Nominal voltage unbalance: An unbalance between modules where the module is simulated to have values near cell "plateau" voltage. The weak module is set to $V_{M,W}$= 12,4 V (4·3,1 V) and the strong modules $V_{M,S}$= 12,8 V (4·3,1 V).
- Extreme unbalance situation: The modules are set to the worst unbalance situation with the weak module $V_{M,W}$= 8 V and the 3 strong modules $V_{M,S}$= 14,6 V.
- Variable unbalance: The 4 modules are set to a variable voltage unbalance to evaluate the balancing system characteristics. The modules are set to $V_{M,1}$= 8 V, $V_{M,2}$= 10 V, $V_{M,3}$= 12 V and $V_{M,4}$= 14 V.

All the unbalance scenarios presented in Table 4.7 give the clear result that natural balancing process is executed for all the different scenarios.

During low voltage module unbalance series connected flyback extracts more energy than the parallel connected full bridge from the strong module. The energy is redistributed to all the other modules with slightly higher current for the weak module in series connected flyback. The other modules obtain the same balancing current as they have the same voltage. The parallel connected full bridge inserts low current to the weak module (11 mA), but nearly zero current (3 mA) to the other modules due to its selective behaviour. In nominal voltage unbalance the behaviour is similar. The series flyback increases the current due to higher magnetizing voltage. However the parallel connected flyback gives similar currents because the current depends on the difference between the weak and strong module voltages. During extreme unbalance the current in series connected flyback does not increase much, although the difference between the weak module current ($I_{Mb,1}$=$I_{Mb,W}$) and other modules current($I_{Mb,2}$, $I_{Mb,3}$) increases. The parallel connected full bridge increases highly the current difference between the weak and strong module. This is due to a higher voltage difference. The current inserted to other modules is zero ($I_{Mb,2}$=$I_{Mb,3}$=0) keeping the selective behaviour. For the variable

unbalance scenario the current distributed to all the modules is depedent on the voltage of each module for the series connected flyback. The low voltage module j=1 receives more current than the higher voltage module j=3. For the parallel connected full bridge the balancing current also depends on the voltage difference between the strong and the weak module voltages. The system behaviour is selective, although a very little current flows to the second weak module j=2.

The intermodule balanced analysis has been simulated for the situation where all the modules are fully charged. This situation permits to evaluate the behaviour of the intermodule balancing systems for the situation where all the cells are charged. In contrary to the intramodule single switch balancing systems the intermodule systems could transfer energy between modules even if the modules are balanced. This is because a switching element is presented in each module stage. During the tests, the switched intermodule system is the 4^{th} module m=4. The balancing current results are presented in Table 4.8.

The series flyback converter has higher current capacity when the modules are balanced because the strong module current is only dependent on the module voltage. The parallel connected full bridge ideally would not insert any current into the modules, however a current flows due to the non-idealities of the components and specially due to the effect of the magnetizing inductance of the transformer (L_M 220 µH, L_S 15 µH). In both intermodule balancing systems the energy transferred to all the weak modules is equal giving good balancing performance with no deviation between balancing currents.

The comparison between the ideal/lossless model and the power loss model with the experimental results is made in the extreme unbalance scenario with $V_{M,W}$= 8 V and 3 strong modules $V_{M,S}$= 14,6 V. The balancing power results $P_{Mb,T}$ and $P_{Mb,Loss}$ are

Table 4.8 Module balancing current $I_{Mb,j}$ for a fully charged balanced scenario. The switching module is the number j=4.

Balanced scenario	**Topology**	$\boldsymbol{I_{Mb,j}}$			
		$I_{Mb,1}$ [mA]	$I_{Mb,2}$ [mA]	$I_{Mb,3}$ [mA]	$I_{Mb,4}$ [mA]
Fully charged	4.5.1	50	50	50	-188
	4.5.2	10	10	10	-90

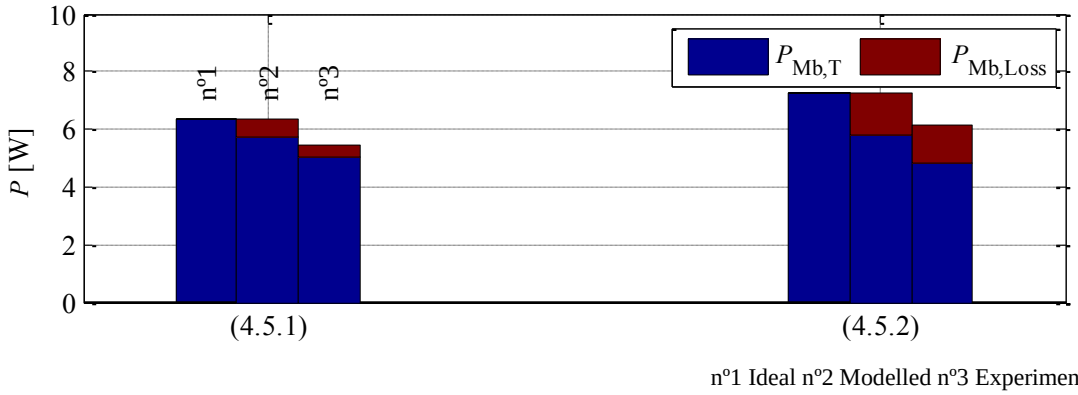

Fig 4.19 Model validation regarding balancing power $P_{Mb,T}$ and power losses of the balancing system $P_{Mb,Loss}$ for an unbalancing situation of a weak module voltage $V_{M,W}$ = 8 V and 3 strong module voltages $V_{M,S}$= 14,6 V. Power losses and balancing power distribution for 2 different intermodule systems. Column nº1= ideal/lossless model. Column nº2: Power loss model. Columnnº3: Experimental results.

presented in Fig 4.19. Bigger power capability is presented for ideal and power loss models. The reason is the higher inductance of experimental prototypes due to series and parallel connection of transformers secondaries. The ideal/lossles models gave good initial point for evaluation of the balancing behaviour and capability of the intermodule systems. However, for good accuracy the power losses models based on AV and RMS currents presented in **Annex B B.2** have to be used.

The series connected flyback presents high efficiency η_{Mb}= 92,18. Low current and energy transfer from strong module to weak modules are the key for high efficiency.

The parallel connected full bridge has lower efficiency than the series connected flyback system (η_{Mb}=72,29), because high number of semiconductors are switched on in each energy transfer (2 mosfets and 2 diodes during ON; 4 diodes during OFF). The parallel connected inductor should be controlled to avoid high mismatch between modelling and experimental results.

Table 4.9 Data resume for comparison between ideal/lossless, power loss modelled and experimental results of intermodule balancing systems for an unbalancing situation of a weak module voltage $V_{M,W}$= 8 V and 3 strong module voltages $V_{M,S}$= 14,6 V.

	$P_{Mb,T}$ [W]			η_{Mb} [%]			$I_{Mb,W}$ [mA]		
Topology	Ideal	Model	Exp.	Ideal	Model	Exp.	Ideal	Model	Exp.
4.5.1	6,345	5,72	5,037	100	89,07	92,18	125	102	73
4.5.2	7,27	5,77	4,8	100	74	72,29	426	342	217

4.8 Conclusions of the chapter

During the present chapter a modular active balancing system approach has been presented, divided in intramodule and intermodule balancing systems. Intramodule systems balance the cells inside a module and intermodule systems balance the modules inside the battery pack balancing the whole system.

Main criterias for balancing system selection are:

- Simplicity.
- Open loop control strategy.

The consolidation of these characteristics is basic for finding an active balancing system that could finally compete against passive balancing systems.

During the chapter an ideal/ lossless modelling approach has been presented for intramodule and intermodule systems. This first approach model is a good initial point to analyse the behaviour and characteristics of balancing systems. However if high accuracy is needed the power loss model has to be taken into account, to recalculate the balancing currents.

Main conclusion for intramodule systems is that good balancing behaviour is presented only using a single active switch in open loop control mode. Multiple core series connected flyback is the less suitable system due to non-selective behaviour. Table 4.10 presents main advantages and disadvantages of presented topologies. Transformer based topologies give a freedom degree for the duty cycle determination. For single switch balancing systems the duty cycle should be higher than 5 % (critical duty cycle design D_C>5%) to avoid high peak currents. The minimum duty cycle will limit the maximum number of series connected Li-ion cells. Sepic, Zeta and Isolated Cuk designs are better balancing options because it is easier to find commercial inductors than transformers.

Good repeatability is presented independent of the weak cell position inside the module. Under balanced situation there is not power distribution between cells, only the power losses of the converter are compensated.

Table 4.10 Main advantages and disadvantages of the analysed intramodule and intermodule balancing systems.

Topology	Advantages	Disadvantages
4.2.1	• Duty cycle extension with transformer ratio	• Transformer non modular
4.2.2	• Modular • Duty cycle extension with transformer ratio	• Higher current paths
4.2.3	• Duty cycle extension due to transformer ratio	• Non selective • Low balancing capability
4.2.4	• Low side switch • No transformers	• Limited in duty cycle
4.2.5	• No transformers	• Limited in duty cycle • High side switch
4.2.6	• Duty cycle extension with transformer ratio	• Transformer and extra capacitor
4.5.1	• High efficiency	• Voltage dependent • Not totally modular • Not selective
4.5.2	• Totally modular. Independent of battery pack voltage • Selective	• 4 switches per full bridge

.

Intermodule balancing systems present good behaviour for module balancing with open loop switching control. Intermodule balancing systems permit to select the strong module independent of the voltage of the module, even if the modules are balanced if the intermodule balancing system is switched on the energy is transferred between modules. The series connected flyback converter gives high efficiency, but the modularity is dependent on the battery pack voltage. The components should be selected for the battery pack voltage specifications. The parallel connected full bridge gives total modularity against battery pack voltage, the components are only dependent on the module voltage. The balancing current is dependent on the difference between the strong module (high voltage module) and the weak module (low voltage module). If low voltage difference is presented low balancing current is injected. The parallel connected full bridge has lower efficiency than the series connected flyback. However is totally selective transferring the energy directly from the strong module to the weak module.

Chapter 5

METHODOLOGY FOR BALANCING SYSTEM DESIGN

During this chapter main equations related to balancing system design are presented. The general equations are suitable for design any type of balancing system architecture.

The first subchapter determines the main equations for a balancing procedure between two cells inside a series connected battery pack.

Second subchapter presents a methodology based on single cell tests to design and evaluate a balancing system performance. The methodology permits to interpret balancing system performance by the use of single cell tests, decreasing the modelling effort requirement. The single cell test based methodology is presented in [PAPER C2].

The third subchapter presents a 16S1P battery pack balancing system design based on previously acquired knowledge. The balancing system is designed with active intramodule and intermodule balancing systems.

5.1 Battery pack balancing theory

A series connected battery pack balancing system is defined to compensate the unbalance between two series connected cells, specifically between the strong cell and the weak cell inside a module. The State Of Charge unbalance ΔSOC is defined as the difference between the SOC of the strong cell SOC_S and the weak cell SOC_W.

$$\Delta SOC_{INI} = SOC_{S,INI} - SOC_{W,INI} \tag{5.1}$$

Ideally the balancing system should meet the requirement that all the cells, and in our case the strong and the weak cell, are balanced (ΔSOC=0). However for practical issues an SOC threshold (ΔSOC_{TH}) is defined. If ΔSOC_{TH} is defined zero, the balancing system will be kept in continuous instability because ΔSOC=0 is practically impossible. Behind ΔSOC_{TH} threshold dispersion the battery pack is considered balanced.

$$\Delta SOC_{TH} \leq SOC_S - SOC_W \quad \rightarrow \text{balanced} \tag{5.2}$$

The balancing SOC (SOC_{Cb}) is them defined by the necessary energy to reduce cell unbalance behind ΔSOC_{TH} from an initial SOC, $SOC_{S,INI}$ and $SOC_{W,INI}$.

$$SOC_{Cb} = \Delta SOC_{INI} - \Delta SOC_{TH} = SOC_{S,INI} - SOC_{W,INI} - \Delta SOC_{TH} \tag{5.3}$$

Equations (2.3) and (2.4) define the SOC of the weak and strong cell as

$$SOC_S = \frac{Q_S}{SOH_S \cdot Q_{Nom}} 100^2 \tag{5.4}$$

$$SOC_W = \frac{Q_W}{SOH_W \cdot Q_{Nom}} 100^2 \tag{5.5}$$

The balancing SOC SOC_{Cb} depends on the weak cell current $I_{C,W}$ and the strong cell current $I_{C,S}$. during the balancing time T_{Cb}.

$$SOC_{Cb} = \frac{\int_0^{t_{Cb}} I_{C,W} dt}{\frac{SOH_W \cdot Q_{Nom}}{100}} - \frac{\int_0^{t_{Cb}} I_{C,S} dt}{\frac{SOH_S \cdot Q_{Nom}}{100}} \tag{5.6}$$

The weak and strong cell current as defined by equation (4.1) could change for different scenarios.

- Balancing while cycling: $I_{C,W}$ and $I_{C,S}$ depend also on battery pack current I_{BP}.
    - Non modular (passive balancing, etc.):

        - $I_{C,W}=I_{BP}+I_{Cb,W}$.
        - $I_{C,S}=I_{BP}+I_{Cb,S}$.
    - Modular balancing systems:
        - $I_{C,W}=I_{BP}+I_{Cb,W}+I_{Mb,W}$.
        - $I_{C,S}=I_{BP}+I_{Cb,S}+I_{Mb,W}$.
- Balancing in standby: No application current, $I_{BP}=0$;
    - Non modular (passive balancing, etc.):
        - $I_{C,W}=I_{Cb,W}$.
        - $I_{C,S}=I_{Cb,S}$.
    - Modular balancing systems:
        - $I_{C,W}=I_{Cb,W}+I_{Mb,W}$.
        - $I_{C,S}=I_{Cb,S}+I_{Mb,W}$.

If the SOH of the weak and strong cell is equal, only the balancing current contributes to the unbalancing compensation between series connected cells, because I_{BP} is equal for all series connected cells.

Redefining equation (5.3) for ΔSOC_{TH} definition and by the use of (5.4)-(5.6) the ΔSOC_{TH} limit is reached when

$$\begin{aligned} \Delta SOC_{TH} &= SOC_{S,INI} - SOC_{W,INI} - SOC_{Cb} \\ \Delta SOC_{TH} &= \frac{Q_{S,INI}}{SOH_S \cdot Q_{Nom}} 100^2 - \frac{Q_{W,INI}}{SOH_{W,INI} \cdot Q_{Nom}} 100^2 - \\ &\quad - \left(\frac{\int_0^{t_{Cb}} I_{C,W} dt}{\frac{SOH_W \cdot Q_{Nom}}{100}} - \frac{\int_0^{t_{Cb}} I_{C,S} dt}{\frac{SOH_S \cdot Q_{Nom}}{100}} \right) \end{aligned} \tag{5.7}$$

As could be seen in (5.7) the balancing system requirement is fully dependent on 4 relations or parameters.

- The initial SOC unbalance between cells.
- The relation between the weak cell current $I_{C,W}$ and the strong cell current $I_{C,S}$.
- The threshold SOC ΔSOC_{TH} where the battery pack is considered balanced.
- The balancing time t_{Cb}.

In most series connected battery applications, cells are voltage balanced (Equal voltage between series connected cells), so the target threshold SOC ΔSOC_{TH} is converted to a target voltage threshold $\Delta V_{C,TH}$.

5.2 Iterative methodology based on single cell tests

In order to simulate the behaviour of a balancing system in a series connected battery pack a battery model is necessary, with different behaviour of each cell inside a battery pack. 3 main battery models are:

- Electro chemical models.
- Analytical and mathematical models.
- Electrical models.

Electro chemical interaction models are the most accurate models representing the real behaviour of a cell. They are based on the knowledge of internal electrochemical reactions to model battery behaviour [102]. The disadvantages are the big computational cost and usually a limited knowledge of the internal structure of the cell [103].

Analytical and mathematical models are based on statistical and analytical expressions based on specific test. Analytical models offer usually expressions about aging, temperature dependency and capacity derating as Peukert [104], [105] and Arrhenius Laws [106], [107]. The disadvantage is that the voltage dynamics are not represented by these models.

Electrical models represent battery behaviour with a combination of electrical sources and impedances. They present good accuracy and low computational cost. The disadvantages are bad voltage modelling in extreme high and low *SOC*s, and high number of tests for good modelling [108]–[110].

For the electronic/electric point of view the electrical model presents the best choice regarding accuracy and knowledge. Therefore for an engineering point of view

Table 5.1 Comparison between main battery cell models

Model	Advantage	Disadvantage
Electro chemical	High accuracy	Computational cost, cell structure knowledge
Analytical/mathematical	Selective	Low accuracy, no voltage dynamics
Electrical	Good accuracy	Differences in extremes, high number of tests for modelling

two types of tests are carried out for specific cells:

- **Modelling tests**: Cell modelling tests (Impedance spectroscopy tests EIS, pulse tests, etc.)
- **Application tests**: Specific tests carried out to determine if the cell is useful for a specific application.

During this research work a simulation approach has been presented that uses specific application test data to evaluate balancing system performance behaviour. With this approach the need of modelling tests is avoided, and the total design procedure time is reduced. The methodology flowchart is presented in Fig 5.1.

The first step **TEST** evaluates single cells under application requirements. A lookup table is generated with the dependency between the capacity Q_i and voltage $V_{C,i}$ of each cell. These characteristics permit to evaluate:

- Dispersion in capacity between cells due to manufacturing process.
- Specific voltage dynamics under application behaviour.

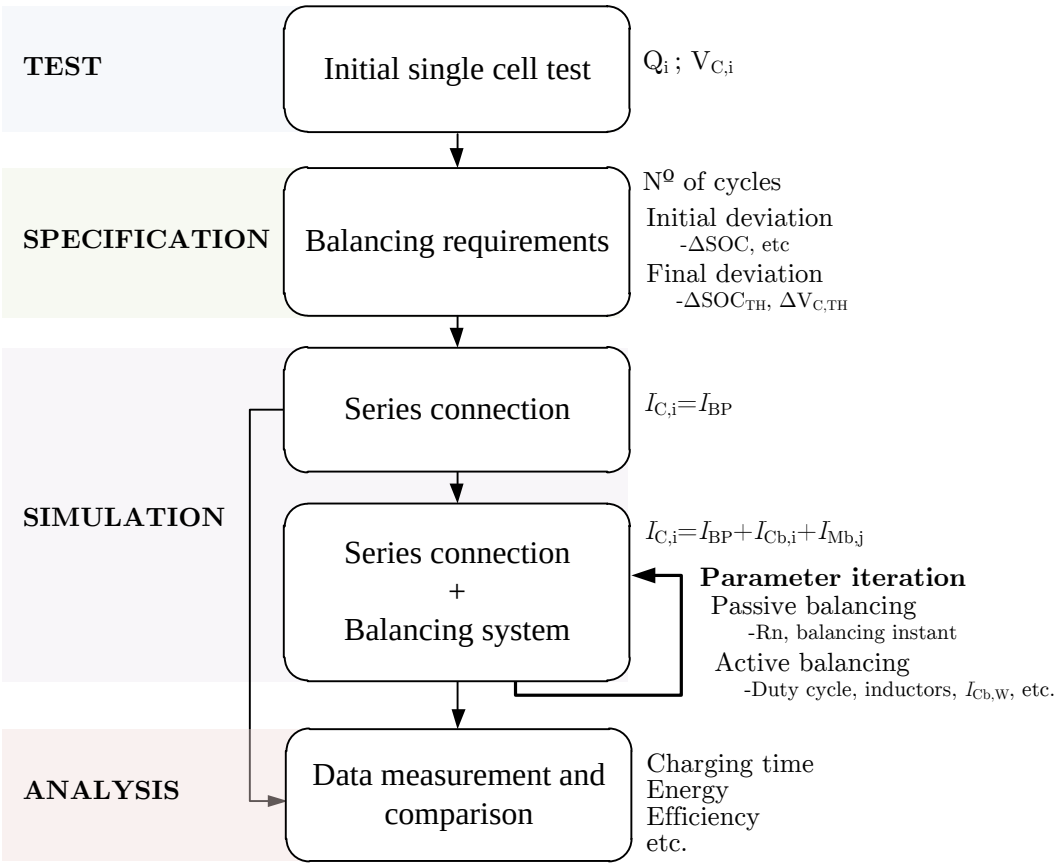

Fig 5.1. Iterative single cell test based balancing system methodology design.

The second step **SPECIFICATION** defines the balancing system actuation criteria with some basic definitions:

- Balancing threshold parameter: ΔSOC_{TH}, $\Delta V_{C,TH}$.
- Balancing time: Number of cycles, balance during charge, discharge, charge-discharge, charge CV period, etc.
- Initial cell deviation: deviation between cells.

During third step **SIMULATION** first the cells are simulated in series connection without balancing. Each cell current $I_{C,i}$ is equal to battey pack current I_{BP}. The integral of each current is inserted to the lookup table as the capacity Q_i. After that the balancing system is connected. The balancing current should be much smaller than the application current not to alter the voltage-capacity dynamics. The cell current is now the battery pack current I_{BP} plus the balancing current of each cell as defined in equation (4.1). The simulation is repeated iteratively to evaluate the sensibility of the series connected battery pack under different balancing system parameters:

- Passive balancing: variation of balancing resistor value R_n.
- Active balancing: variation of duty cycle, inductor value, etc. for intramodule and intermodule balancing systems.

The last step **ANALYSIS** will evaluate the behaviour of the battery pack under different balancing system configurations.

- Energy, efficiency and power losses of the balancing system.
- Charging time, etc.

5.2.1 4S1P passive balancing system iterative design

The iterative process has been implemented for the design of a 4S1P battery pack with passive balancing. The battery pack is performed by 4 LFP Q_{Nom}= 6,5 Ah cells. The passive balancing system is designed for a typical constant current constant voltage charging mode CCCV.

The first step **TEST** charges the 4 cells individually from totally discharged to totally charged under the application requirements of CCCV. The application requirements are presented in Table 5.2. The CC process is done under C/2 current rate

Table 5.2 Application characteristic parameters for a CCCV charging mode.

Application	CCCV		DOD
	CC	CV	
CCCV charge process	C/2	3,65 V until C/20	0-100% (full charge)

and the CV process is made at 3,65 voltage limit until the current decreases to C/20. The single cell test analysis permits to evaluate the capacity deviations presented between the 4 cells under test Table 5.3. If a bigger dispersion analysis is needed, more cells could be tested under the application requirements.

The balancing system **SPECIFICATION** step parameters are defined as:

- **Nº of application cycles:** balancing process during one single charge process.
- **Initial deviation:** All cells fully discharged, SOC =0%, ΔSOC=0.
- **Balancing threshold:** Voltage balancing threshold $\Delta V_{C,TH}$=15 mV.

During **SIMULATION** process the cells are initially connected in series without any balancing system to evaluate the unbalancing behaviour. The biggest unbalancing situation is always held during charge and discharge elbow in LFP technology, where the voltage derivatives are sharper. In this application as the cells are initially discharged, the unbalancing process is bigger during charge elbow.

During the balancing system design an iteration based on the balancing resistor R_n has been implemented. The balancing resistor is iterated from 3 Ω value by 1 until 50 Ohms value R_n=[3:1:50].

The **ANALYSIS** process results are presented in Fig 5.2. The compared parameters are:

- Maximum voltage difference ΔV_{Max}: The maximum voltage difference

Table 5.3 Capacity dispersion between cells under CCCV charging mode. Percentage capacity values respect to Q_{Nom}=6,5 Ah

$Q_{Max,1}$	$Q_{Max,2}$	$Q_{Max,3}$	$Q_{Max,4}$	ΔQ_{Max}	Q_{AV}
7,273	7,51	7,59	7,314	0,317	7,42
112%	115%	117%	112%	4,9%	114%

presented between the 4 series connected cells.

- Wasted energy in balancing system W_{Rn}: The energy wasted in the balancing resistor is evaluated during charge.
- Charging time t_C: The total charging time depending on the balancing resistor.
- Each cell SOC SOC_n: The estimated SOC of each cell is compared.

The minimum voltage difference is presented with lower balancing resistors values Fig 5.2 a). The voltage difference between cells is defined by the index parameters ($|V_1-V_2|$=12). Balancing resistors higher than 10 Ω stabilize the voltage difference near 160 mV. The energy wasted in the balancing resistor increases in an exponential way for low resistor values Fig 5.2 b). This parameter could be critical for origination of hot spots near the battery cells. The charging time Fig 5.2 c) increase with lower resistor values. It is also an important parameter for battery pack and balancing system design. However with the time increase the SOC reached by each cell after charge is also increased with low resistor values Fig 5.2 d).

For the comparison between the simulation approximation and the experimental results a test bench has been implemented with a 4S1P battery pack with a balancing resistor of R_n=12 Ω. The comparison between the experimental results and the simulation tests are presented in Table 5.4 for the main interesting design parameters.

Simulation and experimental results present really good concordance for the scenario without balancing system. The application current is equal to the single cell test currents ($I_{BP}=I_{C,i}$) so it is normal to obtain a good simulation approach. The comparison between the simulation and the experimental results differ with the the balancing system connection. This is due to little deviation in voltage characteristics, because the cell current is the application current I_{BP} plus the injected balancing current $I_{Cb,i}$ ($I_{C,i}=I_{BP}+I_{Cb,i}$). However good accuracy is presented regarding charging time and maximum voltage and SOC deviation are reduced respect to simulation results. The reduction is due to higher balancing time in experimental results and consequently higher resistor energy $W_{Rn,Max}$.

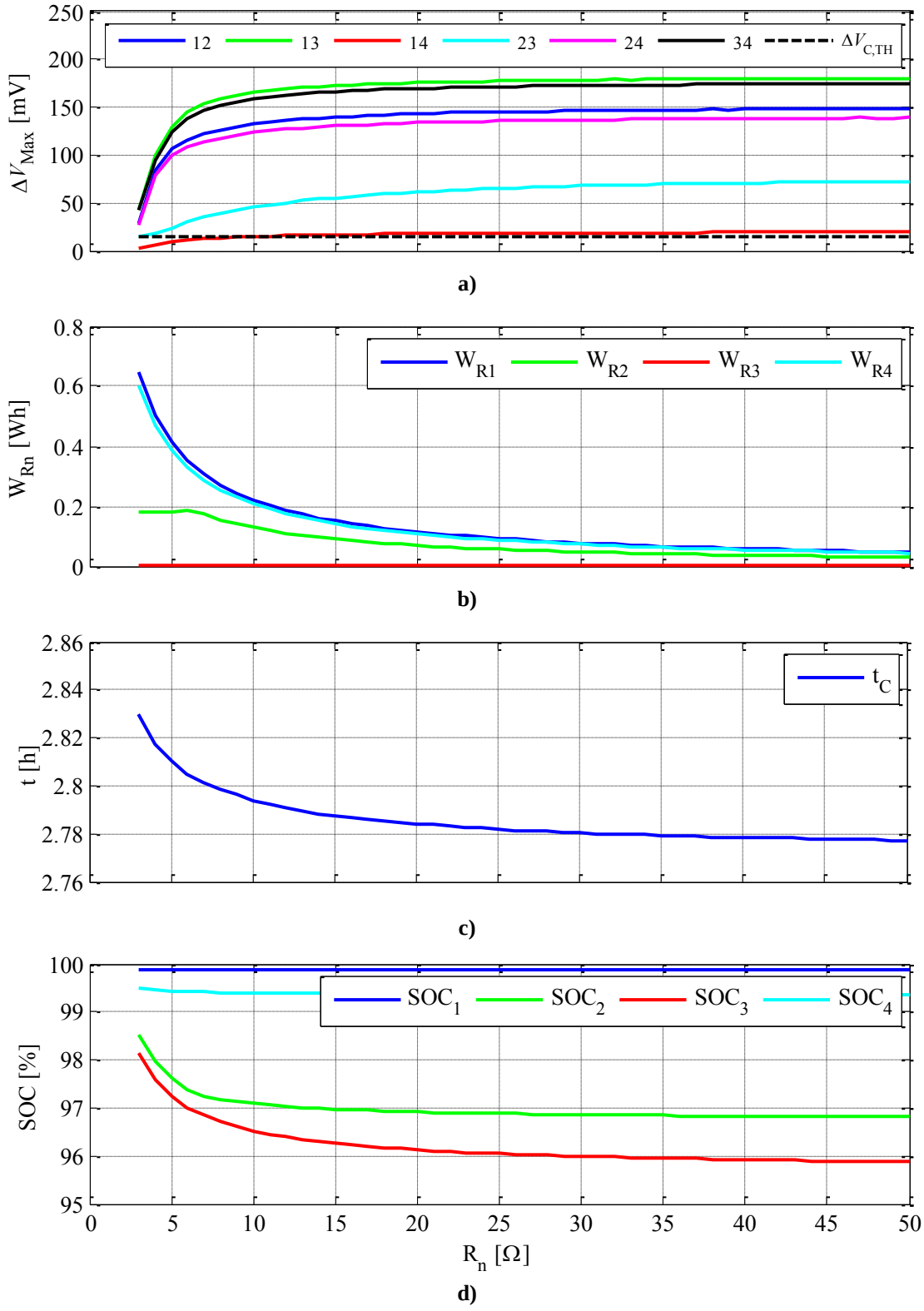

Fig 5.2. Iterative balancing system simulation results respect to R_n iterative value change. a) Maximum deviation between cells ΔV_{Max}, b) Energy wasted in one balancing resistor $W_{Rn,Max}$ c) System charging time t_C. d) Final SOC after charge process.

Table 5.4 Parameter comparisons for a CCCV charging mode for a 4S1P battery pack with and without balancing system. Simulation and experimental comparison. Maximum deviation between cells ΔV_{Max}, maximum deviation in SOC ΔSOC_{Max}, maximum energy wasted in one balancing resistor $W_{Rn,Max}$ and series connected system charging time t_C.

Scenario	Mode	ΔV_{Max}[mV]	ΔSOC_{Max}[%]	$W_{Rn,Max}$[Wh]	t_C [h]
Series connection	Simulation	181	4,182	_	2,796
	Experimental	182	4,2	_	2,802
Series and balancing	Simulation	169	3,609	0,186	2,81
	Experimental	75	1,976	0,39	2,825

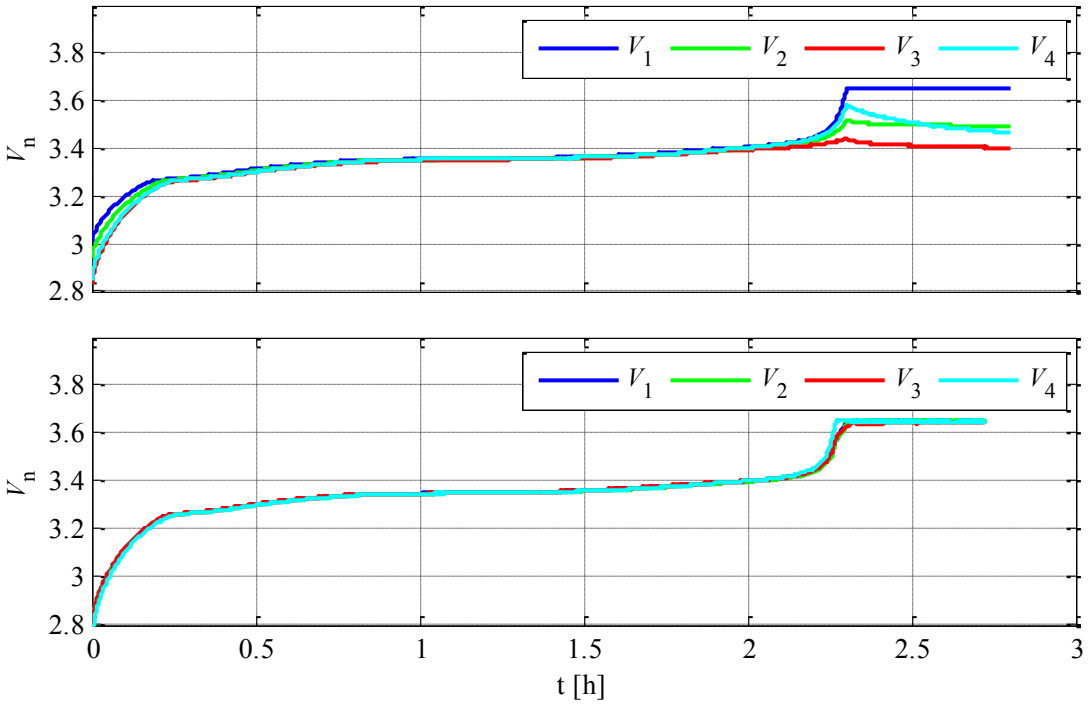

Fig 5.3. Comparison for a CCCV charge process. Experimental results presenting cell voltage charge dynamics. a) Without balancing system. b) With passive balancing system R_n=12 Ω..

5.3 Knowledge based balancing system design

Battery balancing systems are generally designed by knowledge acquired during battery pack cycling. Series connected cells phenomena analysis, permit to decide the magnitude of the balancing current redistributed between the weak cell and the strong cell(s) of the battery pack.

During the Thesis work, and specially focusing in series connected LFP cells, main series connected cells phenomena are:

- LFP cells do not present any unbalance behaviour due to cycling, the differences presented are due to dispersion in initial capacities, so:
  - Small balancing current for equal SOH cells ($I_{Cb,W}$-$I_{Cb,S}$ < 1 A)
  - High balancing current for different SOH cells ($I_{Cb,W}$-$I_{Cb,S}$ >1 A).
- Unbalancing differences could appear due to BMS and monitoring systems.
  - High impedance and low consumption systems should be used.

With this previously acquired knowledge the system designer leads to a balancing system design problem, to be solved with the equations presented in subchapter 5.1. Equation (5.6) determines the relation between the weak cell balancing current $I_{Cb,W}$ and the strong cell balancing current $I_{Cb,S}$, the balancing time $t_{Cb,}$ taking into account the initial deviations between the weak and strong cell state of health (SOH_W and SOH_S).

The battery pack mechanical lay-out configuration it is also an important parameter for balancing system design. Battery cells disposition could be defined for a modular balancing system configuration.

5.3.1 16S1P LFP modular battery pack design

The knowledge acquired during the previous thesis work regarding unbalancing effects in series connected cells, the equations presented in subchapter 5.1 and the analysis of modular systems in Chapter 4, give the basis to design a series connected modular balancing system.

The battery pack under design is a 16S1P LFP cell system with Q_{Nom}=6,5 Ah, with the cells used during the unbalancing effects and causes analysis of Chapter 3. The balancing system behaviour will be analysed during Chapter 6.

The modular balancing system has been implemented with the intramodule and intermodule systems analysed during Chapter 4. These systems assure low complexity and open loop control of the battery pack balancing. The selected systems are the Multi Stacked Sepic (Subchapter 4.2.4) for the intramodule system and the Parallel connected Full Bridge (Subchapter 4.5.2) due to the next reasons:

- Multi Stacked Sepic.
    - No transformers, easier to find commercial inductors.
    - Low side single switch to reduce complexity compared with Multi Stacked Zeta.
- Parallel connected Full Bridge.
    - Totally modular system, independent of the battery pack voltage.

The balancing system will be divided in 4 modules (16S1P=4x4S1P) Fig 5.4. Each module will have an intramodule and intermodule balancing system. The 4 module distribution has been decided due to:

- 4 module analysis of intermodule behaviour gives more importance and impact to the Thesis work.
- The voltage swing of a module composed of 4 series connected LFP cells is V_M=[8V...14,6V]=[4·2V...4·3,65V]. This voltage permits to use CMOS technology drivers self-powered from the module voltage V_M, to generate necessary gate driver signals without the need of external supply nor DCDC converters, reducing the component number, cost and complexity of the system. 4 series connected cells also permit to use duty cycles >5%, even for transformerless intramodule systems.

Table 5.5 Capacity dispersion between 16 cells for a battery pack of 16 S1P. Percentage capacity values respect to Q_{Nom}=6,5 Ah

Q_{Max}	Q_{Min}	ΔQ_{Max}	Q_{AV}
7,312	6,946	0,366	7,09
112%	107%	5,63%	109%

The balancing system is designed for 16 LFP cells with low SOH dispersion (new cells), so the balancing system is designed to only compensate the initial capacity dispersion of the cells. The balancing system will be designed to carry out low balancing currents behind 1 Ampere.

The capacity dispersion between cells is presented in Table 5.5. To inject more energy between the weak cell Q_{Min} and the Strong cell Q_{Max}, each cell will be inserted in different modules to obtain the balancing current of the intramodule $I_{Cb,i}$ and the intermodule $I_{Mb,j}$. With this battery lay-out the current for the weak and strong cells only taking into account the balancing system is:

$$I_{C,W} = I_{Mb,W} + I_{Cb,W} \tag{5.8}$$

$$I_{C,S} = I_{Mb,S} + I_{Cb,S} \tag{5.9}$$

The intramodule and intermodule balancing systems will work under the critical duty cycle D_C to work safely even the worst unbalance situation is presented in the system.

- Intramodule Multi Stacked Sepic: D_C= 13% equation (4.19) with weak cell $V_{C,W}$=2 V and $V_{C,S}$ = 3,65 V and V_M in this configuration = 12,95 V.
- Intermodule Parallel connected Full Bridge: Constant 50% duty cycle, for all situations.

The weak and strong balancing currents are defined for an unbalancing situation where:

- Strong module: 3 cells 3,65 V one cell 3V.(Module next to charge elbow) Intramodule and intermodule ON ($I_{Cb,S}$ and $I_{Mb,S}$).
  - $I_{Cb,S}$=-72 mA $I_{Mb,S}$=-175 mA
- Weak module: 3 cells 3 V one cell 2 V.(Module next to discharge elbow) Intramodule ON intermodule OFF. ($I_{Cb,W}$ and $I_{Mb,W}$).
  - $I_{Cb,W}$=254 mA $I_{Mb,W}$=223 mA

The balancing currents defined make a difference between $I_{C,W}$ and $I_{C,S}$ of 724 mA ($I_{C,W}$-$I_{C,S}$). If the assumption of constant voltage during balancing could be taken the

dispersion of 0,366 Ah defined in Table 5.5 will disappear in 30 minutes. However due to the power losses and that during balancing the voltage difference is reduced the balancing current will be reduced increasing the balancing time. Even so, low balancing currents criteria is respected and the balancing currents are defined as a good design approach. For this situation the balancing system inductor values are defined as:

- Intramodule Multi Stacked Sepic: L_n=68 µH L_{in}= 470 µH.
- Intermodule parallel connected Full Bridge: L_S= 15 µH.

The balancing inductor values and size are designed to obtain commercial inductor values to decrease the balancing system cost, in order to obtain a competitive design to deal with passive balancing systems.

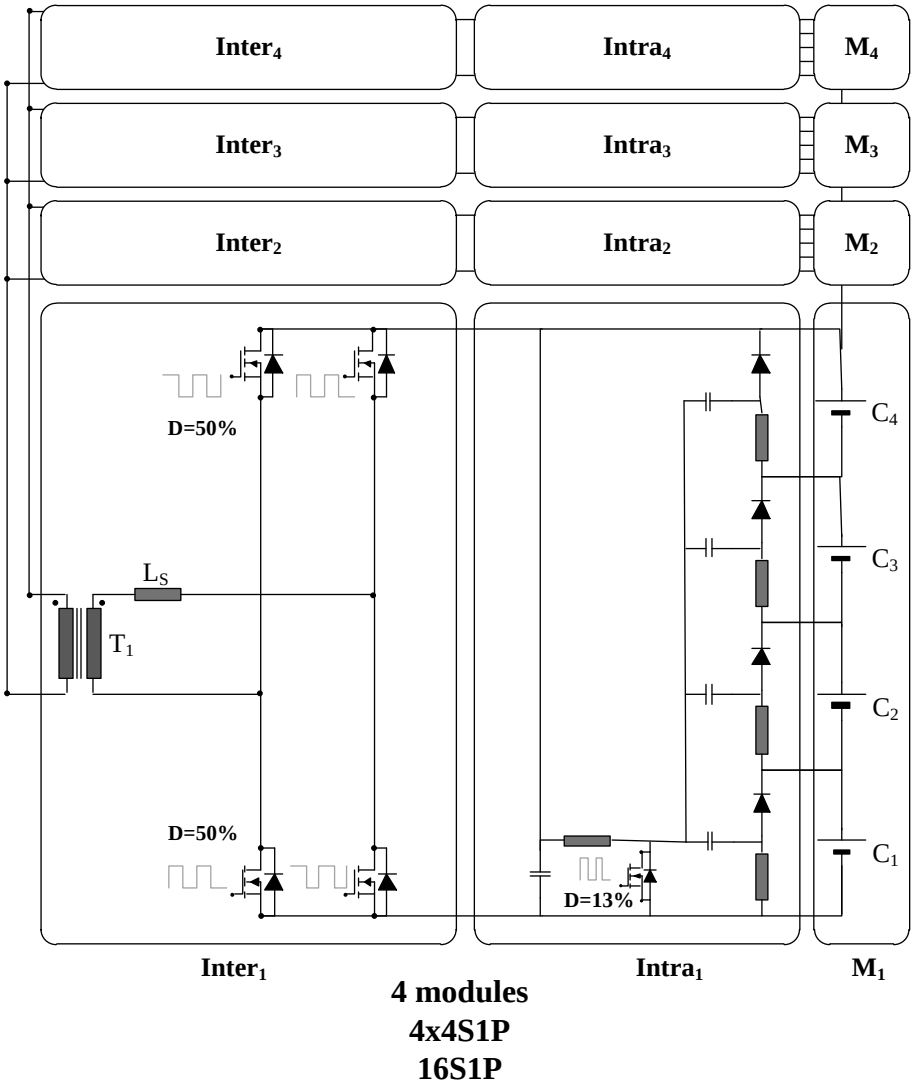

Fig 5.4. 16S1P LFP cells battery pack prototype in 4x4S1P modular configuration. Each module contains an intramodule Multi Stacked Sepic and an intermodule parallel connected Full bridge balancing system.

The final modular design is presented in Fig 5.4. The gate signals are generated by ICs powered by the module voltages, maintaining the duty cycle values independent of the module voltage variations. Each intramodule and intermodule is designed in an individual PCB, giving each module a high modularity. The final prototype design is presented in subchapter C.3, with prototype photographs, schematics and PCB prints.

5.4 Conclusions of the chapter

During the present chapter an analysis about balancing system design for series connected energy storage systems has been presented.

The first subchapter presents the main balancing equations that define the balancing process inside a series connected battery pack. The main parameters are the ones defined by the current difference between the weak cell and strong cell balancing current ($I_{Cb,W}$ and $I_{Cb,S}$), the balancing time (t_{Cb}) and finally the initial capacity or SOC deviation between the strong and the weak cell (SOC_S and SOC_W). With these parameters the necessary balancing SOC can be defined.

A methodology has been presented where a series connected battery pack is simulated via single cell tests data. Single cell tests data is collected from specific tests driven to guarantee that the cell is suitable for the application, so by the use of this data, the modeling necessary tests are avoided reducing the system design time. Different single cell tests permit to take into account capacity dispersion or different voltage dynamics from same manufacturer cells. The simulation methodology permits to iteratively change different balancing system design parameters and evaluate their impact under different battery characteristics (Charge time, voltage unbalance, etc.). The methodology has been implemented for a 4S1P LFP battery pack with a passive balancing system.

Finally a 16S1P modular balancing system design has been presented. The designed modular system is composed of 4 balancing modules, with one multi stacked sepic intramdoule and one parallel connected full bridge in each module. The balancing system has been designed with the general knowledge acquired during the previous Thesis work. The unbalancing knowledge from Chapter 3, the active modular systems design equations from Chapter 4 and general balancing equations from subchapter 5.1 are used during the design process. **The balancing system is designed to obtain a low cost modular balancing system to compete against passive balancing systems**.

Chapter 6

EVALUATION OF ACTIVE BALANCING SYSTEMS

Chapter 6 presents the behaviour evaluation of active balancing systems connected to series connected Li-ion battery packs. The main interest of this chapter is to compare active balancing systems vs passive balancing systems.

During first subchapter, main comparison parameters will be presented focusing on energy considerations, temperature effects and cost. The balancing system influence in temperature is presented in [PAPER J1] *in collaboration with a previous thesis work.*

Second subchapter presents the comparison between a multistacked sepic balancing system and a passive balancing system for a 4S1P Li-ion module. The analysis is focused on new, aged and low energy LFP cells, although other Li-ion technologies analysis is also presented. The results are presented in [PAPER J3]

The third subchapter presents the behaviour analysis of a 16S1P battery pack with passive balancing against active modular balancing. The behavioural analysis is made for the evaluation of fresh cells, a module of 4 cells aged and single cell aged inside the 16S1P battery pack.

The final subchapter deals with an approximated analysis of the energy throughput improvement on a 16S1P battery pack during the whole battery life thanks to the active balancing system. The analysis is performed focusing in energetic improvements and temperature benefits.

Finally, main conclusions are presented.

6.1 Balancing systems evaluation parameters

Energy storage balancing systems are connected to improve battery pack overall behaviour. The balancing system improvement in the battery pack is generally related to energy increase and unbalancing reduction. However during **Chapter 6** 3 different comparison topics of balancing systems will be evaluated:

- **Balancing system energy evaluation**: the energetic evaluation will be held for the point of view of the total battery pack energy. The battery pack charged energy $W_{BP,C}$ the battery pack discharged energy $W_{BP,D}$ and the standby wasted energy W_{SB} will be evaluated.
- **Balancing system temperature behaviour**: Temperature effects of the balancing system will be evaluated under 2 different concepts. The battery pack cell temperatures with the maximum cell temperature T_{Max} and the temperature dispersion between series connected cells ΔT. The balancing system temperature T_{BS} that could generate hot spots in the battery pack.
- **Balancing system cost**: The balancing system cost $C_€$ will be evaluated, as it is the most important parameter for the industry sector.

6.1.1 Balancing system energy evaluation

The energy evaluations presented during these subchapters will be related to the total energy presented in a battery pack. The energy evaluation criteria will be applied for cycling and standby analysis of battery packs (cycle life and calendar life).

Battery pack cycling issues will be presented from two points of view. The energetic diagram is presented in Fig 6.1:

- **Customer point of view W^*_{BP}**: A customer that buys a battery integrated with a balancing system only measures the battery pack voltage V_{BP} and the battery pack current I_{BP}. The balancing system effect is not measurable.
- **Battery pack point of view W_{BP}**: The real energy inserted/obtained to/from the battery pack cells W_{BP} is the difference between the energy from the point of view of the customer W^*_{BP} and the power losses of the balancing system $P_{Cb,Loss}$ ($P_{Cb,Loss}$+$P_{Mb,Loss}$ if modular systems are used).

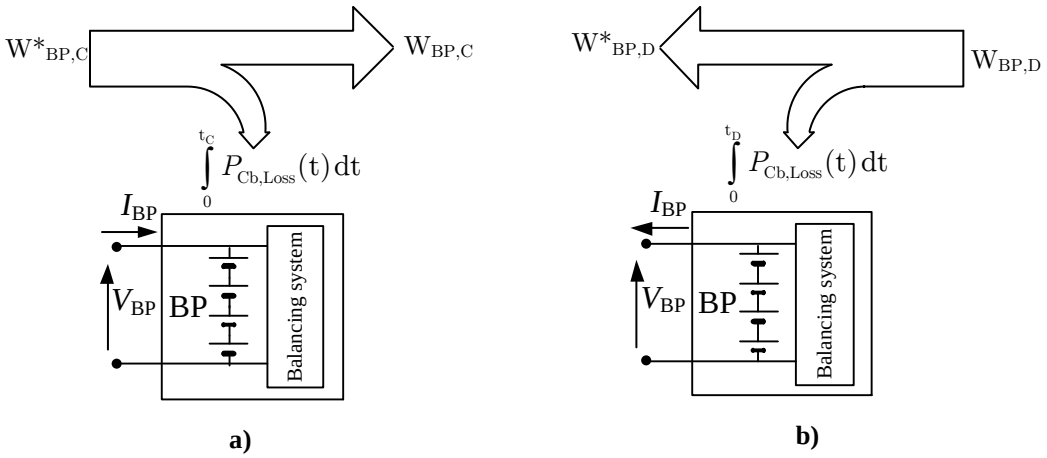

Fig 6.1. Arrow diagram for the energetic evaluation of the battery pack cycling performance. a) Charge process (I_{BP} positive). b) Discharge process (I_{BP} negative).

The charging energy $W^*_{BP,C}$ is the total energy inserted to the system from the point of view of a battery charger during the charge time t_C. $W^*_{BP,C}$ gives the total energy consumed from the power source (electric grid, alternative supply,etc) (6.1). The real energy inserted into the battery pack $W_{PB,C}$ is less due to the power losses of the balancing system during charging process. $W_{PB,C}$ is also defined as the sum of the total energy inserted to all series connected cells [$V_{C,i}$, $I_{C,i}$] (6.2) during charge process.

$$W^*_{BP,C} = \int_0^{t_C} V_{BP}(t) I_{BP}(t)\,dt \tag{6.1}$$

$$W_{BP,C} = \int_0^{t_C} \sum_{i=1}^{m\times n} V_{C,i}(t) I_{C,i}(t)\,dt = W^*_{BP,C} - \int_0^{t_C} P_{Cb,Loss}(t)\,dt \tag{6.2}$$

The total energy inside the battery pack is dependent of the initial energy that was inside the battery cells before the charge process is started and it is not quantified during this evaluation.

The discharge process energy is calculated in a similar way. The customer or the battery user has a discharged battery energy $W^*_{BP,D}$ that is the energy obtained from the whole battery during discharge time t_D (6.3). However the battery gives more energy $W_{BP,D}$ during discharge because has to yield with balancing system losses (6.4) (internal battery resistance losses are excluded).

$$W^*_{BP,D} = \int_0^{t_D} V_{BP}(t) I_{BP}(t)\,dt \tag{6.3}$$

$$W_{BP,D} = \int_0^{t_D} \sum_{i=1}^{m\times n} V_{C,i}(t) I_{C,i}(t)\,dt = W^*_{BP,D} - \int_0^{t_D} P_{Cb,Loss}(t)\,dt \tag{6.4}$$

Remaining energy is usually inside the battery pack after the discharge process because all the cells are not fully discharged.

The subtraction of the balancing power losses in both processes, charge equation (6.2) and discharge equation (6.4), is because positive energy is considered in charge process ($W_{BP,C}>0$ → positive) and negative energy is considered during discharge ($W_{BP,D}<0$ → negative). The subtraction of power losses for charge and discharge process is clearly presented in Fig 6.1.

The battery pack energetic efficiency (do not confuse with coulombimetric efficiency which is ≈99%...100% in Li-ion cells) could be expressed from the point of view of the customer or the point of view of the battery pack as expressed in equations (6.5) and (6.6).

$$\eta^*_{BP} = \frac{W^*_{BP,D}}{W^*_{BP,C}} \cdot 100 \tag{6.5}$$

$$\eta_{BP} = \frac{W_{BP,D}}{W_{BP,C}} \cdot 100 \tag{6.6}$$

For the point of view of a customer it is clear that the battery pack efficiency η^*_{BP} is the most important parameter to know the exploitation level of the battery pack. The battery pack designer must try to equal η^*_{BP} and η_{BP} ($\eta_{BP}= \eta^*_{BP}$) to give the maximum amount of energy to the customer. However if a balancing system is used ALWAYS, $\eta_{BP} > \eta^*_{BP}$; the costumer receives or uses less energy than the battery pack gives.

In applications where the battery pack is going to be in standby, or stored until the battery energy is used (UPS application, Electric vehicles, etc) the standby energy consumption W_{SB} due to the BMS, measurement system or balancing system is an important parameter. If the energy leakage during standby operation is high, the battery could be inoperative when the customer requires it.

6.1.2 Balancing system temperature behaviour

Even if the balancing system behaviour is generally related to energetic issues during a previous Thesis work presented in [14] and the Journal article [PAPER J1] the influence of the balancing system on the battery pack temperature was analyzed,

specially focusing on maximum cell temperature T_{Max} and temperature dispersion between cells ΔT. During the thesis work also the influence of the balancing system temperature T_{BS} will be evaluated, as a key factor for the generation of hot spots within the battery pack.

Cell temperature depends on the power losses generated inside the cell $P_{Loss,i}$. The power losses can be calculated by the power generation in the internal resistance of the cell $R_{in,i}$ and the square of the cell current $I_{C,i}^2$ or by the difference between the cell voltage $V_{C,i}$ and the internal open circuit equivalent voltage $V_{OC,i}$ (and the cell current (6.7)).

$$P_{Loss,i} = R_{in,i} I_{C,i}^2 = \left(V_{C,i} - V_{OC,i}\right) I_{C,i} \rightarrow R_{in,i} = \frac{\left(V_{C,i} - V_{OC,i}\right)}{I_{C,i}} \tag{6.7}$$

In a series connected battery pack the cell current $I_{C,i}$ is equal to the battery pack current I_{BP}. However if a balancing system is connected the cell current is modified by $I_{C,i}=I_{BP}+I_{Cb,i}$ as was presented in (4.1), increasing the current of the weak cell ($I_{Cb,W} > 0$) and decreasing the current through the strong cells ($I_{Cb,S} < 0$).

T_{Max} is generated during final discharge process, due to higher difference between $V_{C,i}$ and $V_{OC,i}$. It is usually generated in the weak cell, which reaches first discharge cut-off voltage. The balancing system could decrease the power losses, decreasing the maximum temperature of the weak cell. Without balancing system or with passive balancing there is not a decrease in power losses, however if an active balancing system is employed current is inserted to the weak cell decreasing the total equivalent discharge current of the cell, and therefore decreasing the power losses (6.8)-(6.9).

DISCHARGE

$$P_{Loss,W} = R_{in,W} I_{C,W}^2 = R_{in,W} I_{BP}^2 \rightarrow P_{Loss,W} = cte \text{ without and passive} \tag{6.8}$$

$$P_{Loss,W} = R_{in,W} I_{C,W}^2 = R_{in,W} \left(I_{BP} + I_{Cb,W}\right)^2 \rightarrow P_{Loss,W} \downarrow\downarrow \text{ active} \tag{6.9}$$

The strong cells temperature increases during discharge process because passive and active balancing systems increase the discharge current of the strong cells, increasing the power losses.

DISCHARGE

$$P_{Loss,S} = R_{in,S} I_{C,S}^2 = R_{in,S} \left(I_{BP} + I_{Cb,S}\right)^2 \rightarrow P_{Loss,S} \uparrow\uparrow \text{ active and passive} \tag{6.10}$$

If the maximum temperature will be generated during a charge process, both passive and active balancing systems will decrease the power losses of the cell, by decreasing the current of the most charged cell or strong cell.

$$\underline{\text{CHARGE}}$$
$$P_{Loss,S} = R_{in,S} I_{C,S}{}^2 = R_{in,S} \left(I_{BP} + I_{Cb,S} \right)^2 \rightarrow P_{Loss,S} \downarrow\downarrow \text{ active and passive} \tag{6.11}$$

The weak cell (low voltage cell) power losses, are increased for active balancing systems and kept constant for passive balancing systems.

$$\underline{\text{CHARGE}}$$
$$P_{Loss,W} = R_{in,W} I_{C,W}{}^2 = R_{in,W} I_{BP}{}^2 \rightarrow P_{Loss,W} = cte \text{ without and passive} \tag{6.12}$$
$$P_{Loss,W} = R_{in,W} I_{C,W}{}^2 = R_{in,W} \left(I_{BP} + I_{Cb,W} \right)^2 \rightarrow P_{Loss,W} \uparrow\uparrow \text{ active} \tag{6.13}$$

Temperature dispersion between cells ΔT is also decreased with balancing systems respect to battery packs without balancing system. Balancing systems equalize the voltages of the cells in the series strings. The balancing procedure matches the voltages between cells equalling the power losses of the cells by definition of equation (6.7). So for charge or discharge processes, if a temperature dispersion reduction is aimed, a balancing process is beneficial. Cell power losses analysis from equation (6.8)-(6.13) confirms this assumption where $P_{Loss,W}$ and $P_{Loss,S}$ difference decreases with balancing systems.

Regarding the temperature generated in the balancing system T_{BS}, temperature depends on the balancing system power losses $P_{Cb,Loss}$ analytically expressed in **Annex A A.2** and experimentally calculated during chapters **4.3 and 4.6** for modular balancing systems. For ideal active balancing systems no temperature increase will be generated in the balancing system board, however due to power losses a temperature increase is generated. Nevertheless the power losses generated in equivalent passive balancing systems are ALWAYS higher, so passive balancing systems can generate higher temperature hot spots than active balancing systems.

6.1.3 Balancing system cost

The relative low complexity and low cost of passive balancing systems, keep passive balancing as the most implemented system for battery pack balancing. The

analysis made during the Thesis work focusing on modular balancing systems, with low switch number and low complexity, permits to obtain a competitive design to compete against the passive balancing. An approximated cost of the balancing systems $C_€$ will be presented as it is a major design parameter for industry partners.

6.2 No balancing vs Passive balancing vs intramodule Sepic for 4S1P battery module

4S1P battery li-ion modules are widely used in applications as portable solutions (laptops, drills, etc) and in substitution of common Lead Acid 12V nominal batteries.

The passive balancing and the intramodule multi Stacked Sepic are compared for a 4S1P Li-ion battery disposition (Fig 6.2). The passive balancing system uses R_n=12 Ω as the dissipative element while the Sepic balancing system uses the same design as presented in **Chapter 4 subchapter 4.4** in Table 4.2. The duty cycle is kept constant to 13 % D=0,13. The different balancing systems behaviour is evaluated under 3 different situations:

- **LFP 6,5 Ah 100% SOH cells:** The balancing system behaviour with a new assembled battery pack will be evaluated.
- **LFP 6,5 Ah one 80% SOH aged cell:** The 4S1P module is assembled with 3

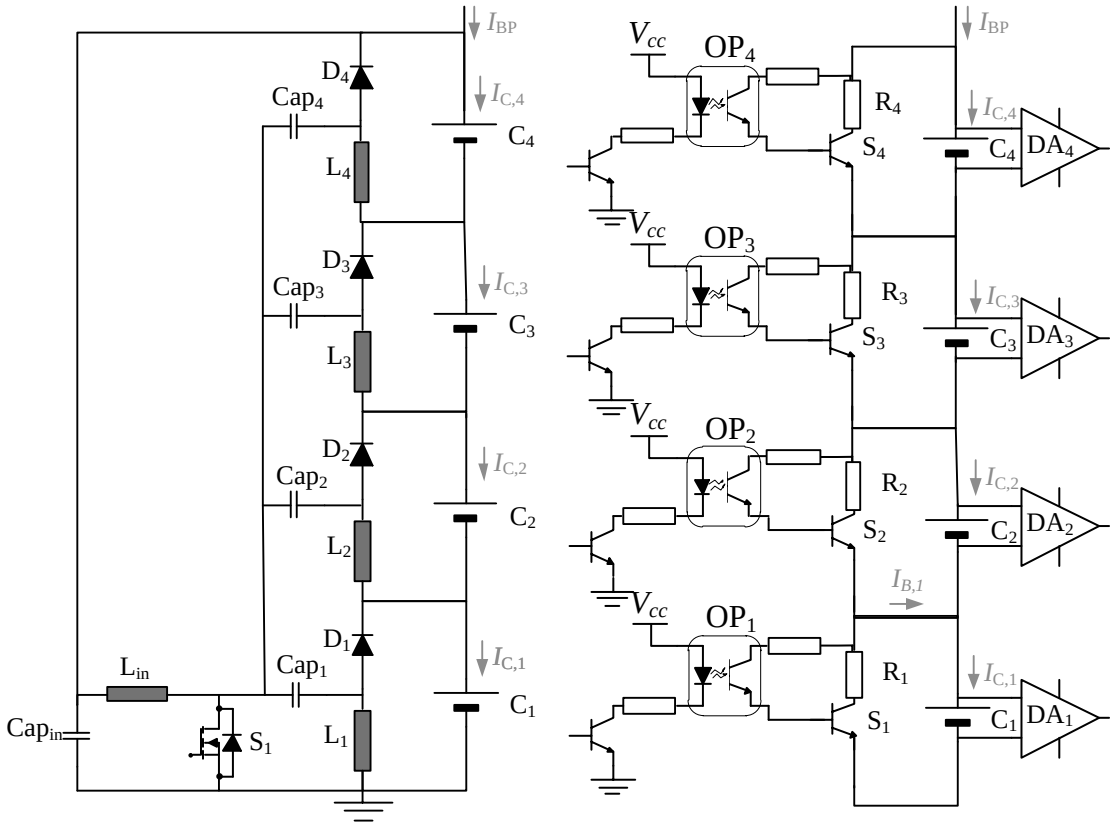

Fig 6.2. Passive and multi stacked Sepic balancing systems with real measurement and conditioning systems for a 4S1P battery module. a) Passive balancing system. b) Multi stacked Sepic balancing system.

100% SOH cells and one 80% SOH cell to evaluate the balancing systems behaviour under high SOH unbalance. The tests are interesting for second life application of Li-ion cells.

- **Different Li-ion technology low energy cells Q ≤ 3A:** Passive and multi stacked Sepic balancing systems are tested with low capacity different technology cells. With these tests the behaviour of the balancing systems with different technologies and the influence of balancing current in smaller capacity cells will be evaluated.

The 3 presented situations will be analysed for the energetic, temperature and cost evaluation parameters presented in subchapter 6.1.1. The balancing system temperature T_{BS}, standby energy consumption W_{SB} and balancing system cost $C_€$ are independent of the Li-ion technology under test, so will be analysed only during subchapter 6.2.1, and is equal during following subchapters.

The test bench used during the evaluation process has a similar architecture as the test bench presented for unbalancing process analysis in **Chapter 3**.

- Charge/Discharge system: Power supply and electronic load
  - Chroma 62024P-80-60: Power supply to charge the 4S1P battery pack.
  - Chroma 63201: Electronic Load to discharge the 4S1P battery pack.
- Acquisition and control system: National Instruments based system:
  - Host: Ni program based to control Chroma power supply and electronic load via series communication.
  - Real Time: Crio 9022 real time controller in a 9114 chassis.
    - NI 9205: Measure 4 cell voltages ($V_{C,1}$...$V_{C,4}$) and the battery pack current I_{BP} via differential measurement.
    - NI 9213: Temperature on centre of the surface of each cell of the 4S1P module is measured by the connection of 2 k type thermocouples to each cell (8 temperature measurements overall).
    - NI 9403: 32 DIO module, the passive balancing system activation (4 DO) and the security relays control (2 DO, charge discharge relays) under overcurrent, overvoltage or over temperature situations.

- Temperature chamber: Prebatem 80L temperature chamber at constant 25ºC temperature.
- Precision shunt resistors: 15 mΩ 1% shunt resistor to measure I_{BP} and to calculate accurate capacity values.

Temperature and energetic analysis will be analysed for **10 consecutive charge /discharge cycles**. All the cells are initially fully charged balanced by a passive balancing system.

- **Charge cycle**: CCCV charge mode.1C charge until V_{Max} cell, and CV at V_{Max} cell until the current decreases to C/20.
- **Discharge cycle**: CC discharge: 1 C discharge until V_{Min} is reached.

The energetic and temperature results will be presented as the mean value of the 10 consecutive cycles. The Multi stacked Sepic and passive balancing system results will be compared respect to a reference test evaluation without balancing system (No Balancing). The behavioural results will present the comparison between:

- No Balancing **NB**.
- Passive Balancing **PB.**
- Active Balancing **AB.**

6.2.1 LFP 6,5 Ah 100% SOH cells

The first evaluation of the balancing systems behaviour is made for a 4S1P module assembled with 4 LFP Q_{Nom}=6,5 Ah new cells (≈100% SOH). These cells are also used during **Chapter 3** for unbalancing effects and causes estimation and in **Chapter 5 5.2.1** during the iterative methodology design. The initial capacity of the 4S1P cells is presented in Table 5.3. The capacity dispersion ΔQ between the 4 cells is 0,317 Ah (4,9 % of the nominal capacity).

In order to avoid temperature influence between nearby positioned cells, cells are distanced 1 cm. Distancing the series connected cells, isolates each cell from the heat generation of adjacent cells, taking only into account the performance of the balancing system for the temperature behaviour.

Table 6.1 Energetic results for 10 charge discharge cycles for a 4S1P battery module of ≈100% SOH cells. The energetic results (charging energy, discharging energy and efficiency) are given from the point of view of the battery and the point of view of the customer. Not Balancing NB Passive Balancing PB and Active Balancing AB.

	Customer			**Battery**		
	$W^*_{BP,C}$ [Wh]	$W^*_{BP,D}$ [Wh]	η^*_{BP} [%]	$W_{BP,C}$ [Wh]	$W_{BP,D}$ [Wh]	η_{BP} [%]
NB	96,575	-92,113	95,38	96,575	-92,113	95,379
PB	97,89	-92,28	94,28	97,21	-92,61	95,27
AB	96,96	-92,48	95,38	96,78	-92,54	95,62

The maximum voltage V_{Max} for CV charge mode is set to 3,65 V and the minimum voltage for the discharge cut-off V_{Min} = 2 V. The voltage threshold where the balancing system is switched on is set to 10 mV ($\Delta V_{C,TH}$=10 mV)

6.2.1.1 Energy evaluation

The energetic cycling results for no balancing NB passive balancing PB and active balancing AB are presented in Table 6.1. PB losses $P_{CB,Loss}$ are calculated in a data post-process, by acquiring the instant when each cell balancing resistor is active. The AB system losses are estimated to be 0,2 W. The value is measured in 4.4 intramodule experimental validation for the worst balancing situation, and therefore it is overestimated for different charge discharge cycling situations. However, it is considered accurate enough for comparison, taking into account that real results are better than presented values.

During charge process AB and PB balancing systems consume more energy from the grid, from a customer point of view (PB +1,4% more and AB +0,4% more than

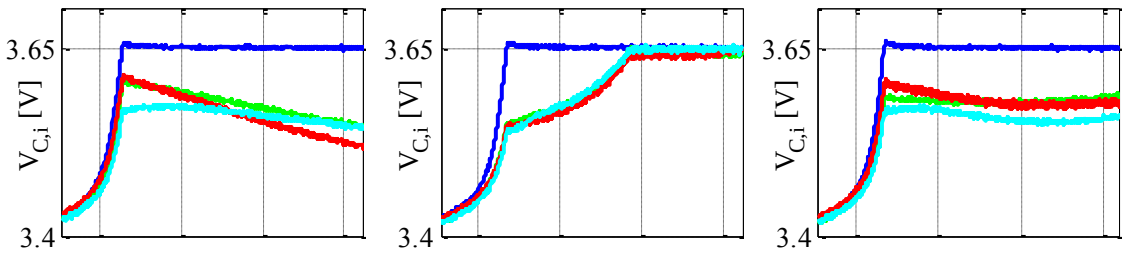

a) **b)** **c)**

Fig 6.3. CV charge process for 3 different balancing systems in a 4S1P battery module. a) No balancing NB. b) Passive balancing PB. c) Sepic Active balancing AB.

Table 6.2 Standby results for a 15 day rest period with balancing systems connected to a fully charged 4S1P battery module. No balancing system connected NB, passive balancing system connected PB and Active balancing system connected AB. The discharged energy $W^*_{BP,D}$ and the standby wasted energy W_{SB} are evaluated respect to the no balancing system.

	$W^*_{BP,D}$ [Wh]	W_{SB} [Wh]
NB	-91,33 (100%)	0 (0%)
PB	-91,13 (99,78%)	0,2 (0,22%)
AB	-91,24 (99,9%)	0,09 (0,1%)

NB), which increases the power bill $W^*_{BP,C}$. However the battery pack is better charged than without balancing $W_{BP,C}$ and therefore more energy is delivered during discharge. The passive balancing system inserts more energy and balances better all the cells during charge as presented in Fig 6.3. The energy delivered to the customer $W^*_{BP,D}$ is increased +0,18% for the PB and +0,40% for the AB. The efficiency of the system η^*_{BP} is reduced -1,1% for the PB and kept equal for the AB. There is not big difference between AB and NB systems, because the cells are 100% SOH equals, even if the results have shown that more energy is extracted.

To analyse the standby energy consumption W_{SB} the 4 S1P battery module is fully charged with the passive balancing system. The decision to fully charge the module is to obtain the worst standby scenario where the leakage current is higher. After 15 days storage with the balancing system connected the 4S1P battery module is discharged at 1C rate. The difference between wasted standby energy is very low between different selected balancing systems. The PB system wastes 0,22% more of energy and the AB 0,1% respect to the total discharged energy of the No balancing reference as presented in Table 6.2. The balancing systems due not contribute in leakage energy consumption as was concluded also in the analysis presented during **Chapter 3**, that the leakage contributing devices where the measurement or monitoring systems. The data presented in Table 6.2 compared to data of Table 6.1 gives an important conclusion: Battery pack self-discharge process during storage or standby time reduces the battery pack discharge energy from 92,113 Wh to 91,33 Wh (reduction of 0,85%). The self-discharge impact in wasted energy is much higher than the wasted standby energy of the balancing systems.

Table 6.3 Maximum temperature T_{Max} and temperature deviation ΔT for 10 consecutive charge discharge cycles. The temperature values are the mean values for the 10 consecutive discharge cycles, during the final process of discharge when T_{Max} and ΔT are maximum.

	T_{Max} [ºC]	ΔT [ºC]
NB	29,16	0,37
PB	28,61	0,4
AB	29,23	0,3

6.2.1.2 Temperature behaviour

Temperature behaviour of the 4S1P cells is analysed during the consecutive 10 charge discharge cycles at 1C rate. The maximum temperature T_{Max} and temperature deviation ΔT are presented during the final discharge process, when one cell reaches V_{Min}= 2 V. Each cell has 2 thermocouples connected in the centre of the surface of the front and rear faces.

The temperature behaviour of the balancing systems is presented in Table 6.3. The T_{Max} results present that PB reduces the maximum temperature (-0,55 ºC) because all the cells are fully charged and in the final discharge instant the reached temperature is smaller. AB maintains T_{Max} nearly constant respect to NB (+0,07 ºC). Related to the temperature dispersion between cells PB presents the higher dispersion (+0,03 ºC respect to NB). This result is conflicting with analysis presented in (6.8)-(6.13). The explanation is that as the 4S1P cells are fully charged with PB, during final discharge process there is higher voltage difference between cells than with NB and AB, increasing the temperature dispersion. AB decreases temperature dispersion (-0,07 ºC), thanks to injecting current to the weak cell.

Temperature results obtained present low deviation respect to NB situation because the cells have equal SOH (and very similar internal impedance), and the 1C current rate does not increase much the temperature of the cell.

The analysis of the balancing system temperature T_{BS} is made for a constant voltage situation where the weak cell is kept to 2 V ($V_{C,W}$=2V) and the strong cells are charged to 3,65 V ($V_{C,S}$=3,65 V). The PB system extracts energy from the 3 strong cells

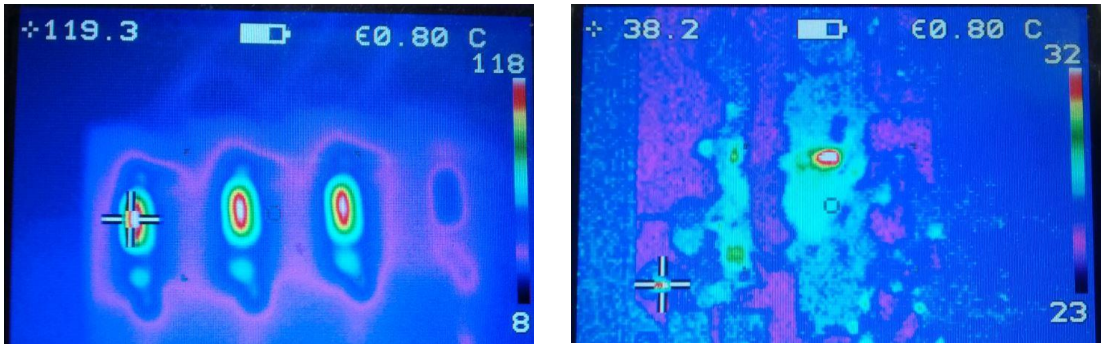

a)		b)	
$P_{Cb,Loss}$ [W]	T_{BS} hot spot[ºC]	$P_{Cb,Loss}$ [W]	T_{BS} hot spot [ºC]
3,5	119,3	0,195	38,2

Fig 6.4. Thermography analysis of a) PB and b) AB balancing systems. $P_{Cb,Loss}$ values calculated experimentally and T_{BS} measured by thermography camera.

while the AB system extracts energy from the 3 strong cells and inserts energy to the weak cell. The temperature is measured by a termography camera where the temperature dispersion in the balancing systems is presented in Fig 6.4.

Fig 6.4 b) presents the results of the AB balancing system. 0,195W of power losses are generated for a high unbalance situation, and the T_{BS} hot spot reaches 38,2 ºC (13,2 ºC increase respect to 25 ºC ambient). The PB system generates 3,5 W of power losses $P_{Cb,Loss}$, generating a hot spot of 119,3 ºC (94,3 ºC increase respect to 25 ºC ambient). The excessive power losses generated by the PB system respect to the AB system, and the potential hot spot creation, could generate a temperature aging issue in a battery module. The AB system is presented as a better option if the balancing system temperature and losses need to be minimized.

6.2.1.3 Balancing system cost

The system cost issue $C_€$ is the biggest constraint when deciding for a balancing system for an industrial application. PB balancing systems are the most used systems in industrial applications due to their low cost and reliability. However, single switch balancing systems and during this evaluation process specifically the multi Stacked Sepic topology, is a good candidate to replace passive balancing systems, thanks to low switch number and reduced balancing complexity. The AB single switch systems permit also to balance the series connected cells without the need of a voltage measurement system, reducing the overall system cost.

Table 6.4 Balancing system cost for a 4S1P battery module. Passive balancing PB and Active Balancing AB component and price distribution. Component price corresponds to quotation of www.farnell.com for a minimum of 10 pcs order.

PB				AB			
Component	**Reference**	**pcs**	**€/pcs**	**Component**	**Reference**	**pcs**	**€/pcs**
OP_n	TLP523	4	0,71	D_n	SL13-E3/61T	4	0,26
R_n	ER7412RJT	4	0,28	L_n	74459168 Würth	4	2,18
S_n	BD437	4	0,233	Cap_n	C1206C106K3PACTU	4	0,195
DA_n	INA 148	4	3,49	Lin	74459247 Würth	1	2,02
				S_1	IRF8721PBF	1	0,6
Total price 4S1P $\mathbf{C_{€}}$	18,852 €			Total price 4S1P $\mathbf{C_{€}}$	13,16 €		

Table 6.4 presents the system cost for the 2 schematics of PB and AB presented in Fig 6.2. The price of the AB system is cheaper than the PB, mainly due to the high price of differential amplifiers DA_n. AB open loop control strategy permits to avoid voltage measurement systems decreasing the balancing system price. The PB system price could be reduced by using commercial ICs for passive balancing issues. The AB balancing system is also oversized, and could be redesigned to obtain a more competitive price.

Even if a voltage measurement system should be used also in the AB system solution (because the Li-ion cells voltages must be measured for security reasons), the multi Stacked Sepic presents a good solution to compete against passive balancing systems for industrial applications.

6.2.2 LFP 6,5 Ah one 80%SOH aged cell

The evaluation of the balancing systems will be held for the case where a 4S1P battery module has an aged cell. To evaluate the balancing systems behaviour for the

Table 6.5 Capacity dispersion between 4 cells for a battery pack of 4S1P with one 80% SOH cell. Percentage capacity values respect to Q_{Nom}=6,5 Ah

$\mathbf{Q_{Max}}$	$\mathbf{Q_{Min}}$	$\mathbf{\Delta Q_{Max}}$	$\mathbf{Q_{AV}}$
7,59	5,2	2,39	6,9
117%	80%	36,77%	106%

Table 6.6 Energetic results for 10 charge discharge cycles for a 4S1P battery module of 3 ≈100% SOH cells and one 80% SOH cell. The energetic results (charging energy, discharging energy and efficiency) are given from the point of view of the battery and the point of view of the customer. Not Balancing NB Passive Balancing PB and Active Balancing AB.

	Customer			**Battery**		
	$W^*_{BP,C}$ [Wh]	$W^*_{BP,D}$ [Wh]	η^*_{BP} [%]	$W_{BP,C}$ [Wh]	$W_{BP,D}$ [Wh]	η_{BP} [%]
NB	65,22	-62,33	95,60	65,22	-62,33	95,60
PB	70,69	-63,24	89,49	68,77	-65,22	94,86
AB	66,96	-63,94	95,51	66,60	-64,17	96,36

extreme situation a 80% SOH cell has been connected in series with 3 100% SOH cells. The 3 100% SOH cells are the cells used during the previous subchapter and the 80% SOH cell is a cell aged during aging tests performed in the laboratory. The capacity of the aged cell Q_{Min} is $80\%Q_{Nom}$=5,2 Ah as presented in Table 6.5. The capacity mismatch between the strongest cell and the weak-aged cell is 2,39 Ah, 36,77% of the nominal capacity.

The standby energetic issues W_{SB}, the balancing system temperature T_{BS} and the balancing system cost $C_€$ analysis are equal to the 100% SOH 6,5 Ah cell case, as these parameters are equal independent of the cell used during the behaviour analysis.

6.2.2.1 Energy evaluation

The energetic behaviour of the NB, PB and AB systems for a high SOH unbalance system is presented in Table 6.6. As presented in the previous subchapter the $P_{Cb,Loss}$ are calculated in a post-process analysis.

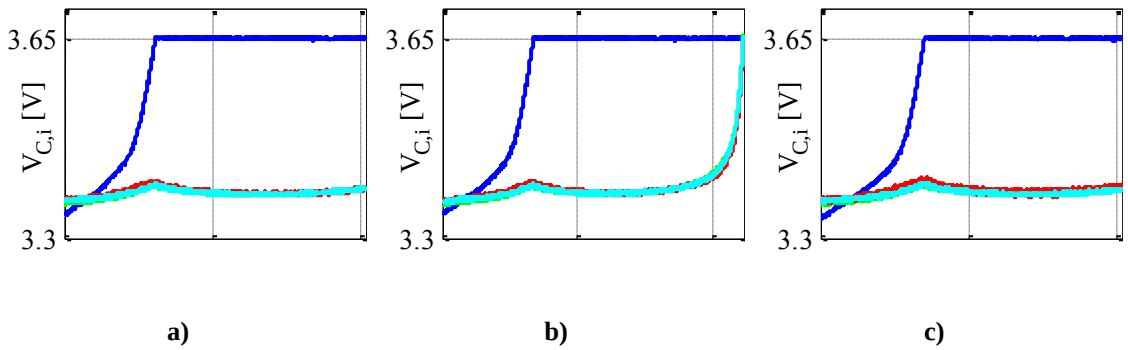

a) **b)** **c)**

Fig 6.5. CV charge process for 3 different balancing systems in a 4S1P battery module with unbalanced SOH cells. The weak cell (80% SOH cell) is presented in blue. a) No balancing NB. b) Passive balancing PB. c) Sepic Active balancing AB.

The energy discharged from the point of view of customer $W^*_{BP,D}$, is increased respect to the NB system, first of all because more energy is inserted in the charging process Fig 6.5. The PB increases +0,91 Wh (1,46 %) the discharged energy for one single discharge and the AB system increases the discharged energy +1,61 Wh, a 2,5 % increase in $W^*_{BP,D}$ respect to the NB system.

The PB system efficiency is reduced a lot because it uses excess energy to charge the battery pack Fig 6.5 b) that is not utilized during discharge. The AB system utilizes the strong cells energy to insert energy to the weak cell, increasing the battery pack efficiency nearly to the NB system value.

6.2.2.2 Temperature behaviour

The 80% SOH aged cell has a higher supposed internal resistance, so the maximum temperature of one cell in the battery pack should be higher than the temperature registered for 100% SOH cells. Also the temperature difference should be higher because the difference in internal resistance or cell voltage ($V_{C,i}$ or open circuit voltage), will be higher due to SOH unbalance. All these issues are confirmed in the results presented in Table 6.7.

Compared to the results of ≈100% SOH cells, the maximum temperature T_{Max} reaches nearly +0,5 ºC more, and ΔT reaches 2,2 ºC for the NB case, when in ≈100% SOH cells the ΔT was only 0,37 ºC. The initial SOH unbalance leads to an increase in maximum cell temperature and a further increase in temperature deviation between cells. Therefore it is clearly concluded that an initial SOH unbalance, leads to a further increase in SOH unbalance during cycling.

Table 6.7 Maximum temperature T_{Max} and temperature deviation ΔT for 10 consecutive charge discharge cycles for an SOH unbalanced 4S1P battery module. The temperature values are the mean values for the 10 consecutive discharge cycles, during the final process of discharge when T_{Max} and ΔT are maximum.

	T_{Max} [ºC]	ΔT [ºC]
NB	29,76	2,2
PB	29,59	2,07
AB	29,53	1,95

The balancing systems behaviour clearly presents an improvement in order to decrease the effect of temperature in SOH unbalance. PB and AB systems reduce T_{Max} from 29,76 ºC to 29,59ºC and 29,53 ºC respectively. The temperature dispersion between cells ΔT is also reduced from 2,2 ºC for the NB case, to 2,07 in the PB case and 1,95 ºC to the AB case. It is clearly demonstrated that the balancing systems reduce the SOH unbalance increase due to temperature.

6.2.3 Different Li-ion technology low energy cells Q < 3Ah

The comparative of the passive balancing system and the active Multi Stacked Sepic have been presented for 6,5 Ah LFP cells in a 4S1P configuration. The same balancing systems will be compared with lower capacity cells (Q<3Ah) and other chemistry cells with the following purposes:

- Investigate the balancing systems behaviour where the relation between the

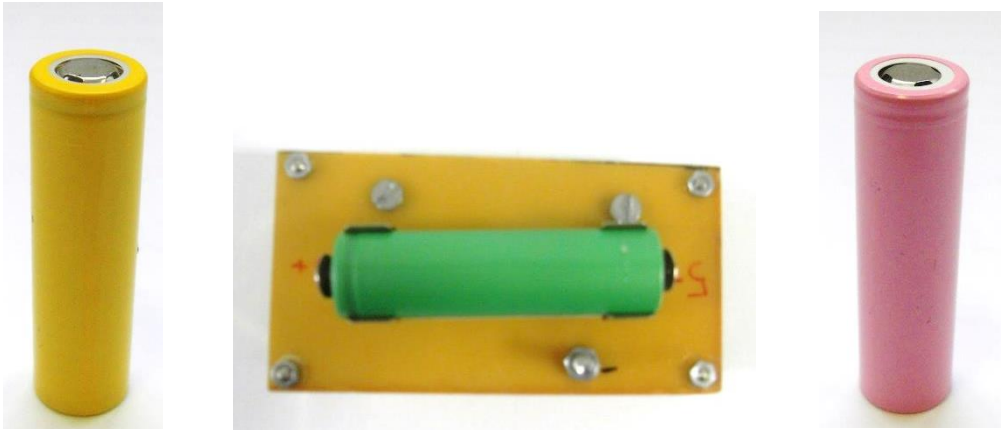

a) **b)** **c)**

Fig 6.6. Low capacity 18650 cells for different chemistry behaviour analysis and high balancing current rate tests. a) Q_{Nom}=1,1 Ah LFP cell . b) Q_{Nom}=1,6 Ah LMO cell . c) Q_{Nom}=3 Ah LCO energy cell.

Table 6.8 V_{Max} and V_{Min} limits for the 3 low capacity 18650 cells under test.

LFP		LMO		LCO	
V_{Max} [V]	V_{Min} [V]	V_{Max} [V]	V_{Min} [V]	V_{Max} [V]	V_{Min} [V]
3,65	2	4,25	2,5	4,25	3

balancing current and the capacity is smaller (faster balancing systems analysis).

- Evaluate the series connection and the balancing system requirements for other Li-ion technologies.

The 3 low capacity cells are have a 18650 cylindrical shape to evaluate different performances under the same cell format Fig 6.6. The cells under test are presented in the following list.

- Q_{Nom}=1,1 Ah LFP cell.
- Q_{Nom}=1,6 Ah LMO cell.
- Q_{Nom}=3 Ah LCO energy cell.

The LFP and LMO cells present good power qualities (High charge and discharge C-rates). However the LCO cell, presents poor charge/discharge capacity (C/2 maximum), but a high energy density.

The low capacity cells are tested for 10 consecutive charge discharge cycles, with the same current rates as the 6,5Ah LFP cell, except the LCO cell where the rate is limited to C/2 due to temperature issues and manufacturer datasheet limits. The voltage ratings V_{Max} and V_{Min} for the end of charge and discharge are presented in Table 6.8.

The 4S1P battery module is constructed connecting in series 4 18650 specific connection cases. The use of specific 18650 cases permits simplicity and versatility to change between the 3 different cells presented in Fig 6.6 b).

The balancing voltage threshold $\Delta V_{C,TH}$ is set to 50 mV, due to higher internal impedance of low capacity cells. Tests have been made with lower threshold voltage ($\Delta V_{C,TH}$=10 mV) and instability has been appreciated (balancing ringing outside threshold).

Table 6.9 Capacity dispersion between 4 cells for a battery pack of 4S1P and low capacity cells. LFP, LMO and LCO 18650 capacity characteristics. The percentage value is calculated to their respective Q_{Nom}.

	Q_{Max}	Q_{Min}	ΔQ_{Max}	Q_{AV}
LFP	1,01	0,97	0,04	0,99
	91,66%	88,34%	3,33%	90,25%
LMO	1,52	1,50	0,02	1,51
	94,84%	93,84%	1,00%	94,48%
LCO	2,53	2,50	0,03	2,51
	84,46%	83,40%	1,06%	83,71%

6.2.3.1 Energy evaluation

The energetic evaluation of the low capacity LFP, LMO and LCO 4S1P battery modules, is made with 4 new series connected cells. The capacity measurements and dispersion is presented in Table 6.9. Results present very low capacity dispersion (1%-3%) specially for LMO and LCO (1% capacity dispersion).

The low capacity dispersion presented between cells suggests that low balancing effort is required to maintain the 4 series connected cells balanced. To confirm the low balancing effort, Fig 6.7 present the charge discharge profile of the 10th cycle with No balancing system NB. The voltage profiles are kept nearly equal, without any unbalancing effect due to good capacity matching between cells.

The highest voltage unbalance is presented in LFP cells during final charge discharge processes, due to the change in open circuit voltage during low and high SOC

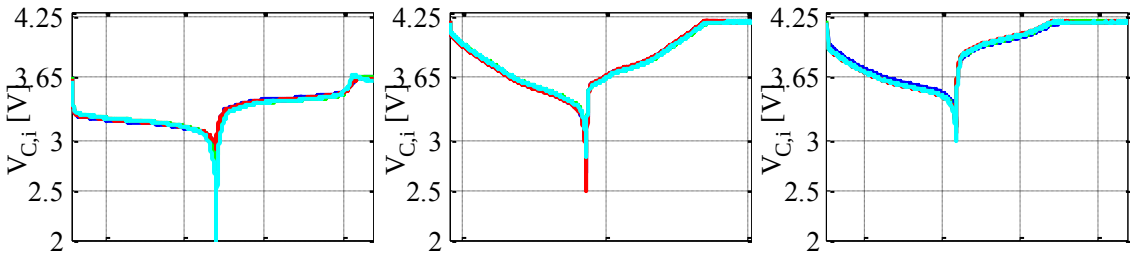

Fig 6.7. Single charge discharge cycle of the low capacity 4S1P battery module without balancing system. $V_{C,i}$ cell voltages i=[1...4]. No balancing system NB. a) LFP cells. b) LMO cells. c) LCO cells.

Table 6.10 Energetic results for 10 charge discharge cycles for a 4S1P battery module of low capacity cells. Yellow shaded LFP, Green shaded LMO and Red shaded LCO as the original cell colours. Not Balancing NB Passive Balancing PB and Active Balancing AB.

		Customer			**Battery**		
		$W^*_{BP,C}$ [Wh]	$W^*_{BP,D}$ [Wh]	η^*_{BP} [%]	$W_{BP,C}$ [Wh]	$W_{BP,D}$ [Wh]	η_{BP} [%]
LFP	NB	13,43	-12,52	93,23	13,43	-12,52	93,23
	PB	13,79	-12,59	91,4	13,64	-12,7	93,11
	AB	13,60	-12,66	93,19	13,53	-12,69	93,80
LMO	NB	23,44	-21,99	93,86	23,44	-21,99	93,86
	PB	23,31	-21,83	93,71	23,30	-21,84	93,74
	AB	23,27	-21,80	93,72	23,26	-21,81	93,77
LCO	NB	39,56	-35,02	88,54	39,56	-35,02	88,54
	PB	40,03	-35,68	89,17	40,03	-35,69	89,19
	AB	39,78	-35,58	89,47	39,78	-35,58	89,49

values. The nearly constant slope waveforms of LMO and LCO cells, as presented in state of the art Fig 2.3 a) and confirmed in Fig 6.7, keeps the series connected cells balanced even in low and high SOC values.

The energetic analysis presented in Table 6.10 confirms the expected results. LMO and LCO results are the same from the battery and consumer point of view ($X^*_{BP} \approx X_{BP}$). This is due to no balancing system work during charge discharge cycles, so it is also confirmed that SOH matched cells reduce balancing system effort. Deviation in LFP cell voltages induce balancing system to work. The discharged energy from the point of view of the customer $W^*_{BP,D}$ is increased with the PB +0,07 Wh (0,6 %) and +0,14 Wh (1,2 %) for the AB. The results are good taking into account the low dispersion of the tested cells.

The PB system for the LFP cells is the worst customer efficiency system η^*_{BP} reducing the efficiency nearly 2% compared to the NB and AB system.

Table 6.12 Maximum temperature T_{Max} and temperature deviation ΔT for 10 consecutive charge discharge cycles without balancing system for a 4S1P battery module of LFP, LMO and LCO cells. The charge discharge cycles of the LCO are featured at C/2 rate due to datasheet requirements.

	T_{Max} [ºC]	ΔT [ºC]
LFP	27,57	0,54
LMO	29,22	1,31
LCO	35,06	1,92

6.2.3.2 Temperature behaviour

The temperature analysis is only evaluated for the LFP 4S1P low capacity battery module for the 3 different balancing systems. Temperature analysis of LCO and LMO is only presented for the No Balancing NB case, as the balancing systems do not work for the LMO and LCO cells. Table 6.12 presents that LCO cell reaches the highest maximum temperature. It was predictable as it is an energy cell and the internal resistance is higher. LMO cells reach higher temperature than LFP cells for 1C charge discharge, and it is also seen that higher T_{Max} higher is the temperature deviation between cells.

The impact of the balancing system in the temperature has been analysed for the LFP topology. In order to verify the temperature behaviour at different rates the charge discharge rate of 1C, has been compared with 2C and 3C rates in Table 6.11. The

Table 6.11 Maximum temperature T_{Max} and temperature deviation ΔT for 10 consecutive charge discharge cycles for a low capacity 4S1P battery module of LFP cells. 1C, 2C and 3C current rate influence is analysed.

		T_{Max} [ºC]	ΔT [ºC]
1C	NB	27,57	0,54
	PB	27,86	0,59
	AB	27,64	0,54
2C	NB	31,60	1,35
	PB	31,94	1,34
	AB	31,73	1,4
3C	NB	36,61	2,24
	PB	36,80	2,27
	AB	36,71	2,27

influence of the balancing system is low in matched capacity cells. PB reaches the higher average maximum temperature T_{Max}. It is also confirmed that higher C-rates increase cell temperature and temperature dispersion, which would originate accelerated and non-regular aging. If a SOH dispersion is generated due to temperature mismatch, the AB and PB balancing systems will reduce the maximum temperature T_{Max} and ΔT as was presented in Table 6.7 for the 6,5 Ah 80% SOH cells analysis.

6.2.4 LFP technology results comparative review

As LFP technology has been the Li-ion chemistry under research during the thesis work a result summary will be presented for 3 different LFP 4S1P scenarios:

- LFP 6,5Ah new cells.
- LFP 6,5 Ah one 80% SOH aged cell.
- Low energy 1,1 Ah new cells.

The results under review will be mainly from the customer point of view. The battery pack for the customer is the composition between the balancing system and the battery cells. The parameters under review are:

- Energetic parameters: Charged energy $W^*_{BP,C}$, Discharged energy $W^*_{BP,D}$ and battery pack efficiency η^*_{BP}. The standby consumed energy W_{SB} is also presented. These parameters give an estimation of the utilization of the battery pack.
- Temperature parameters: Maximum cell temperature T_{Max}, temperature dispersion between cells ΔT and balancing system temperature T_{BS} represent battery pack behaviour respect to temperature, where temperature is a critical parameter in battery life.
- Cost: The balancing system cost $C_€$ is evaluated, which is one of the most important parameters besides of reliability, that keeps passive balancing as the most used balancing system in industry.

W_{SB}, T_{BS} and $C_€$ are kept equal for the 4 different LFP scenarios because the same balancing systems are used for the 3 different scenarios. The standby consumption is kept equal because it is assumed that the energy consumption of the balancing system is

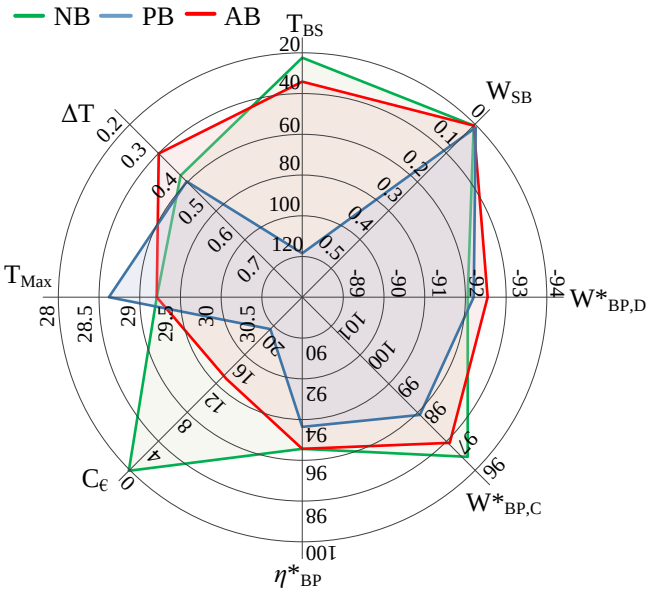

Fig 6.8. Comparison parameters for a 4S1P LFP Q_{Nom}=6,5 Ah battery pack scenario with new cells. NB, AB and PB system under comparison.

only voltage dependent. The No Balancing (NB), Passive balancing (PB) and multistacked Sepic active balancing system (AB) are compared in a spider chart waveform to visualize different parameters weight in a single view. The parameter values are collected from the results presented in previous subchapters.

For the analysis of 4S1P 6,5 Ah new cells presented in Fig 6.8, NB system is the best situated in cost (no balancing system), T_{BS} (no balancing system) and battery charged energy. The efficiency is also the highest however the discharged energy is the lowest.

PB system is the best system according to maximum cell temperature T_{Max}, under the test specifications. It offers worse characteristics in cost $C_€$, temperature dispersion ΔT and energy charge and efficiency. The worst result is presented for T_{BS}, presenting the highest balancing system temperature which could yield to problematic hot spots in the battery pack.

AB system presents the best results for temperature dispersion and total discharged energy. For other parameters presents similar behaviour to the NB system, with little higher T_{Max} and of course higher cost.

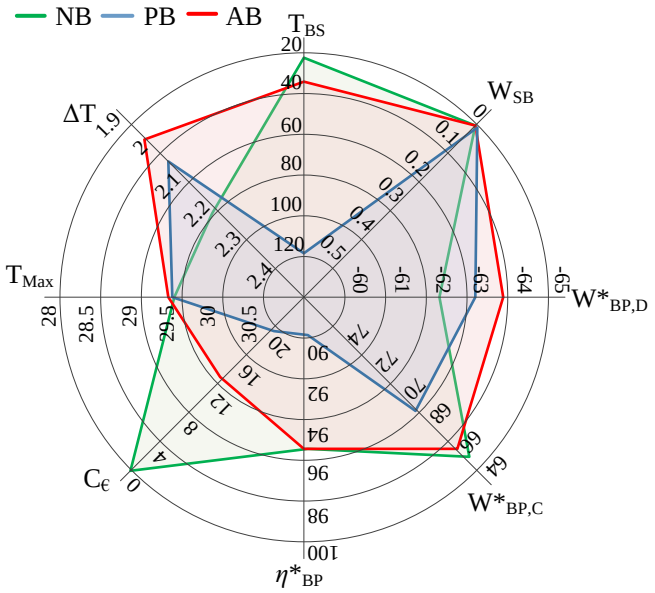

Fig 6.9. Comparison parameters for a 4S1P LFP Q_{Nom}=6,5 Ah battery pack scenario with one 80% aged cell. NB, AB and PB system under comparison.

Fig 6.9 presents the results for the 4S1P battery pack with a single cell aged. The NB system only performs best results for the charging energy. However due to less energy charged less energy is also obtained during discharge.

PB system improves NB temperature results; however it decreases a lot the efficiency due to much higher charging energy requirements. The efficiency could be improved for the PB system if the PB system would be disabled during discharge. However the temperature difference between cells would increase.

AB system performs superior characteristics with aged cells. It keeps the efficiency near NB systems and improves performance regarding to temperature and discharge energy.

The comparison chart for Q_{Nom}=1,1 Ah cells is presented in Fig 6.10. NB system presents the best performance in efficiency, maximum temperature and specially in charged energy. This is due to low capacity dispersion between cells. However the discharged energy is much lower than with the AB and PB systems.

The PB system performs the worst behaviour, with the lowest efficiency and highest temperature deviation, maximum temperature and charged energy. The energetic issues could be improved if the PB system is disabled during discharge.

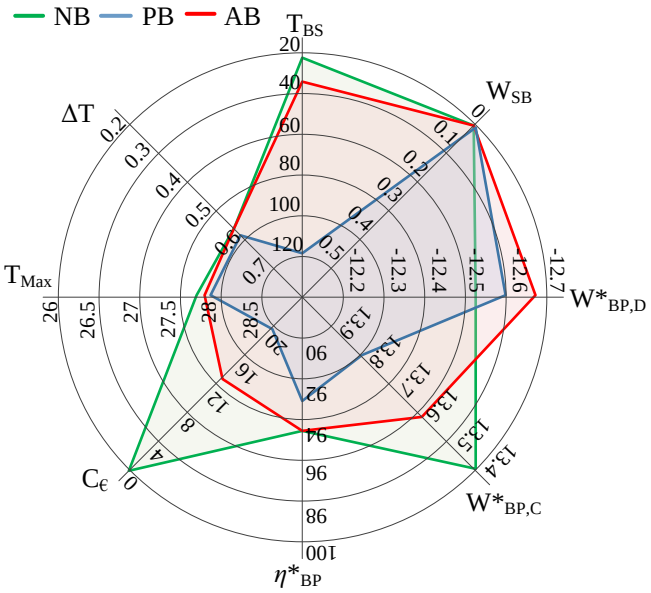

Fig 6.10. Comparison parameters for a 4S1P LFP Q_{Nom}=1,1 Ah battery pack scenario with new cells. NB, AB and PB system under comparison.

AB system performs the best related to discharged energy, higher energy is obtained than with PB and NB. The temperature deviation is equal to NB and T_{Max} slightly higher than without balancing.

6.3 No balancing vs Passive balancing vs Active modular for a 16S1P LFP battery pack

A 16S1P battery pack composed by Q_{Nom}=6,5 Ah LFP cells has been assembled to evaluate a high voltage battery pack behaviour with different balancing systems. The cells mechanical lay-out has the next characteristics: (Assembly photograph presented in Annex C C.3 Fig C. 11)

- 4 modules of 4S1P cells connected in series (4x4S1P): The 16S1P battery pack is divided in 4 independent modules. The modularity gives easiness to change battery pack configuration with different cells. The battery pack cells are expressed in two formats: $X_{j,i}$: j=number of module j=[1,4]; i= number of cell in the module i=[1,4]. X_i= i number of cell in the battery pack i=[1,16]
- Cells 1 cm distance isolated: In order to avoid temperature influence between nearby cells, the cells are separated and assembled with 1 cm air gap between adjacent cells.

The balancing systems used are equally defined as the balancing systems used in the previous subchapter. However they have different characteristics:

- No Balancing **NB**: The 16S1P battery pack will be cycled without balancing system.
- Passive balancing **PB**: 16S1P passive balancing system with a balancing resistor value of R_n=12 **Ω** (the same schematic as Fig 6.2 b) but sized to 16 cells).
- Active balancing **AB**: The active balancing system used is the balancing system designed in subchapter 5.3.1 Fig 5.4. Each module has an intramodule multi stacked Sepic and an intermodule parallel connected Full bridge balancing system. The 4 modules are scalable and interchangeable.

The 3 different balancing systems are evaluated for 3 different battery pack aging situations:

- **16S1P new cells SOH ≈100%:** The battery pack behaviour will be evaluated under the assembly of 16 new cells with low SOH dispersion values. These

tests will give information about the battery pack behaviour in the beginning of life BOL.

- **16S1P with one module 4S1P of aged cells**: The battery pack behaviour will be evaluated with 3 new modules SOH≈100% and one aged module connected in series. This battery topology will simulate a battery pack aged differently, or a battery pack where battery modules have been replaced.
- **16S1P with single cell SOH<80%:** The battery pack behaviour will be evaluated with one single cell in the end of life EOL. The scenario simulates a single cell that fails in the battery due to an accelerated aging process.

The test bench used is equal to previous subchapter and Chapter 3. However some extra devices are listed following:

- Temperature chamber: Prebatem 150L temperature chamber at constant 25 ºC. A bigger temperature chamber is needed due to 16S1P battery pack size.
- Real time: Crio 9022 real time controller in a 9114 chassis:
  - NI 9213: The temperature of the surface of each cell is measured with one single thermocouple, using the 16 thermocouple measurements to measure the 16 single cells.
  - NI 9403 module: 32 DIO module with 16 passive balancing activation signals (1...16 DO), 4 intramodule system signals (17...20 DO) 4 intermodule system signals (21...24 DO) and 2 security relay signals (25-26 DO). The wiring complexity is increased.
  - NI 9205: Measure 16 cell voltages ($V_{C,1}$...$V_{C,16}$) and the battery pack current I_{BP} via differential measurement. To overcome the high common mode voltage, intermediate differential amplifier has been used based on INA148.

The 16S1P battery pack will be analysed related to energetic (customer point of view and battery point of view), temperature issues (T_{Max} and ΔT when the end of discharged is reached) and balancing system cost $C_€$. Standby energy W_{SB} and balancing system temperature T_{BS} are not evaluated.

Temperature and energetic behaviour will be analysed for **10 consecutive charge /discharge cycles**. All the cells are initially fully charged and balanced by the passive balancing system PB.

- **Charge cycle**: CCCV charge mode.1C charge until V_{Max} cell, and CV at V_{Max} cell until the current decreases to C/20.
- **Discharge cycle**: CC discharge: 1 C discharge until V_{Min} is reached.

The maximum voltage V_{Max} for CV charge mode is defined as 3,65 V and the minimum voltage for the discharge cut-off V_{Min}=2 V, LFP cell limit values. The voltage threshold where the balancing system is switched on is set to:

- 10 mV for passive and intramodule balancing systems ($\Delta V_{C,TH}$=10 mV).
- 40 mV for intermodule balancing system ($\Delta V_{M,TH}$=40 mV). The intermodule balancing will balance the deviations between modules.

6.3.1 16S1P 16 new cells SOH≈100%

The 16S1P battery pack with 16 new cells is assembled simulating a newly constructed battery pack. The Q_{Nom}=6,5 Ah cells capacity values are presented in Table

Table 6.13 Capacity dispersion between 16 new cells SOH ≈100%. for a 16S1P or 4x4S1P battery pack (16 cells in series or 4 modules of 4 cells in series). The cells are expressed in two formats: $Q_{j,i}$: j=number of module j=[1,4]; i= number of cell in the module i=[1,4]. Q_i= i number of cell in the battery pack i=[1,16]. Percentage calculated related to nominal capacity Q_{Nom}=6,5 Ah

	$Q_{1,1}$-Q_1	$Q_{1,2}$-Q_2	$Q_{1,3}$-Q_3	$Q_{1,4}$-Q_4	$\Delta Q_{Max,1-4}$	$Q_{AV,1-4}$	$\Delta Q_{Max,1-16}$	$Q_{AV,1-16}$
M_1	7,07	7,08	7,05	7,02	0,06	7,06		
	109%	109%	108%	108%	0,92%	108,62%		
	$Q_{2,1}$-Q_5	**$Q_{2,2}$-Q_6**	**$Q_{2,3}$-Q_7**	**$Q_{2,4}$-Q_8**	**$\Delta Q_{Max,5-8}$**	**$Q_{AV,5-8}$**	0,36	7,1
M_2	6,95	6,99	6,96	6,99	0,04	6,97		
	107%	108%	107%	108%	0,62%	107,23%		
	$Q_{3,1}$-Q_9	**$Q_{3,2}$-Q_{10}**	**$Q_{3,3}$-Q_{11}**	**$Q_{3,4}$-Q_{12}**	**$\Delta Q_{Max,9-12}$**	**$Q_{AV,9-12}$**		
M_3	7,28	7,19	7,17	7,31	0,14	7,24		
	112%	111%	110%	112%	2,15%	111,38%		
	$Q_{4,1}$-Q_{13}	**$Q_{4,2}$-Q_{14}**	**$Q_{4,3}$-Q_{15}**	**$Q_{4,4}$-Q_{16}**	**$\Delta Q_{Max,13-16}$**	**$Q_{AV,13-16}$**	5,54%	109%
M_4	7,17	7,09	7,13	7,15	0,08	7,14		
	110%	109%	110%	110%	1,23%	109,85%		

Table 6.14 Energetic results for 10 charge discharge cycles for a 16S1P battery module of new cells. The energetic results (charging energy, discharging energy and efficiency) are given from the point of view of the battery and the point of view of the customer. Not Balancing NB Passive Balancing PB and Active Balancing AB.

	Customer			**Battery**		
	$W^*_{BP,C}$ [Wh]	$W^*_{BP,D}$ [Wh]	η^*_{BP} [%]	$W_{BP,C}$ [Wh]	$W_{BP,D}$ [Wh]	η_{BP} [%]
NB	381,92	-366,44	95,95	381,92	-366,44	95,95
PB	391,42	-366,97	93,75	387,04	-370,45	95,72
AB	388,26	-367,45	94,64	387,72	-367,61	94,81

6.13. The maximum dispersion between the 16 cells $\Delta Q_{Max,1\text{-}16}$ =0,36 Ah a 5,54 % respect to nominal capacity. The second module with cells from 2,1 to 2,4 is the weakest module but with low difference compared with the other modules.

6.3.1.1 Energy evaluation

The energetic results for 10 consecutive charge discharge cycles of the 16S1P battery pack are presented in Table 6.14. The active balancing system power losses are calculated from experimental results presented in Chapter 4. The intramodule balancing system losses $P_{Cb,Loss}$ are 0,2 W (equal to the balancing system power losses for the 4S1P active balancing, because the same balancing system is used), and the intermodule balancing system losses $P_{Mb,Loss}$ are 1,3 W (calculated in subchapter 4.7). Both experimentally measured power losses are quantified for the worst unbalancing situation (3 cells 3,65V and 1 cell 2 V for intramodule balancing system; 3 modules fully charged to 14,6 V and one module fully discharged to 8 V). The real power losses will be lower, so the real results will be better than the presented results.

Table 6.14 results from the customer point of view present that the energy consumed to charge the battery pack $W^*_{BP,C}$ is 2,49% higher (+9,5 Wh) in the PB and 1,66% in the AB case (+6,34 Wh). However the energy obtained during discharge is increased 0,14% in the PB case and 0,28% in the AB case.

The results present that, when the cells are matched in SOH the balancing system improvement is not high in the battery pack. Even more, the efficiency of the battery pack from the customer point of view is reduced -1,31 % for the AB system and -2,34% for the PB system. The charging time is not presented in the results of Table 6.14. The

Table 6.15 Maximum temperature T_{Max} and temperature deviation ΔT for 10 consecutive charge discharge cycles for 16S1P new cells battery pack. The temperature values are the mean values for the 10 consecutive discharge cycles, during the final process of discharge when T_{Max} and ΔT are maximum.

	T_{Max} [ºC]	ΔT [ºC]
NB	29,6	1,2
PB	29,8	1,3
AB	29,55	1,18

results of the increased charge energy for the AB and PB systems respect to NB, clearly present that the charging time is increased with balancing systems. NB charging time is of 1,3 hours, while PB increases charging time 9,8% (1,43 hours) and AB 3,8 % (1,35 hours). The charging time could also be an important issue to take into account depending on the final application.

6.3.1.2 Temperature behaviour

The results for the temperature analysis related to T_{Max} and ΔT should be ideally equal or similar to the results obtained in the analysis of the 4S1P battery module of new cells presented in subchapter 6.2.1. This assumption is made assuming that 1cm air gap between cells eliminates the influence of temperature between adjacent cells.

The temperature results for the 16S1P are presented in Table 6.15. Even 1 cm air gap distribution has been maintained to avoid temperature influence between cells, the maximum temperature T_{Max} and the temperature dispersion between cells ΔT have increased respect to the 4S1P case presented in Table 6.3.

PB balancing increases T_{Max} +0,3 ºC respect to NB and AB decreases -0,05ºC respect to NB. The temperature dispersion is decreased -0,02ºC for the AB and increased +0,1ºC for the PB.

6.3.1.3 Balancing system cost

The balancing system cost of the 16S1P active balancing is compared to the passive balancing system PB for 16 cells.

Table 6.16 PB balancing system cost for a 16S1P battery pack. Component price corresponds to quotation of www.farnell.com for a minimum of 10 pcs order.

PB 16S1P			
Component	**Reference**	**pcs**	**€/pcs**
OP_n	TLP523	16	0,71
R_n	ER7412RJT	16	0,28
S_n	BD437	16	0,233
DA_n	INA 148	16	3,49
Total price 16S1P $\mathbf{C_€}$		75,40 €	

The PB system price includes the differential amplifier price. The price could be reduced if a commercial IC could be used to measure the cell voltage. 16 digital signals are necessary to activate the 16 independent optocouples.

The AB system designed in subchapter 5.3.1 is a modular active balancing system dividing the 16S1P battery pack in 4 independent modules. Each balancing module is composed of a multi stacked Sepic intramodule balancing system with a parallel connected full bridge intermodule balancing system. The voltage monitoring system is omitted in the price, in spite of a monitoring system is indispensable due to security reasons.

The voltage presented in 4 series connected cells V_M between 8 V and 14,6 V permit to use direct connected drivers to the 4S1P module with CMOS technology. CMOS technology is used to reduce current consumption of the systems. The constant duty cycle signals for the intramodule and intermodule system are generated by a 7555 oscillator. The intramodule and intermodule balancing systems are switched on by a digital signal optocoupled OP, which inhibits the 7555 pulse to switch off the active balancing system. The double pulses necessary for the intermodule full bridge are generated by a frequency divider circuit using a D flip-flop and a 4 AND logic gate IC. No current loop is necessary because the current is limited with the constant duty cycles. 2 digital inputs are necessary to control each module, so for the 16 S1P battery pack 8 digital signals are required. The schematic and the PCB of the modular balancing system is presented in Annex C C.3. The AB system price could be reduced by buying magnetic components directly to the manufacturer (Würth), and reducing the current

Table 6.17 AB balancing system cost for a 16S1P battery pack. Component price corresponds to quotation of www.farnell.es for a minimum of 10 pcs order.

AB 16S1P					
	Comp	**Reference**	**Pcs/ module**	**pcs**	**€/pcs**
INTRAMODULE	D_n	SL13-E3/61T	4	16	0,26
	L_n	74459168 Würth	4	16	2,18
	Cap_n	C1206C106K3PACTU	4	16	0,195
	Lin	74459247 Würth	1	4	2,02
	Oscillator	ICM7555	1	4	0,653
	S_1	IRF8721PBF	1	4	0,6
	OP	HCPL-817-500E	1	4	0,18
INTERMODULE	L_S	74459115 Würth	1	4	2,15
	Transformer	744873221 Würth	1	4	2,84
	S_n	IRF8721PBF	4	16	0,6
	Oscillator	ICM7555	1	4	0,653
	D flip-flop	CD4013BM	1	4	0,362
	AND	CD4081BM	1	4	0,362
	OP	HCPL-817-500E	1	4	0,18
Total price 16S1P $\mathbf{C_{€}}$			91,76 €		

rate of the power mosfets and inductors, which have been oversized for the prototype design.

The AB system cost is only increased from 75,4 € to 91,76 € in the prototype design.

6.3.2 16S1P with one module 4S1P of aged cells

A 16S1P battery pack is assembled with one 4 aged cells module. This configuration simulates an accelerated aging behaviour of a single module that could be due to incorrect thermal management or different batch cells with high capacity dispersion. It could also simulate a battery pack where modules are substituted during life aging. The cell capacity values are presented in Table 6.18 where the aged module is M_3. The maximum dispersion between cells is 0,99 Ah, 15,23% respect to the nominal 6,5 Ah capacity.

Table 6.18 Capacity dispersion between 12 new cells SOH ≈100% and an aged module for a 16S1P or 4x4S1P battery pack (16 cells in series or 4 modules of 4 cells in series). The aged module is number 3 (M_3 j=3) The cells are expressed in two formats: $Q_{j,i}$: j=number of module j=[1,4]; i= number of cell in the module i=[1,4]. Q_i= i number of cell in the battery pack i=[1,16]. Percentage calculated related to nominal capacity Q_{Nom}=6,5 Ah

	$Q_{1,1}$-Q_1	$Q_{1,2}$-Q_2	$Q_{1,3}$-Q_3	$Q_{1,4}$-Q_4	$\Delta Q_{Max,1-4}$	$Q_{AV,1-4}$	$\Delta Q_{Max,1-16}$	$Q_{AV,1-16}$
M_1	7,07	7,08	7,05	7,02	0,06	7,06		
	109%	109%	108%	108%	0,92%	108,62%		
	$Q_{2,1}$-Q_5	**$Q_{2,2}$-Q_6**	**$Q_{2,3}$-Q_7**	**$Q_{2,4}$-Q_8**	**$\Delta Q_{Max,5-8}$**	**$Q_{AV,5-8}$**	**0,99**	**6,89**
M_2	6,95	6,99	6,96	6,99	0,04	6,97		
	107%	108%	107%	108%	0,62%	107,23%		
	$Q_{3,1}$-Q_9	**$Q_{3,2}$-Q_{10}**	**$Q_{3,3}$-Q_{11}**	**$Q_{3,4}$-Q_{12}**	**$\Delta Q_{Max,9-12}$**	**$Q_{AV,9-12}$**		
M_3	6,24	6,24	6,26	6,18	0,08	6,23		
	96%	96%	96%	95%	1,23%	95,85%	**15,23%**	106%
	$Q_{4,1}$-Q_{13}	**$Q_{4,2}$-Q_{14}**	**$Q_{4,3}$-Q_{15}**	**$Q_{4,4}$-Q_{16}**	**$\Delta Q_{Max,13-16}$**	**$Q_{AV,13-16}$**		
M_4	7,17	7,09	7,13	7,15	0,08	7,14		
	110%	109%	110%	110%	1,23%	109,85%		

6.3.2.1 Energy evaluation

The energetic evaluation presents in the first view the importance of balancing systems if a good battery pack use is expected as presented in Table 6.19. Even if with the NB system the battery efficiency is the highest (there are not power losses), the discharged energy is much lower. $W^*_{BP,D}$ increases +11,52 Wh for the PB case (3,6 %) and 15,22 Wh for the AB system (4,53 %). Those discharged energy increases represent a big improvement for applications as for example EV.

Table 6.19 Energetic results for 10 charge discharge cycles for a 16S1P battery pack with one aged module (4 cells inside a module aged). The energetic results (charging energy, discharging energy and efficiency) are given from the point of view of the battery and the point of view of the customer. No Balancing NB Passive Balancing PB and Active Balancing AB.

	Customer			**Battery**		
	$W^*_{BP,C}$ [Wh]	$W^*_{BP,D}$ [Wh]	η^*_{BP} [%]	$W_{BP,C}$ [Wh]	$W_{BP,D}$ [Wh]	η_{BP} [%]
NB	331,59	-313,83	94,66	331,59	-313,83	94,66
PB	360,61	-325,35	90,23	352,22	-334,73	95,04
AB	349,75	-329,05	94,08	348,07	-330,03	94,82

The battery charged energy $W^*_{BP,C}$ continues being much higher in the PB case, than in the AB case. PB system increases 29,02 Wh the charging energy respect to NB and AB 18,16 Wh. The excess charged energy respect to the NB increases the electric bill.

Even if the AB system is designed for low SOH dispersion cells (new cells) as presented in the design of subchapter 5.3.1, a good behaviour is presented with aged modules. During the tests performed the intermodule balancing system is working nearly full time because a big unbalance between modules is presented. However, the intramodule systems do not work so much because the cells inside the modules are well matched in capacity.

6.3.2.2 Temperature behaviour

The temperature behaviour of the 16 cells is summarized in Table 6.20. The maximum temperature T_{Max} is increased +0,46 ºC for the PB case and decreased -0,3 ºC for the AB case. The temperature dispersion between cells clearly increases respect to the 4S1P case, even with the 80% SOH cell where the temperature dispersion was 2,2 ºC for the NB case Table 6.7. The temperature dispersion for the 16S1P case decreases 0,6 ºC for the PB case and 0,23 ºC for the AB case respect to the NB.

The temperature behaviour improves with AB system, decreasing T_{Max} and ΔT.

6.3.3 16S1P with single cell SOH <80%

The final battery pack is assembled with one aged cell inserted into the module number 3 with a capacity of 4,9 Ah, 75% of Q_{Nom}=6,5 Ah. The battery pack is

Table 6.20 Maximum temperature T_{Max} and temperature deviation ΔT for 10 consecutive charge discharge cycles for a 16S1P battery pack with one module composed of 4 cells aged. The temperature values are the mean values for the 10 consecutive discharge cycles, during the final process of discharge when T_{Max} and ΔT are maximum.

	T_{Max} [ºC]	ΔT [ºC]
NB	29,95	3,34
PB	30,41	3,28
AB	29,65	3,11

Table 6.21 Capacity dispersion between 15 new cells SOH ≈100% and an aged cell 75% SOH for a 16S1P or 4x4S1P battery pack (16 cells in series or 4 modules of 4 cells in series). The aged cell is inserted in the 3rd module 4th position (3-4 or 12th cell) The cells are expressed in two formats: $Q_{j,i}$: j=number of module j=[1,4]; i= number of cell in the module i=[1,4]. Q_i= i number of cell in the battery pack i=[1,16]. Percentage calculated related to nominal capacity Q_{Nom}=6,5 Ah

	$Q_{1,1}$-Q_1	$Q_{1,2}$-Q_2	$Q_{1,3}$-Q_3	$Q_{1,4}$-Q_4	$\Delta Q_{Max,1-4}$	$Q_{AV,1-4}$	$\Delta Q_{Max,1-16}$	$Q_{AV,1-16}$
M_1	7,07	7,08	7,05	7,02	0,06	7,06		
	109%	109%	108%	108%	0,92%	108,62%		
	$Q_{2,1}$-Q_5	**$Q_{2,2}$-Q_6**	**$Q_{2,3}$-Q_7**	**$Q_{2,4}$-Q_8**	**$\Delta Q_{Max,5-8}$**	**$Q_{AV,5-8}$**	**4,9**	**7**
M_2	6,95	6,99	6,96	6,99	0,04	6,97		
	107%	108%	107%	108%	0,62%	107,23%		
	$Q_{3,1}$-Q_9	**$Q_{3,4}$-Q_{12}**	**$Q_{3,3}$-Q_{11}**	**$Q_{3,4}$-Q_{12}**	**$\Delta Q_{Max,9-12}$**	**$Q_{AV,9-12}$**		
M_3	7,28	4,9	7,17	7,31	2,41	6,67		
	112%	75%	110%	112%	37,08%	102,62%		
	$Q_{4,1}$-Q_{13}	**$Q_{4,2}$-Q_{14}**	**$Q_{4,3}$-Q_{15}**	**$Q_{4,4}$-Q_{16}**	**$\Delta Q_{Max,13-16}$**	**$Q_{AV,13-16}$**	**37,08%**	107,69%
M_4	7,17	7,09	7,13	7,15	0,08	7,14		
	110%	109%	110%	110%	1,23%	109,85%		

assembled simulating a single cell with an accelerated aging pattern and with its EOL already reached. Table 6.21 presents the capacity dispersion of the 16 series assembled cells and the position of each single cell. The maximum capacity dispersion between cells is 4,9 Ah representing a dispersion of 37,08% respect to the nominal capacity.

6.3.3.1 Energy evaluation

The energetic evaluation results presented in Table 6.22, confirm that a good charge process benefits for consecutive discharge, as for the aged module analysis from the previous subchapter.

The total discharged energy $W^*_{BP,D}$ increases +34,06 Wh for the PB (14,47%) and +20,62 Wh (8,75%) for the AB. The big difference for the PB is that the AB is not designed for high SOH unbalance processes, and also lower energy is inserted during charge process. The total energy inserted to the battery pack $W^*_{BP,C}$ is much higher for the PB system inserting +51,32 Wh more than the NB. The AB system inserts 21,79 Wh more than the NB system.

Table 6.22 Energetic results for 10 charge discharge cycles for a 16S1P battery pack with one single cell aged with 75% SOH. The energetic results (charging energy, discharging energy and efficiency) are given from the point of view of the battery and the point of view of the customer. No Balancing NB Passive Balancing PB and Active Balancing AB.

	Customer			**Battery**		
	$W^*_{BP,C}$ [Wh]	$W^*_{BP,D}$ [Wh]	η^*_{BP} [%]	$W_{BP,C}$ [Wh]	$W_{BP,D}$ [Wh]	η_{BP} [%]
NB	250,61	-235,71	94,06	250,61	-235,71	94,06
PB	301,93	-269,77	89,36	292,07	-280,22	95,95
AB	272,40	-256,33	94,10	271,54	-257,18	94,72

The efficiency is decreased nearly 5 % for the PB system, and increased 0,04% for the AB system because much more energy is charged than for the NB system.

6.3.3.2 Temperature behaviour

The temperature behaviour resumed in Table 6.23 presents that the maximum temperature is increased in the PB system +0,37ºC and decreased -0,19 ºC for the AB system. The temperature dispersion is reduced -0,63ºC until 3,32 ºC with the PB system and -0,4ºC until 3,45ºC for the AB system. ΔT and T_{Max} values increase nearly 1ºC compared to the values obtained for the 4S1P aged battery module presented in Table 6.7.

Table 6.23 Maximum temperature T_{Max} and temperature deviation ΔT for 10 consecutive charge discharge cycles for a 16S1P battery pack with one single cell aged to SOH=75%. The temperature values are the mean values for the 10 consecutive discharge cycles, during the final process of discharge when T_{Max} and ΔT are maximum.

	T_{Max} [ºC]	ΔT [ºC]
NB	30,12	3,85
PB	30,49	3,32
AB	29,93	3,45

6.4 Life time energy evaluation of series connected battery packs.

After presenting the energetic and temperature experimental behaviour of different battery packs with No Balancing NB, PB Passive Balancing and Active Balancing AB, a life time energy estimation of a battery pack will be presented for the 3 different balancing systems.

The battery pack energy during cycle life is influenced by 2 different mechanisms:

- The battery pack cycle life is influenced by the maximum working temperature T_{Max}. Higher temperature battery packs suffer faster aging processes.
- The battery pack cycle life total discharged energy is improved by the balancing system.

The battery pack under evaluation will be a 4S1P Q_{Nom}=6,5 Ah battery pack with constant 1C charge discharge cycles with 100% DOD. The 4S1P battery pack life time energy evaluation will be done with the experimental results obtained in subchapters 6.2.1 and 6.2.2. The results and analysis obtained during this estimation work, could be extrapolated or used for other Li-ion technologies, high number of series connected cells, etc.

The capacity loss (Q_{Loss}) or aging of the battery pack is assumed that it is only influenced by the maximum temperature T_{Max} generated in the battery pack. The capacity loss due to temperature is typically modelled by an Arrhenius equation. In the absence of aging data relating capacity loss with surface cell temperature of evaluated Q_{Nom}=6,5 Ah LFP cells, a bibliography work presented by Wang et al. [55] is used as the aging pattern. The capacity loss of a LFP cell is estimated by equation (6.14).

$$Q_{Loss} = Be^{\left(\frac{-31700+370,3\cdot C\_rate}{RT}\right)}(A_h)^{0,55} \tag{6.14}$$

B[ ] is defined as the pre-exponential factor, R [J/mol ºK] is the gas constant, T [ºK] is the cell temperature (T_{Max} of the cell in our case), C_rate[ ] is the current rate of the application and A_h [Ah] are the throughput ampere-hours defined us

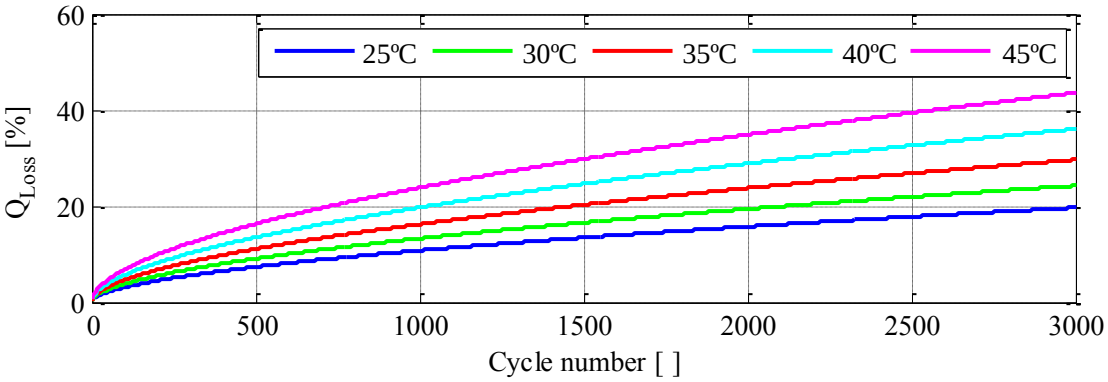

Fig 6.11. Capacity loss Q_{Loss} respect to cycle number for a constant 1C charge discharge cycle, for different cell temperatures.

(A_h=Cycle_number·DOD·Q_{Nom}). For the presented 4S1P application the values are the following ones:

- B=26655.
- R=8,314.
- C_rate= 1. 1C charge and discharge cycles.
- DOD= 100% full charge discharge cycles. The DOD is inserted in per unit value (DOD=1).
- Q_{Nom}=6,5 Ah.
- T=T_{Max} of the cells of the 4S1P battery pack. The temperature is inserted in Kelvin degrees K.

The temperature dependency with the capacity loss presented in (6.14) is plotted in Fig 6.11. Q_{Loss} of 20 % is estimated in 3000 cycles for 25ºC cell temperature and in 750 cycles for 45 ºC.

The temperature T_{Max} and energetic issues ($W^*_{BP,C}$, $W^*_{BP,D}$ and η^*_{BP}) are estimated in function of the SOH of the weakest cell by a linear interpolation. The linear interpolation equations are presented as:

$$T_{Max}(SOH) = \frac{T_{Max}(SOH_{EOL}) - T_{Max}(SOH_{BOL})}{SOH_{EOL} - SOH_{BOL}} SOH + T_{Max}(SOH_{BOL}) \quad (6.15)$$

$$W^*_{BP,D}(SOH) = \frac{W^*_{BP,D}(SOH_{EOL}) - W^*_{BP,D}(SOH_{BOL})}{SOH_{EOL} - SOH_{BOL}} SOH + W^*_{BP,D}(SOH_{BOL}) \quad (6.16)$$

$$W^*_{BP,C}(SOH) = \frac{W^*_{BP,C}(SOH_{EOL}) - W^*_{BP,C}(SOH_{BOL})}{SOH_{EOL} - SOH_{BOL}} SOH + W^*_{BP,C}(SOH_{BOL}) \quad (6.17)$$

Table 6.24 Energetic and temperature parameters obtained during subchapters 6.2.1 and 6.2.2 for 1C charge discharge cycling of a 4S1P LFP 6,5 Ah battery module. Parameters are used for linear interpolation of equations (6.15)-(6.18).

	T_{Max} [ºC]		$W^*_{BP,C}$ [Wh]		$W^*_{BP,D}$ [Wh]		η^*_{BP} [%]	
	SOH_{BOL}	SOH_{EOL}	SOH_{BOL}	SOH_{EOL}	SOH_{BOL}	SOH_{EOL}	SOH_{BOL}	SOH_{EOL}
NB	29,16	29,76	96,575	65,22	-92,379	-62,33	95,379	95,60
PB	28,61	29,59	97,89	70,69	-92,28	-63,24	94,28	89,49
AB	29,23	29,53	96,96	66,96	-92,48	-63,94	95,39	95,51
	Q_{BOL} [Ah]		SOH_{BOL} [%]		Q_{EOL} [Ah]		SOH_{EOL} [%]	
	7,273		112%		5,2		80%	

$$\eta^*_{BP}(SOH) = \frac{\eta^*_{BP}(SOH_{EOL}) - \eta^*_{BP}(SOH_{BOL})}{SOH_{EOL} - SOH_{BOL}} SOH + \eta^*_{BP}(SOH_{BOL}) \quad (6.18)$$

The parameters for equations (6.15)-(6.18) for the 4S1P battery module under life time energy estimation are presented in Table 6.24. The listed parameters are obtained from the experimental results presented in subchapters 6.2.1 and 6.2.2. The capacity loss from BOL to EOL is of 32% (112%-80%).

The life time energy estimation is carried out by the flow chart presented in Fig 6.12. The estimation flow chart could be used with a different aging pattern, or different temperature and energetic results.

During **INITIALIZATION** step the beginning of Life BOL and end of life EOL parameters are measured for writing equations (6.15)-(6.18). The minimum capacity cell limits the values for SOH_{BOL} which is the limiting aging cell with the maximum temperature T_{Max}. The DOD of the application is also defined.

Afterthet, during **AGING** step the aging pattern is introduced where the capacity loss is calculated depending on temperature (T_{Max} cell for our case) and the number of cycles.

After calculating the capacity loss, during **ESTIMATION** step the new SOH is calculated. The SOH value is introduced in equations (6.15)-(6.18) to estimate the new temperature and energetic values.

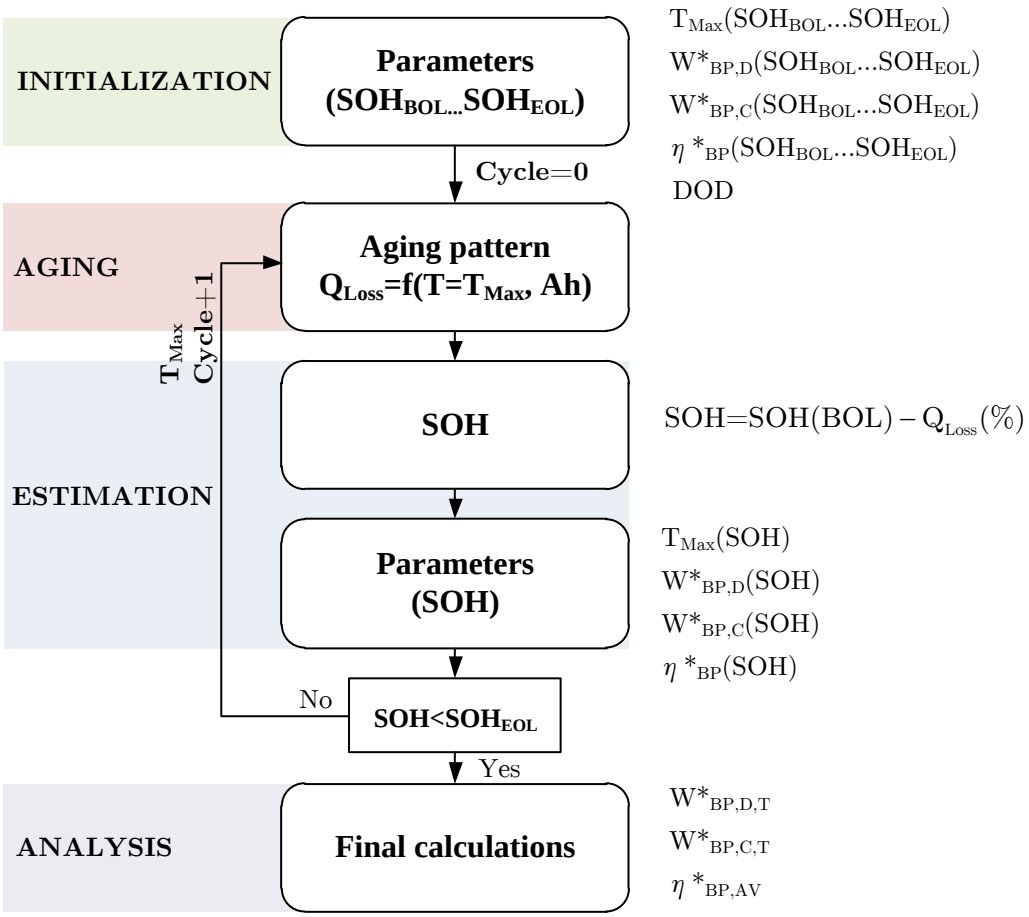

Fig 6.12. Flow chart presentation of the life time energy estimation of a battery pack where the temperature influence affects the aging process and different balancing systems energetic behaviour is taken into account.

If the SOH is smaller than end of life SOH, the total charged energy $W^*_{BP,C,T}$, total discharged energy $W^*_{BP,D,T}$ and the average efficiency $\eta_{BP,AV}$ during the whole cycle life are calculated during **ANALYSIS** step. If SOH_{EOL} is not reached, the cycle life number is increased, and the capacity loss is recalculated.

The cycle life evolution of the temperature T_{Max}, total discharged energy $W^*_{BP,D,T}$ during cycle life , total charged energy $W^*_{BP,C,T}$ and battery pack efficiency η^*_{BP} evolution during cycle life are presented in Fig 6.13. Table 6.25 summarizes final results for energetic estimation during cycle life.

Fig 6.13 a) presents the total discharged energy during the cycle life. The AB balancing system discharges 382,26 kWh, 3,27% more than the NB case, and the PB discharges 378,60 kWh 2,28% more than the NB.

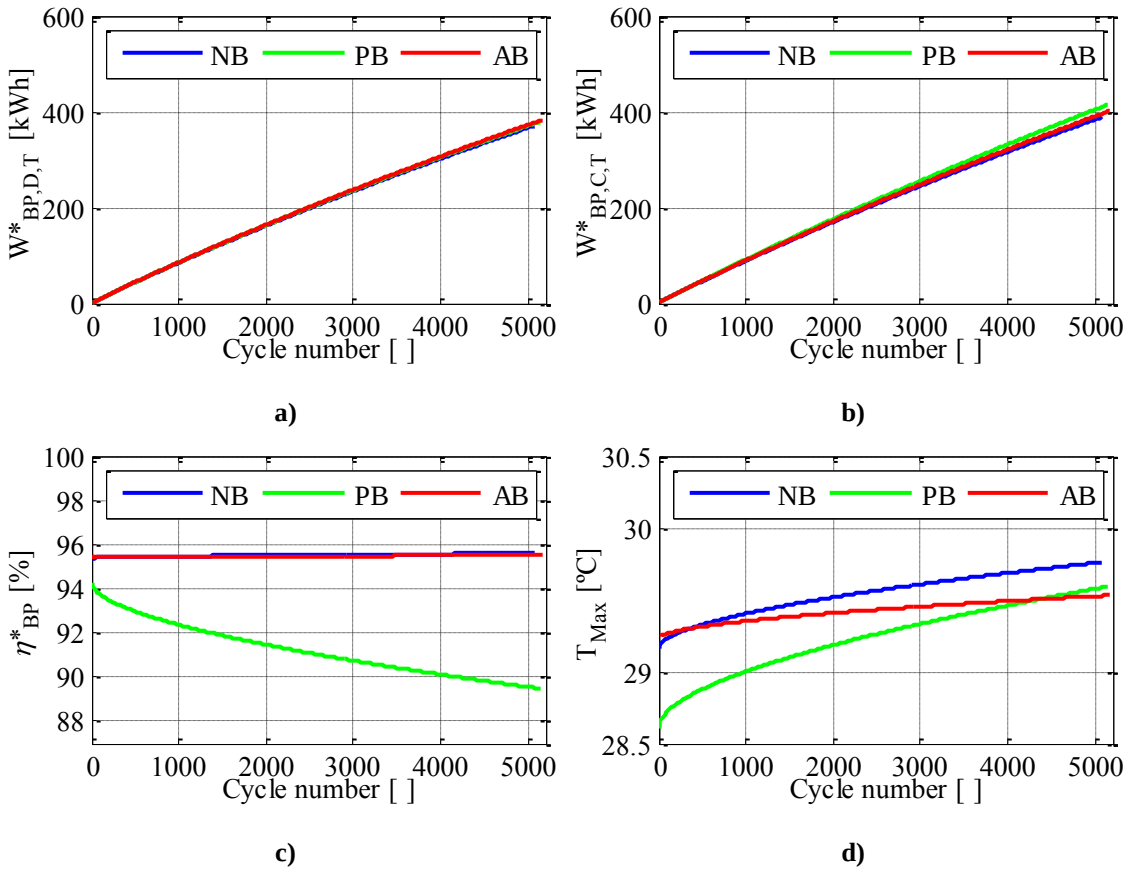

Fig 6.13. Energetic and temperature evolution respect to cycle number for a 4S1P battery module with NB, PB and AB systems. A) Total discharged energy $W^*_{BP,D,T}$ b) Total charged energy $W^*_{BP,C,T}$ c) Battery module efficiency η^*_{BP} d) Battery module maximum temperature T_{Max}.

Analysing the total charged energy to the battery pack in Fig 6.13 b), which impacts directly in the wasted money to charge the battery, the AB balancing system charges 400,52 kWh, 3,33% more than the NB case, and the PB charges 413,43 kWh 6,64% more than the NB. The electric bill is increased respect to the NB system with balancing systems.

The efficiency analysis presented in Fig 6.13 c) concludes that for NB and AB case the efficiency is nearly kept constant during the whole cycle life. However for the PB case, the efficiency is reduced while SOH is reduced.

The temperature evolution presented is plotted in Fig 6.13 d) respect to the cycle number instead of the SOH (respect to SOH is modelled as a linear interpolation exposed in equation (6.15)). The temperature impact is very high in the energetic issues during cycle life. As presented before, the capacity loss estimation is made with the

Table 6.25 Total energetic predicted results during a 4S1P battery life time.

	Cycle number [ ]		$W^*_{BP,C,T}$ [kWh]		$W^*_{BP,D,T}$ [kWh]		$\eta^*_{BP,AV}$ [%]	
NB	5069	0 %	387,66	0%	370,15	0%	95,52	0%
PB	5134	+1,28%	413,43	+6,64%	378,60	+2,28%	91,22	-4,3%
AB	5157	+1,73%	400,52	+3,31%	382,26	+3,27%	95,47	-0,05%

aging pattern presented in bibliography work [55] and summarized with equation (6.14). However, the flow chart analysis presented is prepared to work with the aging pattern of the 6,5 Ah cells under test when data is available.

The cycle number during battery life time is increased 1,28% until 5134 cycles with the PB and 1,73% until 5157 cycles with the AB, increasing the total discharged energy. Temperature difference T_{Max} in 6,5 Ah LFP cells with NB, PB or AB balancing system does not increase so much with the cycle number because the capacity loss Q_{Loss} as presented in Fig 6.14, does not differ so much between different balancing systems.

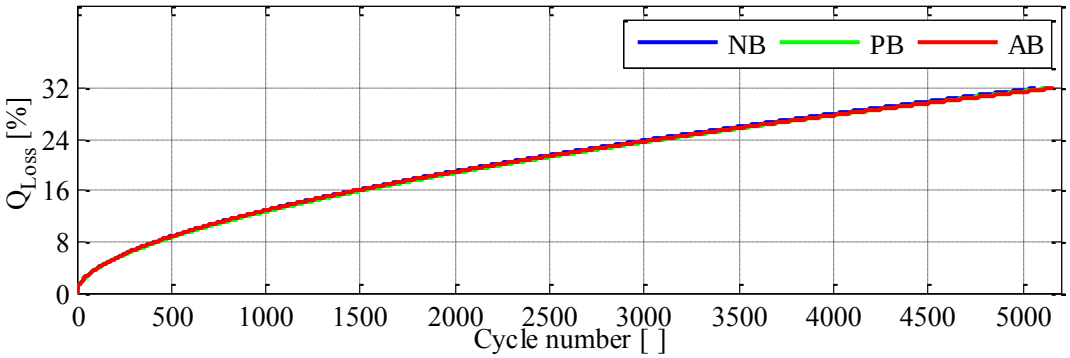

Fig 6.14. Capacity loss Q_{Loss} respect to cycle number for a constant 1C charge discharge cycle, for NB, PB and AB systems from BOL to EOL for a 4S1P battery module.

6.5 Conclusions of the chapter

During the present chapter an evaluation process has been presented to compare balancing systems.

The comparison parameters are divided in energetic issues, temperature behaviour and balancing system cost. The energetic issues of the battery pack are evaluated via the charged energy $W_{BP,C}$, the total discharged energy $W_{BP,D}$ and the efficiency between the charged energy and the discharged energy η_{BP}. The energetic behaviour from the point of view of the customer ($W^*_{BP,C}$ $W^*_{BP,D}$ η^*_{BP}), considering the battery pack the composition of the battery cells and the balancing system is the most interesting parameter. The temperature behaviour is analysed for the maximum cell temperature T_{Max} of a battery pack, the temperature dispersion of the cells inside a battery pack ΔT and the maximum temperature reached in the balancing system T_{BS} due to power losses. Finally the cost of the balancing systems $C_€$ is evaluated.

The analysis is performed for 10 consecutive charge/discharge cycles to measure balancing system performance under cycling. The results presented are the 10 consecutive cycles mean values, reducing measurement dispersion and deviation errors.

The balancing systems under comparison are no balancing (NB) system, a passive balancing system (PB) and an active balancing (AB) system. The AB balancing system is a multi stacked sepic balancing system for the 4S1P configuration, and a mixed balancing system between intramodule sepic balancing and parallel connected full bridge intermodule balancing system for the 16S1P configuration.

The cycling analysis of LMO and LCO cells has presented that due to very low dispersion between cells ($\Delta Q_{Max} \approx 1\%$) the balancing system does not improve the battery pack performance because it does not act the battery cells module.

First a 4S1P LFP battery module has been analysed, with 6,5 Ah cells (new and aged configuration), and a 1,1 Ah new cells.

NB system performs the best battery pack efficiency of all the system because there are not power losses, however it limits the battery pack discharge process because

less energy is charged. The maximum temperature and temperature deviation is also typically higher than for PB and AB, although due to 1C low rate current the temperature differences are low. The cost and the temperature of the balancing system are the minimum because no balancing system is used.

PB balancing system charges more the battery pack, and therefore obtains more energy during discharge increasing +0,18% for new 6,5 Ah cells, 1,46 % with one 6,5 Ah aged cell, and 0,6 % for 1,1 Ah cells. The temperature behaviour is also deteriorated when the cells are aged. Other big disadvantages are the increase in the electric bill due to higher charge energy and the generated hot spots in the balancing system with a maximum temperature of 119,3 ºC. The energetic efficiency of the battery pack is also reduced with PB, however if the PB system is disabled during discharge the efficiency could be improved.

AB balancing system charges the battery pack less than the PB system but performs superior behaviour respect to total discharged energy. An increase of 0,4% for 6,5 Ah new cells, 1,2 % for 1,1 Ah new cells and 2,5 % discharge energy increase for an aged 6,5 Ah battery module is performed, even if the balancing system is not designed for high SOH unbalances (low current balancing system is designed for low SOH differences). The cost is low due to low complexity single switch structure, being competitive (even lower) against the PB, because the voltage measurements could be avoided (however a BMS is necessary to measure voltage to guarantee Li-ion cells secure working). The temperature of the balancing system is also low due to low power losses and the maximum temperature of the cells, and temperature dispersion is reduced during aging process.

The results of a 16S1P 6,5 Ah LFP battery pack reveal that the presented intramodule-intermodule modular active balancing system is a suitable low complexity balancing system option for high number of series connected battery packs. The energetic and temperature issues are only compared in the 16S1P battery pack, for 3 different configurations: 16 new cells (newly constructed battery pack), 4 aged cells(one module aged), one aged cell (accelerated aging of single cell). The spyder chart resume for the 100% SOH low SOH dispersion cells is presented in Fig 6.15.

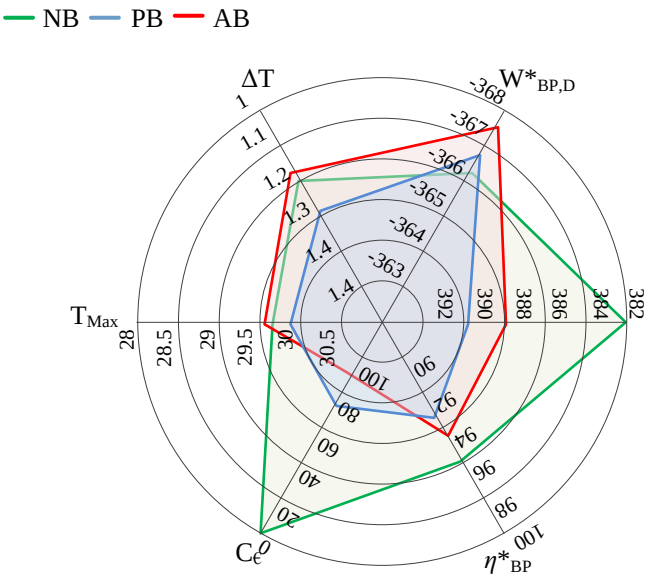

Fig 6.15. Comparison parameters for a 16S1P LFP Q_{Nom}=6,5 Ah battery pack scenario with new cells 100% SOH and low SOH dispersion. NB, AB and PB system under comparison.

NB system continues performing the highest efficiency, however the discharged energy is highly decreased, especially for accelerated aging processes.

PB system charges the best the battery pack, and increases the discharged energy +0,14% with 16 new cells +3,6% with one 4 cell module aged and the awesome +14,47% if one cell is accelerated aged, always respect to NB system. The maximum temperature of the cells is also increased which could yield to faster aging processes.

The AB system maintains efficiency near NB due to low power losses, charges less than PB system and discharges higher energy. Compared to NB system, increases discharged energy +0,28% for new cells, +4,53% for one aged module and +8,75% for one single aged cell. The maximum temperature of the cells in the battery pack is also reduced, and the temperature dispersion as well. The energetic behaviour could be improved if the balancing system is designed for higher SOH unbalances, with higher balancing currents.

During the final subchapter a battery life time energy analysis has been presented based on an aging pattern proposed in the literature [55] for LFP cells, that has been used for the 6,5 Ah LFP cells under study during the thesis work. The aging pattern temperature influence has been changed while the battery pack ages due to cycling with experimental temperature data obtained for 4S1P 6,5 Ah temperature analysis. An

approximated energetic analysis has been presented comparing NB, PB and AB during a 4S1P battery cycle life.

The PB system increases the total charged energy +6,64% (more expensive electric bill), the total discharged energy is increased +2,28% (more battery energy), and the mean efficiency of the battery pack during cycle life is reduced -4,3%.

The AB system increases the charged energy +3,31 % (half passive balancing), increases the discharged energy 3,27 % (increased battery energy) and the efficiency is kept nearly constant to NB with a little reduction of -0,05%.

These results should be corroborated by experimental aging patterns of 6,5 Ah LFP cells, but present a first estimation of balancing systems improvement in LFP battery packs.

Chapter 7

CONCLUSIONS AND FUTURE WORK

During this chapter main conclusions of the thesis work are presented. The first paragraph presents the main objective achievement.

A summarize of each subchapter conclusions is presented during the conclusions chapter.

Finally, future work lines will be presented.

7.1 Conclusions

The main objective of the thesis work is the "Energy and efficiency improvement of an energy storage system based on Lithium-ion technology". The results presented in chapter 6 present an energy increase in Li-ion battery packs due to passive and active balancing systems, and active balancing maintains battery efficiency close to the efficiency without balancing system. The life time energy approach for 4S1P battery packs presented in subchapter 6.4 exhibits and energy improvement of 2,28% for the passive balancing system and 3,27% for the active balancing system. The efficiency is decreased -4,3 % for the passive balancing system and only -0,05% for the active balancing system, concluding that the active balancing system is superior in order to improve the energetic behaviour of the battery pack. The main objective has been fulfilled by one main requirement: low complexity active balancing systems to compete against passive balancing systems. Modular balancing systems divided in intramodule and intermodule balancing systems present an affordable solution to replace passive balancing systems in series connected Li-ion battery packs.

Each chapter conclude with the chapter most important conclusions. The main qualitative conclusions (for quantitative conclusions refer to each chapter conclusions) are presented following.

Chapter 2 STATE OF THE ART conclusions give main weaknesses found in literature respect to series connected Li-ion battery packs. The weaknesses found in the state of the art give the main pads where the research work has been carried out. The main weaknesses are briefly listed in the following.

- There is not lack of information related to unbalancing effects in series connected cells.
- Passive balancing is the most used balancing system. A competitive active balancing system is necessary.
- There balancing system design and sizing is not well presented in literature.

Chapter 3 LFP SERIES CONNECTED UNBALANCING EFFECTS AND CAUSES presents a methodology to test series connected LFP battery packs. The results present that due to C-rate the battery performance is highly reduced and that the battery pack is not

unbalanced due to cycling. Great effort has to be made in BMS measurement systems as could be main cause for unbalance in series connected Li-ion battery packs.

During **Chapter 4** SERIES CONNECTED ENERGY STORAGE MODULAR BALANCING SYSTEMS active balancing systems design is presented. Modular balancing systems are presented as the best approach to solve the balancing problem of high number of series connected cells. Modular balancing systems are defined as intramodule balancing systems (balance cells inside a module) and intermodule balancing systems (balance modules inside the battery pack). The balancing systems have been designed to work in open loop control reducing the balancing system complexity to the minimum in order to obtain a competitive solution against the passive balancing system.

6 intramodule balancing systems have been modelled and designed, obtaining good accuracy between modelled and experimental results. The multi stacked Sepic balancing system has been chosen for future designs as the most promising balancing system due to the use of a low side switching device and the absence of transformers.

2 intermodule systems have been modelled and designed. The full bridge parallel connected intermodule system presents higher performance, specially due to selective energy transfer, and the most important; no voltage limitation in high number of series connected Li-ion battery packs. The intermodule balancing systems could be connected in large battery packs modularly, without any change in the electronic design.

All the different balancing systems are tested in a power supply- power resistor based test bench. Even if the thesis orientation is related to Li-ion cells, the analysed balancing systems could work with any other technology (lead- acid, Nickel based, ultracaps...) where a voltage unbalance between cells could be presented.

Chapter 5 METHODOLOGY FOR BALANCING SYSTEM DESIGN presents a methodology design based on single cell test data. The methodology gives the possibility to evaluate a balancing system performance in a series connected battery pack without the need of a cell model. Knowledge based design is also presented where main battery balancing equations are presented. With the previously obtained knowledge a new balancing system design for a 16S1P battery pack has been designed

composed of 4 modular intramodule-intermodule balancing systems The intramodule balancing system is composed of a multi stacked sepic balancing system and the intermodule system is a parallel connected full bridge topology.

Chapter 6 EVALUATION OF ACTIVE BALANCING SYSTEMS presents a comparative review of no balancing, passive balancing and active balancing system for Li-ion series connected battery packs. The results are calculated for 10 consecutive charge discharge cycles to evaluate average performance during cycling, not only a single cycle. The results obtained present that active balancing systems have the best mean results, relating temperature and energetic issues, for 4S1P battery modules with intramodule design and for 16S1P battery pack with a mixed intramodule intermodule balancing system. The battery pack without balancing system is better related to cost and the charged battery to the battery pack is smaller. However the discharged energy is lower. Passive balancing systems charge better the battery pack, with the disadvantage that more energy is consumed from the electric grid due to passive balancing power losses.

7.2 Future work

After thesis defence, future work will be focused on improving characteristics of modular active balancing systems. Main relevant working points will be:

- Increase of the balancing current of active balancing systems when low voltage difference is presented to better charge the battery during CV charge process.
- Evaluate the active balancing behaviour for power applications:
  - High C-rate applications.
  - Pulse power applications, for example specific EV patterns as the New European Driving Cycle NEDC.
- Design high current active balancing systems for high SOH unbalance cells, for second life Li-ion exploit.
- Apply active balancing systems designs for other battery chemistries as series connected lead-acid batteries.

Annex A

ANALYTICAL MODELLING OF HIGH FREQUENCY CONVERTERS

During this Annex main modelling methods are presented for analytical analysis of high frequency switching converters.

First subchapter will introduce piecewise modelling equations. The piecewise modelling equations are expressed in order to relate the average AV, Root mean square RMS and differential ΔX magnitudes.

Second subchapter presents main power loss equations of common power converters.

Final subchapter will present power limits and device rating specifications, necessary in order to choose a power device for a converter application.

A.1 Piecewise waveform analysis

The piecewise waveform analytical models are the most common method for analysing power converters behaviour. Literature reference power converter books as [111] present this type of analysis. During this subchapter a relation between the RMS and AV parameters will be presented for the next waveforms:

- **Triangular waveforms:** Hard switching and Discontinuous conduction mode DCM waveforms.
- **Constant waveforms:** Zero voltage constant current shape for power converters.
- **Trapezoidal waveforms:** Constant current and current ripple as CCM operation of DCDC converters.
- **Fully sinusoidal:** AC excitation systems and subresonant resonant converters.
- **Sinusoidal segment:** Above resonant converters and soft switching resonant behaviours.

Triangular waveforms

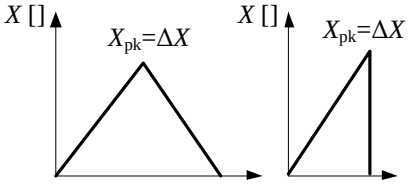

$$X_{AV} = \frac{X_{pk}}{2} = \frac{\sqrt{3}X_{RMS}}{2}$$

$$X_{RMS} = \frac{X_{pk}}{\sqrt{3}} = \frac{2X_{AV}}{\sqrt{3}}$$

Constant waveforms

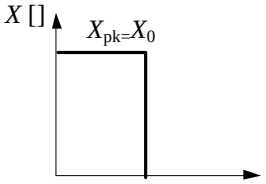

$$X_{AV} = X_{pk} = X_0 = X_{RMS}$$

$$X_{RMS} = X_{AV} = X_{pk} = X_0$$

Trapezoidal waveforms

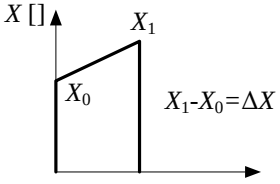

$$X_{AV} = X_0 + \frac{\Delta X}{2} = \frac{X_0 + X_1}{2}$$

$$X_{RMS} = \frac{\sqrt{\Delta X^2 + 3\Delta X \cdot X_0 + 3X_0^2}}{\sqrt{3}} = \frac{\sqrt{X_0^2 + X_1^2 + X_1 X_0}}{\sqrt{3}} = \frac{\sqrt{4X_{AV}^2 + 2X_{AV}X_0 + X_0^2}}{\sqrt{3}}$$

Full Sinusoidal

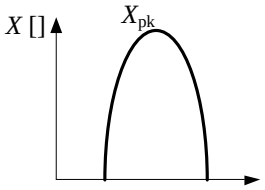

$$X_{AV} = \frac{2X_{pk}}{\pi} = \frac{2\sqrt{2}X_{RMS}}{\pi}$$

$$X_{RMS} = \frac{X_{pk}}{\sqrt{2}} = \frac{X_{AV}\pi}{2\sqrt{2}}$$

Sinusoidal segments

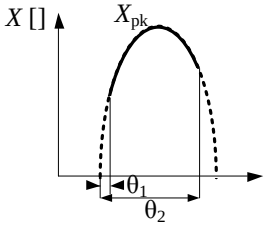

$$X_{AV} = \frac{X_{pk}}{\theta_2 - \theta_1}\left[-\cos\theta_2 + \cos\theta_1\right]$$

$$X_{RMS} = \frac{X_{pk}}{\sqrt{2}}\sqrt{\frac{\sin(\theta_1)\cos(\theta_1) - \sin(\theta_2)\cos(\theta_2) + \theta_2 - \theta_1}{\theta_2 - \theta_1}}$$

The analysis of the total RMS and AV value is made for a complete switching period. The switching period is divided in k period times:

$$\left.\begin{aligned} &D_1+D_2+...+D_p+...+D_k=1 \\ &T_1+T_2+...+T_p+...+T_k=T_S \end{aligned}\right\} \quad p=[1,k] \quad D_p = \frac{T_p}{T_S} \tag{A.1}$$

The piecewise analysis of the total RMS $X_{RMS,T}$ and total AV $X_{AV,T}$ values is calculated via equations (A.2) and (A.3).

$$\begin{aligned} X_{AV,T} &= \sum_{p=1}^{k} X_{AV,p}D_p = \frac{X_{AV,1}T_1 + X_{AV,2}T_2 + ... + X_{AV,k}T_k}{T_S} = \\ &= X_{AV,1}D_1 + X_{AV,2}D_2 + ... + X_{AV,k}D_k \end{aligned} \tag{A.2}$$

$$\begin{aligned} X_{RMS,T} &= \sqrt{\sum_{p=1}^{k} X_{RMS,p}{}^2 D_p} = \sqrt{\frac{X_{RMS,1}{}^2T_1 + X_{RMS,2}{}^2T_2 + ... + X_{RMS,k}{}^2T_k}{T_S}} = \\ &= \sqrt{X_{RMS,1}{}^2D_1 + X_{RMS,2}{}^2D_2 + ... + X_{RMS,k}{}^2T_k} \end{aligned} \tag{A.3}$$

The steady state analysis of all high frequency converters is based on two general laws. The volt-second balance of inductors and the charge balance of capacitors.

$$\begin{aligned} &\lambda = \int_0^{T_S} v_L(t)\,dt = 0 \\ &\frac{\lambda}{T_S} = V_{L,AV} = 0 \ \text{(Inductor volt second balance)} \end{aligned} \tag{A.4}$$

$$\begin{aligned} &Q = \int_0^{T_S} i_C(t)\,dt = 0 \\ &\frac{Q}{T_S} = I_{C,AV} = 0 \ \text{(Capacitor charge balance)} \end{aligned} \tag{A.5}$$

A.2 Power losses analysis

Switching power converters behaviour is typically analysed under ideal circuit behaviour. The three main elements of any high frequency converter are power switches, inductors and capacitors with ideal properties:

- Ideal switches: Zero voltage drop and instantaneous ON and OFF time.
- Ideal inductors: Non-resistance inductors.
- Ideal capacitors: Non-resistance capacitors.

However the non-idealities of power switches and resistive pads perform a power loss in the power converter. The power losses for a switching period in any active switch (diode, Mosfet, IGBT...) or resistive pad are expressed by (A.6)

$$P_{\mathrm{Loss}} = \frac{1}{\mathrm{T_S}} \int_0^{\mathrm{T_S}} v(\mathrm{t}) i(\mathrm{t})\, \mathrm{dt} \tag{A.6}$$

The converter power losses can also be calculated via analytical modelling of the Average AV and Root Mean Square Values RMS of the current values. The current values are typically calculated for the ideal converter analysis, with linear inductor and capacitor current waveforms. This approximation is possible thanks to keep the relation between the inductor value L and the resistance R low, and therefore the time constant τ=L/R has to be kept much higher than the switching period T_S (τ>>T_S).

The power switches are typically divided between bipolar systems (IGBT, BJT, etc.) and field effect transistors (MOSFET, FET, etc.). The power losses of power switches are divided in conduction losses P_{ON} and switching losses P_{SW}.

$$P_{\mathrm{Loss}} = P_{\mathrm{ON}} + P_{\mathrm{SW}} \tag{A.7}$$

The conduction losses of bipolar systems are calculated via their colector-emitter voltage drop and the field effect switches are evaluated as a power resistor behaviour between the drain and source.

$$P_{\mathrm{ON}} = V_{\mathrm{CE}}\left(v, T^{\circ}, \ldots\right) \cdot I_{\mathrm{AV}} \quad \text{(Bipolar)} \tag{A.8}$$

$$P_{\mathrm{ON}} = R_{\mathrm{DS}}\left(v, T^{\circ}, \ldots\right) \cdot {I_{\mathrm{RMS}}}^2 \quad \text{(Field Effect)} \tag{A.9}$$

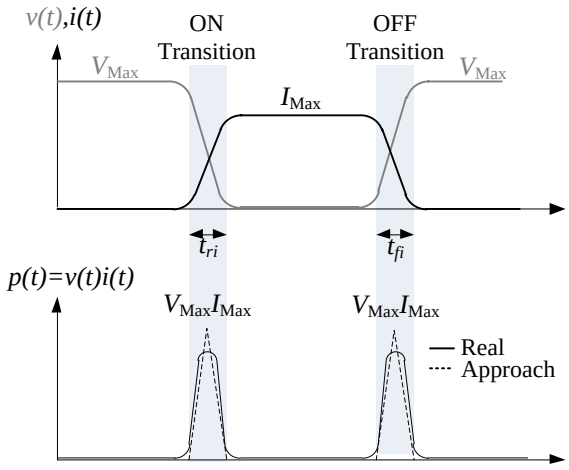

Fig A.1 Switching power losses estimation during ON and OFF transition for power transistors. Power losses triangular approach presented.

The conduction characteristics (V_{CE} or R_{DS}) are dependent on application voltage or chip temperature, so are typically calculated for the design working point.

The switching losses in power switches are dependent on the rising (t_{ri}) and falling times (t_{fi}) during the transitions between conduction ON state and blocking OFF state Fig A.1. The switching power losses are approximated by a triangular waveform analysis and calculated as:

$$P_{SW} = P_{SW\text{-}ON} + P_{SW\text{-}OFF} = \frac{1}{2} V_{Max} I_{Max} t_{ri} f_S + \frac{1}{2} V_{Max} I_{Max} t_{fi} f_S \quad \text{(Bipolar and Field Effect)} \tag{A.10}$$

Power diode losses are also divided in conduction losses and switching losses as described in (A.7). Conduction losses are evaluated via (A.11)

$$P_{ON} = V_D(v, T^\circ, ...) I_{AV} + r_D I_{RMS}^2 \quad \text{(Diode)} \tag{A.11}$$

Related to switching losses of power diodes, there are not ON transition power losses and the switching losses are only evaluated for the OFF transition. The diode OFF transition losses are due to reverse recovery and expressed as:

$$P_{SW} = \frac{1}{2} V_{Max} I_{rr} t_B f_S \quad \text{(Diode)} \tag{A.12}$$

Reverse recovery current I_{rr} also influences in power switches losses, because reverse recovery current appears during ON transition. However Schottky diodes are

typically used in power converters where reverse recovery losses can be neglected and also conduction losses are reduced respect to conventional diodes.

Resistive losses are calculated with the RMS current flowing through the capacitors and inductors. The power losses on the capacitors are dependent on the ESR and in for the inductor the series resistance R_L.

$$P_{RL} = R_L I_{RMS}^2 \tag{A.13}$$

$$P_{ESR} = \mathrm{ESR} I_{RMS}^2 \tag{A.14}$$

The total losses of the converter $P_{LOSS;T}$ are the sum of all the power losses of the individual power switches, diodes and resistors. The power converter efficiency is the division between the output power P_{out} and the input power P_{in}

$$\eta = \frac{P_{out}}{P_{in}} = \frac{P_{out}}{P_{out} + P_{LOSS,T}} = \frac{1}{1 + \frac{P_{out}}{P_{LOSS,T}}} \tag{A.15}$$

A.3 Power device rating

The power devices used in a power converter should be correctly rated in order to choose the correct device for the application. During this subchapter basic rating concepts will be presented. The power devices are typically rated for:

- Voltage.
- Current.

The voltage and current ratings should be fulfilled different working modes: Maximum, RMS or AV. The power device ratings are also influenced by the device temperature and also for the working ambient temperature. As a brief analysis main device necessary specifications are defined:

- Transistors (S).
  - V_{Max}: Not to overcome breakdown voltage
  - I_{Max}: Maximum device current for a limited time.
  - I_{RMS}: Maximum RMS device current for steady state operation.
- Diodes (D).
  - V_{Max}: Maximum voltage not to overcome breakdowm voltage.
  - I_{AV}: maximum AV device current under steady state.
- Inductors (L)
  - I_{AV}, I_{DC}= Maximum AV current and indication of stored magnetic energy on the inductor.
  - I_{RMS}: maximum RMS current. Conduction power losses and limitation for wire burning.
  - I_{Max}: Maximum instantaneous current, related with saturation and decrease of the autoinductance value.
  - V_{Max}: Maximum voltage related to isolation requirements and saturation.
  - Frequency: Working frequency is related with magnetic power losses. Different material selection (ferrites, iron powders...)
- Capacitors (Cap)
  - V_{Max}: Maximum voltage limit not overcharge capacitor.
  - I_{RMS}: Maximum RMS current. Related with power losses and heating of the capacitor.

- Frequency: Working frequency of the capacitor. Higher working frequencies reduce voltage capability of the system.

Annex B

ANALYSIS AND DESIGN OF ACTIVE BALANCING SYSTEMS

Annex B presents main analysis and design equations for active balancing systems. The active balancing systems are modelled with under ideal system evaluation. The RMS and AV values of main currents will be defined. Each component design equations are defined. Furthermore each component voltage and current ratings are defined.

The analysis and design will be held for intramodule and intermodule devices presented in Chapter 4. The analysis will express the behaviour of different components during each time interval of a complete switching period.

B.1 Intramodule balancing systems

Intramodule balancing systems analysis will be divided between design process and interval analysis. The design process gives the main equations to define all the circuit component values as inductors and capacitors. The interval analysis of intramodule systems will be held under assumption of equation (4.3) where the DCM is guaranteed, and 3 time interval periods are obtained: [$T_{ON}=DT_S$; $T_1=D_1T_S$.;$T_2=D_2T_S$]. The interval analysis gives the necessary waveform analysis to calculate RMS and AV values with equations presented in Annex A.1 and calculate power losses via equations of Annex A.2. Interval analysis also presents main values for power device rating.

B.1.1 Single core Flyback

B.1.1.1 Design process

Single core Flyback design process only calculates the magnetizing inductor L of the primary side of the core. D_C ($D \leq D_C$), N and $I_{Cb,W}$ are parameter designs presented in equations (4.3)-(4.5). Inductance value is them calculated as:

$$L=\frac{V_M D^2 T_s}{2I_{Cb,W}}\left(\frac{V_M}{V_{C,W}}-1\right) \tag{B.1}$$

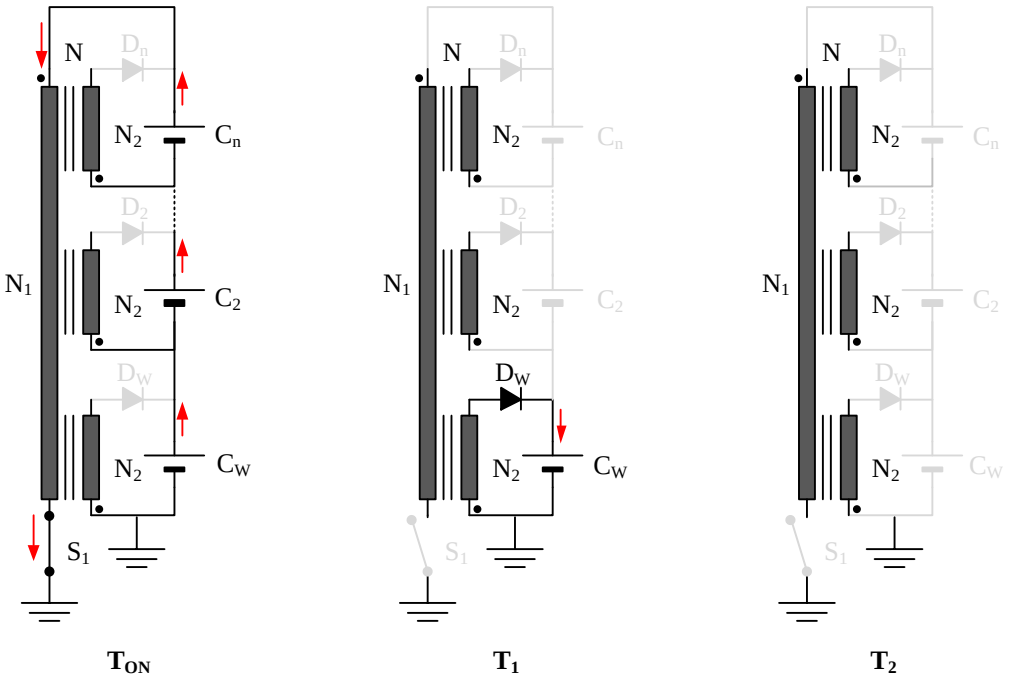

Fig B.1. Single core flyback intramodule active balancing system current paths during T_{ON}, T_1 and T_2

Table B.1 Current distribution for each time interval T_{ON}, T_1 and T_2 for the single core flyback

	L	**S_1**	**D_W**	**D_S**	**Annex A.1**
T_{ON}	I_{pk}	I_{pk}	0	0	Triangular
T_1	0	0	$I_{pk}N$	0	Triangular
T_2	0	0	0	0	Constant

D_1 period is directly related to the module voltage V_M and the weak cell voltage $V_{C,W}$. D_2 is the DCM guaranteeing period.

$$D_1 = \frac{V_M D}{N V_{C,W}}; \quad D_2 = 1 - D - D_1 \tag{B.2}$$

B.1.1.2 Interval Analysis

Single core flyback time interval analysis will be focused on the current value analysis for the weak cell and strong cells components for T_{ON}, T_1 and T_2 periods. Main current waveforms are presented in Fig 4.3 and interval current paths are highlighted in Fig B.1. The current values are referenced to the peak current or current variation value in the primary magnetizing inductor.

$$I_{pk} = \Delta I = \frac{V_M}{L} D T_s \tag{B.3}$$

With the knowledge of each period D, D_1 and D_2, and the peak value of the currents presented in Table B.1, RMS and AV can be calculated via equations presented in Annex A.1. The resulting analytical equations are not presented to reduce document complexity. The maximum instantaneous values are calculated when the module is fully charged $V_M = V_{M,Max} \rightarrow I_{pk,Max}$. Maximum value is necessary for power device rating.

B.1.2 Multiple core parallel connected Flyback

B.1.2.1 Design process

The design process of the multiple core parallel connected Flyback is focused on the determination of the value of the magnetizing inductance of the primary side L_n of each of the parallel connected transformers. D_C ($D \leq D_C$), N and $I_{Cb,W}$ are determined via balancing system design, as well as the number of cells n inside the intramodule system. The inductance L_n is defined as:

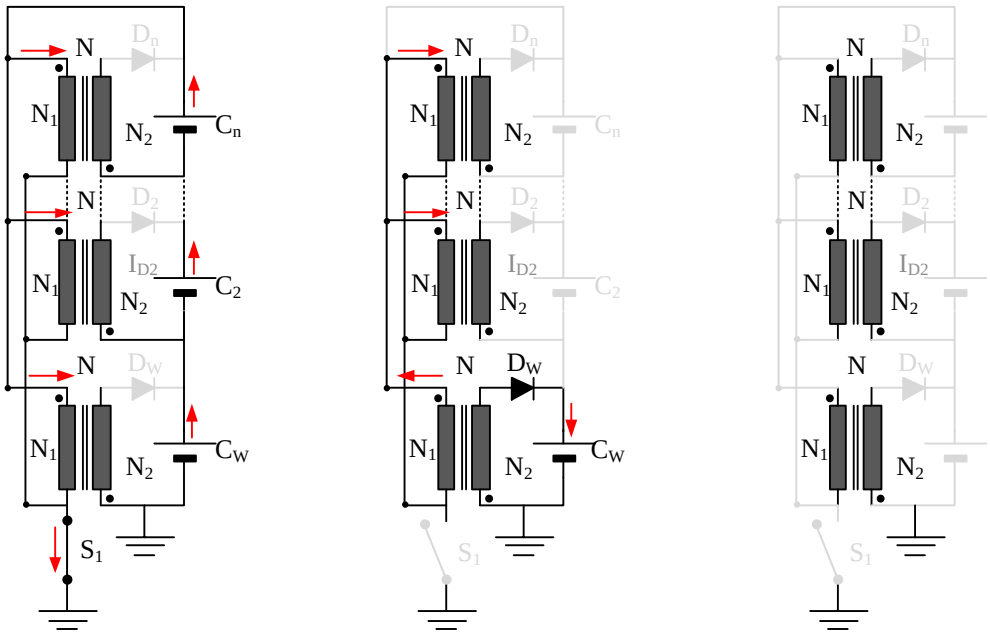

Fig B.2. Single core flyback intramodule active balancing system current paths during T_{ON}, T_1 and T_2

$$L_n = \frac{V_M D^2 T_s n}{2 I_{Cb,W}} \left(\frac{V_M}{V_{C,W}} - 1 \right) \tag{B.4}$$

The D_1 period and D_2 period are defined as:

$$D_1 = \frac{V_M D}{N V_{C,W}}; \quad D_2 = 1 - D - D_1 \tag{B.5}$$

B.1.2.2 Interval Analysis

The interval analysis of the multiple core parallel connected flyback permits to know the current distribution for the different time intervals T_{ON}, T_1 and T_2. The current distribution and the time interval knowledge permits to evaluate the RMS and AV values for all the different system devices.

The current distribution is calculated dependent on the peak current or current variation generated during T_{ON} on a single core.

$$I_{pk} = \Delta I = \frac{V_M}{L_n} D T_s \tag{B.6}$$

The maximum values for device rating are calculated with module voltage $V_M = V_{M,Max}$.

Table B.2 Current distribution for each time interval T_{ON}, T_1 and T_2 for the multiple core parallel connected Flyback.

	L_n	S_1	D_W	D_S	**Annex A.1**
T_{ON}	I_{pk}	$I_{pk}n$	0	0	Triangular
T_1	0	0	$I_{pk}nN$	0	Triangular
T_2	0	0	0	0	Constant

B.1.3 Multiple core series connected Flyback

B.1.3.1 Design process

During the design process of the multiple series connected Flyback, the magnetizing inductor L_n of the primary side of each transformer is designed. The L_n value is defined D_C ($D \leq D_C$), N and $I_{Cb,W}$ are determined.

$$L_n = \frac{V_M D^2 T_s}{2n I_{Cb,W}} \left(\frac{V_M}{n V_{C,W}} - 1 \right) \tag{B.7}$$

D_1 and D_2 value is different for each series connected cell [$D_{1,i}$, $D_{2,i}$]. The highest D_1 value is for the weak cell case.

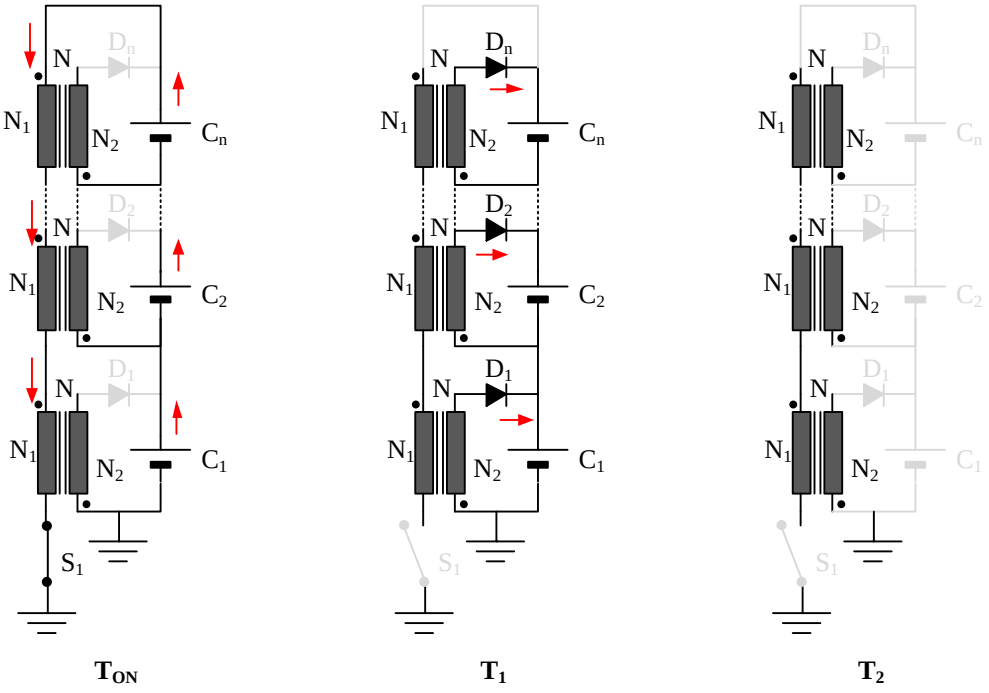

Fig B.3. Multiple core series connected flyback intramodule active balancing system current paths during T_{ON}, T_1 and T_2

Table B.3 Current distribution for each time interval T_{ON}, T_1 and T_2 for the multiple core series connected Flyback.

	L_i	S_1	D_i	**Annex A.1**
T_{ON}	I_{pk}	I_{pk}	0	Triangular
T_1	0	0	$I_{pk}N$	Triangular
T_2	0	0	0	Constant

$$D_{1,i}=\frac{V_M D}{nN\,V_{C,i}};\quad D_{2,i}=1-D-D_{1,i}\quad i=[1,n] \tag{B.8}$$

B.1.3.2 Interval analysis

The evaluation of RMS and AV values for multiple core series connected Flyback is different for each element that conducts during period D_1 Fig B.3. The current behaviour is modelled based on peak current of the primary side magnetizing inductor L_n and resumed in Table B.3. Maximum values for component rating are calculated for $V_M=V_{M,Max}$.

$$I_{pk}=\Delta I=\frac{V_M}{nL_n}DT_s \tag{B.9}$$

B.1.4 Multi stacked Sepic

B.1.4.1 Design process.

The design process of the Multi Stacked Sepic consists on the definition of L_{in}, L_n and Cap_n. During the balancing system sizing process D_C ($D \le D_C$), and $I_{Cb,W}$ are defined for a module working point. L_{in} and L_n are defined by solving equations (B.10) and (B.11).

$$I_{Cb,W}=\frac{V_M D^2 T_s\left(L_n+nL_{in}\right)}{2L_n L_{in}}\left(\frac{V_M}{V_{C,W}}-1\right) \tag{B.10}$$

$$\frac{L_{in}}{L_n}=\frac{D_{1C}}{D_C} \tag{B.11}$$

Equation (B.11) is obtained by the assumption presented in equation (B.12). The relation between the average current and the ripple current is kept equal for inductors L_n and L_{in}. This approximation is generally used in Sepic circuit design.

$$\frac{\Delta I_{Lin}}{I_{Lin,AV}}=\frac{\Delta I_{Ln}}{I_{Ln,AV}} \tag{B.12}$$

The capacitor value Cap_n is defined by the assumption that the voltage is kept constant. The capacitor voltage value is defined by (B.13).

$$V_{Cap,i} = V_M - \sum_{\substack{k=1 \\ i>1}}^{i-1} V_{C,k} \tag{B.13}$$

To maintain the voltage constant the resonant frequency of the LC tank has to be much smaller than the switching frequency $F_r << F_S$. During the Thesis work a relation of 40 ($F_S=40F_r$) has been implemented. With this approximation, Cap_n is defined by equation (B.14).

$$Cap_n = \frac{1}{(2\pi F_r)^2 (nL_{in}+L_n)} \tag{B.14}$$

D_1 and D_2 periods are defined by:

$$D_1 = \frac{V_M D}{V_{C,W}}; \quad D_2 = 1 - D - D_1 \tag{B.15}$$

B.1.4.2 Interval analysis

The interval analysis of the Multi Stacked Sepic converter permits to evaluate the RMS, AV and maximum limits of all the elements. The current values for each period will be approximated with the current values of 3 inductors: The weak cell inductor L_W the strong cells inductors $L_{i\ i\neq W}$ and the input inductor L_{in}. Due to trapezoidal waveform of the current during D and D_1 periods Fig 4.6, the interval analysis will be done with the initial current value I_0 and the ripple current value ΔI. The equations for the different inductors are:

$$\Delta I_{Li} = \Delta I_{L,W} = \frac{V_M}{L_n} DT_S \tag{B.16}$$

$$\Delta I_{Lin} = \frac{V_M}{L_{in}} DT_S \tag{B.17}$$

$$I_{0,Li} = -\frac{V_M DT_S (D+D_1)}{2L_i} \tag{B.18}$$

$$I_{0,Lw} = -\frac{V_M DT_S (DL_{in} - D_1 L_i - D_1 L_{in} n + D_1 L_{in})}{2L_i L_{in}} \tag{B.19}$$

$$I_{0,Lin} = \frac{V_M DT_S (DL_{in} - D_1 L_i - D_1 L_{in} n + D_1 L_{in})}{2L_i L_{in}} + (n+1)\frac{V_M DT_S (D+D_1)}{2L_i} \tag{B.20}$$

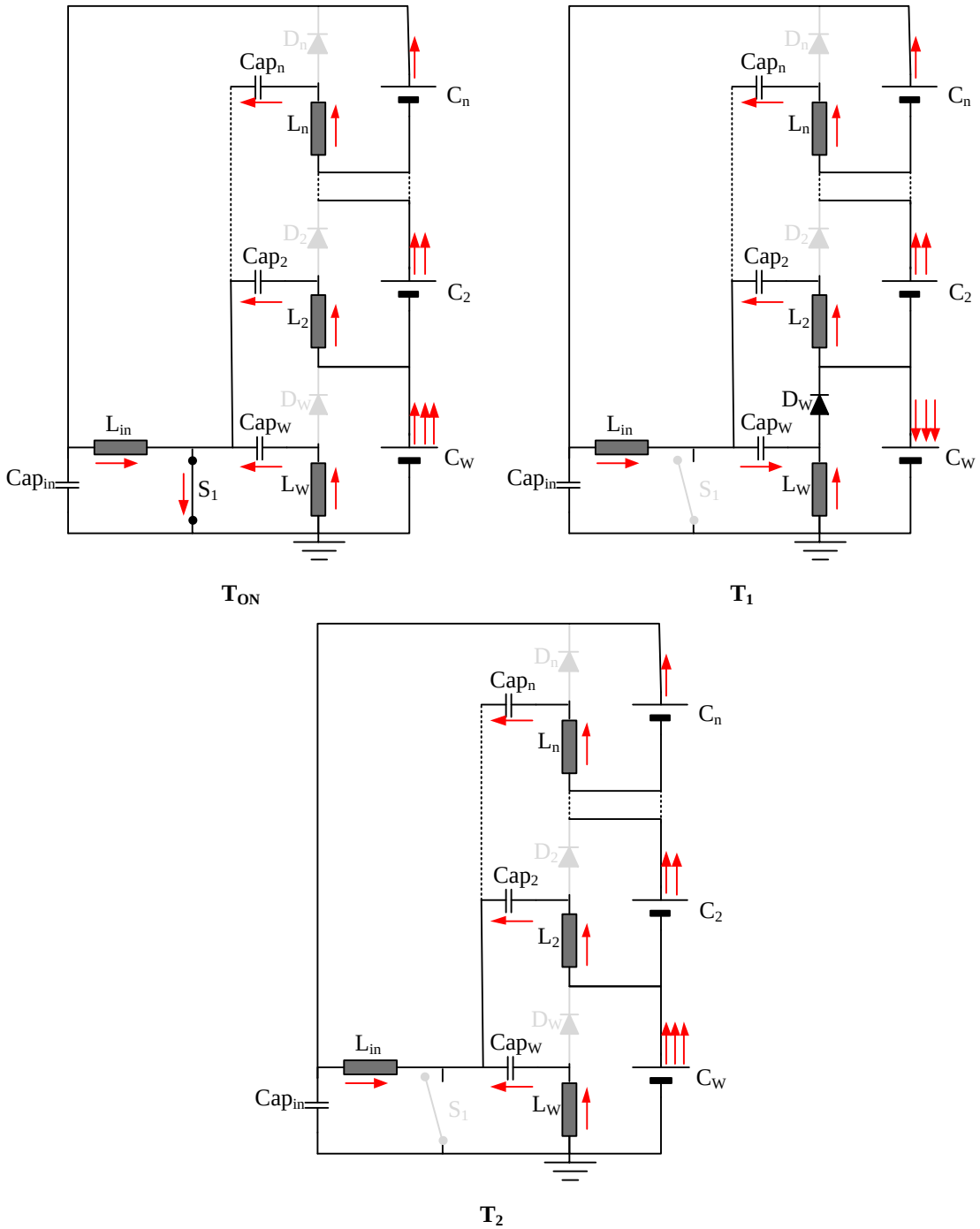

Fig B.4. Multi Stacked Sepic intramodule active balancing system current paths during T_{ON}, T_1 and T_2

The current paths during intervals are presented in Fig B.4. The analysis of time period T_1 clarifies that only the weak cell receives energy. The capacitor charge balance equation also gives that if the strong cell diode average currents are zero, the strong cell inductors current are also zero. Fig 4.6 represents the strong cell inductors current with a zero average value.

Table B.4 Current distribution for each time interval T_{ON}, T_1 and T_2 for the Multi Stacked Sepic.

	L_W	**Li**	**Lin**	**S_1**	**Annex A.1**
T_{ON}	$\Delta I = \Delta I_{Li}$	$\Delta I = \Delta I_{Li}$	$\Delta I = \Delta I_{Lin}$	$\Delta I = n\,\Delta I_{Li} + \Delta I_{Lin}$	Trapezoidal
	$I_0 = I_{0,Lw}$	$I_0 = I_{0,Li}$	$I_0 = I_{0,Lin}$	$I_0 = I_{0,Lin} + (n-1)I_{0,Li} + I_{0,Lw}$	
T_1	$\Delta I = \Delta I_{Li}$	$\Delta I = \Delta I_{Li}$	$\Delta I = \Delta I_{Lin}$	0	Trapezoidal
	$I_0 = I_{0,Lw}$	$I_0 = I_{0,Li}$	$I_0 = I_{0,Lin}$	0	
T_2	$I_0 = I_{0,Lw}$	$I_0 = I_{0,Li}$	$I_0 = I_{0,Lin}$	0	Constant
	D_W	**Di**	**Cap_W**	**Cap_i**	**Annex A.1**
T_{ON}	0	0	$\Delta I = -\Delta I_{Li}$	$\Delta I = -\Delta I_{Li}$	Trapezoidal
	0	0	$I_0 = -I_{0,Lw}$	$I_0 = -I_{0,Li}$	
T_1	$\Delta I = n\,\Delta I_{Li} + \Delta I_{Lin} + I_{0,Lin} + (n-1)I_{0,Li} + I_{0,Lw}$	0	$\Delta I = (n-1)\Delta I_{Li} + \Delta I_{Lin}$	$\Delta I = \Delta I_{Li}$	Trapezoidal
	$I_0 = 0$	0	$I_0 = -I_{0,Lw}$	$I_0 = -I_{0,Li}$	
T_2	0	0	$I_0 = -I_{0,Lw}$	$I_0 = -I_{0,Li}$	Constant

The ripple current ΔI and initial current I_0 value for the RMS, AV and maximum analysis is presented in Table B.4.

B.1.5 Multi Stacked Zeta

B.1.5.1 Design process

The Multi Stacked Zeta design process is equivalent to Sepic process, and calculates the L_n, L_{in} and Cap_n values via equations (B.10)-(B.12) and (B.14). The constant voltage supported by the capacitors is different and is expressed by equation (B.21).

$$V_{Cap,i} = \sum_{k=1}^{i} V_{C,k} \tag{B.21}$$

D_1 and D_2 periods are expressed by equation (B.15).

B.1.5.2 Interval analysis

The interval analysis of the Zeta converter, combines with the D,D_1 and D_2 period result permit to evaluate the RMS, AV and maximum values during a switching period.

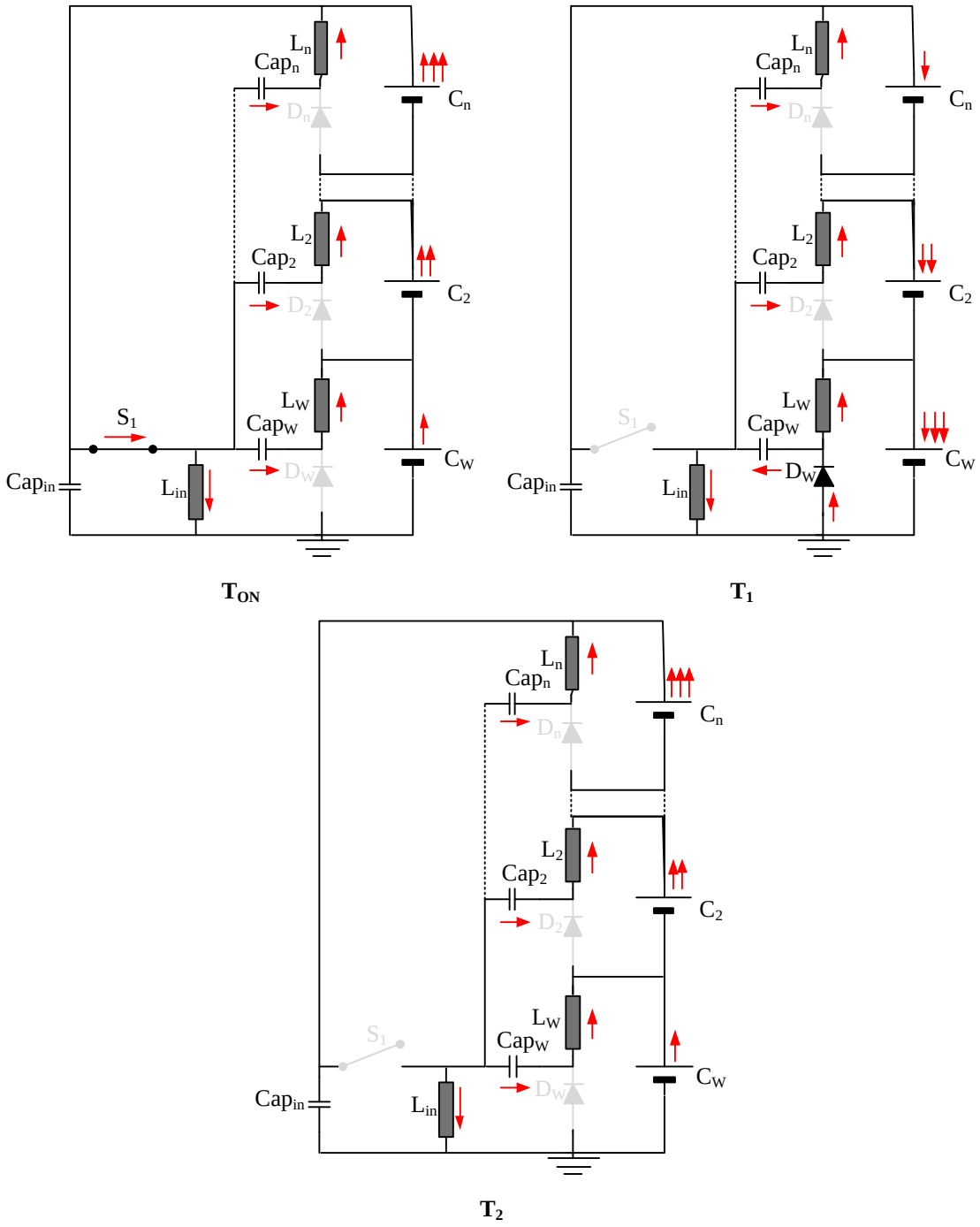

Fig B.5. Multi Stacked Zeta intramodule active balancing system current paths during T_{ON}, T_1 and T_2

The equations representing current ripple and initial current (B.16)-(B.20) and the expressions presented in Table B.4 are equal for the Sepic and the Zeta. However, the current waveform in the series connected cells is different for each system. The current distribution is highlighted in Fig B.5.

B.1.6 Multi Stacked Isolated Cuk

B.1.6.1 Design process

The design process of the Multi Stacked Cuk intramodule system relies on defining L_n, L_{in}, Cap_n and the split capacitor for the Cuk configuration named Cap_{Cuk}. The transformation ratio N, critical duty cycle D_C ($D \leq D_C$) and the weak balancing current $I_{Cb,W}$ are defined during the balancing system sizing process. L_{in} and L_n are calculated by solving the equations (B.22) and (B.23).

$$I_{Cb,W} = \frac{V_M D^2 T_s \left(L_n + \frac{n L_{in}}{N^2} \right)}{2 N_2 L_n L_{in}} \left(\frac{V_M}{V_{C,W}} - 1 \right) \tag{B.22}$$

$$\frac{L_{in}}{L_n} = \frac{D_{1C}}{D_C} N^2 \tag{B.23}$$

(B.23) is obtained maintaining the relation of average current and ripple current between L_n inductors and input inductor L_{in}. Capacitors Cap_n and Cap_{Cuk} maintain their voltage constant.

$$\begin{aligned} V_{Cap,i} &= \sum_{k=1}^{i} V_{C,k} \\ V_{Cap,Cuk} &= V_M \end{aligned} \tag{B.24}$$

The voltage of the capacitors is constant due to the resonant frequency is much lower than the switching frequency $F_r << F_S$. The capacitor values are set to:

$$\begin{aligned} Cap_n &= \frac{1 + N^2}{N^2 (2\pi F_r)^2 \left(n L_{in} + N^2 L_n \right)} \\ Cap_{Cuk} &= n Cap_n \end{aligned} \tag{B.25}$$

D1 and D2 periods are defined as

$$D_1 = \frac{V_M D}{N V_{C,W}}; \quad D_2 = 1 - D - D_1 \tag{B.26}$$

B.1.6.2 Interval analysis

The current paths for intervals D, D_1 and D_2 are presented in Fig B.6. The analysis of the current during different intervals permits to obtain the RMS, AV and maximum values for different circuit components. The analysis is presented as for the Sepic and Zeta converters by the analysis of the initial current I_0 and ripple current ΔI of the

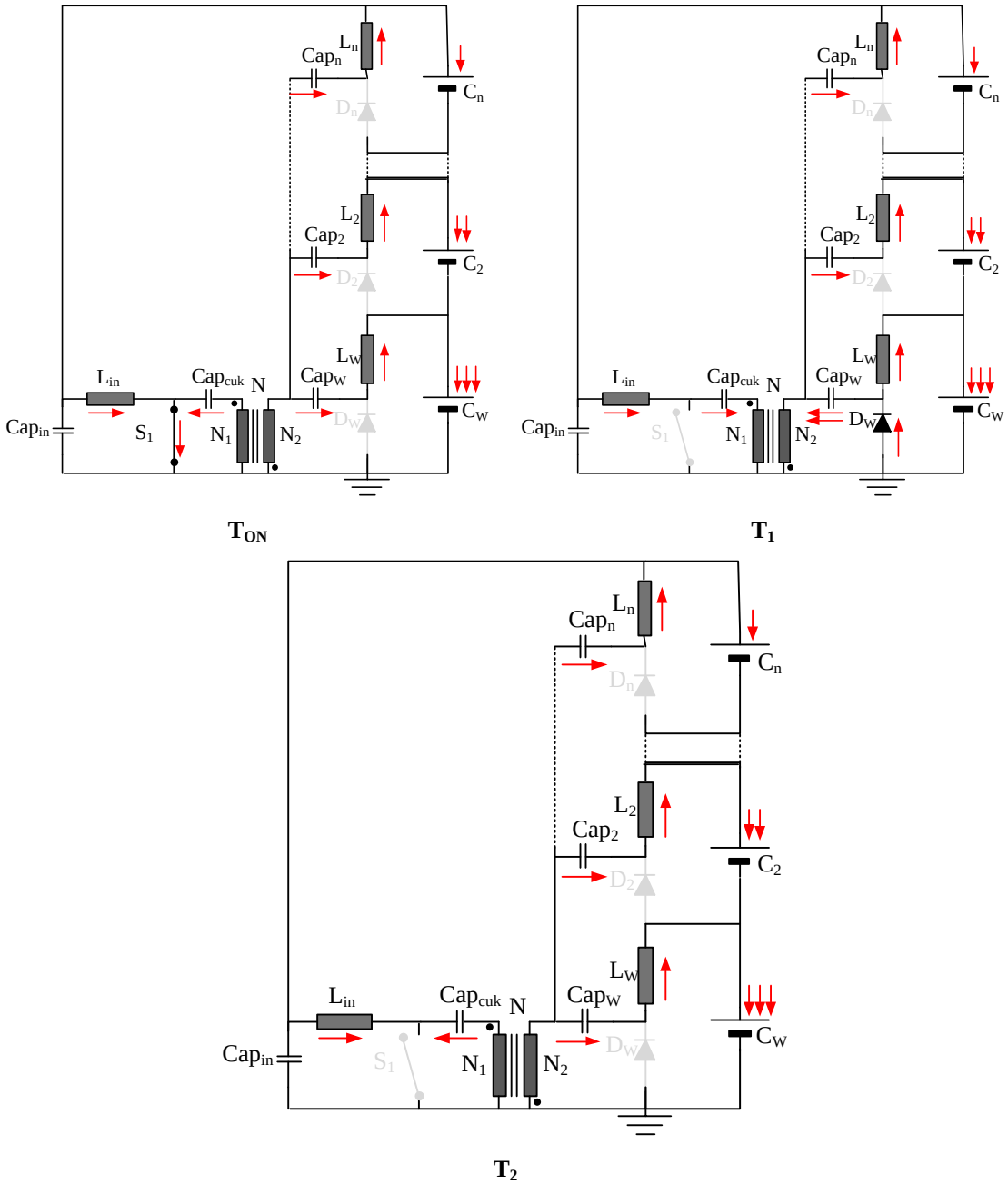

Fig B.6. Multi Stacked Isolated Cuk intramodule active balancing system current paths during T_{ON}, T_1 and T_2

circuit inductors. The equations (B.27) to (B.31) give current ripple and initial current values. Table B.5 gives main values for the RMS and AV analysis.

$$\Delta I_{Li} = \Delta I_{L,W} = \frac{V_M}{NL_n} DT_S \tag{B.27}$$

$$\Delta I_{Lin} = \frac{V_M}{L_{in}} DT_S \tag{B.28}$$

$$I_{0,Li} = -\frac{V_M DT_S (D+D_1)}{2NL_i} \tag{B.29}$$

Table B.5 Current distribution for each time interval T_{ON}, T_1 and T_2 for the Multi Stacked Isolated Cuk.

	$\mathbf{L_W}$	**Li**	**Lin**	$\mathbf{S_1}$	**Annex A.1**
T_{ON}	$\Delta I = \Delta I_{Li}$	$\Delta I = \Delta I_{Li}$	$\Delta I = \Delta I_{Lin}$	$\Delta I = n\,\Delta I_{Li}/N + \Delta I_{Lin}$	Trapezoidal
	$I_0 = I_{0,Lw}$	$I_0 = I_{0,Li}$	$I_0 = I_{0,Lin}$	$I_0 = I_{0,Lin} + (n-1)I_{0,Li}/N + I_{0,Lw}/N$	
T_1	$\Delta I = \Delta I_{Li}$	$\Delta I = \Delta I_{Li}$	$\Delta I = \Delta I_{Lin}$	0	Trapezoidal
	$I_0 = I_{0,Lw}$	$I_0 = I_{0,Li}$	$I_0 = I_{0,Lin}$	0	
T_2	$I_0 = I_{0,Lw}$	$I_0 = I_{0,Li}$	$I_0 = I_{0,Lin}$	0	Constant

	$\mathbf{D_W}$	**Di**	$\mathbf{Cap_W}$	$\mathbf{Cap_i}$	$\mathbf{Cap_{Cuk}}$	**Annex A.1**
T_{ON}	0	0	$\Delta I = -\Delta I_{Li}$	$\Delta I = -\Delta I_{Li}$	$\Delta I = -n\,\Delta I_{Li}/N$	Trapezoidal
	0	0	$I_0 = -I_{0,Lw}$	$I_0 = -I_{0,Li}$	$I_0 = -(n-1)I_{0,Li}/N - I_{0,Lw}/N$	
T_1	$\Delta I = n\,\Delta I_{Li} + N\Delta I_{Lin} + NI_{0,Lin} + (n-1)I_{0,Li} + I_{0,Lw}$	0	$\Delta I = (n-1)\Delta I_{Li} + N\Delta I_{Lin}$	$\Delta I = \Delta I_{Li}$	$\Delta I = \Delta I_{Lin}$	Trapezoidal
	$I_0 = 0$	0	$I_0 = -I_{0,Lw}$	$I_0 = -I_{0,Li}$	$I_0 = I_{0,Lin}$	
T_2	0	0	$I_0 = -I_{0,Lw}$	$I_0 = -I_{0,Li}$	$I_0 = I_{0,Lin}$	Constant

$$I_{0,Lw} = -\frac{V_M D T_S \left(DL_{in} - D_1 N^2 L_i - D_1 L_{in} n + D_1 L_{in}\right)}{2N L_i L_{in}} \tag{B.30}$$

$$I_{0,Lin} = \frac{V_M D T_S \left(DL_{in} - D_1 N^2 L - D_1 L_{in} n + D_1 L_{in}\right)}{2N^2 L_i L_{in}} + (n+1)\frac{V_M D T_S \left(D + D_1\right)}{2N^2 L_i} \tag{B.31}$$

B.2 Intermodule balancing systems

Intermodule balancing systems will be analysed as the intermodule system with a previous subchapter related to the design equations of the main components and the switching periods D, D1 and D2 calculation. During the interval analysis main current paths will be presented to analyse the working behaviour of the balancing systems. The AV and RMS values of the currents can then be calculated via Annex A.1 analysis.

B.2.1 Series connected Flyback

B.2.1.1 Design process

The design process of the parameter values of the series connected Flyback requires an iterative process in order to obtain the magnetizing inductor value L_n, the critical D_C and the average weak module current $I_{Mb,W.}$

The design process starts with the definition of the critical voltage situation for the series connected modules $V_{M,W}$ and $V_{M,S}$. The iterative process is defined for a constant L_n value. Consecutive different iterative processes could be performed to evaluate behaviour under different L_n values. After that the maximum duty cycle is defined (D_{Max}=1) and the iteration process starts. As it is presented in Fig 4.15 during T_{ON} only the strong module is switched On, generating a current variation of amplitude I_{pk} in the module current $I_{Mb,S,pk}$.

$$I_{Mb,S,pk} = \frac{V_{M,S}}{L_n (m-1)} mDT_S \tag{B.32}$$

I_{pk} is reflected to the secondary side of all the other module transformers as the initial current magnitude for T_1 period $I_{T1,0}$.

$$I_{T1,0} = I_{Mb,S,pk} \tag{B.33}$$

The highest voltage module cancels first the current generating the first period $T_{1,1}$ of the whole T_1 time period. During each $T_{1,z}$ period the initial current $I_{Mb,j}|T_{1,z}$ and the current variation in each module $\Delta I_{Mb,j}$. After each module current reaches zero, the module current slope changes. The iterative process is finished when all the currents reach zero for T_1 period. If T_{ON} + T_1 is smaller than the design switching period T_S the

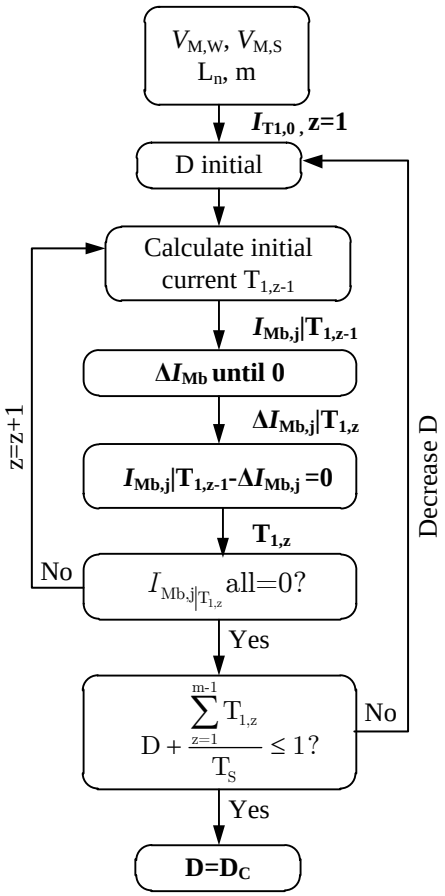

Fig B.7. Flow chart criteria for determination of the critical duty cycle of the series connected Flyback intermodule balancing system

iteration is valid, and the highest obtained D is the critical duty cycle D_C. The flow chart methodology is presented in Fig B.7.

B.2.1.2 Interval analysis

The interval analysis of the series connected Flyback intermodule system will present the current paths of the balancing system during each time interval. The previous design process analysis where each interval currents $I_{Mb,j}|T_{1,z}$, interval variation currents $\Delta I_{Mb,j}|T_{1,z}$ and each interval times T_{ON}, $T_1=[T_{1,1}+T_{1,2}+...+T_{1,m-1}]$, and T_2. Each interval analysis permits to evaluate the RMS and the AV values for each element currents. For further topology understanding an analysis example of a 4 series connected module battery pack is presented in Fig B.8. The battery pack is composed for a strong module (4^{th} module), and consecutive weaker modules until the weakest or weak module (1^{st} module).

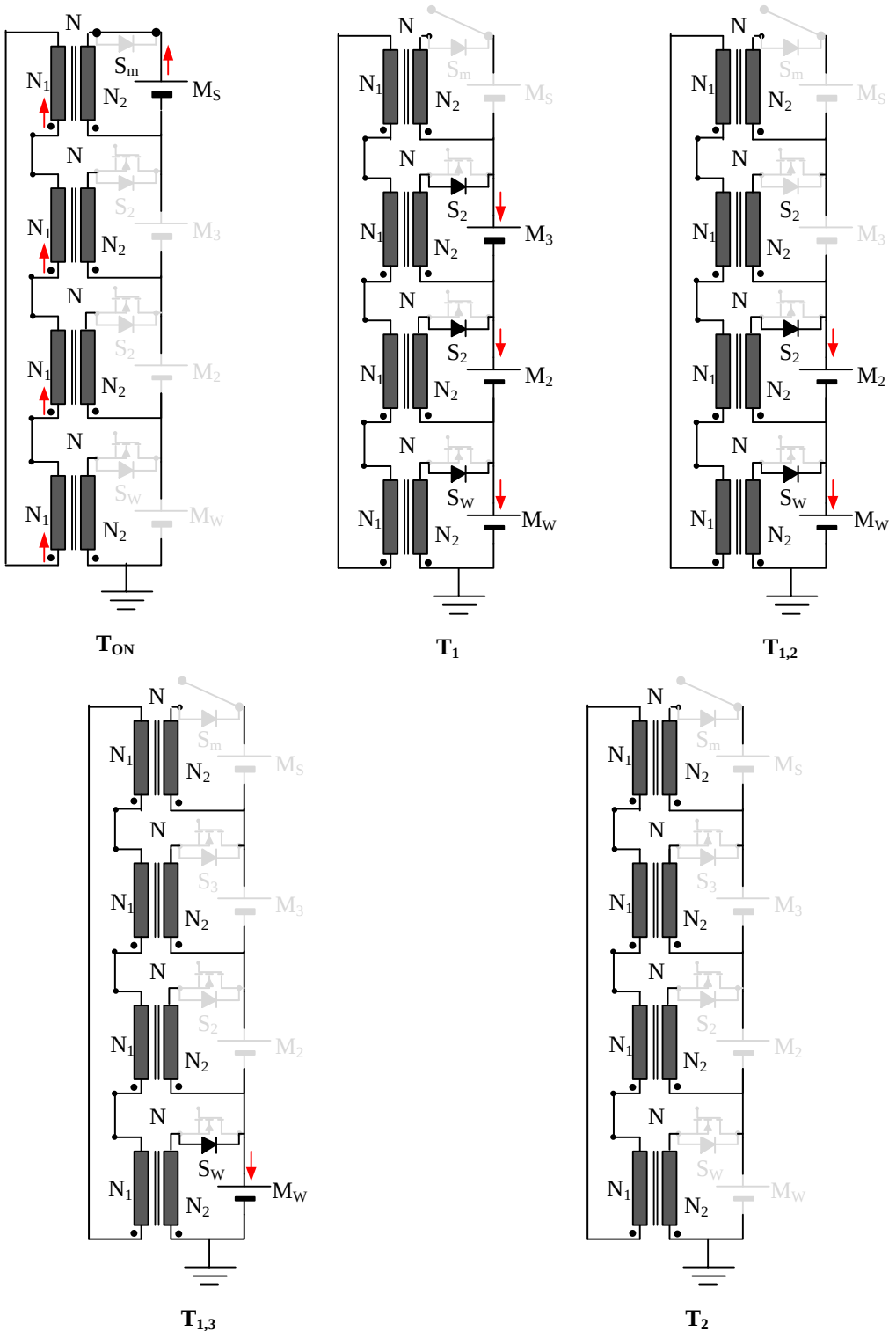

Fig B.8. Series connected flyback intermodule balancing system current path analysis for a specific situation of 4 modules battery pack

Table B.6 presents the current distribution for each interval with the expressions to calculate the RMS and AV values. An analysis for m series connected modules is easily scalable.

Table B.6 Current distribution for each time interval T_{ON}, T_1 and T_2 for the series connected Flyback intermodule balancing system.

		S_S	S_3 (D_3)	S_2 (D_2)	S_W (D_W)	**Annex A.1**
T_{ON}		$\Delta I = I_{Mb,S,pk}$	0	0	0	Triangular
T_1	$T_{1,1}$	0	$\Delta I = \Delta I_{Mb,3\|T1,1}$	$\Delta I = \Delta I_{Mb,2\|T1,1}$	$\Delta I = \Delta I_{Mb,W\|T1,1}$	Trapezoidal
		0	$I_0 = I_{T1,0}$	$I_0 = I_{T1,0}$	$I_0 = I_{T1,0}$	
	$T_{1,2}$	0	0	$\Delta I = \Delta I_{Mb,2\|T1,2}$	$\Delta I = \Delta I_{Mb,W\|T1,2}$	Trapezoidal
		0	0	$I_0 = I_{Mb,2\|T1,1}$	$I_0 = I_{Mb,W\|T1,1}$	
	$T_{1,3}$	0	0	0	$\Delta I = \Delta I_{Mb,W\|T1,3}$	Trapezoidal
		0	0	0	$I_0 = I_{Mb,W\|T1,2}$	
T_2		0	0	0	0	Constant

B.2.2 Parallel connected Full bridge

B.2.2.1 Design process

The design process starts with the definition of the balancing capability by the $I_{Mb,W}$ and D_C definition (4.50) and (4.51). If D=[$D_C \leq D \leq 0{,}5$] is defined as a constant switching period D_C is the time period where the power transistor conducts current. The series inductor L_s is the only design component and is defined as:

$$L_S = \frac{\left(V_{M,S} - V_{M,W}\right) D^2 T_s}{I_{Mb,W}\left(V_{M,S} + V_{M,W}\right)} V_{M,S} \quad (D \leq D_C) \tag{B.34}$$

$$L_S = \frac{\left(V_{M,S} - V_{M,W}\right) {D_C}^2 T_s}{I_{Mb,W}\left(V_{M,S} + V_{M,W}\right)} V_{M,S} \quad (D_C \leq D \leq 0{,}5) \tag{B.35}$$

D_1 is defined for half a period, as the gate signals for the full bridge converter are 180º delayed.

$$D_1 = \frac{\left(V_{M,S} - V_{M,W}\right)}{\left(V_{M,S} + V_{M,W}\right)} D \quad D_2 = 0{,}5 - D_1 - D \quad (D \leq D_C) \tag{B.36}$$

$$D_1 = 1 - D_C \quad D_2 = 0 \quad (D_C \leq D \leq 0{,}5) \tag{B.37}$$

B.2.2.2 Interval analysis

The interval current analysis presents the necessary equations for the RMS and AV current calculations for the Full bridge intermodule balancing system components. The current path distribution for different time periods is presented in Fig B.9 and it

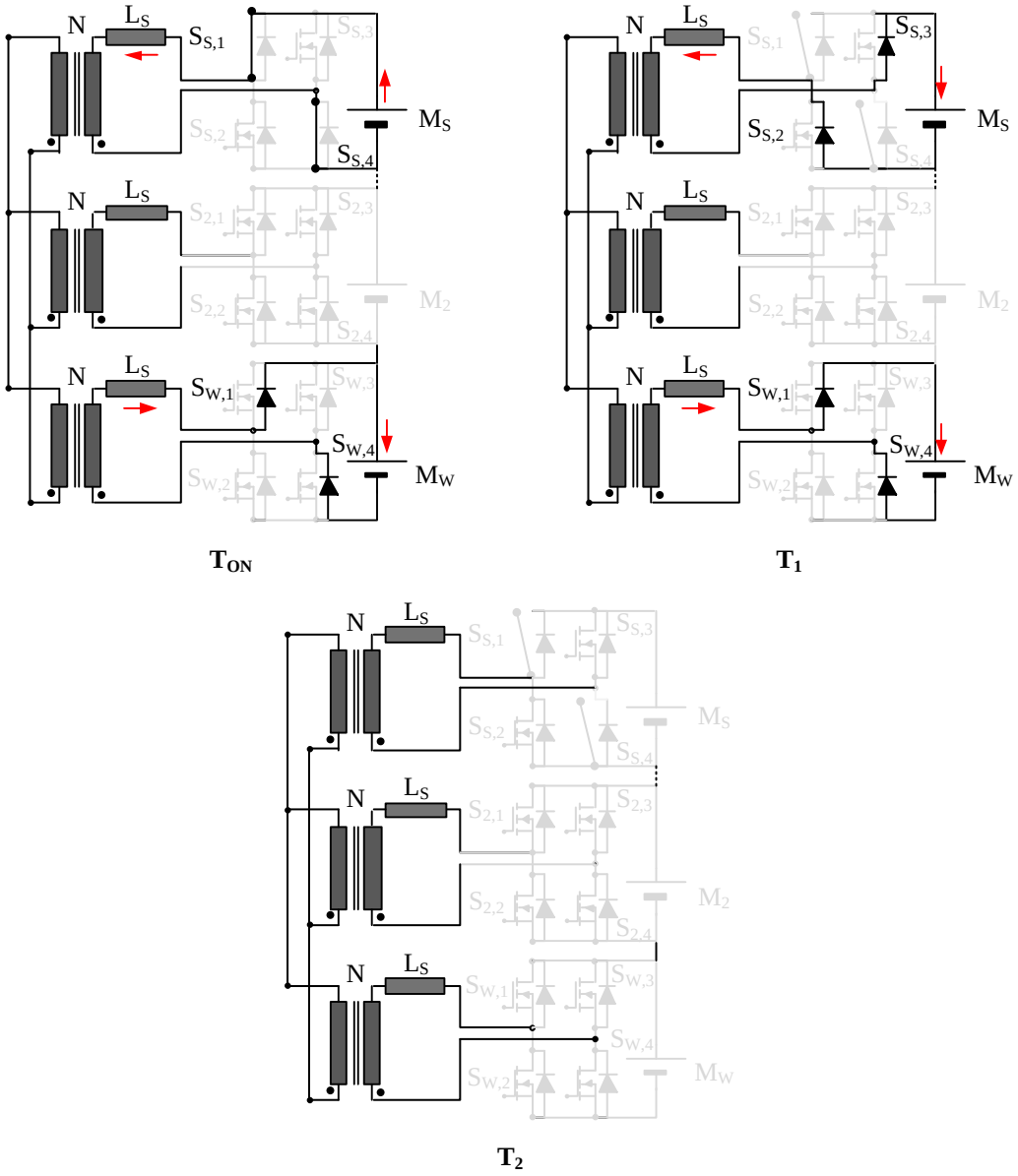

Fig B.9. Parallel connected Full bridge intermodule balancing system current path analysis for T_{ON}, T_1 and T_2 for $T_{ON}+T_1+T_2=T_S/2$. For second interval $[T_S/2,T_S]$ complementary switches are activated. For $D>D_C$ the interval T2 is not presented.

could be seen that the current only flows from the strong module to the weak module. The current analysis is described taking into account the peak current value from the mdoules and series L_S inductors:

$$I_{pk}=\frac{V_{M,S}-V_{M,W}}{2L_S}D \quad (D \le D_C) \tag{B.38}$$

$$I_{pk}=\frac{V_{M,S}-V_{M,W}}{2L_S}D_C \quad (D_C \le D \le 0,5) \tag{B.39}$$

The current distribution analysis is presented in Table B.7.

Table B.7 Current distribution for each time interval T_{ON}, T_1 and T_2 for the parallel connected Full bridge intermodule system $T_{ON}+T_1+T_2=T_S/2$. If $D>D_C$ $T_2=0$. The interval analysis is repeated for interval $[T_S/2,T_S]$. $T_{ON}=D/T_S$ for $D<D_C$ and $T_{ON}=D_C/T_S$ for $D\geq D_C$.

	L_S	S_S [S_S and D_S]	S_W[S_W and D_W]	Annex A.1
T_{ON}	I_{pk}	$-I_{pk}$	I_{pk}	Triangular
T_1	I_{pk}	I_{pk}	I_{pk}	Triangular
T_2	0	0	0	Constant

Annex C

PROTOTYPES

During this chapter thesis work prototype photographs will be presented.

C.1 Intramodule balancing systems

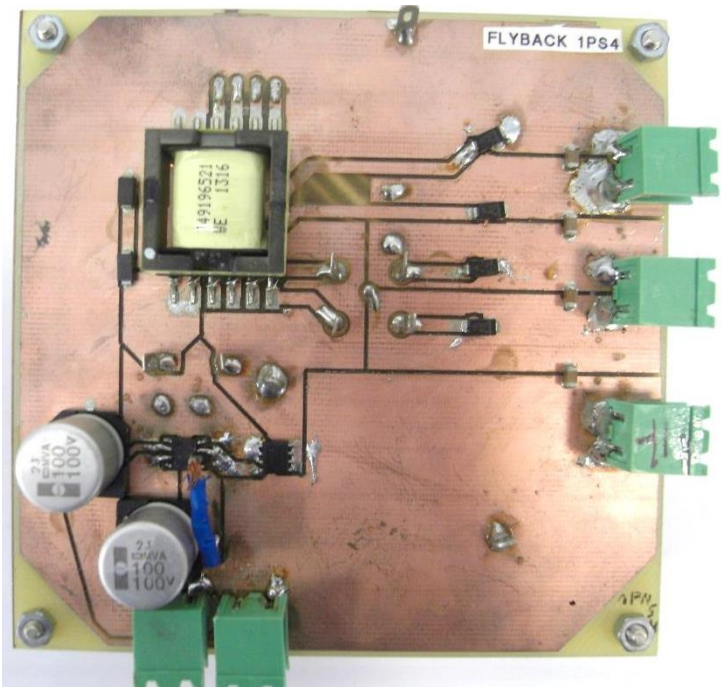

Fig C. 1 Single core Flyback.

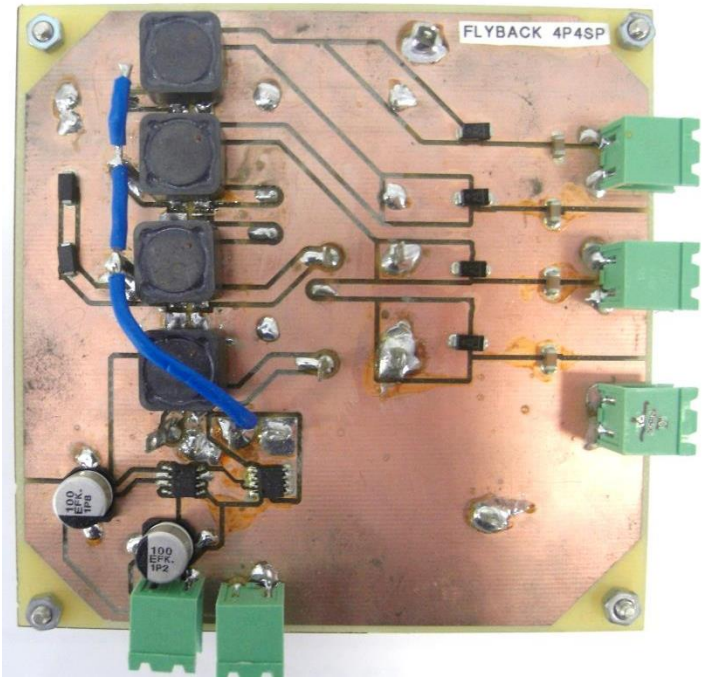

Fig C. 2 Multiple core parallel connected flyback.

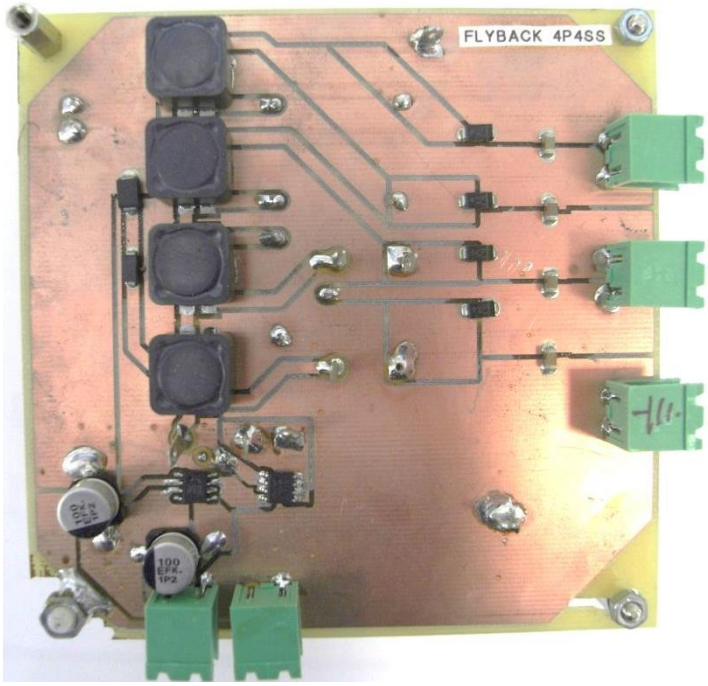

Fig C. 3 Multiple core series connected Flyback.

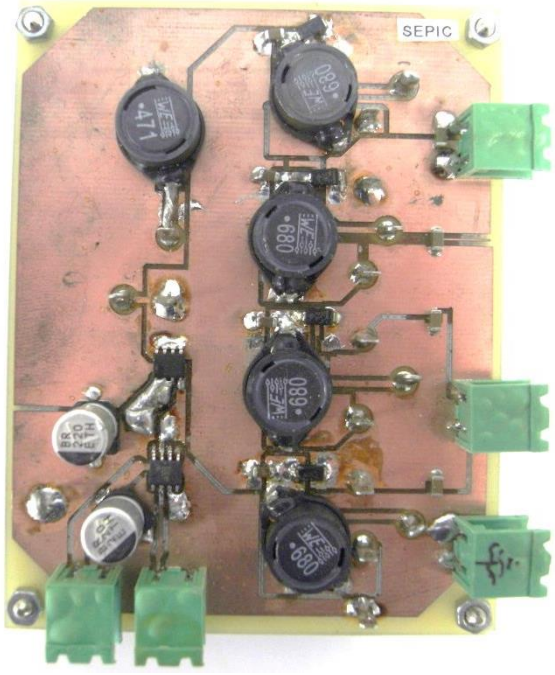

Fig C. 4 Multi stacked Sepic

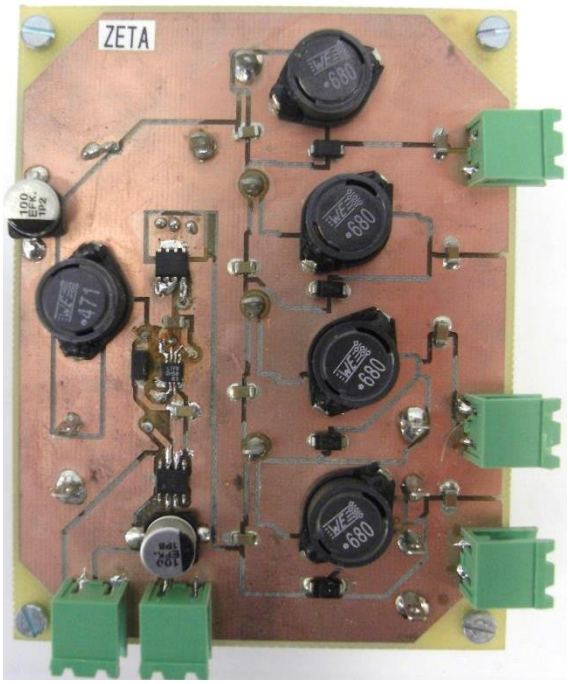

Fig C. 5 Multiple stacked Zeta.

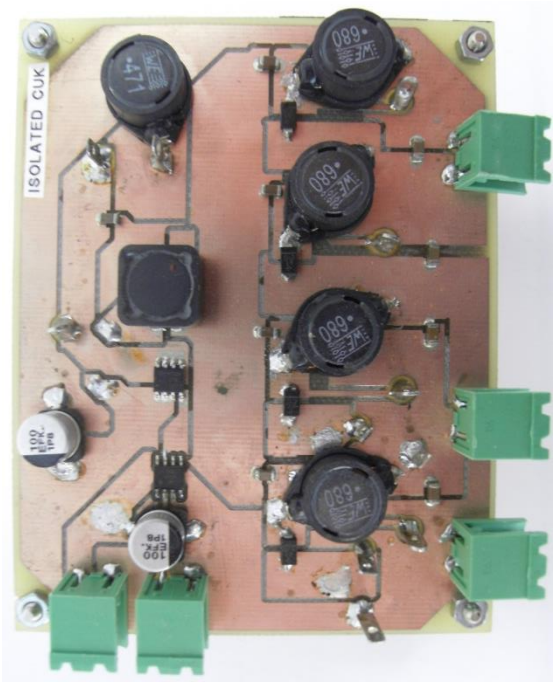

Fig C. 6 Multiple stacked Isolated Cuk

C.2 Intermodule balancing systems

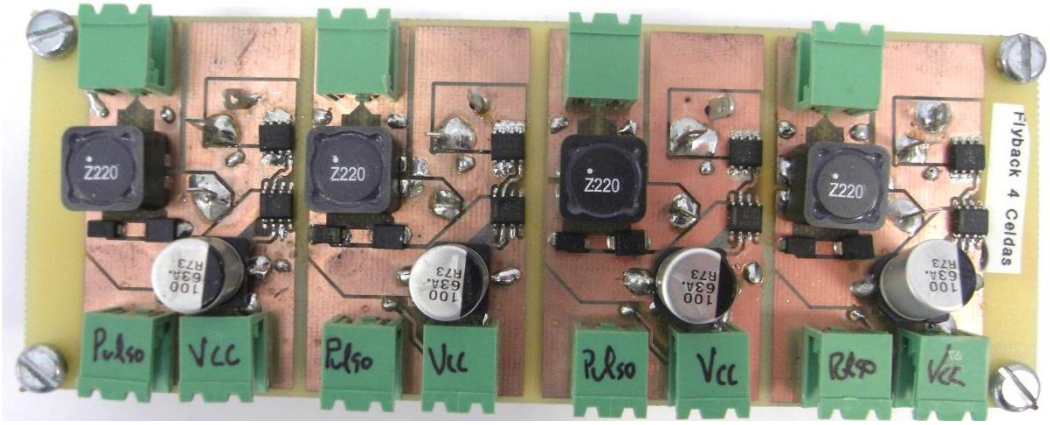

Fig C. 7 Series connected Flyback

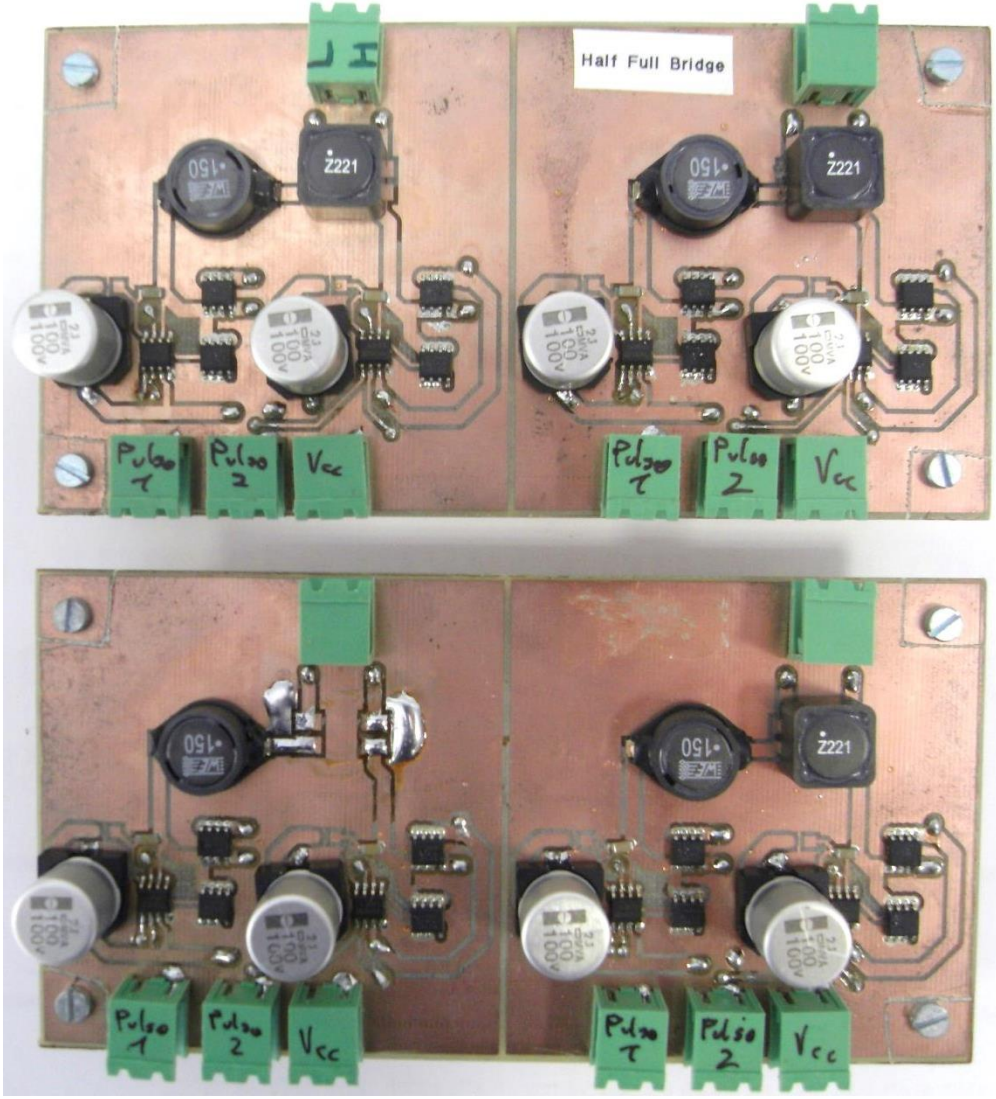

Fig C. 8 Parallel connected Full bridge

C.3 16S1P modular balancing system

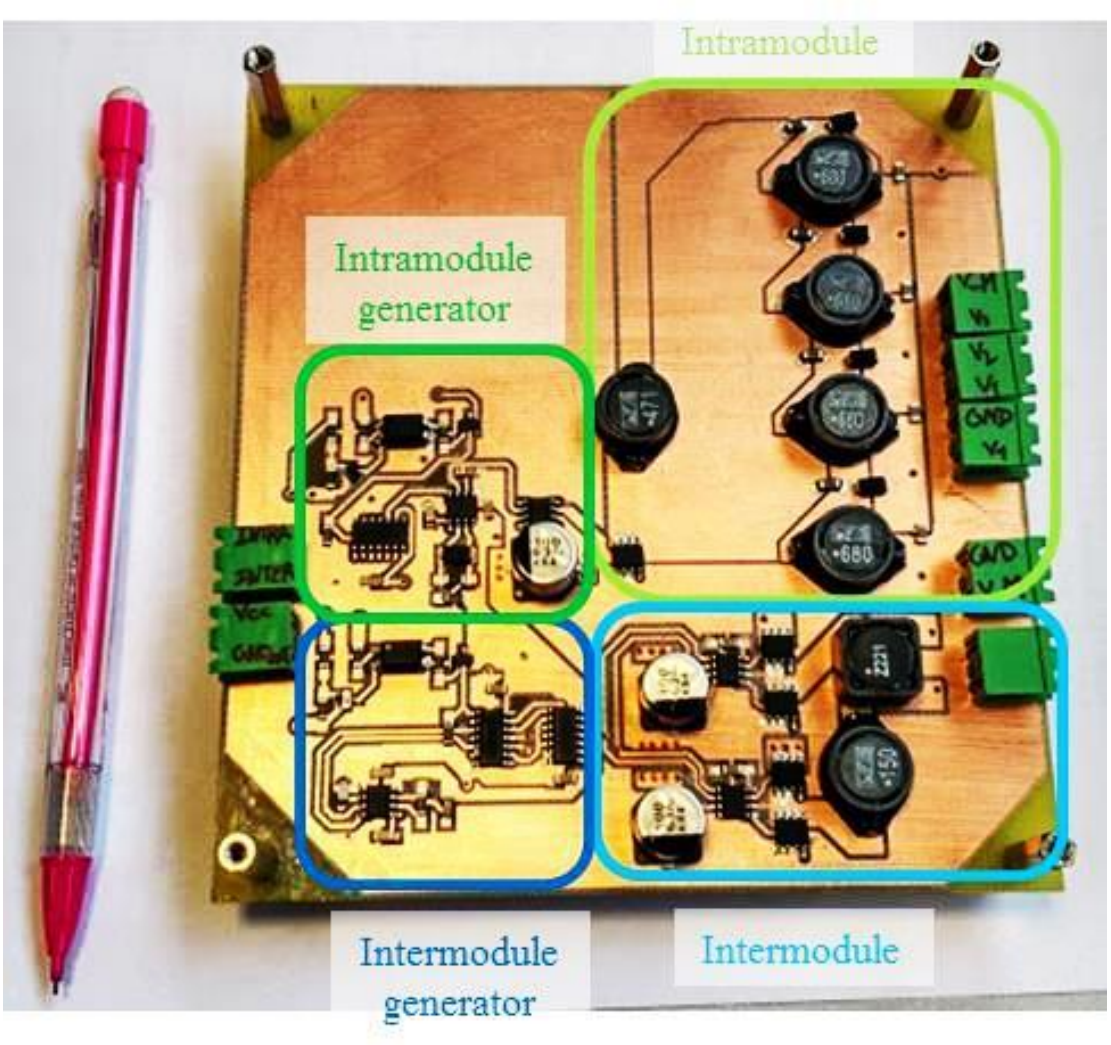

Fig C. 9 Mixed intermodule intramodule balancing system prototype with self-supplied duty cycle generators.

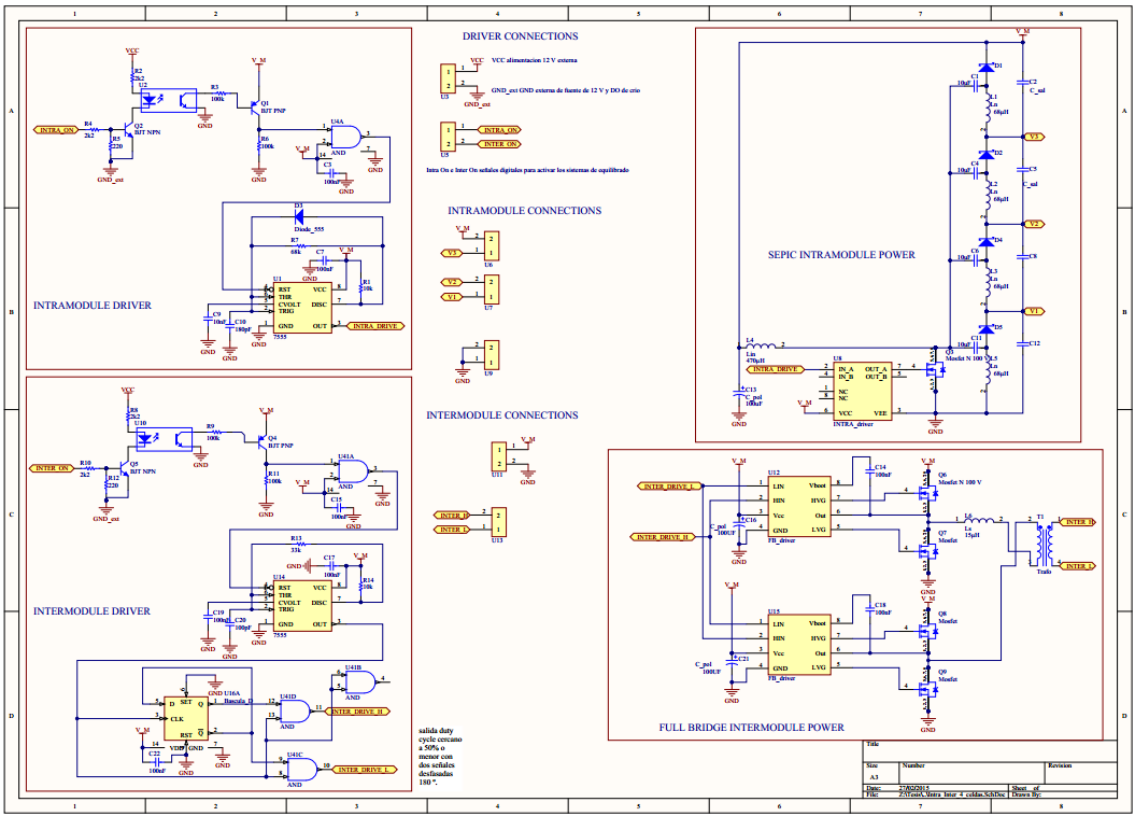

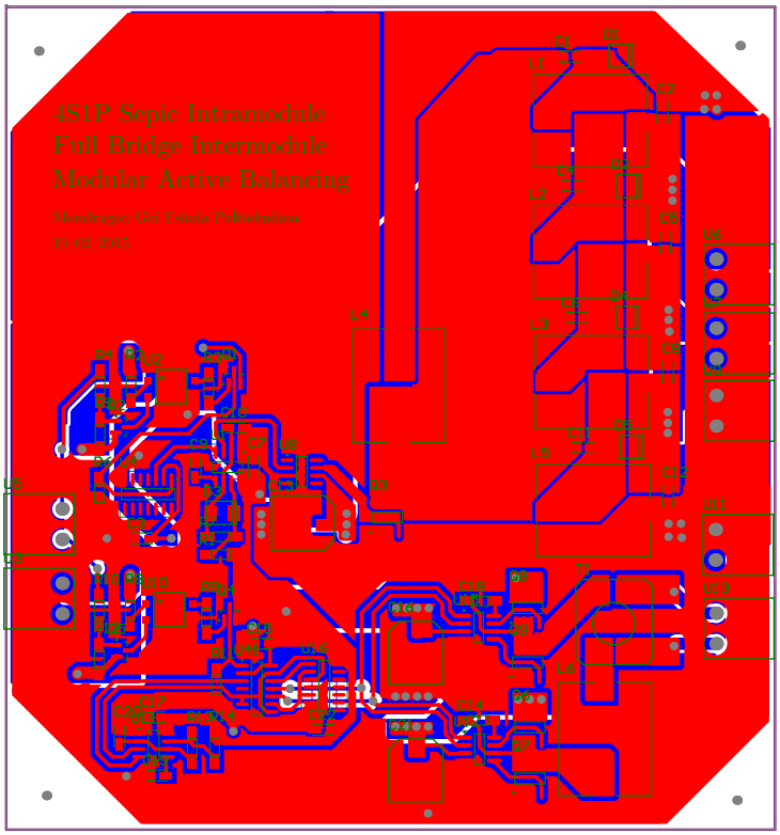

Fig C. 10 Schematic and PCB print of the mixed intramodule and intermodule balancing system

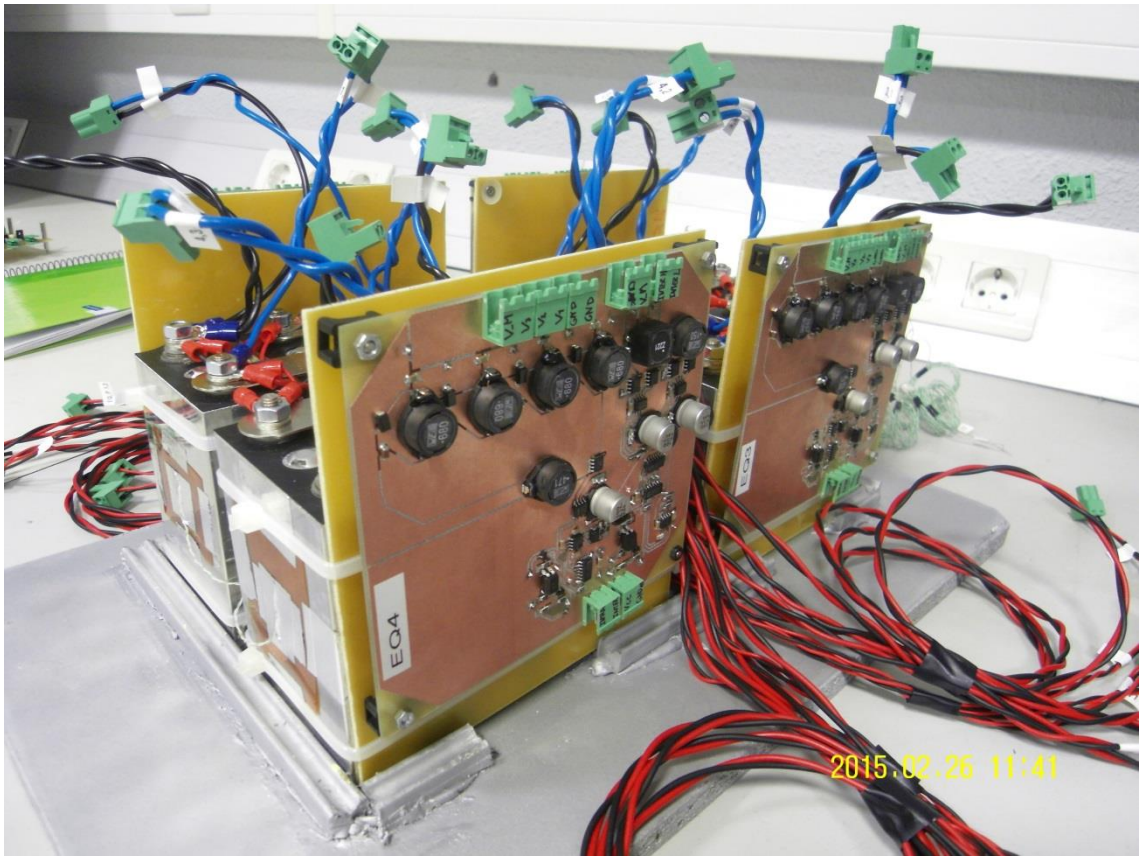

Fig C. 11 16S1P modular lay out. Each 4 cell module is assembled with the mixed modular balancing system for a high modularity battery pack.

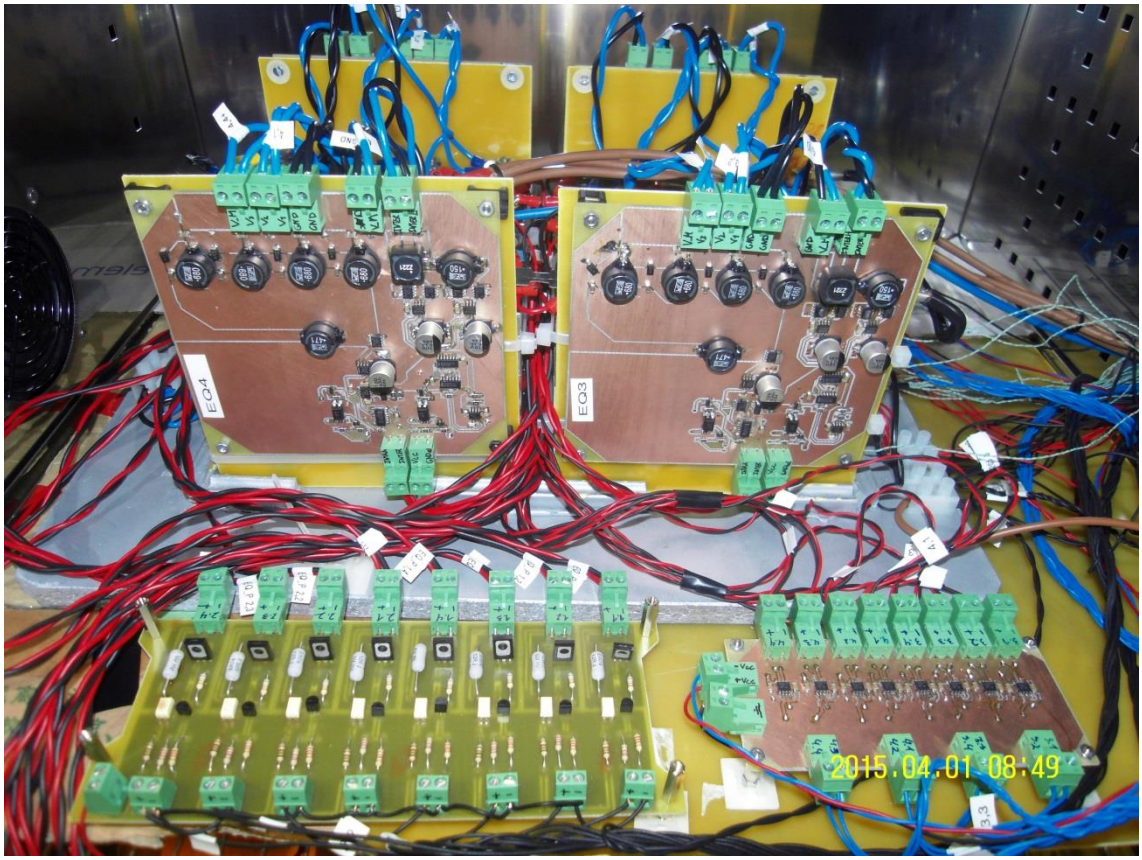

Fig C. 12 16S1P battery pack inside the Prebatem temperature chamber with passive balancing system with passive balancing and active balancing connected

BIBLIOGRAPHY

[1] Red Electrica Española, "Gestión de la demanda de electricidad," 2014. [Online]. Available: www.ree.es.

[2] Fundación Gas Natural Fenosa, "El almacenamiento de electricidad," 2013. [Online]. Available: http://www.fundaciongasnaturalfenosa.org/.

[3] A. Evans, V. Strezov, and T. J. Evans, "Assessment of utility energy storage options for increased renewable energy penetration," *Renew. Sustain. Energy Rev.*, vol. 16, no. 6, pp. 4141–4147, Aug. 2012.

[4] F. Kalhammer, "Status and prospects for Zero Emissions Vehicle Technlogy," in *Report of the ARB Independent expert Panel*, 2007.

[5] P. Poizot and F. Dolhem, "Clean energy new deal for a sustainable world: from non-CO2 generating energy sources to greener electrochemical storage devices," *Energy Environ. Sci.*, vol. 4, no. 6, pp. 2003–2019, 2011.

[6] B. Dunn, H. Kamath, and J.-M. Tarascon, "Electrical Energy Storage for the Grid: A Battery of Choices," *Science (80-.).*, vol. 334, no. 6058, pp. 928–935, Nov. 2011.

[7] R. Padbury and X. Zhang, "Lithium–oxygen batteries—Limiting factors that affect performance," *J. Power Sources*, vol. 196, no. 10, pp. 4436–4444, May 2011.

[8] "Battery University." [Online]. Available: http://www.http//batteryuniversity.com/learn/article/whats_the_best_battery/.

[9] D. Linden, *Linden's Handbook of batteries. Chapter 26*, 4th ed. Mc Graw Hill, 2011.

[10] Lightning global, "Lithium-ion Battery overview," no. 10, 2012.

[11] Boston Consulting Group, "Batteries for Electric Cars," 2009.

[12] Electronic design courtesy of Micro Power, "Understanding The Factors In The Lithium-Battery Equation," 2012. [Online]. Available: ww.electronicdesign.com.

[13] V. Evan House, “Status of Lithium batteries Using Lithium titanate based anode,” *Altair nano*. [Online]. Available: www.altairnano.com.

[14] U. Iraola, “Electro-thermal optimization of an energy storage system based on li-ion batteries,” University of Mondragon, 2014.

[15] J. Vetter, P. Novák, M. R. Wagner, C. Veit, K.-C. Möller, J. O. Besenhard, M. Winter, M. Wohlfahrt-Mehrens, C. Vogler, and A. Hammouche, “Ageing mechanisms in lithium-ion batteries,” *J. Power Sources*, vol. 147, no. 1–2, pp. 269–281, Sep. 2005.

[16] mpoweruk, “Battery performance and characteristics: temperature effects.” [Online]. Available: www.mpoweruk.com.

[17] D. Doughty and E. Roth, “A general discussion of Li ion battery safety,” *Electrochem. Soc. Interface*, pp. 37–44, 2012.

[18] P. Das, B. Laan, S. A. Mousavi, and G. Moschopoulos, “A Nonisolated Bidirectional ZVS-PWM Active Clamped DC-DC Converter,” *Power Electronics, IEEE Transactions on*, vol. 24, no. 2. pp. 553–558, 2009.

[19] F. Krismer, “Modeling and Optimization of Bidirectional Dual Active Bridge DC–DC Converter Topologies,” ETH Zurich, 2010.

[20] N. M. L. Tan, T. Abe, and H. Akagi, “Design and Performance of a Bidirectional Isolated DC-DC Converter for a Battery Energy Storage System,” *Power Electronics, IEEE Transactions on*, vol. 27, no. 3. pp. 1237–1248, 2012.

[21] N. M. L. Tan, T. Abe, and H. Akagi, “Experimental discussions on operating frequencies of a bidirectional isolated DC-DC converter for a battery energy storage system,” *Energy Conversion Congress and Exposition (ECCE), 2013 IEEE*. pp. 2333–2340, 2013.

[22] C.-S. Moo, K. S. Ng, and Y.-C. Hsieh, “Parallel Operation of Battery Power Modules,” *Energy Conversion, IEEE Transactions on*, vol. 23, no. 2. pp. 701–707, 2008.

[23] C.-S. Moo, K.-S. Ng, and J.-S. Hu, “Operation of battery power modules with series output,” *Industrial Technology, 2009. ICIT 2009. IEEE International Conference on*. pp. 1–6, 2009.

[24] S. M. Goetz, A. V Peterchev, and T. Weyh, “Modular Multilevel Converter With Series and Parallel Module Connectivity: Topology and Control,” *Power Electronics, IEEE Transactions on*, vol. 30, no. 1. pp. 203–215, 2015.

[25] W. Chen, X. Ruan, H. Yan, and C. K. Tse, “DC/DC Conversion Systems Consisting of Multiple Converter Modules: Stability, Control, and Experimental

Verifications," *Power Electronics, IEEE Transactions on*, vol. 24, no. 6. pp. 1463–1474, 2009.

[26] X. Ruan, W. Chen, L. Cheng, C. K. Tse, H. Yan, and T. Zhang, "Control Strategy for Input-Series-Output-Parallel Converters," *Industrial Electronics, IEEE Transactions on*, vol. 56, no. 4. pp. 1174–1185, 2009.

[27] D. Sha, Z. Guo, T. Luo, and X. Liao, "A General Control Strategy for Input-Series-Output-Series Modular DC-DC Converters," *Power Electronics, IEEE Transactions on*, vol. 29, no. 7. pp. 3766–3775, 2014.

[28] S. Inoue and H. Akagi, "A Bidirectional Isolated DC–DC Converter as a Core Circuit of the Next-Generation Medium-Voltage Power Conversion System," *Power Electronics, IEEE Transactions on*, vol. 22, no. 2. pp. 535–542, 2007.

[29] S. D'Arco, L. Piegari, and P. Tricoli, "A modular converter with embedded battery cell balancing for electric vehicles," *Electrical Systems for Aircraft, Railway and Ship Propulsion (ESARS), 2012*. pp. 1–6, 2012.

[30] L. Maharjan, S. Member, S. Inoue, and H. Akagi, "State-of-Charge (SOC) - Balancing Control of a Battery Energy Storage System Based on a Cascade PWM Converter," vol. 24, no. 6, pp. 1628–1636, 2009.

[31] L. Lu, X. Han, J. Li, J. Hua, and M. Ouyang, "A review on the key issues for lithium-ion battery management in electric vehicles," *J. Power Sources*, vol. 226, pp. 272–288, Mar. 2013.

[32] A. Kampker, P. Burggraf, C. Deutskens, H. Heimes, and M. Schmidt, "Process alternatives in the battery production," *Electrical Systems for Aircraft, Railway and Ship Propulsion (ESARS), 2012*. pp. 1–6, 2012.

[33] B. University, "Non Correctable Battery Problems." [Online]. Available: http://batteryuniversity.com/learn/article/non_correctable_battery_problems.

[34] C. Wang, X. Zhang, and A. Appleby, "Self-discharge of secondary lithium-ion graphite anodes," *J. Power Sources*, vol. 112, pp. 98–104, 2002.

[35] B. N. Popov, "Calendar life studies of lithium-ion batteries."

[36] C. Martinez, "Cell Balancing Maximizes The Capacity Of Multi-Cell Li-Ion Battery Packs," *Intersil. Inc.*

[37] S. Santhanagopalan and R. E. White, "Quantifying Cell-to-Cell Variations in Lithium Ion Batteries," *Int. J. Electrochem.*, vol. 2012, pp. 1–10, 2012.

[38] R. Gogoana, M. B. Pinson, M. Z. Bazant, and S. E. Sarma, “Internal resistance matching for parallel-connected lithium-ion cells and impacts on battery pack cycle life,” *J. Power Sources*, vol. 252, pp. 8–13, Apr. 2014.

[39] R. Srinivasan, a. Carson Baisden, B. G. Carkhuff, and M. H. Butler, “The five modes of heat generation in a Li-ion cell under discharge,” *J. Power Sources*, vol. 262, pp. 93–103, Sep. 2014.

[40] A. Hausmann and C. Depcik, “Expanding the Peukert equation for battery capacity modeling through inclusion of a temperature dependency,” *J. Power Sources*, vol. 235, pp. 148–158, Aug. 2013.

[41] F. Baronti, G. Fantechi, L. Fanucci, E. Leonardi, R. Roncella, R. Saletti, and S. Saponara, “State-of-charge estimation enhancing of lithium batteries through a temperature-dependent cell model,” *Applied Electronics (AE), 2011 International Conference on*. pp. 1–5, 2011.

[42] J. P. Schmidt, A. Weber, and E. Ivers-Tiffée, “A novel and fast method of characterizing the self-discharge behavior of lithium-ion cells using a pulse-measurement technique,” *J. Power Sources*, vol. 274, pp. 1231–1238, Jan. 2015.

[43] W. Waag, S. Käbitz, and D. U. Sauer, “Experimental investigation of the lithium-ion battery impedance characteristic at various conditions and aging states and its influence on the application,” *Appl. Energy*, vol. 102, pp. 885–897, Feb. 2013.

[44] X. Liu, Z. Chen, C. Zhang, and J. Wu, “A novel temperature-compensated model for power Li-ion batteries with dual-particle-filter state of charge estimation,” *Appl. Energy*, vol. 123, pp. 263–272, Jun. 2014.

[45] M. Uno and K. Tanaka, “Influence of High-Frequency Charge-Discharge Cycling Induced by Cell Voltage Equalizers on the Life Performance of Lithium-Ion Cells,” *Vehicular Technology, IEEE Transactions on*, vol. 60, no. 4. pp. 1505–1515, 2011.

[46] M. Einhorn, W. Guertlschmid, T. Blochberger, R. Kumpusch, R. Permann, F. V Conte, C. Kral, and J. Fleig, “A Current Equalization Method for Serially Connected Battery Cells Using a Single Power Converter for Each Cell,” *Vehicular Technology, IEEE Transactions on*, vol. 60, no. 9. pp. 4227–4237, 2011.

[47] E. Sarasketa-Zabala, I. Gandiaga, L. M. Rodriguez-Martinez, and I. Villarreal, “Calendar ageing analysis of a LiFePO4/graphite cell with dynamic model validations: Towards realistic lifetime predictions,” *J. Power Sources*, vol. 272, pp. 45–57, Dec. 2014.

[48] M. Kassem, J. Bernard, R. Revel, S. Pélissier, F. Duclaud, and C. Delacourt, “Calendar aging of a graphite/LiFePO4 cell,” *J. Power Sources*, vol. 208, pp. 296–305, Jun. 2012.

[49] S. Grolleau, A. Delaille, H. Gualous, and P. Gyan, “Calendar aging of commercial graphite / LiFePO 4 cell e Predicting capacity fade under time dependent storage conditions,” *J. Power Sources*, vol. 255, pp. 450–458, 2014.

[50] M. Ecker, N. Nieto, S. Käbitz, J. Schmalstieg, H. Blanke, A. Warnecke, and D. U. Sauer, “Calendar and cycle life study of Li(NiMnCo)O2-based 18650 lithium-ion batteries,” *J. Power Sources*, vol. 248, no. 0, pp. 839–851, Feb. 2014.

[51] S. Käbitz, J. B. Gerschler, M. Ecker, Y. Yurdagel, B. Emmermacher, D. André, T. Mitsch, and D. U. Sauer, “Cycle and calendar life study of a graphite|LiNi1/3Mn1/3Co1/3O2 Li-ion high energy system. Part A: Full cell characterization,” *J. Power Sources*, vol. 239, pp. 572–583, Oct. 2013.

[52] Y. Barsukov, “Battery cell balancing: what to balance and how,” *Texas Instruments*, 2009.

[53] H. Song, Z. Cao, X. Chen, H. Lu, M. Jia, Z. Zhang, Y. Lai, J. Li, and Y. Liu, “Capacity fade of LiFePO4/graphite cell at elevated temperature,” *J. Solid State Electrochem.*, vol. 17, no. 3, pp. 599–605, Oct. 2012.

[54] N. Omar, M. A. Monem, Y. Firouz, J. Salminen, J. Smekens, O. Hegazy, H. Gaulous, G. Mulder, P. Van den Bossche, T. Coosemans, and J. Van Mierlo, “Lithium iron phosphate based battery – Assessment of the aging parameters and development of cycle life model,” *Appl. Energy*, vol. 113, pp. 1575–1585, Jan. 2014.

[55] J. Wang, P. Liu, J. Hicks-Garner, E. Sherman, S. Soukiazian, M. Verbrugge, H. Tataria, J. Musser, and P. Finamore, “Cycle-life model for graphite-LiFePO4 cells,” *J. Power Sources*, vol. 196, no. 8, pp. 3942–3948, Apr. 2011.

[56] Y. Zhang, C.-Y. Wang, and X. Tang, “Cycling degradation of an automotive LiFePO4 lithium-ion battery,” *J. Power Sources*, vol. 196, no. 3, pp. 1513–1520, Feb. 2011.

[57] E. Sarasketa-Zabala, I. Gandiaga, E. Martinez-Laserna, L. M. Rodriguez-Martinez, and I. Villarreal, “Cycle ageing analysis of a LiFePO4/graphite cell with dynamic model validations: Towards realistic lifetime predictions,” *J. Power Sources*, Oct. 2014.

[58] J. Cao, N. Schofield, and A. Emadi, “Battery balancing methods: A comprehensive review,” *Vehicle Power and Propulsion Conference, 2008. VPPC ’08. IEEE*. pp. 1–6, 2008.

[59] S. Moore, “A review of cell equalization methods for lithium ion and lithium polymer battery systems,” 2001.

[60] J. Gallardo-Lozano, E. Romero-Cadaval, M. I. Milanes-Montero, and M. a. Guerrero-Martinez, “Battery equalization active methods,” *J. Power Sources*, vol. 246, pp. 934–949, Jan. 2014.

[61] M. Daowd, N. Omar, P. Van Den Bossche, and J. Van Mierlo, “Passive and active battery balancing comparison based on MATLAB simulation,” *Vehicle Power and Propulsion Conference (VPPC), 2011 IEEE*. pp. 1–7, 2011.

[62] K. Zhi-Guo, Z. Chun-Bo, L. Ren-Gui, and C. Shu-Kang, “Comparison and Evaluation of Charge Equalization Technique for Series Connected Batteries,” *Power Electronics Specialists Conference, 2006. PESC ’06. 37th IEEE*. pp. 1–6, 2006.

[63] D. Linzen, S. Buller, E. Karden, and R. W. De Doncker, “Analysis and evaluation of charge-balancing circuits on performance, reliability, and lifetime of supercapacitor systems,” *Ind. Appl. IEEE Trans.*, vol. 41, no. 5, pp. 1135–1141, 2005.

[64] B. Lindemark, “Individual cell voltage equalizers (ICE) for reliable battery performance,” *Telecommunications Energy Conference, 1991. INTELEC ’91., 13th International*. pp. 196–201, 1991.

[65] W. C. Lee, D. Drury, and P. Mellor, “Comparison of passive cell balancing and active cell balancing for automotive batteries,” *Vehicle Power and Propulsion Conference (VPPC), 2011 IEEE*. pp. 1–7, 2011.

[66] C. Pascual and P. T. Krein, “Switched capacitor system for automatic series battery equalization,” *Proc. APEC 97 - Appl. Power Electron. Conf.*, vol. 2, pp. 848–854.

[67] A. C. Baughman and M. Ferdowsi, “Double-Tiered Switched-Capacitor Battery Charge Equalization Technique,” *Industrial Electronics, IEEE Transactions on*, vol. 55, no. 6. pp. 2277–2285, 2008.

[68] A. Baughman and M. Ferdowsi, “Double-tiered capacitive shuttling method for balancing series-connected batteries,” *Vehicle Power and Propulsion, 2005 IEEE Conference*. pp. 109–113, 2005.

[69] C. Speltino, A. Stefanopoulou, and G. Fiengo, “Cell equalization in battery stacks through State Of Charge estimation polling,” *American Control Conference (ACC), 2010*. pp. 5050–5055, 2010.

[70] N. H. Kutkut, “A modular nondissipative current diverter for EV battery charge equalization,” *Applied Power Electronics Conference and Exposition, 1998. APEC ’98. Conference Proceedings 1998., Thirteenth Annual*, vol. 2. pp. 686–690 vol.2, 1998.

[71] Y.-S. Lee and G.-T. Cheng, "Quasi-Resonant Zero-Current-Switching Bidirectional Converter for Battery Equalization Applications," *Power Electronics, IEEE Transactions on*, vol. 21, no. 5. pp. 1213–1224, 2006.

[72] T. H. Phung, J. Crebier, A. Chureau, A. Collet, and T. Van Nguyen, "Optimized structure for next-to-next balancing of series-connected lithium-ion cells," *Applied Power Electronics Conference and Exposition (APEC), 2011 Twenty-Sixth Annual IEEE*. pp. 1374–1381, 2011.

[73] S.-H. Park, T.-S. Kim, J.-S. Park, G.-W. Moon, and M.-J. Yoon, "A new battery equalizer based on buck-boost topology," *Power Electronics, 2007. ICPE '07. 7th Internatonal Conference on*. pp. 962–965, 2007.

[74] N. H. Kutkut, "Nondissipative current diverter using a centralized multi-winding transformer," *Power Electronics Specialists Conference, 1997. PESC '97 Record., 28th Annual IEEE*, vol. 1. pp. 648–654 vol.1, 1997.

[75] N. H. Kutkut and D. M. Divan, "Dynamic equalization techniques for series battery stacks," *Telecommunications Energy Conference, 1996. INTELEC '96., 18th International*. pp. 514–521, 1996.

[76] C. Bonfiglio and W. Roessler, "A cost optimized battery management system with active cell balancing for lithium ion battery stacks," *Vehicle Power and Propulsion Conference, 2009. VPPC '09. IEEE*. pp. 304–309, 2009.

[77] H.-S. Park, C.-E. Kim, G.-W. Moon, J.-H. Lee, and J. K. Oh, "Two-Stage Cell Balancing Scheme for Hybrid Electric Vehicle Lithium-Ion Battery Strings," *Power Electron. Spec. Conf. 2007. PESC 2007. IEEE*, pp. 273–279, 2007.

[78] J.-W. Shin, G.-S. Seo, C.-Y. Chun, and B.-H. Cho, "Selective flyback balancing circuit with improved balancing speed for series connected Lithium-ion batteries," *Power Electron. Conf. (IPEC), 2010 Int.*, pp. 1180–1184, 2010.

[79] A. M. Imtiaz, F. H. Khan, and H. Kamath, "Steady state analytical model of a 'time shared li-ion cell blancing circuit' for Plug-in hybrid vehicles and utility energy storage," *Power Electronics and ECCE Asia (ICPE & ECCE), 2011 IEEE 8th International Conference on*. pp. 577–584, 2011.

[80] N. H. Kutkut, D. M. Divan, and D. W. Novotny, "Charge equalization for series connected battery strings," *Industry Applications, IEEE Transactions on*, vol. 31, no. 3. pp. 562–568, 1995.

[81] N. H. Kutkut, "N-dissipative current diverter using a centralized multi- winding transformer," pp. 648–654, 1997.

[82] N. H. Kutkut, H. L. N. Wiegman, D. M. Divan, and D. W. Novotny, "Design considerations for charge equalization of an electric vehicle battery system," *Industry Applications, IEEE Transactions on*, vol. 35, no. 1. pp. 28–35, 1999.

[83] N. H. Kutkut, H. L. N. Wiegman, D. M. Divan, and D. W. Novotny, “Design considerations for charge equalization of an electric vehicle battery system,” *IEEE Trans. Ind. Appl.*, vol. 35, no. 1, pp. 28–35, 1999.

[84] M. Uno and K. Tanaka, “Single-Switch Multioutput Charger Using Voltage Multiplier for Series-Connected Lithium-Ion Battery/Supercapacitor Equalization,” *Industrial Electronics, IEEE Transactions on*, vol. 60, no. 8. pp. 3227–3239, 2013.

[85] M. Uno and K. Tanaka, “Single-switch equalization charger using multi-stacked buck-boost converters for series-connected energy storage cells,” *Power Electronics and ECCE Asia (ICPE & ECCE), 2011 IEEE 8th International Conference on*. pp. 2990–2996, 2011.

[86] M. Uno and K. Tanaka, “Multi-Stacked SEPICs for Series-Connected Energy Storage Cells Single-Switch Cell Voltage Equalizer Based on,” pp. 0–6, 2011.

[87] M. Uno and K. Tanaka, “Single-switch cell voltage equalizer based on multi-stacked SEPICs for series-connected energy storage cells,” *Telecommunications Energy Conference (INTELEC), 2011 IEEE 33rd International*. pp. 1–7, 2011.

[88] S. E. S. Cells, M. Uno, and K. Tanaka, “Single-Switch Cell Voltage Equalizer Using Multistacked Buck-Boost Converters Operating in Discontinuous Conduction Mode for,” vol. 60, no. 8, pp. 3635–3645, 2011.

[89] M. Uno and K. Tanaka, “Single-Switch Cell Voltage Equalizer Using Multistacked Buck-Boost Converters Operating in Discontinuous Conduction Mode for Series-Connected Energy Storage Cells,” *Vehicular Technology, IEEE Transactions on*, vol. 60, no. 8. pp. 3635–3645, 2011.

[90] M. Uno and K. Tanaka, “Single-Switch Multi-Output Charger Using Voltage Multiplier for Series-Connected Lithium-Ion Battery/Supercapacitor Equalization,” *Industrial Electronics, IEEE Transactions on*, vol. PP, no. 99. p. 1, 2012.

[91] M. Uno and A. Kukita, “Bidirectional PWM Converter Integrating Cell Voltage Equalizer Using Series-Resonant Voltage Multiplier for Series-Connected Energy Storage Cells,” *IEEE Trans. Power Electron.*, vol. 1, no. c, pp. 1–1, 2014.

[92] H. Park, C. Kim, and C. Kim, “A modularized charge equalization converter for a hybrid electric vehicle lithium-ion battery stack,” *J. Power …*, pp. 343–352, 2007.

[93] C. Kim, H. Park, G. Moon, and A. C. Description, “A Modularized Two-Stage Charge Equalization Converter for Series Connected Lithium-Ion Battery Strings in an HEV,” pp. 992–997, 2008.

[94] A. Xu, S. Xie, and X. Liu, "Dynamic Voltage Equalization for Series-Connected Ultracapacitors in EV/HEV Applications," *Vehicular Technology, IEEE Transactions on*, vol. 58, no. 8. pp. 3981–3987, 2009.

[95] H.-S. Park, C.-E. Kim, C.-H. Kim, G.-W. Moon, and J.-H. Lee, "A Modularized Charge Equalizer for an HEV Lithium-Ion Battery String," *Industrial Electronics, IEEE Transactions on*, vol. 56, no. 5. pp. 1464–1476, 2009.

[96] C.-H. Kim, M. Kim, J.-H. Kim, and G.-W. Moon, "Modularized charge equalizer with intelligent switch block for lithium-ion batteries in an HEV," *Telecommunications Energy Conference, 2009. INTELEC 2009. 31st International*. pp. 1–6, 2009.

[97] C.-H. Kim, M.-Y. Kim, Y.-D. Kim, and G.-W. Moon, "A modularized charge equalizer using battery monitoring IC for series connected Li-Ion battery strings in an electric vehicle," *Power Electronics and ECCE Asia (ICPE & ECCE), 2011 IEEE 8th International Conference on*. pp. 304–309, 2011.

[98] J. Ewanchuk, D. Yague, and J. Salmon, "A modular balancing bridge for series connected Li-ion batteries," *Energy Conversion Congress and Exposition (ECCE), 2011 IEEE*. pp. 2908–2915, 2011.

[99] C.-H. Kim, M.-Y. Kim, H.-S. Park, and G.-W. Moon, "A Modularized Two-Stage Charge Equalizer With Cell Selection Switches for Series-Connected Lithium-Ion Battery String in an HEV," *Power Electronics, IEEE Transactions on*, vol. 27, no. 8. pp. 3764–3774, 2012.

[100] H.-S. Park, C.-H. Kim, K.-B. Park, G.-W. Moon, and J.-H. Lee, "Design of a Charge Equalizer Based on Battery Modularization," *Vehicular Technology, IEEE Transactions on*, vol. 58, no. 7. pp. 3216–3223, 2009.

[101] Y. Barsukov, "Battery cell balancing: what to balance and how," *Texas Instruments*, 2009.

[102] W. B. Gu and C. Y. Wang, "Thermal-Electrochemical Modeling of Battery Systems," *J. Electrochem. Soc.*, vol. 147, no. 8, p. 2910, 2000.

[103] K. Lee, G. Kim, and K. Smith, "3D Thermal and Electrochemical Model for Spirally Wound Large Format Lithium-ion Batteries," *Energy Meet. Las Vegas*, 2010.

[104] D. N. Rakhmatov and S. B. K. Vrudhula, "An analytical high-level battery model for use in energy management of portable electronic systems," *Computer Aided Design, 2001. ICCAD 2001. IEEE/ACM International Conference on*. pp. 488–493, 2001.

[105] D. Doerffel and S. A. Sharkh, “A critical review of using the Peukert equation for determining the remaining capacity of lead-acid and lithium-ion batteries,” *J. Power Sources*, vol. 155, no. 2, pp. 395–400, Apr. 2006.

[106] R. K. Jaworski, “Effects of nonlinearity of Arrhenius equation on predictions of time to failure for batteries exposed to fluctuating temperatures,” *Telecommunications Energy Conference, 1998. INTELEC. Twentieth International*. pp. 289–296, 1998.

[107] B. Y. Liaw, E. P. Roth, R. G. Jungst, G. Nagasubramanian, H. L. Case, and D. H. Doughty, “Correlation of Arrhenius behaviors in power and capacity fades with cell impedance and heat generation in cylindrical lithium-ion cells,” *J. Power Sources*, vol. 119–121, pp. 874–886, Jun. 2003.

[108] L. Lam, P. Bauer, and E. Kelder, “A practical circuit-based model for Li-ion battery cells in electric vehicle applications,” *Telecommunications Energy Conference (INTELEC), 2011 IEEE 33rd International*. pp. 1–9, 2011.

[109] M. Chen and G. A. Rincon-Mora, “Accurate electrical battery model capable of predicting runtime and I-V performance,” *Energy Conversion, IEEE Transactions on*, vol. 21, no. 2. pp. 504–511, 2006.

[110] L. Gao, S. Liu, and R. A. Dougal, “Dynamic lithium-ion battery model for system simulation,” *Components and Packaging Technologies, IEEE Transactions on*, vol. 25, no. 3. pp. 495–505, 2002.

[111] R. W. Erickson and D. Maksimovic, *Fundamentals of power electronics*. Springer Science & Business Media, 2001.

PUBLICATIONS

This chapter will present the different publications presented during the thesis work. All the presented publications have a final version copyrighted by IEEE ©.

Clean Electrical Power (ICCEP), 2013 International Conference on , vol., no., pp.99,106, 11-13 June 2013.

Battery pack tests to detect unbalancing effects in series connected Li-ion cells

I.Aizpuru
U.Iraola
J.M.Canales
E.Unamuno
I.Gil

DOI: 10.1109/ICCEP.2013.6586974

Battery pack tests to detect unbalancing effects in series connected Li-ion cells

I. Aizpuru*, U. Iraola*, J.M. Canales*, E. Unamuno*, I. Gil**
*Faculty of Engineering, University of Mondragon, Loramendi 4, 20500 Arrasate, (*Spain*)
**Orona eic s. coop, Polígono industrial Lasaola s/n, 20120 Hernani (*Spain*)

***Abstract*—In this work main unbalancing effects and causes in series connected lithium ion cells are analyzed. Literature and research papers are analyzed regarding manufacturing process and environmental issues, detecting main unbalancing aspects. There is not much work in the literature focused in unbalancing effects and causes; due to insufficient knowledge a test procedure to detect unbalancing effects and causes is presented in this work. Main unbalancing causes are detected and their effect in battery pack performance has been tested. Main factors and their influence in battery pack unbalancing and performance are presented as conclusions.**

Keywords*—Batteries, Battery Management Systems Energy storage, Lithium, un

I. INTRODUCTION

Energy demand is growing nowadays. Fuel and fossil energy sources are held of only some countries, so the dependency to this power sources is high for main countries. This dependency is pushing the effort in new and renewable energy sources and is becoming the main investment for governments and private companies.

Renewable energies are clean and attractive technologies. However, they have a big limitation; they cannot produce energy when consumers need it. They are dependent on environmental conditions. The most common examples are the wind and solar energy. Solar energy cannot be produced at night and wind energy cannot feed energy when there is not wind. That's why renewable energy by itself is unable to provide continuous energy to our worldwide energy system.

Renewable energy should go hand in hand with energy storage systems. Energy storage systems can accumulate energy when renewable energies produce it and they can give energy when the consumers need it.

Energy storage systems can be differenced by energy capacity and energy delivery speed. High energy capacity systems as power pump hydroelectric and compressed air have big capacity to store energy, but they are not fast response technologies. Electrochemical energy based systems as batteries, capacitors and mixed systems between batteries and ultracapacitors as lithium-capacitors (LiCs) offer a high speed response but they need to compose large systems to reach high energy capacities.

Li-ion batteries are extendedly used in portable applications and are gaining interest for energy storage and traction applications. For high energy power applications series connection of li-ion batteries is necessary to reach high voltage used in energy storage and traction application building big battery packs [1–4]. The cells of this battery pack are subjected to different conditions of temperature or self discharge, inducing unbalancing between series connection devices [5]. This unbalanced must be controlled by a Battery Management System *BMS* to maximize the life of the entire battery pack. [6].

The motivation for this work is to determine a test methodology and procedure to measure the unbalancing effects in series connected battery packs. Unbalancing effects and causes are not well-known, and there is not much information in literature. This paper presents the main unbalancing causes that influence in Li-ion cells and interprets the unbalancing effects in battery performance and life.

First chapter describes unbalancing causes and effects found in the literature. Second chapter describes the performance issues of a battery pack under unbalancing situation. Third chapter describes the unbalancing detection test procedure. Fourth chapter presents main results during test development and finally the most important conclusions are presented.

These tests will permit to evaluate the amount of balancing that is necessary to perform a good balancing between cells and maximize battery life and performance.

II. UNBALANCING CAUSES AND EFFECTS

Unbalancing causes and effects in battery cells are due to uncontrolled processing disturbances, environmental variations and discharge currents due to external circuitry connections.

Unbalancing effects cause a performance deterioration on the whole battery pack, reducing its characteristics and features [7].

Unbalancing causes and effects are interconnected between them because each variation in a cell affects to the whole battery. The battery pack is a multivariable system as presented in Fig. 1, where all variables are interdependent creating a multivariable interdependent system. Individual cell variation and performance has effect in the whole battery.

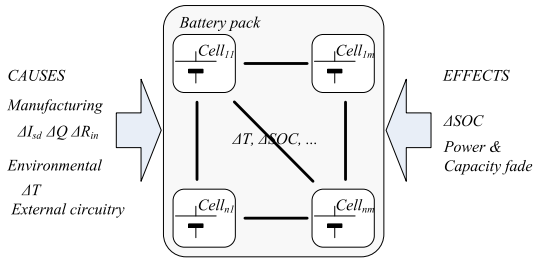

Fig. 1. Battery multivariable system. Unbalancing causes and effects in a multivariable Battery pack.

A. Unbalancing causes

Manufacturing process, environmental variables and external manipulation circuitries cause unbalancing between cells in a battery pack.

1) Manufacturing process

Li-ion cells present differences due to manufacturing process. Starting from the manufacture of the electrodes (mixing the materials, coating, etc.) continuing with the assembly of the cell (filling, packing, welding, etc.) and finishing with the formation and the final quality check; there are little variations that produce mismatch between cells manufactured in the same process.

The main variations in manufacturing process are reflected in capacity variations ΔQ, where low capacity variations are required. Self discharge variations ΔI_{sd}, where a greater self discharge in one cell reduces the whole capacity of the battery pack [8]. Internal resistance variation ΔR_{in}, where little internal variations during the manufacturing of the different materials produce internal resistance variations [5].

2) Environmental influence

ΔT between cells is the main environmental parameter that affects battery performance, due to differences in cell behavior [9], [10]. Temperature affects benefiting capacity and power permance but accelerating aging at High temperatures (>35ºC), and battery deterioration and performance reduction at Low temperatures (<0ºC).

3) External circuitry

External circuitry connected to cells in a battery pack cause unbalances between cells. Voltage measurement and balancing circuitry is necessary to control, measure and guarantee the safety of the cells, but it should affect as low as possible to the cell [11].

B. Unbalancing effects

Due to unbalancing causes not desired behavior happens in the Battery pack presented as unbalancing effects between cells.

1) ΔSOC

State of charge *SOC* variation between cells, ΔSOC, limits battery pack performance. Low *SOC* cell will limit the Battery pack performance during discharge while high *SOC* cells limit battery pack during charge. The whole battery pack performance will be limited if the battery suffers ΔSOC between cells.

2) Capacity & power fade

If a cell in a Battery pack is subjected to extreme temperature, overvoltage or over discharge this cell will experience a premature performance reduction.

Capacity fade is usually due to consecutive overvoltage in one cell [7] and over temperature effects.

Power fade is directly related to an internal impedance R_{in} increment. The internal impedance increases due to aging, and overstress of the cells.

III. Battery Performance with Unbalancing Effects

Battery performance under unbalancing conditions is limited by ΔSOC between cells in a battery pack and differences and limits in capacity and power.

To maximize all the energy of the Battery pack the energy of all the cells has to be obtained. For this objective a balancing system has to be installed in the battery pack.

Balancing systems exchange energy between cells during charge and/or discharge. The excess energy of the strongest cells is supplied to the weakest cell avoiding the *BMS* to shut off the battery because one cell reaches overvoltage or deep discharge.

The maximum energy difference between 2 cells in a battery pack is considered when one cell is new ($Q_{new}=Q_{max}$) and the other cell is in the end of life *EOL* in the 80% of the maximum capacity ($Q_{EOL}=0.8Q_{max}$).

The maximum variation of *SOC*, ΔSOC, depends on the performance and the requirements of the *BMS* and the balancing system.

To understand the behavior of an unbalanced battery pack a 2S1P battery pack, under *SOC* unbalance (ΔSOC) and capacity unbalance (ΔQ), system has been analyzed. The battery pack of Fig. 2 is subjected to a charge and discharge process under different balancing conditions. Total energy obtained after discharge in Watts per hour (Wh) is analyzed to evaluate the balancing system performance in TABLE I.

The 2S1P battery pack is assembled with a $\Delta Q=Q_{new}-Q_{EOL}$ and a $\Delta SOC=|SOC_{new}-SOC_{EOL}|$ of 17.5 %. The *SOC* of each

TABLE I
Battery Performance Behavior for modes in Fig. 2

Mode	Aprox. Wh obtained Fig. 2	Fig. 2 3,2V Q_{new}=10Ah		
		Max. energy	***Energy used***	***Energy unused***
a)	$(V_1+V_2)\cdot min(Q_{1(charge)},Q_{2(charge)})$	57.6	44.8 (77%)	12.8 (23%)
b)	$(V_1+V_2)\cdot Q_{EOL}$	57.6	51.2 (88%)	6.4 (12%)
c)	$V_1\cdot Q_{1(charge)}+V_2\cdot Q_{2(charge)}$	57.6	54.4 (94%)	3.2 (6%)
d)	$V_1\cdot Q_{new}+V_2\cdot Q_{EOL}$	57.6	57.6 (100 %)	0 (0%)

This work was supported by a training research grant under the AE modality via the Basque government program, Basque Contry.

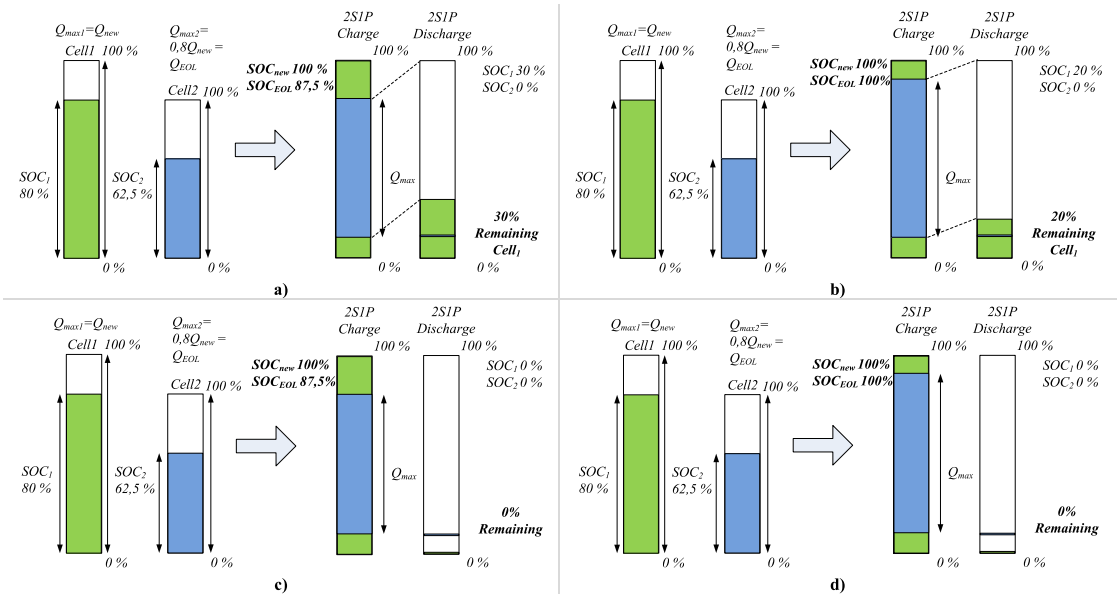

Fig. 2 Performance diagram of 2S1P Battery pack ΔSOC unbalancing and ΔQ unbalancing a) Battery performance without balancing system. b) Battery performance with balancingsystem operating during charging. c) Battery performance with balancing sytem operating during discharging. d) Battery performance with balancing system operating during charging and discharging.

cell is related to the maximum capacity of each cell and their instantaneous capacity Qx, so $SOC_{new}= Q_1/Q_{new}$ and $SOC_{EOL}= Q_2/Q_{EOL}$ where Q_1 and Q_2 are the charge inside each cell respectively.

First operation without any balancing system is analyzed in Fig. 2 a). Both cells are connected in series and charged until "cell new" reaches the maximum 100 % SOC_{new} ($Q_1=Q_{new}$) and charge is stopped. "Cell new" increases the SOC in 20 %. An increase in 20 % of SOC in cell new means a 25% increase in SOC in "cell EOL". "Cell EOL" is not fully charged $SOC_{EOL(charged)}=87,5\%$ ($Q_2=0,875Q_{EOL}$). During discharge "cell EOL" limits the discharge while the 30 % of "cell new" is still unused. The battery pack is shut off because "Cell EOL" is empty.

Second operation presents balancing during charge process in Fig. 2 b). This process charges both cells to 100% of SOC but during discharge the 20% of the available energy of "cell new" is still available, only Q_{EOL} is obtained from the battery.

Third operation presents a balancing system that balances cells during discharge in Fig. 2 c). During charge "cell EOL" is not fully charged with $SOC_{EOL(charged)}=87,5\%$ so all the battery energy is not used. The cells are charged to ($Q_1=Q_{new}$) and ($Q_2=0,875Q_{EOL}$). During discharge both cells are discharged to 0% SOC.

Fourth operation presented in Fig. 2 d) balances the Battery pack during charge and discharge. The whole energy of the cells is obtained.

To quantify the cell balancing benefits and the unbalancing effects an example for 2 liFePO$_4$ cells with a new capacity of Q_{new}=10 Ah is presented in TABLE I with the battery performances of Fig. 2. The maximum available energy with 3.2 nominal voltage of LiFePO$_4$ cells is $V_1Q_{new}+V_2Q_{EOL}=57,6$ Wh. The total energy is only available in case d).

IV. UNBALANCING TEST PROCEDURE

A new test methodology has been implemented to measure and quantify the unbalancing effects in series connected li-ion cells.

The methodology consist of a test bench for Battery packs, to measure the unbalance between different cells and introduce different unbalance effects externally to measure the influence in the whole battery pack. The unbalancing effects will be measured in *Charge/Discharge tests* and *rest tests* to verify the impact of different unbalancing processes as presented in Fig. 3.

A. Charge/Discharge tests

Different unbalancing effects are analyzed during Charge/ Discharge tests. The objective is to detect the most critical parameters for battery pack unbalance.

Temperature effect between cells is analyzed during charge and discharge of the battery pack. Equal temperature between cells and temperature mismatch ΔT between cells is tested.

SOC of single cells affect in battery performance and limit battery total capacity. SOC between cells is analyzed to

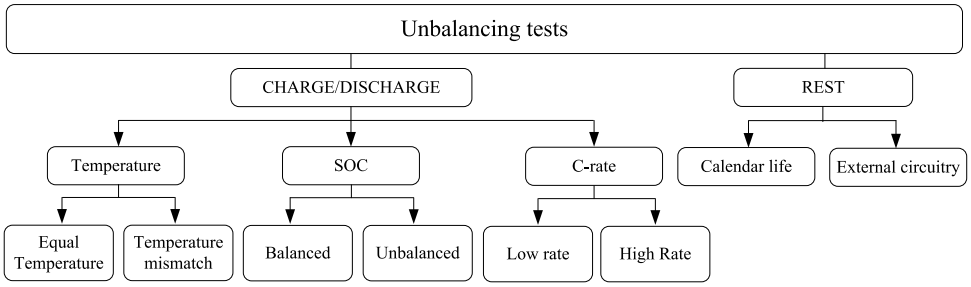

Fig. 3 Unbalancing tests methodology diagram. Charge/ Discharge tests and Rest period tests to measure different unbalancing effects.

compare battery performance between cells with *SOC* variation (*ΔSOC)* and equal *SOC*.

Current rate influence in battery pack unbalancing will be investigated. For this issue Low rate tests and High rate tests will be implemented to a Battery pack.

B. Rest tests

Rest tests analyze battery pack unbalancing effects when the battery pack is in standby or in repose. There are two different tests during rest. The calendar life test and the external circuitry influence test are analyzed.

The calendar life test stores single cells in room temperature and measures the difference in self discharge ΔI_{sd} between different cells. The cells are stored at different *SOC* values to analyze deviation in self discharge due to *SOC* variation.

External circuitry tests permit to analyze unbalancing effect between different measurement systems.

C. Test bench

A Basytec XCTS battery tester is used to initialize the cells of the Battery pack to different initial conditions.

Two Prebatem climate chambers are employed to make controlled temperature tests and generate differential temperatures *(ΔT)* between cells.

A Maynuo M9715 DC load is employed to discharge the battery pack and a ET-SYTEM LAB/SMP 135 DC power supply to execute charge cycles.

All the system parameters (Voltage, current and temperature) are measured by a NI cRIO system and the DC load and supply are controlled via a Labview interface.

The unbalancing effects measurement test starts with an *initialization* of the cells to a determined condition. After that, the *test* is reproduced, and finally the results are *measured and analyzed.*

V. Experimental Results

An experimental Battery pack in a 4S1P configuration of 4 $LiFePO_4$ 6.5Ah cells has been implemented. Test bench configuration and Battery pack are presented in Fig. 5. Main results are presented in TABLE IV.

A. Charge discharge tests

The four cells of the 4S1P are tested separately to measure the initial capacity deviation between cells *ΔQ* TABLE III. This initial deviation introduces the first unbalance in the Battery pack. The cells are measured in a CCCV charging process until 3,65V and C/20 current. After that all the cells are discharged at 1C rate until 2V, and when each cell is initialized the pack is conformed.

TABLE III
Battery Capacity Mismatch

$Cell_1$	$Cell_2$	$Cell_3$	$Cell_4$	Max *ΔQ*	Mean *Q*
7.95 (122%)[a]	7.88 (121%)	7.65 (117%)	7.67 (118%)	0.3 (4.6%)	7.78 (120%)

[a] Percentage respect to nominal capacity 6.5 Ah

To avoid the CV stage during charge tests the battery pack is cycled during charge until one cell reaches 3.65V and during discharge until one cell reaches 2V. After each cycle one hour rest period is introduced as presented in Fig. 4.

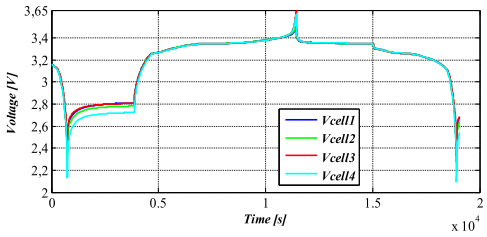

Fig. 4 Charge discharge tests for unbalancing effect detection

TABLE II
External Unbalance Parameters

Temperature		SOC		C-rate	
Equal Temp.	*Temp. mismatch*	*Balanced*	*Unbalanced*	*Low rate*	*High rate*
ΔT=0ºC	*ΔT*=5ºC	*ΔSOC*=0%	*ΔSOC*=3%	C/2 Charge 1C Discharge	3.5C Charge 7C Discharge

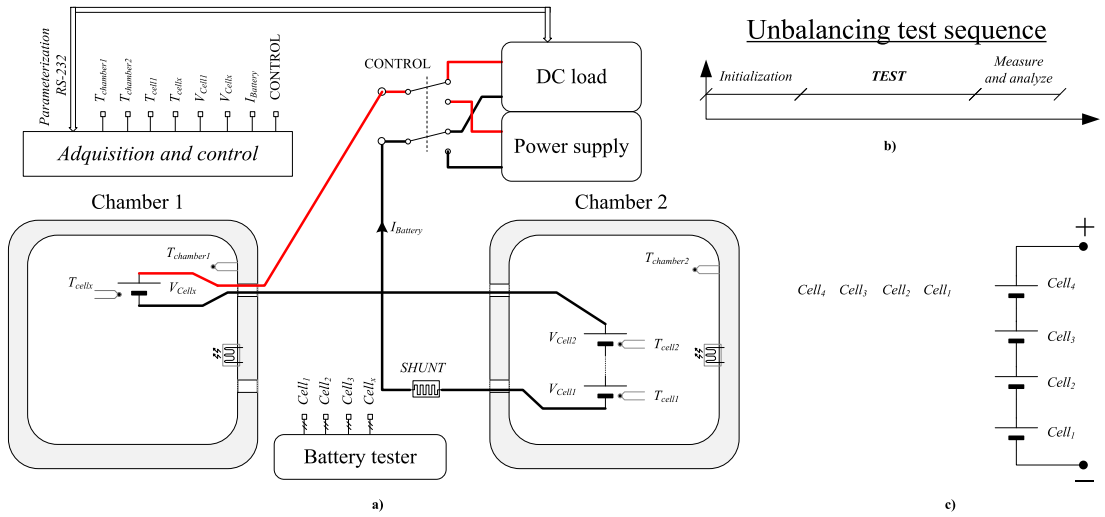

Fig. 5 Test bench for unbalancing effect detection. a) Test bench configuration for a temperature mismatch configuration. b) Unbalancing test sequence with Initialization, TEST and measure and analyze process. c) Battery pack configuration: real photo and diagram.

The capacity is measured with a precision shunt resistor and a low time integration period in order to reduce coulombic measurement error.

The unbalancing parameters dispersion to analyze battery performance are presented in TABLE II.

During Charge/Discharge, voltage variation between cells ΔV and mean capacity obtained from the battery Q_{mean} will be measured.

Four different tests have been implemented to evaluate unbalancing effects in Battery packs. Battery performance in terms of usable capacity during tests and unbalancing generation; measuring if the ΔV_{max} between cells increases during the test will be analyzed.

Most important results are presented in TABLE IV and in chapter *Experimental tests conclusions*.

1) Equal temperature-Balanced-Low rate

The 4S1P testing battery pack is cycled under constant 25ºC, balanced and Low rate configuration. High capacity (6.95Ah) is obtained during charge discharge cycles and big difference in voltage is obtained because the *SOC* of the cells is in the limit regions and the *OCV-SOC* curve has more deviation. (Fig. 5 a)).

2) Equal temperature-Balanced-High rate

High rate tests obtain less capacity because the cell reaches 2V and 3.65V faster and the test is stopped. Due to high rate currents the *SOC* of the cells varies less than in a low rate test so the *OCV-SOC* curve does not affect so much, and the cell voltage variation is not high. (Fig. 5 b))

The whole Battery pack is at a constant temperature of 25ºC and low rate.

3) Temperature mismatch-Balanced-Low rate

A temperature mismatch of ΔT 5ºC is inserted in the Battery pack testing 3 cells at 30ºC and one cell at 25ºC. The cell at lower temperature limits the battery pack performance obtaining less capacity that with equal temperature. The maximum voltage variations are obtained during charge. (Fig. 5 c)).

The cells are balanced and tested in low rate conditions. The test is presented in Fig. 5.

4) Equal temperature-Unbalanced-Low rate

An *SOC* variation of 3% is introduced to one cell respect to the rest of the cells. The Battery performance is reduced due to this variation and voltage variations are increased. (Fig. 5 d)

The battery pack is tested at 25ºC and Low rate conditions.

B. Rest tests

Rest tests permit to identify unbalancing behaviors during standby moments of battery packs.

1) Calendar life

Calendar life tests permit to measure degradation of cells due to time in a storage situation and measure the self discharge of the cells. The cells are stored at room temperature and a capacity measuring test is implemented once a month. Calendar life tests demonstrate that High *SOC* (70%) cells have bigger self discharge 1,5% /month respect to Low *SOC* (50%) cells with 0,76% /month. No difference in self discharge is appreciable between cells with same *SOC*.

2) External circuitry

External circuitry influence is measured and compared to calendar life comparing the influence in self discharge.

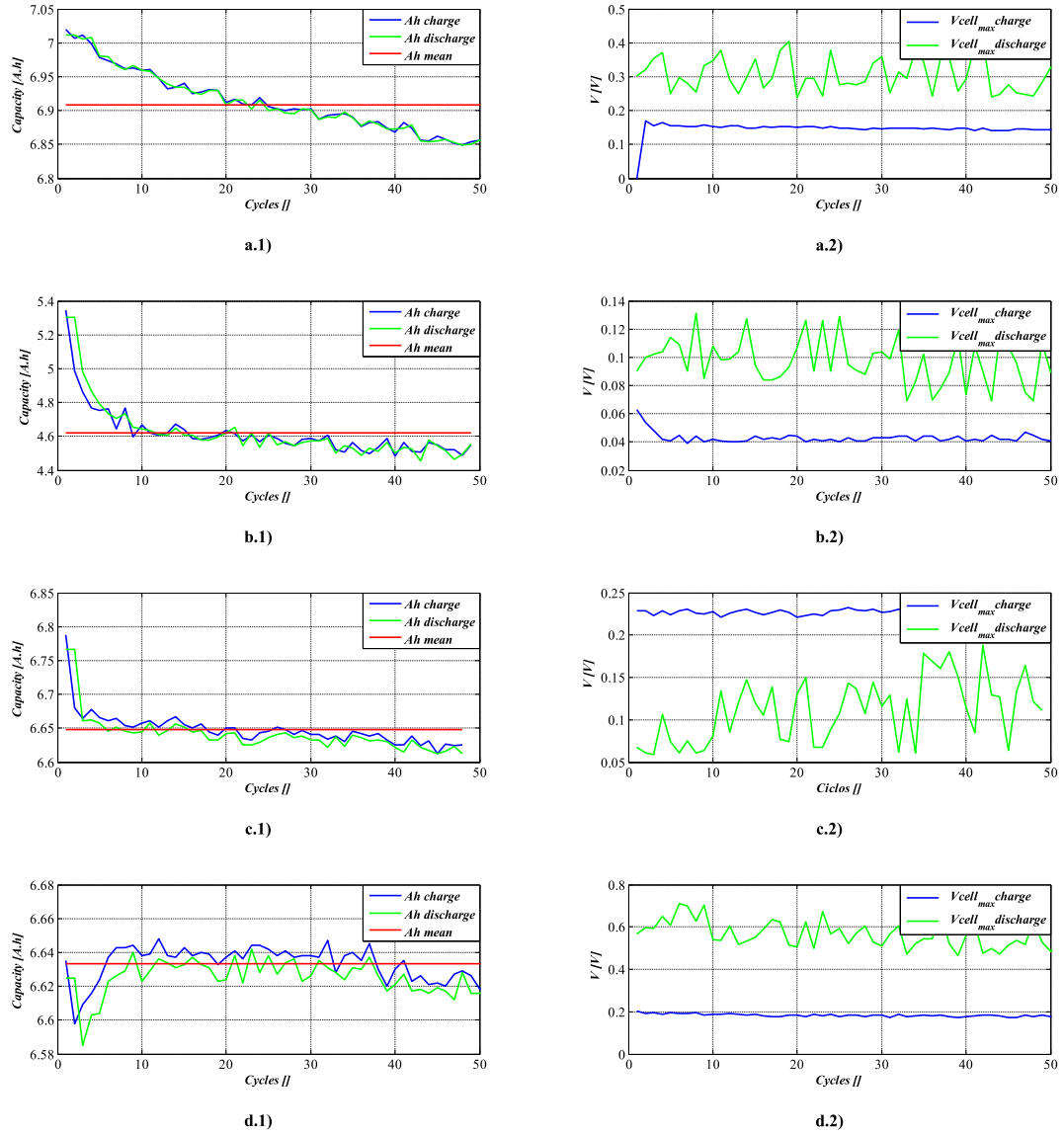

Fig. 6 Battery pack unbalancing tests. a) Equal temperature-Balanced-Low rate. b) Equal temperature-Balanced-High rate. c) Temperature mismatch-Balanced-Low rate. d) Equal temperature-Unbalanced-Low rate. 1) Capacity obtained during charge and discharge. 2) Maximum voltage deviation during charge and discharge.

TABLE IV
BATTERY TESTS RESUME

CHARGE/DISCHARGE TESTS

Values / Tests	Q_{mean} [Ah]	First cycles ΔV_{max} [V]		Last cycles ΔV_{max} [V]	
		Charge	Discharge	Charge	Discharge
Equal temperature-Balanced-Low rate	6.91	0.17	0.35	0.17	0.33
Equal temperature-Balanced-High rate	4.62	0.04	0.12	0.04	0.12
Temperature mismatch-Balanced-Low rate	6.65	0.22	0.1	0.22	0.15
Equal temperature-Unbalanced-Low rate	6.637	0.2	0.6	0.2	0.6

REST TESTS

Values / Tests	Q_{ini}	Q_{lost} max [a]	Q_{lost} min [a]	$\%Q_{lost}/Q_{nominal}/month$ [b]	$\%Q_{lost}/Q_{nominal}/week$ [b]
Calendar life 50%	3.25	0.05		0.76%	0.19%
Calendar life 70%	4.55	0.1		1.5%	0.375%
External circuitry INA 210	3.25	0.36 ($Cell_1$)	0.12 ($Cell_4$)	5.54%	1.38%
External circuitry INA 210+balancing	3.25	0.37 ($Cell_1$)	0.12 ($Cell_4$)	5.7%	1.42%
External circuitry TI bq76PL536	3.25	0.22 ($Cell_4$)	0.16 ($Cell_1$)	3.38%	0.845%
External circuitry NI 9205 cRIO	3.25	0.1	0.1	1.5%	0.375%

[a] Q_{lost} *per month*
[b] Respect to Q_{lost} *max*
[c]

4 different measuring systems are used to measure 4 cell voltages of a 4S1P Battery pack with 50% *SOC* each cell, and compare the tests with 50% and 70% calendar life tests.

The first measuring system is based on a TI INA210 analog differential amplifier system with one amplifier per cell. Each cell is continuously measured, and the cell connected to the negative point ($Cell_1$ Fig. 5 c)) suffers more discharge.

The second measuring system is the same system composed of 4 INA 210 amplifiers with a passive balancing system connected, to evaluate self discharge due to transistors and resistor circuits connected in parallel to the cell. The self discharge of the *BJT* transistors is negligible as is presented in TABLE IV.

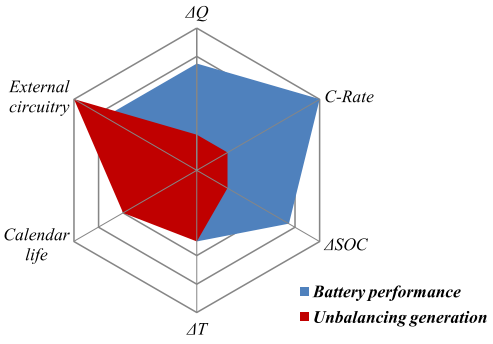

Fig. 7 Spider chart representing unbalancing parameter effect in battery performance and unbalancing generation in the Battery pack.

The third measuring system is based on a TI bq76PL536 battery management IC mounted in a bq76PL536EVM-3 evaluation board. A measurement rate of 1S/s is implemented. The most discharged cell is the cell connected to the positive terminal ($Cell_4$ Fig. 5 c)). The discharge rate is less than for the analog measurement system.

The fourth measuring system is a NI 9205 analog measurement module, controlled by a cRIO system with a 1S/s rate of measurement. The *AD* converters of the cRIO do not cause big discharge effect during measurement, discharging cells as self discharge to 70% of *SOC*.

C. Experimental tests conclusions

Experimental tests affect in battery performance and cell behavior. Battery capacity decrease is one of the most common parameters to detect battery performance characteristics. Another important parameter is the unbalancing generation or degradation in the battery pack. Unbalancing generation is measured if ΔV increases between cells or if capacity discharge varies between cells in a battery pack.

Battery performance is affected mainly by High *C-rates*. ΔQ differences in batteries and ΔSOC of 3%, affect similarly in a capacity decrease of 0.2-0.3 Ah in the battery pack. 5º ΔT between cells in a battery pack affect similarly to a ΔSOC of 3%. One cell with lower temperature suffers from over discharge and overcharge, suffering bigger degradation. The temperature deviation should be controlled by a *BTMS*. A variation in *SOC* limits the battery pack in overcharge and over discharge by different cells. The *SOC* variation produces

the biggest voltage variation. This difference could be controlled with a *BMS.*

Low self discharge of Li-ion cells (1%/month) calendar life is not a big problem regarding battery performance. External circuitry affects in a bigger way in battery performance due to a bigger capacity decrease.

Unbalancing generation or degradation permits to measure how much is unbalanced the battery pack during cycle life. *ΔQ, C-Rate* and *ΔSOC* variations in battery cycling do not increase unbalancing between cells. *ΔT* increases *ΔV* during some cycles but not in a significant way.

External circuitry is the most important parameter in unbalancing generation. Analog measurement systems should be avoided due to high self discharges and variation in common mode behavior as presented in INA 210 results. Passive balancing systems do not discharge the cell, so they do not increase unbalancing degradation.

Digital *AD* converters, with low consumption and sleep mode operation are the best choice for battery measurement systems as presented in the TI cRIO results. Battery management *ICs* must be used with sleep mode or standby functionalities to improve their behavior, and are the best choice when big amounts of cells should be measured.

Calendar life affects in a lower way due to low self discharge in Li-ion cells. Higher *SOC* cells suffer more self discharge so if the battery pack is not balanced the self discharge due to *SOC* differences influences more in unbalancing generation.

VI. CONCLUSIONS

A battery pack test procedure has been implemented to measure unbalancing effects in series connected Li-ion battery packs due to literature misinformation about unbalancing effects and causes in li-ion battery packs.

No unbalancing generation is detected due discharge and charge tests, so the most important parameters that cause unbalance in battery packs are external circuitry and self discharge.

No unbalancing degradation has been observed due to continuous overvoltage to the same cell. This effect could impact in longer charge/discharge tests. To avoid degradation effect in cells is essential to shut off the battery back when one cell of the whole pack reaches charge voltage limit or discharge voltage limit.

Capacity mismatch *ΔQ* due to manufacturing differences presents the first unbalancing effect limiting the pack by the less capacity cell. Cell with matched capacities are required. Capacity mismatch of less than 5% are required.

High *C-rates* reduce the available capacity of the whole battery pack, but do not induce unbalancing between cells.

ΔSOC limits the battery performance. The *BMS* should limit the *SOC* variation between the cells of a battery pack. *SOC* variation produces high voltage variations in charge and discharge limits. A difference in *SOC* of 3% is manageable.

Temperature difference *ΔT* affect in two ways. Low temperature cells limit the battery pack performance, but high temperature cells have higher aging rates. A compromise between temperature and application is required. The temperature of the cells should be controlled by a *BTMS* in high dispersion temperature applications.

Calendar life is not a big issue in battery performance and has not big impact in unbalancing generation in Li-ion technology. Calendar life and self discharge difference between cells with different *SOC* is the main problem.

External circuitry connection is the main problem regarding battery performance and unbalancing generation between series connected cells. Differences between energy consumption in measurement and balancing systems generate unbalancing effects between cells. Analog measurement systems should be discarded and consider low consumption, standby and sleep mode *AD* converters as the best solution.

REFERENCES

[1] F. Jin and K. G. Shin, “Pack Sizing and Reconfiguration for Management of Large-Scale Batteries,” *Cyber-Physical Systems (ICCPS), 2012 IEEE/ACM Third International Conference on*. pp. 138–147, 2012.

[2] J. Kim, J. Shin, C. Chun, and B. H. Cho, “Stable Configuration of a Li-Ion Series Battery Pack Based on a Screening Process for Improved Voltage/SOC Balancing,” *Power Electronics, IEEE Transactions on*, vol. 27, no. 1. pp. 411–424, 2012.

[3] J.-H. Kim, J.-W. Shin, C.-Y. Jeon, and B.-H. Cho, “Screening process of Li-Ion series battery pack for improved voltage/SOC balancing,” *Power Electronics Conference (IPEC), 2010 International*. pp. 1174–1179, 2010.

[4] G. L. Plett and M. J. Klein, “Simulating Battery Packs Comprising Parallel Cell Modules and Series Cell Modules,” no. 1, pp. 1–17, 2009.

[5] S. Santhanagopalan and R. E. White, “Quantifying Cell-to-Cell Variations in Lithium Ion Batteries,” *International Journal of Electrochemistry*, vol. 2012, pp. 1–10, 2012.

[6] A. Affanni, A. Bellini, G. Franceschini, P. Guglielmi, and C. Tassoni, “Battery choice and management for new-generation electric vehicles,” *Industrial Electronics, IEEE Transactions on*, vol. 52, no. 5. pp. 1343–1349, 2005.

[7] Y. Barsukov and T. Instruments, “Battery Cell Balancing : What to Balance and How.”

[8] C. Martinez, “Cell Balancing Maximizes The Capacity Of Multi-Cell Li-Ion Battery Packs,” *Intersil. Inc*.

[9] J. R. Belt, C. D. Ho, T. J. Miller, M. A. Habib, and T. Q. Duong, “The effect of temperature on capacity and power in cycled lithium ion batteries,” *Journal of Power Sources*, vol. 142, no. 1–2, pp. 354–360, Mar. 2005.

[10] M. Broussely, P. Biensan, F. Bonhomme, P. Blanchard, S. Herreyre, K. Nechev, and R. J. Staniewicz, “Main aging mechanisms in Li ion batteries,” *Journal of Power Sources*, vol. 146, no. 1–2, pp. 90–96, Aug. 2005.

[11] M. Uno and K. Tanaka, “Influence of High-Frequency Charge-Discharge Cycling Induced by Cell Voltage Equalizers on the Life Performance of Lithium-Ion Cells,” *Vehicular Technology, IEEE Transactions on*, vol. 60, no. 4. pp. 1505–1515, 2011.

Clean Electrical Power (ICCEP), 2013 International Conference on , vol., no., pp.99,106, 11-13 June 2013.

Passive balancing design for Li-ion Battery Packs based on single cell experimental tests for a CCCV charging mode

I.Aizpuru
U.Iraola
J.M.Canales
M. Echeverria
I.Gil

DOI: 10.1109/ICCEP.2013.6586973

Passive balancing design for Li-ion Battery Packs based on single cell experimental tests for a CCCV charging mode

I. Aizpuru*, U. Iraola*, J.M. Canales*, M. Echeverria*, I. Gil**
*Faculty of Engineering, University of Mondragon, Loramendi 4, 20500 Arrasate, (*Spain*)
**Orona eic s. coop, Polígono industrial Lasaola s/n, 20120 Hernani (*Spain*)

***Abstract*—High power battery systems are composed of big array of series connected single cells. The main reason of increasing battery pack voltage is, to increase power by decreasing current and improve the efficiency. To control the charge and voltage of each cell a *BMS* with balancing system is necessary. Battery modeling is hard work, and battery dispersion and deviations are not taken into account. To overcome this problem, in this work a passive balancing system design procedure is presented based on single cell experimental tests. Battery modeling is avoided and main deviations between batteries are taken into account. Main parameters are taken into account during the design procedure. Finally design procedure is compared with experimental results.**

Keywords—Batteries, Battery Management Systems, Energy storage, balancing systems, Lithium

I. INTRODUCTION

Single cells are widely used in portable solutions like mobile phones. For higher energy demand applications parallel connection of cells is used to obtain an equivalent higher capacity cell. The current diverts according to the internal impedance of each cell. However there are a lot of equipments that work with higher voltages so series connection of cells is necessary. Starting with laptops (connection of 3 cells in series), continuing with Electric Vehicles (tens to hundreds of cells in series) and grid energy storage systems (several hundreds of cells in series) [1], [2].

Due to asymmetrical differences in process manufacturing (capacity mismatch, Self discharge variation…) and environmental variables (temperature mismatch between cells) unbalancing is generated between cells. [3–6]

During battery cycling each cell has a Charging Voltage Limit *CVL* and a Discharging Voltage Limit *DVL* that limits the cell performance. These security limits are vital to guarantee the correct operation of the cell, even exceeding these limits may lead to a security hazard.

To subject one cell to *CVL* continuously or exceed this limit could start an accelerated aging of the cell, or even could damage the cell irreversibly. To protect energy cells of a battery pack from *CVL* or *DVL* excess a Battery Management System *BMS* is necessary to control each cell voltage. [7]

If one cell is overcharged, the *BMS* should outcome the excess of charge. This is made by the Balancing Circuit. The balancing circuit could be passive or active, being the passive balancing the most frequently used balancing system. [8–16]

Passive balancing is used during charging process of cells and is based on discharging overcharged cells to match *SOC* or voltage of different cells of a Battery Pack using a parallel connected resistor and an active switch.

One of the most common charging methods is the CCCV method, to fulfill the battery pack capacity. During the last *CV* part the cell is fully charged to *CVL* until the cell current reaches C/20 of the nominal current.

The motivation of this work is to obtain a methodology to design passive balancing circuits based on single cell tests, avoiding cell battery models. Li-ion cells battery models are based on cell tests, but they cannot simulate battery mismatch, and they are usually inaccurate in *CVL* and *DVL* regions [17], at high and low *SOC*s.

This work will calculate and measure the main important parameters to design a passive balancing circuit with single cell tests of CCCV charging. Single cell tests are usually available from manufacturers or battery testers. Using simulation Software single cells are connected in series to simulate a complete CCCV charging process of a Battery Pack. After connecting cells in series a passive balancing circuit is connected.

II. DESING METHODOLOGY

The design methodology permits to design a balancing circuit for a battery pack based on single cell tests taken into account main design parameters. No cell model is required. With this methodology standard deviation between cells is taken into account.

A. Initial single cell test.

The first step is to test different cells under final application conditions. During initial tests different parameters of the cells could be measured and the balancing system is designed taken into account these deviations.

During the test of each cell the main parameter of deviation is the variation in capacity ΔQ between cells. This deviation occurs between cells of the same manufacturer due to process inaccuracies.

Single cells could be tested with different environmental parameters. For example, it is possible to test cells in different temperatures ΔT, to obtain the behavior of the cell in a Battery pack with different temperature between cells.

This work was supported by a training research grant under the AE modality via the Basque government program, Basque Country.

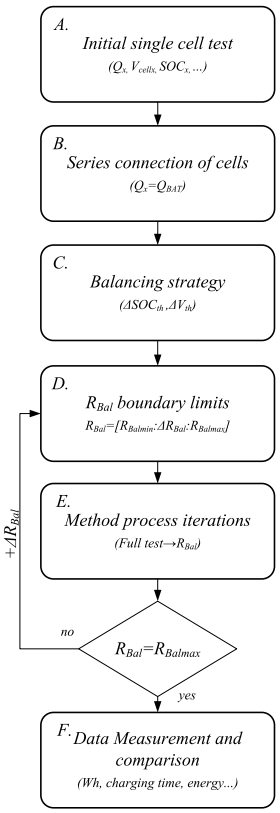

Fig. 1 Design methodology flow chart

It is possible to test single cells with different capacities. For example, it is possible to have new cells and old cells (end of life cells), if our intention is to combine different aged cells.

B. Series connection of cells

After initial single tests all the cells are connected in series by a simulation code programmed on Matlab. The simulation program consists of introducing the same current to all the cells and increase the capacity of each cell Q_x. Due to the cell is tested in specific conditions, the voltage V_{cellx} and the SOC_x of each cell are known as a function of their capacity $V_{cellx}=f(Q_x)$, $SOC_x=f(Q_x)$. During the series connection of cells the capacity of each cell is equal to the battery pack capacity Q_{BAT}.

$$Q_{BAT} \quad Q_x$$

series connection, not balancing

$$SOC_x \quad \frac{Q_x}{Q_{\max_x}}$$

C. Balancing strategy

Main balancing algorithms for passive battery balancing systems are based on voltage balancing strategy and *SOC* balancing strategy. The balancing strategy consists of detecting the weakest cell with V_{min} or SOC_{min}. The other cells are compared to the weakest cell and the result is compared with a threshold value ΔV_{th} or ΔSOC_{th}. If the cell is outside the threshold the balancing system acts discharging the cell through the balancing resistor R_{Bal}.

Passive balancing systems are usually used during charge periods. They are not suitable to use during discharge because the energy of the battery is wasted.

When the passive balancing is switched on the capacity of the cell decreases and the energy is wasted in R_{Bal}.during interval T_{Bal}. The battery capacity Q_{BAT} measured with a coulomb meter is not equal to the cell capacity Q_x. The voltage and the *SOC* of each cell are function of the data obtained during single cell tests.

$$Q_{BAT} \quad Q_x$$

series connection, balancing

$$SOC_x \quad \frac{Q_x}{Q_{\max_x}} \quad Q_x \quad Q_{x_0} \quad \int_0^{T_{Bal}} \frac{V_{cell_x}}{R_{Bal}} dt$$

D. R_{Bal} boundary limits

During the design procedure boundary limits for R_{Bal} are fixed R_{Bal} = (R_{Balmin},R_{Balmax})to limit the iteration process of the balancing system. A minimum ΔR_{Bal} is also

Low R_{Bal} values mean High current with high speed rates, but big amount of heat and energy is wasted in the balancing system. High R_{Bal} values implicate low speed balancing but no heat is generated in the balancing systems.

Low rate balancing currents of C/100 are adequate for battery systems that do not work constantly and stay in standby, like energy storage systems for grid connection.

100 mA balancing current is enough for most applications specially to balance the cells during CCCV charge.

When active balancing is required, for example for high speed equalization and with cells with different capacities or life cycles; higher balancing currents are required, generally bigger than 1A.

E. Method process iterations

After building the battery pack; with series connected cells, the balancing system and the balancing strategy, the battery test is performed for each R_{Bal} value.

The test procedure for the battery pack is the same test procedure of the single cell test described in *A. Initial single cell test.*

F. Data measurement and comparison

After the battery pack is tested under different R_{Bal} values, different parameters are measured and compared to evaluate the passive balancing performance.

Energy wasted during the balancing process, total capacity of the cells, charging time…all the parameters are compared. Depending on the final application different weight for each parameter has to be considered.

III. METHODOLOGY IMPLEMENTATION

The design methodology is implemented for a CCCV charging process for a 4S1P 6.5 Ah $LiFePO_4$ battery pack. The CC charge is made to a C/2 rate, and to maximize the energy of the battery pack the CV charge is made to 3.65V value for the maximum charged cell. To charge the battery pack in CV mode to the maximum cell voltage of 3.65V the *BMS* must send each cell voltage to the battery charger.

A. Initial single cell test.

Initial single cell test is done to measure cell initial deviation and cell performance during CCCV charge. Fig. 3 presents single cell variables (V_{cell}, I_{cell}, *SOC*) as a function of the cell capacity *Q*. Each cell is charged to the 100 % of its *SOC*.

Due to manufacturing process differences capacity mismatch ΔQ appears between same manufacturer cells.1C constant discharge test is implemented to measure the capacity of each cell. The parameter deviation is presented in TABLE I in terms of the nominal capacity.

The capacity dispersion between the cells ΔQ is near 5%,

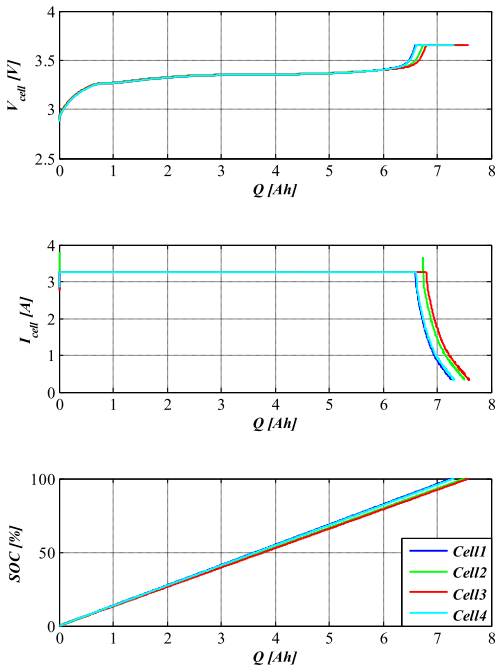

Fig. 3 Single cell test for a CCCV charging process. (Top) V_{cell} *=f(Q)*. (Middle) I_{cell} *=f(Q)*. (Bottom) *SOC =f(Q)*.

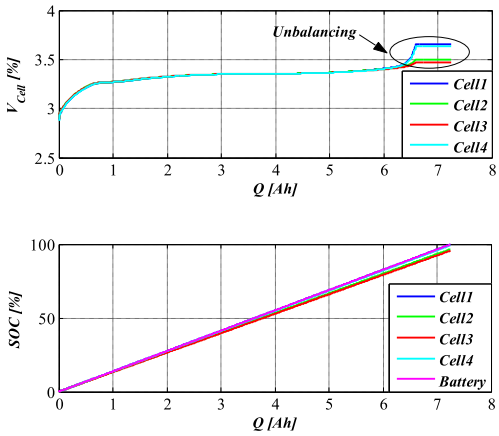

Fig. 2 Series connection of cells without balancing system. (Top) *Vcell =f(Q).* (Bottom) *SOC =f(Q)*

respect to the nominal capacity.

TABLE I
BATTERY CAPACITY MISMATCH

Q_1	Q_2	Q_3	Q_4	Max ΔQ	Mean Q
7.273 (112%)[a]	7.51 (115%)[a]	7.59 (117%)[a]	7.314 (112%)[a]	0.317 (4.9%)[a]	7.42 (114%)[a]

[a] Percentage respect to nominal capacity 6.5 Ah

B. Series connection of cells

4 single tested cells are connected in series via simulation. The series connection implies the same current for all the cells and the same capacity for all the battery pack (Q_x=Q_{BAT}). The weakest cell, with the lowest capacity, limits the pack performance. The capacity of all the cells is the weakest cell capacity Q_1. All the other cells are not fully charged. The cells are charged until a CV 3,65V balancing strategy is reached for the most charged cell. *Cell1* and *Cell4* are nearly fully charged

C. Balancing strategy

SOC and voltage balancing strategies are compared via simulation. *SOC* balancing is the best strategy but it has the big disadvantage that measuring all the cells *SOC* in a battery pack is a very complex issue. To compare both strategies a comparison between a ΔV_{th}=15mV or ΔSOC_{th}=3% is implemented. If one cell is out of the threshold respect to the weakest cell, the passive balancing resistor is switched on during one second. The deviation between all single cells is measured. The capacity of the switched cell decreases as a function of the cell voltage and the balancing resistor. T_{Bal} is set to 1 second as presented in (4).

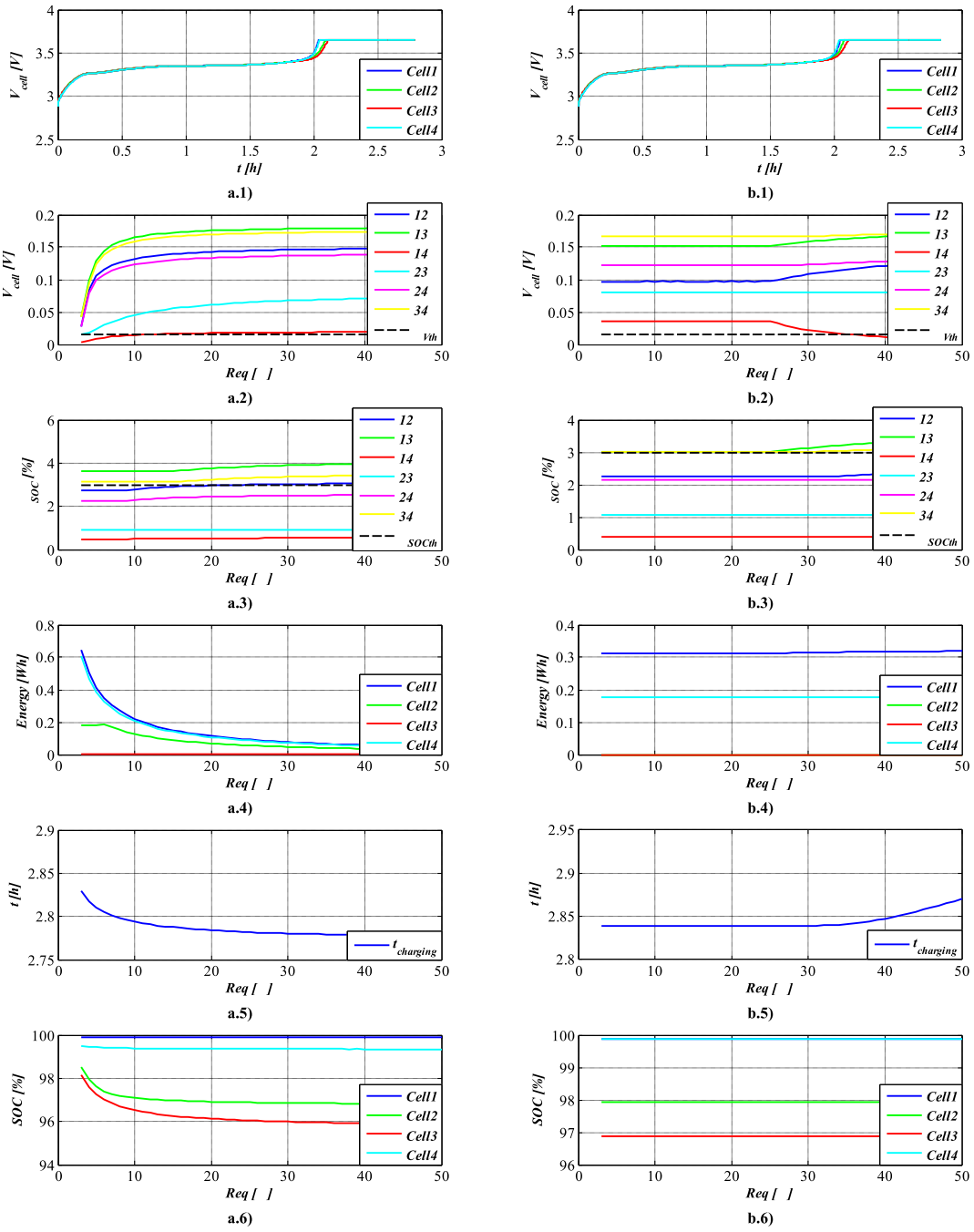

Fig. 4 CCCV test with passive balancing system. a) Voltage strategy ΔV_{th}=15mV b) *SOC* strategy ΔSOC_{th}=3%. 1) Complete CCCV test R_{Bal}=12Ω. 2) ΔV_{max} between cells. 3) ΔSOC_{max} between cells. 4) Energy wasted in balancing circuits. 5) Charging time for the CCCV test. 6) *SOC* of each cell after a CCCV test.

TABLE II
CCCV TESTS RESUME

		ΔV_{max} [V]	ΔSOC_{max} [%]	Max. Energy wasted R_{Bal} [Wh]	t_{charge} [h]
SIMULATION	No balancing	0,181	4,182	_	2,796
	Voltage balancing [a]	0,169	3,609	0,186	2,81
	SOC balancing [a]	0,166	3,001	0,312	2,839
EXPERIMENTAL	No balancing [a]	0,182	4,2	_	2,802
	Voltage balancing [a]	0,075	1,976	0,39	2,825

[a] *Parameters that are compared evaluated with a R_{Bal} of 12Ω.*

D. R_{Bal} boundary limits

R_{Bal} boundary limits for the iteration process are limited between R_{Balmin}=3Ω, and R_{Balmax}=50Ω. The variation of R_{Bal} ,ΔR_{Bal}, is fixed to 1Ω. R_{Bal} is limited to R_{Bal}=(3:1:50). The maximum nominal balancing current is near 1A (3,2V/3Ω), and the minimum balancing current is near 65mA (3,2V/50Ω).

E. CCCV charging process iterations

After choosing all test parameters, the full CCCV test is implemented for each R_{Bal} value and for both *SOC* and voltage strategies. Differences between each cell are measured and compared as presented in Fig. 4.

The CV charging process is implemented to one cell by the communication of the *BMS* and the charger.

F. Data measurement and comparison

Simulation results for a R_{Bal} value of 12Ω are presented in TABLE II and Fig. 4. The most important parameters to design a balancing system are presented in sections (2-5) Fig. 4.

1) ΔV_{cell}

The voltage difference between cells is presented in section 2 of Fig. 4.

Voltage strategy cannot fulfill the requirements of ΔV_{th}=15mV. The balancing current is not enough to fulfill this requirement during the full charging cycle.

SOC strategy keeps the voltage difference equal until the R_{Bal} reaches to 26Ω. With bigger balancing resistors the voltage difference increases.

2) ΔSOC

ΔSOC increases with R_{bal} bigger than 8Ω with the voltage strategy. When R_{bal} reaches 40Ω, the ΔSOC_{max} is near 4%, which is the maximum difference of the no series connection without balancing.

With the *SOC* balancing strategy for smaller values than 25Ω for R_{Bal}, the *SOC* difference is kept constant. With bigger R_{Bal} values the balancing current is not able to maintain the *SOC* difference during the charging process inside the limits.

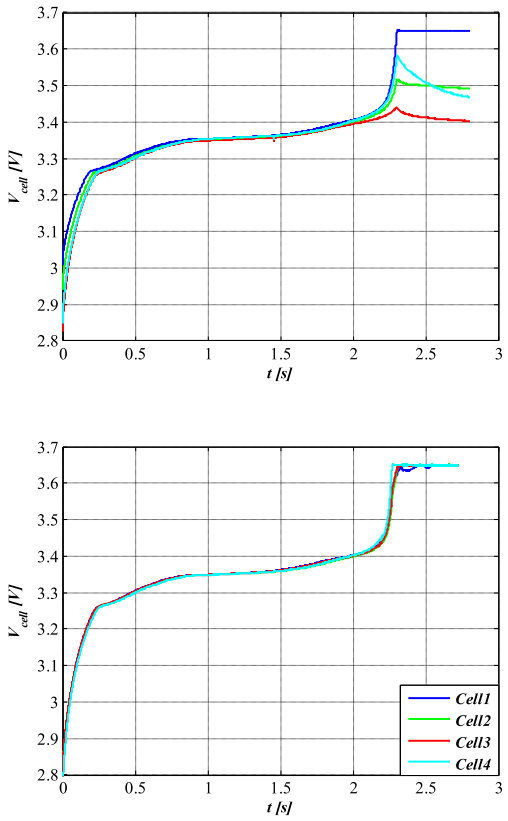

Fig. 5 Experimental tests. (Top) No balancing system. (Bottom) Voltage strategy ΔV_{th}=15mV

3) Max energy wasted R_{Bal}

For the voltage balancing strategy the energy wasted in the balancing circuit increases exponentially with low resistor values.

For the *SOC* balancing strategy, the value is constant because you have to balance the *SOC* difference and this difference is constant for all balancing resistor values.

4) Charging time

The charging time increases if more energy is introduced to the cells for both voltage strategy and *SOC* balancing strategy.

IV. EXPERIMENTAL RESULTS

Experimental test for a 4S1P configuration for the no balancing system connection and voltage balancing connection has been implemented. These experimental results are compared to simulation parameters in TABLE II and presented in Fig. 5.

The balancing resistor R_{Bal} is fixed to 12Ω, to compare simulation results to experimental results.

The no balancing connection obtains the same results in experimental and simulation. The voltage relaxation effect is different in simulation and experimental, because all the cells do not reach 3,65V equally.

The voltage balancing system wastes more energy than the simulation system but decreases the voltage unbalance respect to simulation. This is due to a different behavior between cells during the CV charge process. However the results are good compared to simulation. All the cells are charged to 3,65V thanks to the CV strategy for one single cell. This charging strategy is better than the CV strategies referred to pack voltage.

V. CONCLUSIONS

A passive balancing design methodology has been presented based on single cell tests. The methodology compares main parameters that influence the balancing procedure, giving the designer the option to select the optimum balancing system for the requirements.

Single cell tests permit to take into account cell deviations due to manufacturing processes that are difficult to take into account in battery cell models.

Wasted energy in balancing system is bigger with voltage balancing strategy for low resistor values. When *SOC* balancing strategy is implemented the wasted energy is equal for all the resistor values because the amount of energy to balance is the same.

Experimental results are equivalent to simulation results, with small differences in the CV region, because all cells reach CV at different voltage and this is not taken into account in single cell tests.

VI. FUTURE WORK

Future work is focused on balancing strategy for active balancing systems and bigger difference capacity and *SOC* ranges, for example new cells and cells in “end of life” *EOL* or the 80% of its nominal capacity.

REFERENCES

[1] F. Jin and K. G. Shin, “Pack Sizing and Reconfiguration for Management of Large-Scale Batteries,” *Cyber-Physical Systems (ICCPS), 2012 IEEE/ACM Third International Conference on*. pp. 138–147, 2012.

[2] J. Kim, J. Shin, C. Chun, and B. H. Cho, “Stable Configuration of a Li-Ion Series Battery Pack Based on a Screening Process for Improved Voltage/SOC Balancing,” *Power Electronics, IEEE Transactions on*, vol. 27, no. 1. pp. 411–424, 2012.

[3] Y. Barsukov and T. Instruments, “Battery Cell Balancing : What to Balance and How.”

[4] J. R. Belt, C. D. Ho, T. J. Miller, M. A. Habib, and T. Q. Duong, “The effect of temperature on capacity and power in cycled lithium ion batteries,” *Journal of Power Sources*, vol. 142, no. 1–2, pp. 354–360, Mar. 2005.

[5] S. Santhanagopalan and R. E. White, “Quantifying Cell-to-Cell Variations in Lithium Ion Batteries,” *International Journal of Electrochemistry*, vol. 2012, pp. 1–10, 2012.

[6] M. Uno and K. Tanaka, “Influence of High-Frequency Charge-Discharge Cycling Induced by Cell Voltage Equalizers on the Life Performance of Lithium-Ion Cells,” *Vehicular Technology, IEEE Transactions on*, vol. 60, no. 4. pp. 1505–1515, 2011.

[7] M. Einhorn, W. Roessler, and J. Fleig, “Improved Performance of Serially Connected Li-Ion Batteries With Active Cell Balancing in Electric Vehicles,” *Vehicular Technology, IEEE Transactions on*, vol. 60, no. 6, pp. 2448–2457, 2011.

[8] G. Landrum and T. a. Stuart, “Fast equalization for large Lithium Ion batteries,” *Oceans 2008*, pp. 1–6, Sep. 2008.

[9] B. Lindemark, “Individual cell voltage equalizers (ICE) for reliable battery performance,” *Telecommunications Energy Conference, 1991. INTELEC ’91., 13th International*. pp. 196–201, 1991.

[10] D. Linzen, S. Buller, E. Karden, and R. W. De Doncker, “Analysis and evaluation of charge-balancing circuits on performance, reliability, and lifetime of supercapacitor systems,” *Industry Applications, IEEE Transactions on*, vol. 41, no. 5, pp. 1135–1141, 2005.

[11] W. C. Lee, D. Drury, and P. Mellor, “Comparison of passive cell balancing and active cell balancing for automotive batteries,” *Vehicle Power and Propulsion Conference (VPPC), 2011 IEEE*. pp. 1–7, 2011.

[12] M. Uno, “Interactive charging performance of a series connected battery with shunting equalizers,” *Telecommunications Energy Conference, 2009. INTELEC 2009. 31st International*. pp. 1–4, 2009.

[13] M. Uno, “Interactive charging performance of a series connected battery with shunting equalizers,” *Telecommunications Energy Conference, 2009. INTELEC 2009. 31st International*. pp. 1–4, 2009.

[14] M. Daowd, N. Omar, P. Van Den Bossche, and J. Van Mierlo, “A Review of Passive and Active Battery Balancing based on MATLAB/Simulink,” vol. xx, no. September, 2011.

[15] M. Uno and K. Tanaka, “Single-switch cell voltage equalizer based on multi-stacked SEPICs for series-connected energy storage cells,” *Telecommunications Energy Conference (INTELEC), 2011 IEEE 33rd International*. pp. 1–7, 2011.

[16] H.-S. Park, C.-H. Kim, K.-B. Park, G.-W. Moon, and J.-H. Lee, “Design of a Charge Equalizer Based on Battery Modularization,” *Vehicular Technology, IEEE Transactions on*, vol. 58, no. 7. pp. 3216–3223, 2009.

[17] M. Chen and G. A. Rincon-Mora, “Accurate electrical battery model capable of predicting runtime and I-V performance,” *Energy Conversion, IEEE Transactions on*, vol. 21, no. 2. pp. 504–511, 2006.

Industrial Electronics Society, IECON 2013 - 39th Annual Conference of the IEEE , vol., no., pp.6752,6757, 10-13 Nov. 2013.

Methodology for thermal modelling of lithium-ion batteries

U.Iraola
I.Aizpuru
J.M.Canales
A. Etxeberria
I.Gil

DOI: 10.1109/IECON.2013.6700250

Methodology for thermal modelling of lithium-ion batteries

U.Iraola, I.Aizpuru, J.M.Canales, A.Etxeberria
Computing and Electronics department
Faculty of Engineering, University of Mondragon
Mondragon-Arrasate, Spain

I.Gil
Electronics department
Orona eic s.coop
Hernani, Spain

***Abstract*— Temperature is a determinant parameter in terms of performance, lifespan and safety working with li-ion batteries. Working above 45ºC, in hot climates, has direct influence in the cycle life of the battery and can cause a dangerous failure if higher temperatures are reached; besides, performance of li-ion batteries in cold climates is very poor due to the high internal resistance they present under these ambient conditions. Being able to predict the temperature of a li-ion cell or the temperature distribution in a module for any working condition without testing the device is considered important when designing energy storage systems based on li-ion batteries. Thus, this paper presents a methodology to achieve the equivalent thermal parameters governing the behavior of a single li-ion cell and the power losses within it; different experimental tests are combined with an analytical expression of the power losses inside a cell to reach this target. The parameters obtained are used to develop a model in *matlab/simulink* and another model solved with *CFD* software. Simulation results show good agreement with experimental results with a maximum error of 2ºC committed during the validation of the methodology.**

***Keywords*— Thermal equivalent model; Li-ion cell; behavioural model.**

I. INTRODUCTION

Advances in the field of energy have contributed significantly to the development of society up to the present situation, and its consumption is increasing day by day. The lack of natural resources joined to the high consumption requires looking for the highest possible efficiency and adding alternatives to support the energy demand; renewable energies are a real alternative to support energy production, but there are other alternatives to improve the present situation. Energy storage is presented as an important option because it presents important advantages: the ability to work without a grid connection and make autonomous systems; and the capacity to accumulate energy from different energy sources and use it to support the grid when the energy demand is higher. There are different ways to accumulate energy; mechanically with flywheels, electrically with supercapacitors or thermally with steam accumulators... However, nowadays, energy storage systems based on electrochemical devices, also called batteries, are commonly used in several applications.

Different battery technologies have been grown up since the first battery appeared; lead-acid, nickel metal hydride, nickel cadmium and lithium-ion (li-ion) batteries are the most representative ones. However, li-ion technology is mostly used today in portable applications, and there is increasing interest in using this technology for power applications. High power applications require high voltage and current levels and thus, large battery packs. The high energy and power density of li-ion batteries is then an important advantage against other technologies when large battery packs are needed.

High power demands increase Joule effect power losses and temperature can reach undesirable values. This hot ambient directly affects the cycle life of the battery [1] and can be dangerous if temperature is not under control above 60 ºC because *thermal runaway* phenomenon can be triggered [2]. Conversely, cold climates (0-10ºC) also worsen the performance of the li-ion battery because of the increase in their internal resistance under cold environments; besides, cycling the battery in very cold climates (<10ºC) can damage the battery irreversibly and reduce its capacity under 80% in a few cycles [1]. Thus, it is important to keep the battery temperature within a safe range (commonly 20-40 ºC) for any working condition [3].

In this context, it is considered essential to study the thermal modeling and simulation as a tool to predict the behavior of the temperature within the battery under different working and ambient conditions without the necessity of doing the experimental test.

Internal heat generation (*q)* is the first parameter to calculate for any thermal model. In bibliography different equations are found depending on the assumptions made by the author. In *electrochemical models* chemical and electrical aspects are taken into account when calculating *q* [4–7]. However, *models based on experimental tests* commonly use the equation proposed by *Bernardi et al*. in [8]; experimental data and electrical variables are needed to calculate the internal heat generation parameter with this equation [9–12].

Temperature distribution is the other parameter achieved in a thermal model; two different modeling techniques have been identified in this field, *behavioral models* and *analytical models*. The *analytical models* solve the differential equation governing the energy balance in the battery [12], as in *finite element models*, since *behavioral models* use electrical equivalent circuits to predict the evolution of the cell

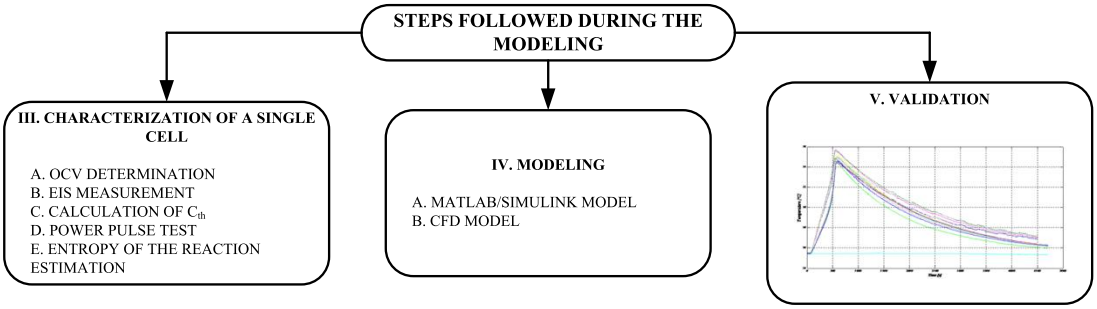

Fig. 1. Steps followed during the modeling of a single cell.

Figure 1 Steps followed during the methodology

temperature [13]. *Finite element models* are commonly time consuming but also more accurate since a temperature distribution is calculated throughout the battery. *Behavioral models* instead, are faster and easier to develop but usually calculate an average temperature for the whole battery and thus, are less accurate.

The lack of information concerning the different materials within the cell in terms of thermal properties and dimensions makes the option of the *behavioral model* very attractive to reach the desired thermal model. Thus, this paper presents a methodology to obtain the parameters of a *behavioral model* for a concrete li-ion battery, the parameters of the equivalent electrical circuit that predicts the behavior of the cell under different working conditions.

Besides, the average thermal properties of the cell obtained from the *behavioral model* are used to define a simple 3D model solved with *CFD*; the target is to conduct module level simulations with different ambient conditions.

The cell used in this work to obtain the results presented is a prismatic 6.5 Ah $LiFePO_4$ power cell.

II. CHARACTERIZATION OF A SINGLE CELL

The following chapter presents the experimental tests done to do the thermal characterization of a single lithium-ion cell.

A. OCV determination

In this work a *linear interpolation method* [14] has been developed to determine the *OCV*. The *linear interpolation method* consists of doing a complete charge and discharge to the battery with a very low current rate *(C/20)*; the overpotential effect is neglected and the *OCV* is considered equal to the terminal voltage. Resulting *OCV* curves for the cell under test are shown in Fig. 2.

B. EIS measurement

An *electrochemical impedance spectroscopy* analysis has been done to measure the impedance of the cell in different points of the *SOC* at different frequencies. The frequency range used for this analysis has been 6.5 kHz to 1Hz. The goal is to find the value of the frequency at which the impedance of the cell is purely resistive for a concrete *SOC*, and the value of this impedance. Fig. 3 shows the resulting curve for a *SOC* value of 50% and at room temperature.

C. Power pulse generation test

After determining the values of the impedance R_0 and the frequency f_0 for a concrete *SOC*, in this case *50%*, the *power pulse generation test* has been conducted. This experimental test consists of applying a sinusoidal current of frequency f_0 and big amplitude (30 A rms in this work) to the cell to generate a constant power losses profile within it (1). In this case the amplitude of the constant pulse has been 0.879 W.

$$q_0 \quad R_0 (I_{rms})^2 \qquad (1)$$

This procedure has been obtained from Schmidt et al. work [15]. Fig. 4 shows the results obtained from this test; the evolution of the measured temperature is similar to a 1st order model response.

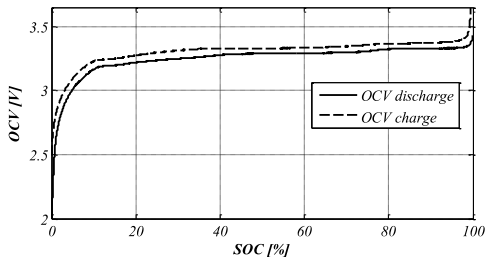

Fig. 2. *OCV* results for the cell under test.

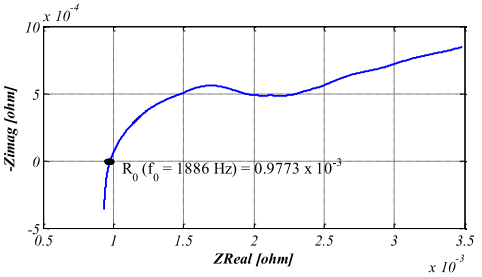

Fig. 3. EIS measurement at 50% of the *SOC*.

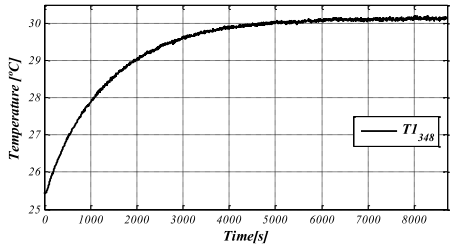

Fig. 4. Experimental results of the temperature on the surface of the cell during the power pulse generation test.

D. Calculation of the heat capacity of the cell (C_{th})

An important parameter to be able to predict the thermal behavior of the li-ion cell is the heat capacity C_{th}. In this work an average value of the heat capacity for the overall cell has been calculated conducting an experimental test. Other authors estimate it from the heat capacities of each material within the li-ion cell; however, this data about the materials and their thermal properties is not usually accessible and experimental estimations are conducted with calorimeters in some studies.

Due to the absence of such equipment, another experimental test has been conducted to estimate C_{th}. Four thermocouples are placed on the surface of a single cell under test, and the cell is covered by a protection layer; then the cell and the protection layer are inserted in a tube and this tube is filled with a thermal insulation material. This material solidifies and the cell is trapped in it with the connection and measurement wires out from the structure; Fig. 5 shows the final assembly of the experimental test. With this assembly heat cannot be evacuated to the environment and all the heat generated inside the cell is accumulated within it.

In order to generate heat inside the cell the same procedure as in *power pulse generation test* is followed. In this case a constant heat pulse of $q_0 = 0.543$ watts has been generated.

Fig. 6 shows one of the surface temperatures resulting from the experimental test. From these results the value of $\Delta t/\Delta T$ is obtained, and the average heat capacity C_{th} of the cell is calculated with (2). In this case, the value achieved for C_{th}

Fig. 5. Final assembly of the experimental test.

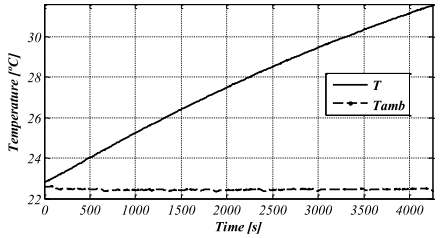

Fig. 6. Resulting evolution of the surface temperature of the cell.

is 272 [J/ºC].

$$C_{th} \quad \frac{q_0 dt}{dT} \qquad (2)$$

E. Experimental determination of the entropic heat coefficient ($\partial OCV_{avg}/\partial T$)

The last step is to conduct another experimental test to evaluate the *entropic heat coefficient* of the li-ion cell. This experimental test consists of evaluating the variation of the *OCV* for different *SOC* values when the temperature of the cell changes. In order to do that, the cell is placed inside a climate chamber and the temperature is varied; meanwhile, the *OCV* of the cell and the surface temperature are measured and their variation is quantified. The same process is applied for 8 different *SOC* values.

Fig. 7 shows the resulting variation of *OCV* and surface

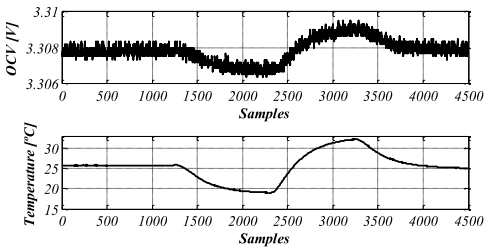

Fig. 7. Variation of the *OCV* when the room temperature changes.

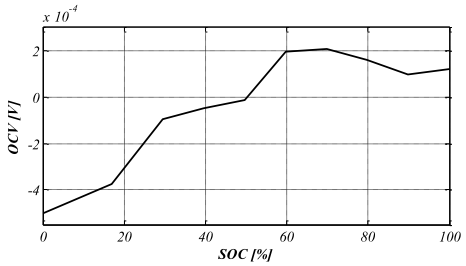

Fig. 8. *Entopic heat coefficient* depending on the value of *SOC*.

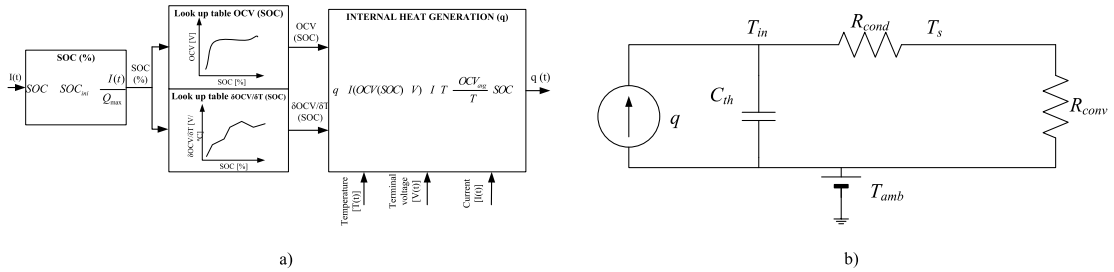

Fig. 9. a) Internal heat generation model in matlab/simulink; b) Thermal equivalent model of the cell utilized in matlab/simulink.

temperature for a *SOC* of 58%. The quantification of the *entropic heat coefficient* has been done when temperature rises from 18º C to 32º C following (3).

$$\frac{OCV_{avg}}{T} \quad \frac{OCV_{avg}(T_{\max})}{T_{\max}} \quad \frac{OCV_{avg}(T_{\min})}{T_{\min}} \qquad (3)$$

After doing the same process for 8 different *SOC* values, Fig. 8 shows the resulting *entropic heat coefficient.* The values obtained show good agreement with other authors values; in power applications, the demanded current levels are quite high, and thus, power losses due to *Joule effect* will be high comparing them with the *entropic losses.* When a power application current profile is studied, the *entropic power losses* in li-ion cells could be neglected.

III. MODELING

During next chapter the simulation models used in this work are going to be explained. Firstly, a model developed with *matlab/simulink*, and after that, a simulation model solved with a *Computational fluid dynamics* (*CFD)* simulation tool. The parameters achieved during the *characterization chapter* are used to develop both simulation models.

A. Matlab/Simulink model

This model is divided into two main parts, the internal heat generation of the li-ion cell, and the estimation of the surface temperature. It is an iterative process, each time step the surface temperature of the cell is calculated and feed backed to the internal heat generation calculator because this variable is temperature dependent. Then, the internal heat generation is applied into the thermal equivalent model shown in Fig. 9 b) to calculate the surface temperature again.

1) Internal heat generation

The internal heat generation calculation in this work is based on the equation of Bernardi et al.[8], equation (4) in this document. The *q* value calculated is an average value of the whole cell, it is not spatially dependent.

$$q \quad I(OCV_{avg}(SOC) \quad V) \quad I(T(\frac{OCV_{avg}}{T}(SOC))) \qquad (4)$$

Fig. 9 a) shows the *internal heat generation* model used in this work. The *OCV* and the $\partial OCV_{avg}/\partial T$ are *SOC* dependent; the instantaneous values of these parameters are calculated using look up tables. Equation (4) also requires the instantaneous value of the terminal voltage *(V)* , the charge or discharge current *(I)*, and cell temperature *(T)*. The terminal voltage and the current are measured during the experimental test and are inputs of the equivalent model. Temperature instead is calculated by the equivalent model and fed back to calculate the *internal heat generation* of the cell.

2) Calculation of the parameters of the equivalent model

Once the *internal heat generation* is calculated, the estimation of the surface temperature is done. Fig. 9 b) shows the thermal equivalent model of the cell used in this work [13]; this model is composed by an internal heat generation inside the cell *q (W)*, a thermal capacity C_{th} *(J/ºC)*, a resistor modelling the conduction R_{cond} *(ºC/W)*, and a resistor modelling the convection R_{conv}*(ºC/W)*. T_s*(ºC)* is the temperature on the surface of the cell, T_{amb}*(ºC)* is the ambient temperature and T_{in}*(ºC)* is the temperature inside the cell. The value of the conduction resistor determines the temperature difference between inside and the surface of the cell. The convective resistor instead, the temperature difference between the surface and the ambient. Heat capacity determines the dynamics of the temperature inside and on the surface of the cell.

The equation governing the evolution of the surface temperature (T_s) of the cell for a constant ambient temperature T_{amb} has been calculated (5).

C_{th} has been previously calculated in II.D; convection resistor R_{conv} and conduction resistor R_{cond} have been obtained from Fig. 4 results.

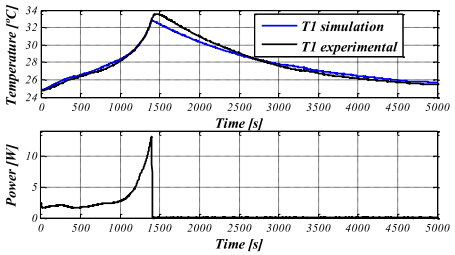

Fig. 10. Comparison between simulation and experimental results for a 3C complete discharge.

TABLE I

THERMAL EQUIVALENT CIRCUIT PAREMETERS

Parameter	*Value*
C_{th}	*272 [J/ºC]*
R_{cond}	*1.8 [ºC/W]*
R_{conv}	*3.371 [ºC/W]*

$$T_s(t) \quad T_{amb} \quad R_{conv} q \quad 1 \quad e^{\frac{t}{C_{th} \; R_{cond} \quad R_{conv}}} \qquad (5)$$

When the surface temperature reaches the steady state, the convection resistor can be calculated with equation (6). Then, the conduction resistor R_{cond} is calculated from (5) because it is the last unknown term.

$$R_{conv} \quad \frac{T_s \quad T_{amb}}{q_0} \qquad (6)$$

The values of the parameters of the equivalent thermal circuit obtained for the cell under test are presented in TABLE I.

3) Model validation

Fig. 10 shows the results obtained by the model for a 3C complete discharge process. In the upper figure the predicted surface temperature and the experimental measurement; in the down figure the *internal heat generation* estimated by the model. This estimation has not been validated due to the absence of a calorimeter to compare the results. However, the results obtained predicting the surface temperatures of the cell under test are accurate enough to think that the error committed is not excessive. The error committed in the temperature approximation during the simulation is acceptable since a *behavioral model* with average parameter estimation has been used.

B. CFD model

The absence of information regarding to the materials within cells and their dimensions make difficult to build up a layered 3D model of a single li-ion cell like in [16]. Although the accuracy obtained with a layered model is high for a single cell model, the time consumed by the simulation in a layered 3D model for a battery module or pack could be excessive.

Thus, a simple 3D model has been developed in this work to evaluate the surface temperature of li-ion cells for single

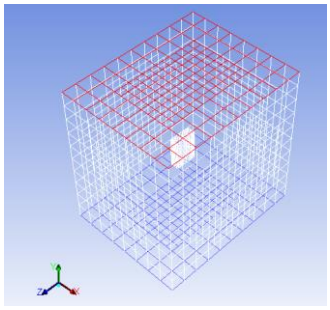

Fig. 11. Single cell simulation model.

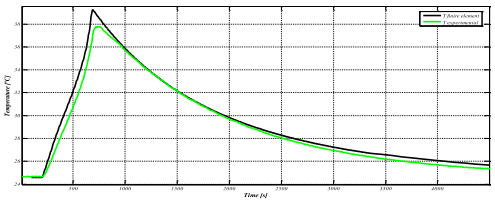

Fig. 12. 7.69C complete discharge results for the *CFD* model.

cells and modules. The assumptions made for a single cell level simulation are the following ones:

> Cell is considered a single body with user defined thermal properties; *specific heat (J/kgºC)*, *isotropic thermal conductivity (W/ºC m)* and *constant density (kg/m^3)*.
> The *internal heat generation rate (W/m^3)* of the cell is considered uniform for the whole body.

The *specific heat* and the *isotropic thermal conductivity* are the same values as the ones obtained for the *matlab/simulink* thermal equivalent model III.A; the value of *density* is obtained from the specifications of the cell; the *internal heat generation rate* is also obtained from this model and applied as an input to the *CFD* model.

Fig. 11 shows the setup of the single cell level 3D simulation. In all the simulations, heat is transferred from the surface of the cell to the ambient by *natural convection*.

Fig. 12 shows the result obtained from the simulation for a 7.69C complete discharge of the cell under test. As mentioned before, the *internal heat generation* applied in this model is first obtained with *matlab/simulink*. The result shown is the average value of the surface temperature of the cell and it is compared with the measurement acquired on the surface of the cell experimentally. An error is committed in the prediction but it is considered a good result due to the simplicity of the model.

IV. CONCLUSIONS

This paper presents a methodology based on experimental tests to calculate the parameters of an equivalent thermal model for lithium ion cells. These parameters are used to build up a model in *matlab/simulink* and a 3D model solved with *CFD* software. According to the modeling of the internal heat generation of a li-ion cell, it is concluded that *Bernardi´s* equation and the assumptions made are adequate to achieve a good approximation of this parameter. The validation of the equation has been done in an indirect way, measuring temperatures on the surface of the cell and comparing them

TABLE II

THERMAL PROPERTIES OF THE CELL FOR THE 3D MODEL

Parameter	*Value*
Specific heat [c_{th}]	*700 [J/kgºC]*
Density [ ]	*2089 [kg/m^3]*
Thermal conductivity [k]	*1.08 [W/mºC]*

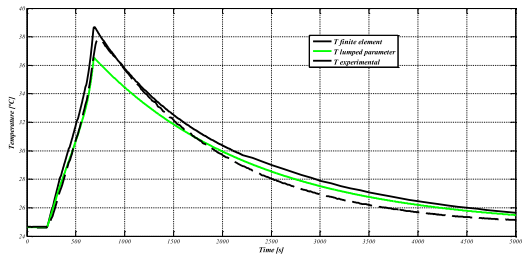

Fig. 13. Comparison between the experimental results and both models under a 7.69C discharge rate.

with the ones achieved from the *matlab/simulink* model, in which the heat generation is calculated. However, it is considered important to have special equipment to measure the amount of heat generated by the cell permitting a direct validation of the equation of *Bernardi*.

Talking about the *matlab/simulink*, it is concluded that a 1st order *RC* thermal equivalent circuit is able to predict the behavior of the surface average temperature in the cell under test. However, an error is committed during the simulations and improvements in terms of accuracy during experimental tests and increasing the order of the equivalent thermal circuit could benefit the overall results. On the other hand, the methodology described to estimate the parameters of the equivalent *RC* circuit is considered to be adequate according to the results obtained during the fitting of the parameters.

The main advantage of a 3D model is that temperature distributions can be calculated and in the model presented in this paper average surface temperatures are presented. The reason for this is because this model is going to be used in the future to calculate temperature distributions within li-ion battery modules, not in a single cell level. However, the validation of the model has been done with a single cell before including battery modules. Furthermore, in commercial battery packs it is typical to have at most a single measurement per cell; thus, it is considered useful to have a 3D battery model to get an average temperature per cell when battery modules or packs are under simulation.

REFERENCES

[1] J. Wang, P. Liu, J. Hicks-Garner, E. Sherman, S. Soukiazian, M. Verbrugge, H. Tataria, J. Musser, and P. Finamore, "Cycle-life model for graphite-LiFePO4 cells," *Journal of Power Sources*, vol. 196, no. 8, pp. 3942–3948, Apr. 2011.

[2] T. M. Bandhauer, S. Garimella, and T. F. Fuller, "A Critical Review of Thermal Issues in Lithium-Ion Batteries," *Journal of The Electrochemical Society*, vol. 158, no. 3, p. R1, 2011.

[3] A. Pesaran, S. Burch, and M. Keyser, "An approach for designing thermal management systems for electric and hybrid vehicle battery packs," *Fourth Vehicle Thermal Management Systems Conference and Exhibition*, no. January, 1999.

[4] G. G. Botte, V. R. Subramanian, and R. E. White, "Mathematical modeling of secondary lithium batteries," *Electrochimica Acta*, vol. 45, no. 15–16, pp. 2595–2609, May 2000.

[5] P. M. Gomadam, R. E. White, and J. W. Weidner, "Modeling Heat Conduction in Spiral Geometries," *Journal of The Electrochemical Society*, vol. 150, no. 10, p. A1339, 2003.

[6] K. Kumaresan, G. Sikha, and R. E. White, "Thermal Model for a Li-Ion Cell," *Journal of The Electrochemical Society*, vol. 155, no. 2, p. A164, 2008.

[7] M. W. Verbrugge, "Three-dimensional temperature and current distribution in a battery module," *AIChE Journal*, vol. 41, no. 6, pp. 1550–1562, 1995.

[8] D. Bernardi, E. Pawlikowski, and J. Newman, "A general energy balance for battery systems," *Journal of The Electrochemical Society*, vol. 132, no. 1, 1985.

[9] S. Al Hallaj, H. Maleki, J. S. Hong, and J. R. Selman, "Thermal modeling and design considerations of lithium-ion batteries," *Journal of Power Sources*, vol. 83, no. 1–2, pp. 1–8, Oct. 1999.

[10] S. Chen, Y. Wang, and C. Wan, "Thermal analysis of spirally wound lithium batteries," *Journal of the Electrochemical Society*, vol. 153, no. 4, 2006.

[11] K. Onda, T. Ohshima, M. Nakayama, K. Fukuda, and T. Araki, "Thermal behavior of small lithium-ion battery during rapid charge and discharge cycles," *Journal of Power Sources*, vol. 158, no. 1, pp. 535–542, Jul. 2006.

[12] S. Chen, C. Wan, and Y. Wang, "Thermal analysis of lithium-ion batteries," *Journal of power sources*, vol. 143, no. 9, 2005.

[13] C. Forgez, D. Vinh Do, G. Friedrich, M. Morcrette, and C. Delacourt, "Thermal modeling of a cylindrical LiFePO4/graphite lithium-ion battery," *Journal of Power Sources*, vol. 195, no. 9, pp. 2961–2968, May 2010.

[14] V. Pop, H. J. Bergveld, D. Danilov, P. P. L. Regtien, and P. H. L. Notten, *Battery Management Systems: Accurate State-of-Charge Indication for Battery-Powered Applications (Philips Research Book Series) (Philips Research Book Series)*, 1st ed. Springer Publishing Company, Incorporated, 2008.

[15] J. P. Schmidt, D. Manka, D. Klotz, and E. Ivers-Tiffée, "Investigation of the thermal properties of a Li-ion pouch-cell by electrothermal impedance spectroscopy," *Journal of Power Sources*, vol. 196, no. 19, pp. 8140–8146, Oct. 2011.

[16] S. C. Chen, C. C. Wan, and Y. Y. Wang, "Thermal analysis of lithium-ion batteries," *Journal of Power Sources*, vol. 140, no. 1, pp. 111–124, Jan. 2005.

Power Electronics, Electrical Drives, Automation and Motion (SPEEDAM), 2014 International Symposium on , vol., no., pp.154,160, 18-20 June 2014.

Li-ion battery modeling optimization based on Electrical Impedance Spectroscopy measurements

E.Unamuno
L. Gorrotxategi
I. Aizpuru
U. Iraola
I. Fernadez
I.Gil

DOI: 10.1109/SPEEDAM.2014.6872015

Li-ion Battery Modeling Optimization Based on Electrical Impedance Spectroscopy Measurements

Eneko Unamuno, Lorea Gorrotxategi,
Iosu Aizpuru, Unai Iraola, and Iosu Fernandez
Electronics and Computing Department
University of Mondragon
Mondragon, Spain 20500

Iñigo Gil
Drives – R & D
Orona eic s. coop
Hernani, Spain 20120

***Abstract*—Li-ion batteries are a very attractive energy storage technology due to their high energy density and their capability for high charge and discharge rates. This makes them very suitable for power applications such as Electric Vehicles (EV), Hybrid Electric Vehicles (HEV) or electric grid oriented applications. However, in order to take advantage of Li-ion batteries' good properties, an accurate battery model is needed, as it provides a tool to know how the cell will behave without doing time consuming tests. Although many battery models can already be found in the literature, the need to compare different models' accuracy appears. This paper presents an analysis and testing of second and third order electrical equivalent models for a 6.5Ah, $LiFePO_4$ cell type, whose parameters are obtained from an Electrochemical Impedance Spectroscopy (EIS) and a subsequent model fitting process. In addition, an optimization criterion is presented for the fitting process, which improves the accuracy of the models and reduces the parameter estimation time from 61h to 6h for the presented models.**

***Index Terms*—Batteries, electrochemical impedance spectroscopy, EIS, li-ion, modeling, optimization, randles, V-I performance.**

I. Introduction

Nowadays, due to the high dependency on fossil fuels (e.g., energy generation or vehicles), new renewable energy generation technologies are being developed. In addition, the improvements made in power electronics have contributed to the development of this energy generation and other kind of applications such as electric vehicles, vertical transportation or electrical energy transportation and distribution. For this reason, applications with integrated energy storage systems are becoming more important.

Several systems can be used depending on the application, such as ultra-capacitors, flywheels, electrochemical batteries (Ni-Cd, Ni-MH, Flow batteries, Li-ion etc.) and so on. However, electrochemical batteries offer the best energy density out of the above mentioned storage systems, and as Li-ion ones offer the best performance in this group [1], the following development will be focused on this type of technology.

The use of this kind of technology involves many laboratory tests and simulations in order to know exactly the characteristics of the storage system before bringing it to the real application. This is necessary because the behavior of many variables such as temperature, voltage and current must be known so as to make a correct use of the electric storage system. For safety reasons and system reliability, it is also important to know in which conditions the cell will reach its limit values.

An accurate battery model provides a way to simulate different situations of the system without having to make real tests, what means long waiting time and the use of expensive measuring and controlling systems. In addition, the battery model gives the chance to estimate the State of Charge (SOC) and the State of Health (SOH) of the storage system [2]–[5], comparing the real model with the simulation.

A wide variety of models have already been developed in the literature, which are explained briefly in the following paragraphs.

On the one hand, electrochemical models characterize the batteries' behavior related to the electrical and thermal variables with the chemical processes occurring inside it [6], [7]. However, it is a complex and computationally expensive method, as it involves a system of coupled time-variant spatial partial differential equations.

On the other hand, mathematical and analytic models define the batteries' behavior with mathematical equations [8]–[10]. Different analytic variables such as battery capacity or internal resistance are modeled by mathematical methods, helping to predict the system behavior. Despite that, these methods only work for specific applications, and provide relatively inaccurate results. Moreover, they require a lot of knowledge to be applied to the batteries' model.

On top of that, electrical models represent the dynamic characteristics and behavior of Li-ion batteries with equivalent circuit models that are composed of passive elements (e.g., capacitors, resistors or inductances) and active elements (e.g., voltage sources or current sources) [11]–[13]. Those models are considerably intuitive and simple to develop, although getting the required parameters is not that clear.

This paper covers the development and comparison of different equivalent electrical models due to the simplicity regarding the implementation. This kind of models offer the best relation between accuracy and simplicity, as the dynamics of the cell can be properly approximated in a relatively simple way.

In addition, the importance of choosing properly the frequency range when making the parameter fitting process for

the models is shown.

Regarding the structure of the paper, the following sections are explained.

To begin with, Section II presents the state of art of the most common electrical battery models and their main characteristics.

After that, Section III collects the way to obtain the needed parameters for the proposed models based on experimental tests, and their implementation in Matlab/Simulink environment.

In section Section IV, the validation test is described and the validation of the models is explained, comparing the real test results with the ones obtained in the equivalent models. It also contains the explanation of the optimization process made to improve the models' accuracy and shows the result comparison.

Finally, the last two sections contain the main conclusions obtained during the development and the future work that is going to be done based on the results obtained in this paper.

II. State of Art of Electrical Battery Models

Different types of electrical models exist depending on the components used and how they are connected [14]. Generally, a voltage source is used to represent the Open Circuit Voltage (OCV or V_{OC}) of the cell, resistors to portray battery internal resistance, and capacitors to depict the dynamic behavior of the batteries. It has to be mentioned that all these parameters are function of temperature, current rate, SOC and SOH [15], [16]. However, during the following analyses, only the dependence with the SOC will be taken into account.

A. Internal resistance electrical model

This model is the simplest electrical model, which can be seen in Fig. 1. It is composed by a DC source and a resistor, that represent the V_{OC} and the internal resistance of the battery, respectively.

Equation (1) is the electrical equivalent circuit formula, which tries to approximate the real V-I behavior of the cell, giving an output voltage response, V_{Batt}, for a given battery current, I_{Batt}.

$$V_{Batt} = V_{OC} + R_{Int} \cdot I_{Batt} \tag{1}$$

As it can be appreciated, this model is not able to simulate the transient behavior of the battery, as it does not contain any capacitors. For this reason, it can be concluded that this model is not accurate enough for the purpose of this paper, because the transient dynamics of the cell must be modeled.

B. n order Randles models

This model is composed by an internal resistance model with *n* RC parallel circuits connected in series. This way, the transient behavior of the cell for different input current pulses can be modeled by the RC branches.

Depending on the battery type, in many occasions the battery does not behave in the same way for all the range of input current frequencies. For this reason, each technology

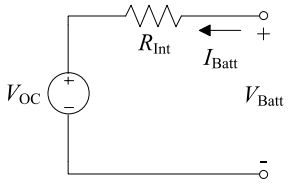

Fig. 1. Internal resistance electrical model circuit.

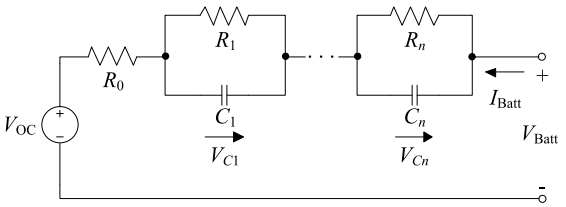

Fig. 2. *n* order Randles model circuit.

model must be composed of a specific number of RC parallel circuits, so as to model the V-I response of the cell in a proper way.

In each model there will be *n* time constants, which correspond to the *n* RC branches connected in series.

The advantage of this kind of equivalent electrical circuits is that they can model different behaviors for a wide range of frequencies. For example, if a second order model is used, one of the RC branches will model the high frequency response, while the second one will model the low frequency one.

It can be said that as the equivalent circuit model is more complex, the V-I response of the cell is modeled in a better way. However, most of the times (e.g., [12], [13], [17], [18]), second or third order models are used because of their good relation between response accuracy and complexity.

Fig. 2 shows an *n* order Randles equivalent electrical circuit.

Besides that, the *n* order model state space equations are represented in (2) and (3), which model the dynamics of the cell with the V_{Batt} as the output variable (taking into account that V_{OC} is a known variable).

$$\begin{bmatrix} \dot{V}_{C1} \\ \vdots \\ \dot{V}_{Cn} \end{bmatrix} = \begin{bmatrix} \frac{-1}{R_1 \cdot C_1} & 0 & 0 \\ 0 & \ddots & 0 \\ 0 & 0 & \frac{-1}{R_n \cdot C_n} \end{bmatrix} \begin{bmatrix} V_{C1} \\ \vdots \\ V_{Cn} \end{bmatrix} + \begin{bmatrix} \frac{1}{C_1} \\ \vdots \\ \frac{1}{C_n} \end{bmatrix} I_{Batt} \tag{2}$$

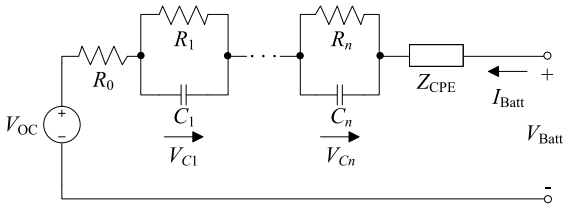

Fig. 3. *n* order Randles model circuit with a CPE in series.

$$V_{Batt} - V_{OC} = \begin{bmatrix} 1 & \cdots & 1 \end{bmatrix} \begin{bmatrix} V_{C1} \\ \vdots \\ V_{Cn} \end{bmatrix} + R_0 I_{Batt} \quad (3)$$

C. n order Randles models with a constant phase element in series

In this kind of equivalent electrical circuits a Constant Phase Element (CPE) is used to improve the frequency response of the battery model.

This impedance is connected in series with the circuits explained in II-B, and (4) shows its frequency domain formula.

$$Z_{CPE} = \frac{K_{CPE}}{(j\omega)^m} \quad (4)$$

The CPE element is used to improve the accuracy of the model, because it models the constant phase behavior of the cell at low frequency input signal ranges [19], [20]. This way, the RC branches are able to model the high frequency behavior in a better manner. Fig. 3 shows the equivalent electrical circuit for the models with the CPE element.

Although the frequency response accuracy of the model is improved considerably with this kind of model, the complexity regarding the implementation makes it a less attractive method than the ones explained in II-B.

III. Parameter Estimation and Cell Modeling Based on Experimental Data

Fig. 4 shows the steps followed to make the different measurements, parameter estimation and model validation (which is explained in Section IV).

Regarding the parameter measurement and estimation, the OCV has been measured for the entire SOC range.

In addition, Electrochemical Impedance Spectroscopy (EIS) measurements have been made at different SOC-s so as to get the frequency response of the cell at different states.

The estimated parameters are used to build the cell model in the Simulink environment, and a validation test is carried out in order to compare the real data with the experimental one.

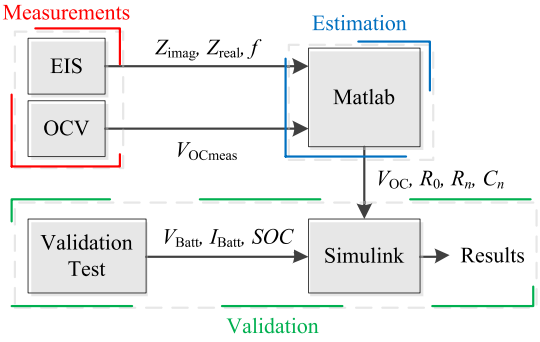

Fig. 4. Parameter measurement, estimation and validation schematic.

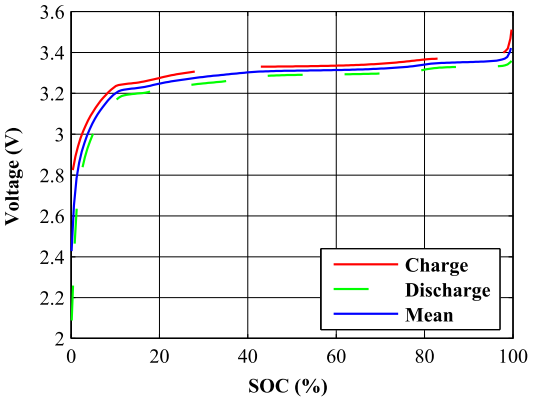

Fig. 5. OCV vs. SOC curves at 25ºC and C/20 current rate.

A. Open circuit voltage determination

By definition, the V_{OC} is equal to the terminal voltage of the cell when no current is flowing through it and the voltage has reached the steady-state point, at a concrete SOC.

According to literature, two different methods have been found in order to model the V_{OC} of the cell [17], [21]; the first one called Linear Interpolation method and the other known as the Voltage Relaxation method.

The Linear Interpolation method consists on consecutive full charge and discharge cycles at a very low current rate (e.g., C/20). In addition, it is assumed that the over potential (difference between the cells' real V_{OC} and the measured charge/discharge voltage), is symmetrical during the charge and discharge of the cell [21].

In Fig. 5, the over potential effect in the hysteresis curve can be clearly seen. Thus, in the developed models, and taking into account the assumption made previously, the mean value of the charge and discharge curves is taken as the V_{OC} in function of SOC.

The Voltage Relaxation method consists on partially charging and discharging the cell by applying current pulses and

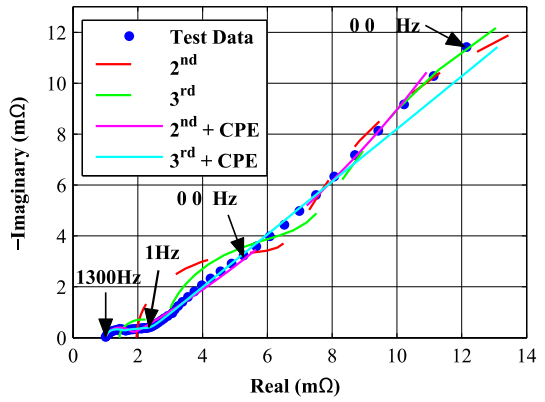

Fig. 6. Nyquist plot for different electrical equivalent models with EIS measurement approximation at 25ºC and 50% of SOC.

permitting the cell to relax after each pulse. After that, the last voltage value of the relaxation period is taken as the V_{OC} voltage value of the cell at this SOC [17].

In this paper, the Linear Interpolation method has been used to model the V_{OC} behavior of the cell. It can be said that the result obtained with this method at very small current rates is really close to the one obtained with the Voltage Relaxation method. Moreover, the implementation of the Linear Interpolation method is simpler than the other one, and the test needs less time to be concluded, as almost all the relaxation periods are avoided.

B. Model passive element estimation based on EIS measurements

The passive components of the equivalent electrical models are obtained from the EIS measurements at [0-100]% SOC range, in steps of 10%. These tests give the impedance response of the cell for different input current frequencies [9].

Once the results are obtained, the equivalent impedance of the model can be approximated to the experimental data, calculating the optimal passive element values to fit properly the frequency response of the cell. In this paper, the Non-Linear Least Squares method has been used in order to make that fitting process in the Matlab environment.

Four models have been used to fit the response of the cell (Second and third order Randles models with/without CPE in series).

Fig. 6 shows the obtained approximations for the EIS results at 50% SOC and a frequency range of 6500-0.001Hz in a Nyquist diagram (the figure shows a range of 1300-0.001Hz because the inductive behavior of the cell has been neglected). In this diagram, the real and imaginary impedance values can be seen for different input current frequencies.

As it can be concluded from the figure, the more complex the circuit used to make the fitting is, the more accurate the response of the model is. However, as it has been mentioned

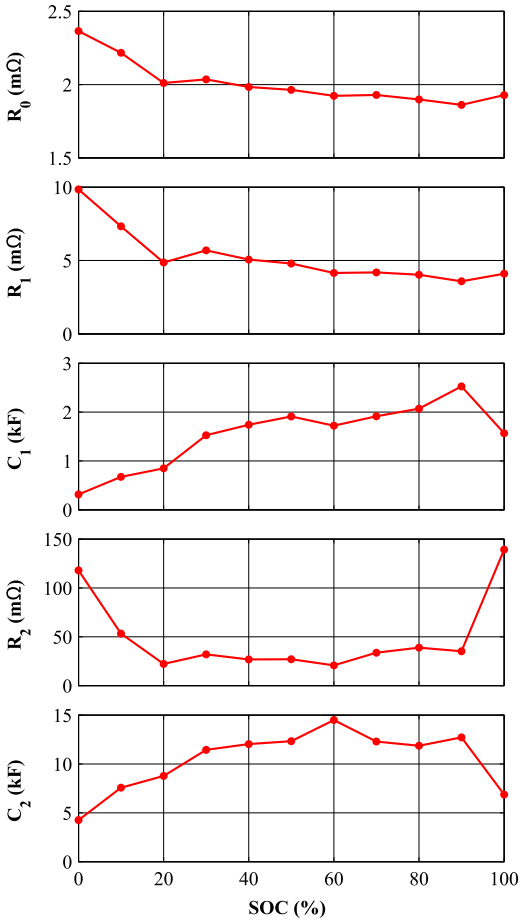

Fig. 7. Parameters for the second order Randles model at 25ºC.

before, second and third order Randles models with a CPE in series have been discarded due to their complexity regarding the implementation.

This same fitting procedure has been repeated at all the range of SOC 0-100% for the chosen equivalent electrical models (second and third order Randles models). The results for the obtained parameters from this process can be seen in Fig. 7 for the second order Randles model.

C. Developed electrical models in Matlab/Simulink environment

In order to implement the above mentioned two models, (2) and (3) have been used. In these equations it can be appreciated that the current has been taken as the input variable, whereas V_{Batt} has been chosen as the output variable.

As it has been mentioned in II, the dependency of the parameters with the SOC has been taken into account. For

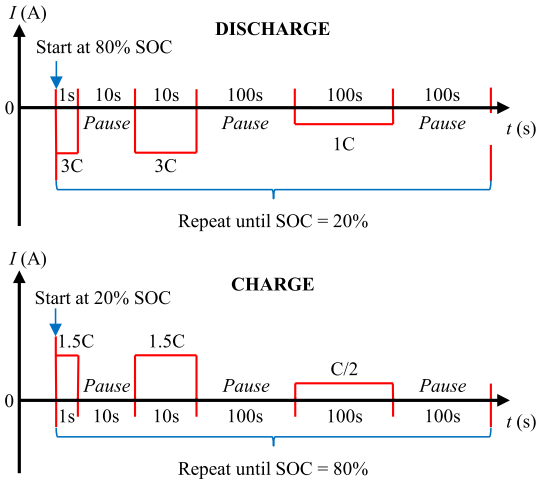

Fig. 8. Model validation testing cycles' current profile.

this reason, the SOC must be a known variable. In case this data is not provided, a Coulomb counter can be implemented to derive the SOC of the cell from the input current. However, this data will not be as accurate as the one provided by the measurement system.

In this paper, as the SOC is a known parameter, it has been taken as an input for the model, together with the cell current. A Linear Interpolation method has been used in order to get the model parameter values for the cases where the EIS measurements have not been done (e.g., 5%, 15%, 25% etc.).

IV. Model Validation

This section collects the proposed validation testing cycle and the results obtained from the different models, without and with parameter optimization process.

A. Validation test

As the behavior of the cell for different input currents has to be modeled, a specific current profile has been proposed in order to observe the evolution of the models' cell voltages against the real data obtained from the test.

On the one hand, different length pulses have been implemented, because the behavior of the cell for varying input frequencies must be observed.

On the other hand, the amplitude of the current pulses changes during the cycle, as the cell will not respond equally for different magnitude currents. Fig. 8 shows the validation cycle for both the discharging and the charging processes.

It can be seen from the figure that the validation test is done in the range of 20-80% of SOC. This is done in order to avoid the most critic zones of the battery V_{OC}.

On top of that, many applications used nowadays do not operate outside these bounds (e.g., hybrid electric vehicles [22] or vertical transportation systems), as this way the cycling life of the cells is improved.

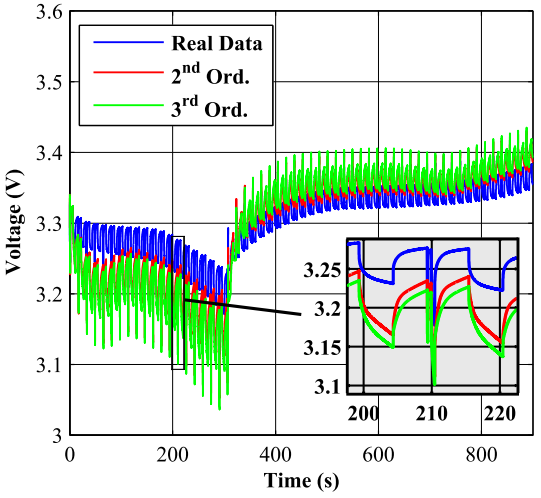

(a)

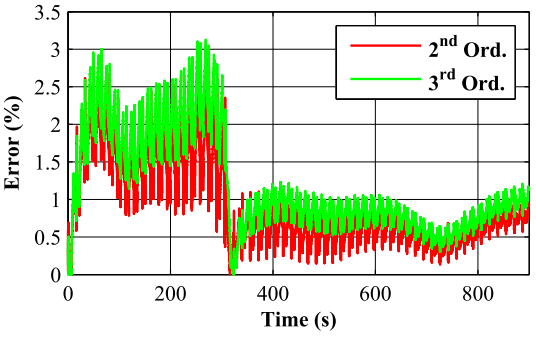

(b)

Fig. 9. Results for the non-optimized Randles models: (a) Voltage comparison and (b) Error comparison.

B. Models' accuracy without parameter optimization

Based on the validation test, the models explained in III-C have been simulated in the Matlab/Simulink environment, and a comparison between the real data and the models' outputs has been done (Fig. 9a).

As it can be observed, the behavior of the models match relatively well the real voltage of the cell, so it can be said that the models are valid to use them in simulation. A zoom has been made in order to see the dynamics of both models more in detail.

Apart from that, Fig. 9b shows the absolute errors obtained in the models, comparing the instantaneous real and simulated voltages. It can be observed that the maximum errors of the second and third order Randles models are near 2.9% and 3.1%, respectively. In addition, the mean errors during the validation cycle have been calculated (0.9% and 1.1%), together with the EIS measurements' total duration (61h).

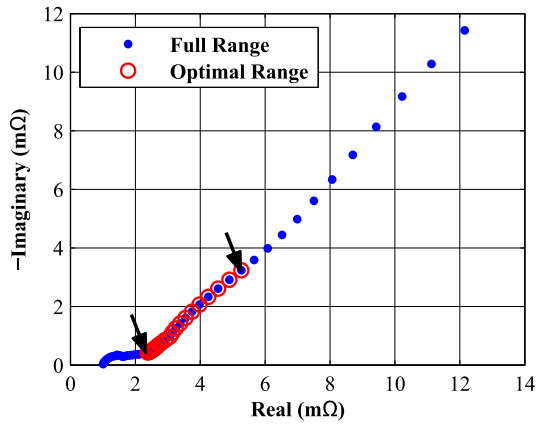

Fig. 10. Reduced frequency range for the models' optimization, [0.01-1]Hz.

C. Models' accuracy with parameter optimization

During the simulation process, the importance of having properly estimated parameters has become crucial in order to have good accuracy in the models. For that reason, different tests have been done to improve the parameter estimation quality and consequently the models' accuracy. This subsection presents the followed procedure.

The optimization process basically consists of reducing the frequency range when making the fitting to the obtained curves in the EIS measurements.

As the models' validation is done for a concrete current pulse profile, the frequency range of the input current signals is known. Hence, depending on the application where the cell is going to work, a bigger or smaller frequency range will be chosen.

This makes the fitting process to be adjusted to the application where the battery is going to be working, what means better accuracy in the model and less time for modeling the cell.

In this case, as the longest pulse in the validation test (explained in IV-A) lasts 100s, a frequency of 0.01Hz has been chosen as the smallest one for the approximation. In addition, having a smallest pulse in the test of 1s, a frequency of 1Hz has been taken as the biggest frequency for the fitting process. This reduced frequency range can be observed on Fig. 10.

Based on all that, the same fitting as in IV-B has been done, and the results in the models have been obtained, which are shown in Fig. 11.

As it can be seen, even if the results are better than the previous ones, there is still some error between the real voltage and the voltages of the models (0.85% and 0.71% maximum error for the second and third order models, respectively). However, it can be said that this phenomenon occurs because of the implemented V_{OC} model, as the models' voltage stays above the real one during the discharge process, and below it during the charge process.

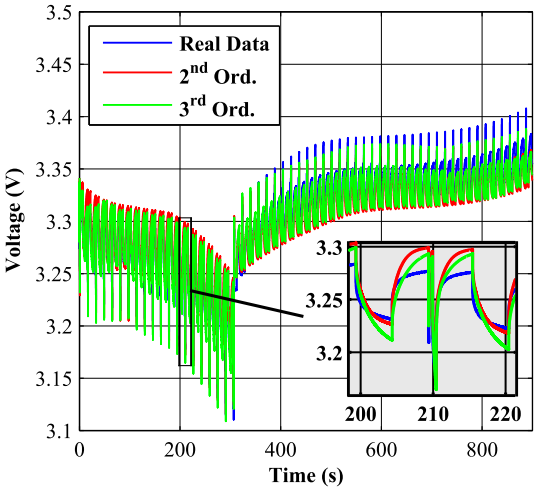

(a)

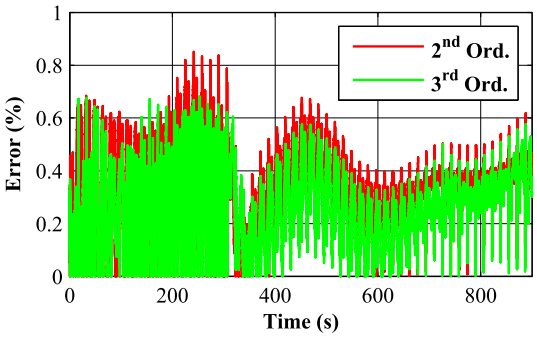

(b)

Fig. 11. Results for the optimized Randles models: (a) Voltage comparison and (b) Error comparison.

TABLE I
MODELS' VOLTAGE AND TIME ERRORS.

Model	*Optimized*	*Mean error (%)*	*Max. error (%)*	*EIS meas. tot. duration (h)*
Second order	No	*0.91*	*2.94*	*61*
Third order		*1.167*	*3.126*	
Second order	Yes	*0.3535*	*0.8504*	*6*
Third order		*0.2612*	*0.7134*	

Once more, the mean errors obtained during the entire validation test (0.35% and 0.26%), and the EIS measurements' total duration have been calculated (6h).

Finally, the results for all the optimized and the non-optimized models have been collected in TABLE I.

V. Conclusions

A comparison between different equivalent electrical models has been done in order to choose the most suitable ones depending on the application. Second and third order Randles models have been chosen as the models with best relation between ease to implement and accuracy.

Regarding the V_{OC} of the cell, the Linear Interpolation method has been used in order to model it. Further research in this field could bring better results, but this method has been chosen because of its good relation between test duration and accuracy.

The model parameter estimation method has been presented and an optimization criterion has been proposed so as to improve the models' accuracy and the EIS measurements' duration.

TABLE I presents the results for the second and third order models without/with the parameter estimation optimization, showing that the models' accuracy is improved and the parameter estimation time is reduced considerably.

References

[1] B. Lawson, "Battery Performance Characteristics." [Online]. Available: http://www.mpoweruk.com/performance.htm

[2] J. Kim and B. H. Cho, "Pattern Recognition for Temperature-Dependent State-of-Charge/Capacity Estimation of a Li-ion Cell," *IEEE Transactions on Energy Conversion*, vol. 28, no. 1, pp. 1–11, Mar. 2013. [Online]. Available: http://ieeexplore.ieee.org/lpdocs/epic03/wrapper.htm?arnumber=6339034

[3] M. A. Roscher, O. S. Bohlen, and D. U. Sauer, "Reliable State Estimation of Multicell Lithium-Ion Battery Systems," *IEEE Transactions on Energy Conversion*, vol. 26, no. 3, pp. 737–743, Sep. 2011. [Online]. Available: http://ieeexplore.ieee.org/lpdocs/epic03/wrapper.htm?arnumber=5893927

[4] L. Liu, L. Y. Wang, Z. Chen, C. Wang, F. Lin, and H. Wang, "Integrated System Identification and State-of-Charge Estimation of Battery Systems," *IEEE Transactions on Energy Conversion*, vol. 28, no. 1, pp. 12–23, Mar. 2013. [Online]. Available: http://ieeexplore.ieee.org/lpdocs/epic03/wrapper.htm?arnumber=6341065

[5] J. Zhang and J. Lee, "A review on prognostics and health monitoring of Li-ion battery," *Journal of Power Sources*, vol. 196, no. 15, pp. 6007–6014, Aug. 2011. [Online]. Available: http://www.sciencedirect.com/science/article/pii/S0378775311007865

[6] K. A. Smith, C. D. Rahn, and C.-Y. Wang, "Model-Based Electrochemical Estimation and Constraint Management for Pulse Operation of Lithium Ion Batteries," *IEEE Transactions on Control Systems Technology*, vol. 18, no. 3, pp. 654–663, May 2010. [Online]. Available: http://ieeexplore.ieee.org/lpdocs/epic03/wrapper.htm?arnumber=5256311

[7] R. Klein, N. A. Chaturvedi, J. Christensen, J. Ahmed, R. Findeisen, and A. Kojic, "Electrochemical Model Based Observer Design for a Lithium-Ion Battery," *IEEE Transactions on Control Systems Technology*, vol. 21, no. 2, pp. 289–301, Mar. 2013. [Online]. Available: http://ieeexplore.ieee.org/lpdocs/epic03/wrapper.htm?arnumber=6121920

[8] Z. Chen, L. Y. Wang, G. Yin, F. Lin, and C. Wang, "Accurate Probabilistic Characterization of Battery Estimates by Using Large Deviation Principles for Real-Time Battery Diagnosis," *IEEE Transactions on Energy Conversion*, vol. PP, no. 99, pp. 1–11, 2013. [Online]. Available: http://ieeexplore.ieee.org/lpdocs/epic03/wrapper.htm?arnumber=6600908

[9] C. Forgez, K. El Kadri Benkara, and G. Friedrich, "Impedance Observer for a Li-Ion Battery Using Kalman Filter," *IEEE Transactions on Vehicular Technology*, vol. 58, no. 8, pp. 3930–3937, Oct. 2009. [Online]. Available: http://ieeexplore.ieee.org/lpdocs/epic03/wrapper.htm?arnumber=5184857

[10] R. Al Nazer, V. Cattin, P. Granjon, M. Montaru, and M. Ranieri, "Broadband Identification of Battery Electrical Impedance for HEVs," *IEEE Transactions on Vehicular Technology*, vol. 62, no. 7, pp. 2896–2905, Sep. 2013. [Online]. Available: http://ieeexplore.ieee.org/lpdocs/epic03/wrapper.htm?arnumber=6516985

[11] M. Greenleaf, H. Li, and J. P. Zheng, "Modeling of Li FePO Cathode Li-Ion Batteries Using Linear Electrical Circuit Model," *IEEE Transactions on Sustainable Energy*, vol. 4, no. 4, pp. 1065–1070, Oct. 2013. [Online]. Available: http://ieeexplore.ieee.org/lpdocs/epic03/wrapper.htm?arnumber=6557099

[12] M. Chen and G. A. Rincon-Mora, "Accurate Electrical Battery Model Capable of Predicting Runtime and I–V Performance," *IEEE Transactions on Energy Conversion*, vol. 21, no. 2, pp. 504–511, 2006. [Online]. Available: http://ieeexplore.ieee.org/lpdocs/epic03/wrapper.htm?arnumber=1634598

[13] S. Abu-Sharkh and D. Doerffel, "Rapid test and non-linear model characterisation of solid-state lithium-ion batteries," *Journal of Power Sources*, vol. 130, no. 1–2, pp. 266–274, May 2004. [Online]. Available: http://www.sciencedirect.com/science/article/pii/S0378775303011455

[14] H. He, R. Xiong, H. Guo, and S. Li, "Comparison study on the battery models used for the energy management of batteries in electric vehicles," *Energy Conversion and Management*, vol. 64, pp. 113–121, Dec. 2012. [Online]. Available: http://linkinghub.elsevier.com/retrieve/pii/S0196890412001987

[15] L. Lam and P. Bauer, "Practical Capacity Fading Model for Li-Ion Battery Cells in Electric Vehicles," *IEEE Transactions on Power Electronics*, vol. 28, no. 12, pp. 5910–5918, Dec. 2013. [Online]. Available: http://ieeexplore.ieee.org/lpdocs/epic03/wrapper.htm?arnumber=6387312

[16] L. Lam, "A Practical Circuit-based Model for State of Health Estimation of Li-ion Battery Cells in Electric Vehicles," M.Sc. Thesis, University of Technology Delft, 2011. [Online]. Available: http://repository.tudelft.nl/view/ir/uuid:a7446a0a-4c29-4c68-bbe2-273f68f85ed7/

[17] M. Petzl and M. A. Danzer, "Advancements in OCV Measurement and Analysis for Lithium-Ion Batteries," *IEEE Transactions on Energy Conversion*, vol. 28, no. 3, pp. 675–681, Sep. 2013. [Online]. Available: http://ieeexplore.ieee.org/lpdocs/epic03/wrapper.htm?arnumber=6517504

[18] L. Lam, P. Bauer, and E. Kelder, "A practical circuit-based model for Li-ion battery cells in electric vehicle applications," in *2011 IEEE 33rd International Telecommunications Energy Conference (INTELEC)*. IEEE, Oct. 2011, pp. 1–9. [Online]. Available: http://ieeexplore.ieee.org/lpdocs/epic03/wrapper.htm?arnumber=6099803

[19] A. Cuadras and O. Kanoun, "SoC Li-ion battery monitoring with impedance spectroscopy," in *2009 6th International Multi-Conference on Systems, Signals and Devices*. IEEE, Mar. 2009, pp. 1–5. [Online]. Available: http://ieeexplore.ieee.org/lpdocs/epic03/wrapper.htm?arnumber=4956761

[20] D. Andre, M. Meiler, K. Steiner, H. Walz, T. Soczka-Guth, and D. U. Sauer, "Characterization of high-power lithium-ion batteries by electrochemical impedance spectroscopy. II: Modelling," *Journal of Power Sources*, vol. 196, no. 12, pp. 5349–5356, Jun. 2011. [Online]. Available: http://www.sciencedirect.com/science/article/pii/S0378775310012942

[21] V. Pop, H. J. Bergveld, D. Danilov, P. P.L. Regtien, and P. H.L. Notten, *Battery Management Systems: Accurate State-of-Charge Indication for Battery-Powered Applications*. Springer Science+Business Media B.V., 2008.

[22] B. Lawson, "Traction Batteries for EV and HEV Applications." [Online]. Available: http://www.mpoweruk.com/traction.htm

Energy Conversion, IEEE Transactions on 2014.

Influence of voltage balancing in the temperature distribution of a li-ion battery module

U. Iraola
I. Aizpuru
L. Gorrotxategi
J.M. Canales
A. Etxeberria
I.Gil

DOI: 10.1109/TEC.2014.2366375

Influence of voltage balancing in the temperature distribution of a li-ion battery module

U.Iraola, *Student Member, IEEE*, I.Aizpuru, *Student Member, IEEE*, L.Gorrotxategi, J.M.Canales, A.Etxeberria, I.Gil

***Abstract*-- Temperature is one of the key factors when working with lithium ion battery modules due to its influence in safety, performance and lifespan concerns in these devices. High working temperatures reduce the available capacity of each cell within the module after several cycles due to aging; non uniform temperature distributions in the module lead to different aging processes in each cell and thus it will be impossible to take advantage of all the energy available in the li-ion storage system because the most aged cell will limit the available energy. This paper is focused on the minimization of the maximum temperature gradient of a battery module for high depth of discharge applications to avoid different aging processes of the cells within the module. Voltage balancing is proposed as a solution for this purpose and different strategies and their results are presented in this work.**

***Index Terms*—Aging, battery modules, lithium-ion, temperature distribution, voltage balancing.**

I. Introduction

ENERGY storage systems are presented nowadays as an alternative to support the main grid during high energy demand periods because they can store energy during the low consumption ones. Besides, their possibility to work without a grid connection makes them an attractive possibility for electro-mobility applications. Lithium ion batteries are one of the most promising technologies for different purposes since they cover a wide range of applications due to their high energy and power density. Modeling the electrical and thermal behavior of these devices has been one of the challenges of researchers until now. According to the electrical behavior, it is compulsory to be able to predict the state of charge (SOC) of the cells to know the available capacity in the energy storage systems; there are several works researching this field [1]–[4]. According to the thermal modeling it is important to predict the thermal behavior of the battery under the power requirements of the application [5]. Besides, temperature has a big influence in the performance and lifespan of li-ion batteries; low temperatures (below 10ºC) reduce the performance of these batteries [6] while high temperatures (over 40ºC) have direct influence into the acceleration of their ageing processes. In fact, predicting the state of health (*SOH*) of li-ion batteries is another big challenge nowadays due to the importance of knowing this parameter for power applications; there are several works in bibliography analyzing the *SOH* estimation [7]–[10]. Moreover, if higher temperatures are reached (over 70ºC), the security of the whole system could be in distress.

In this context, it is important to control the working temperature of the cells within the battery to guarantee their best performance for the longest time. According to thermal management of batteries, two main variables are taken into account, maximum temperature of the module, and temperature distribution within the module. Pesaran et al. in [11] mention the maximum differences in temperature distributions of single battery modules to be 2-6ºC. However it is important to minimize this value because different average working temperatures between cells of the same module will lead to different aging processes; after certain cycles, this effects will have significant influence in the maximum capacity of the module since the most aged cell will determine the maximum energy delivered, and cells with less aging will not deliver all their accumulated energy. Several authors studied temperature related ageing mechanisms in li-ion batteries; some of them talk about 1 month earlier ageing if one cell is cycling 1ºC over its optimum working temperature. Other ones talk about cycles, 1000 less cycles done with a cell working 8ºC over its optimum temperature, from 3500 cycles to 2500 cycles [12]–[17]. Maximum temperature of the module can be kept below certain temperature value by the battery thermal management system or *BTMS* (commonly liquid or air forced cooling); however, these systems hardly compensate the temperature distribution within the module, thus, it is important to minimize this effect by electrical or mechanical improvements in the design of the module.

Each cell in a battery module has its own characteristics (for instance internal impedance and maximum capacity), thus, their thermal behavior is not the same despite the same current is flowing through them in a module. These small differences in capacity and impedance for different state of charges (*SOC*) lead to different heat generation rates in each cell; this effect is

U.Iraola, I.Aizpuru, L.Gorrotxategi, J.M.Canales and A.Etxeberria are with Mondragon University, Mondragon 20500, Spain (e-mail: uiraola@mondragon.edu; iaizpuru@mondragon.edu; lorea.gorrotxategi@alumni.mondragon.edu; jmcanales@mondragon.edu; aetxeberria@mondragon.edu).

I.Gil is with Orona eic s.coop, Hernani 20120, Spain (e-mail: igil@orona-group.com).

a) b)

Figure 1. Layout of the modules used during the experimental testing: a) prismatic Lishen 6.5 Ah cell module; b) cylindrical Lifebat 8 Ah cell module.

better seen when deep discharges are reached because of the faster increase of the internal impedance when these SOC ranges are reached. Depending on the layout of the module, this effect has less influence on the temperature distribution; in modules with cells in touch, heat is usually accumulated in the middle of the module, so the distribution is mainly affected by the layout, (Figure 1a). However, in modules with air gaps between cells, power losses determine the temperature distribution of the module, (Figure 1b).

In this kind of modules, differences between the *SOC* of the cells can determine the temperature distribution of the module. The main target of this paper is to analyze the influence of the voltage balancing to compensate this temperature distribution and evaluate the energy delivered by the module in each experimental test. For this purpose, the experimental results obtained for the temperature distribution of an 8S1P battery module composed by 8 Ah LiFebat cylindrical power cells for constant current discharges from 100% *SOC* to 0% *SOC* are presented. Three different voltage balancing systems will be analyzed; low current passive balancing, high current passive balancing, and an active inductive voltage balancing.

II. Influence of Layout in the Temperature Distribution of Battery Modules

When li-ion based energy storage systems are thermally designed, special attention has to be paid in the mechanical assembly and the layout of the cells within the module; these parameters have direct influence in the thermal behaviour of the module but also in other important issues like in the size and shape of the module. Besides, the *BTMS* of the battery will be influenced by these issues as well. Thus, it is important to find a compromise between all factors according to the final application.

Depending on the type of the cell selected, the layout of the module will be different; prismatic cells give the opportunity to minimize the size of the module when the cells are in touch, without any air gap between them. However, cylindrical cells are typically mounted between holders, being impossible to avoid an air gap between them. Besides, thermal interface materials (*TIM*) are added between cells in the case of prismatic cells to correct possible irregularities in the surface of the cells and improve heat transfer between them (Figure 1a).

The thermal behaviour of the prismatic cell module (Figure 1a) depends on the layout of the module mainly; although different power losses are generated within each cell, heat is accumulated in the centre of the module because these cells are further from the ambient air. This effect is seen in Figure 3, since thermocouples *T8* and *T9* are the highest ones. Besides, the first and last cells have a bigger surface in contact with air, and as a consequence, the highest temperature difference is measured between these cells and the ones in the centre (between *T1* and *T9* in Figure 3). However, this layout will help to make uniform the temperature distribution because of the high thermal conductivity of the *TIM* between cells (ΔT of 3ºC at the end of discharge).

In the case of the cylindrical cell module (Figure 1b), all the cells have similar surface in contact with air, thus, layout is not as important as in the case of prismatic module. In this module the differences in the internal heat generation play the most important role in the temperature distribution of it.

That is why this module is selected for the experimental testing of the voltage balancing to compensate temperature distributions. The air gaps between cells and the mismatch in the internal heat generation make the temperature distribution of the module to be less uniform than in the case of prismatic one. For the case of 1C complete discharge, at the end of

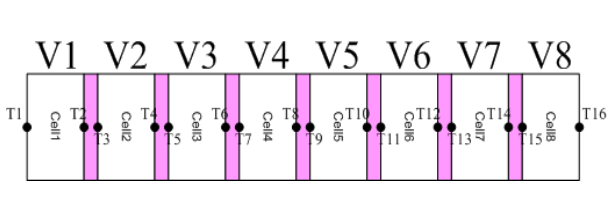

a)

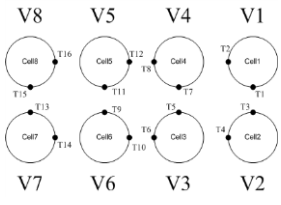

b)

Figure 2. Thermocouples locations: a) Prismatic module; b) Cylindrical module.

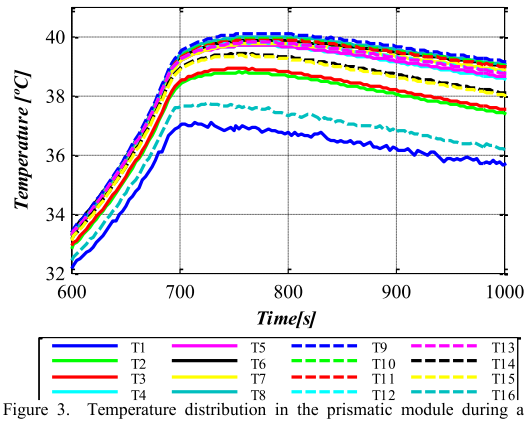

Figure 3. Temperature distribution in the prismatic module during a 7C complete discharge. (End of discharge zoom)

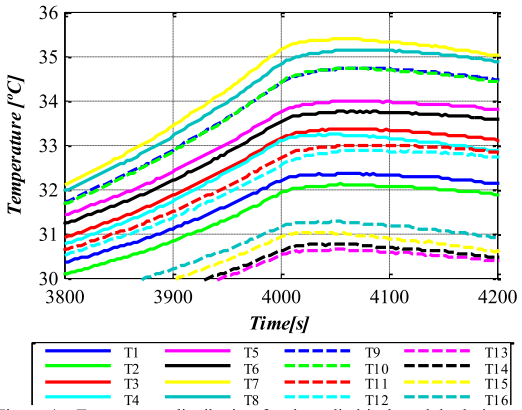

Figure 4. Temperature distribution for the cylindrical module during a 1C complete discharge without voltage balancing. (End of discharge zoom)

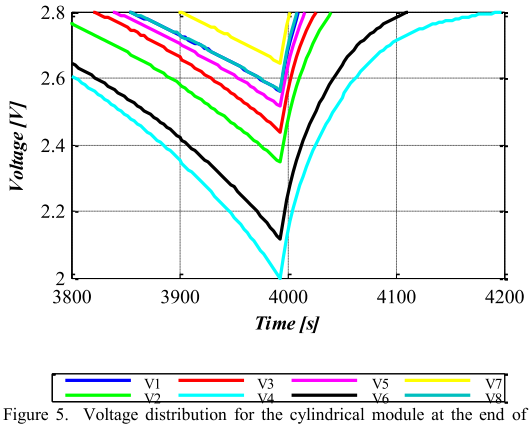

Figure 5. Voltage distribution for the cylindrical module at the end of 1C discharge without voltage balancing. (End of discharge zoom)

discharge, the maximum ΔT is 4.8ºC (Figure 4). The target of this work is to compensate the temperature gradient in this module as much as possible to reduce the influence of this mismatch in the ageing processes of the different cells within the battery module.

III. Relation between terminal voltage and cell temperature

Before all the following discharge experimental tests with the cylindrical module, the module is charged with a constant C/20 current until 3.65 volts and a passive voltage balancing connected to ensure that all the cells reach this voltage and thus, the 100% of their *SOC* is considered. The maximum Q_{max} of the cells are between 9 Ah and 8.72 Ah. However, the maximum capacity of the cells is not the same and when the constant discharge current is applied to the module cells with lower Q_{max} will increase their internal resistance first, generating more power losses than in the cells with higher Q_{max}. This mismatch will lead to a non uniform temperature distribution in the module. The evolution of the terminal voltage of each cell reflects the mismatch in the evolution of the internal impedances. Figure 5 shows the evolution of the terminal voltages of the cells in the cylindrical module and Figure 4 presents the temperature distribution during the same discharge; voltages 4 and 6 reach faster the end of discharge (Figure 5) and the thermocouples located in that cells (*T7*, *T8*, *T9* and *T10*) reach higher temperatures (Figure 4) due to higher internal heat generation of the cells. Thereby, the balancing of the voltages and at the same time the *SOC* is considered to compensate the temperature distribution.

IV. Different voltage balancing systems used to achieve the experimental results

A. Passive voltage balancing 1(PB1, 12 Ω)

The passive voltage balancing system (Figure 6) consists of an electronic switch and a 12 ohm resistor in parallel with each cell working independently. When one of the voltages in the module is higher than the lowest one, the electronic switch is closed and the current I_{Bal} is discharged during a fixed period to do the balancing. The value of this current depends on the actual voltage of the cell and the fixed value of the resistor (2).

A threshold value is defined to fix the value when the voltage balancing is going to start working following equation (1). V_{lim} is the voltage limit, V_{low} is the lowest voltage of one of the cells and $V_{threshold}$ is a user defined value, 5 mV during these experimental tests.

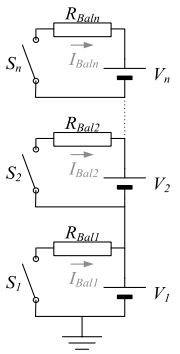

Figure 6. Structure of the passive voltage balancing used

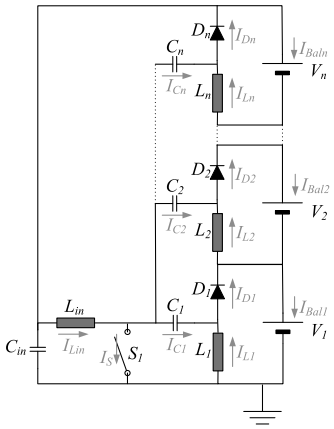

Figure 7. Structure of the active inductive voltage balancing used threshold voltage ($V_{threshold}$) as in equation (1).

B. Passive voltage balancing 2(PB2, 3.8 Ω)

The second balancing system is equal to the previous one but with a lower fixed resistor value to increment the value of the balancing current I_{Bal}. In this case, the value of the resistor is 3.8 ohm.

$$V_{lim} \quad V_{low} \quad V_{threshold} \qquad (1)$$

C. Active voltage balancing (AB)

The active balancing system (Figure 7) consists of a sepic based multistacked converter [18]. When the switch is on the inductors are charged from all the cells and when the switch is off the energy is released. In the single switch balancing system the energy is released to the lowest voltage cell. This natural behavior of the converter permits to balance the voltages with a fixed duty cycle of the switch.

$$I_{Bal} \quad \frac{V}{R_{Bal}} \qquad (2)$$

V. Results and Discussion

The experimental tests conducted for this analysis are summarized in **TABLE I**; the 8 cylindrical cells are characterized before the tests in terms of internal impedance and nominal capacity at 1C discharge rate. The maximum mismatch between the maximum capacities of the cells is 0.28 Ah and the maximum internal impedance mismatch is 0.24 mΩ; constant current discharges from the 100% of *SOC* until one of the cells reaches 2 volts and under two different current rates, 1C and 2C (8 and 16 A). The evaluated variables have been the maximum voltage difference $(\Delta V)_{max}$ and the maximum temperature difference $(\Delta T)_{max}$ between cells, both evaluated when the end of discharge is reached. Besides, as the voltage balancing systems consume energy, the total amount of energy delivered by the battery module (E) has been quantified in each case. These constant current discharges have been applied for the case without voltage balancing, and for the previously mentioned three different voltage balancing systems. Results show better temperature distributions when the voltages of the cells within the module are more balanced

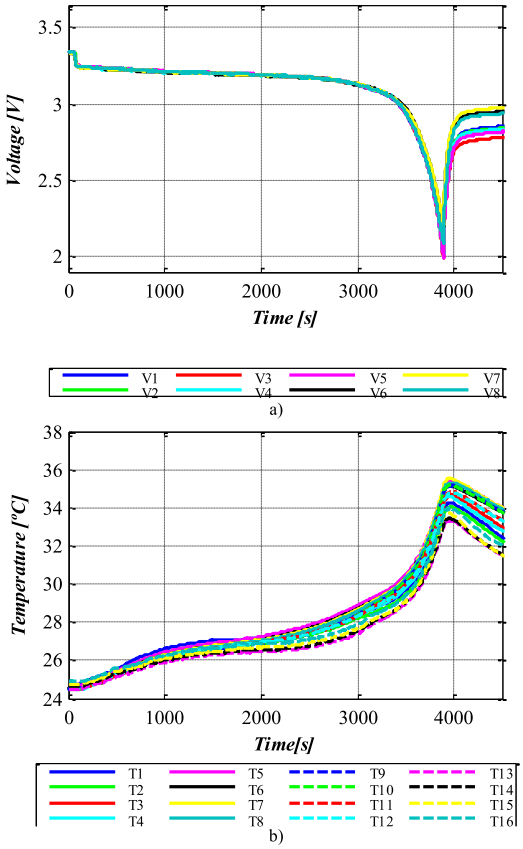

Figure 8. Results for passive balancing 2 (*PB2*) during a 1C complete discharge; a) Voltage distribution; b) Temperature distribution

for passive balancing systems. When active voltage balancing systems are used temperature distribution is improved because of the compensation of the power losses although voltage mismatch is similar to the case without voltage balancing.

A. Passive voltage balancing (PB1 and PB2)

PB1 and *PB2* voltage balancing systems improve the voltage distribution when the end of discharge is reached; as a consequence, temperature distribution is also improved. For 1C discharge rate, the $(\Delta V)_{max}$ without voltage balancing is 0.64 V; *PB1* reduces this value to 0.414 V and with *PB2*, this value is reduced until 0.21 V.

According to temperature distribution, when no voltage balancing system is used (ΔT)max is about 4.75 ºC; for PB1 this value is reduced to 3.22 ºC and with PB2 the maximum improvement is obtained with 2.17 ºC. Figure 8 shows the results for 1C rate and PB2 voltage balancing. PB2 gets better results since it has a higher current capability, but also higher power losses.

For 2C rate, results are similar since *PB2* is the system with better results; however, as the current rate is increased, the effect of *PB1* and *PB2* in the temperature distribution is less important. Besides, with this rate the end of discharge is

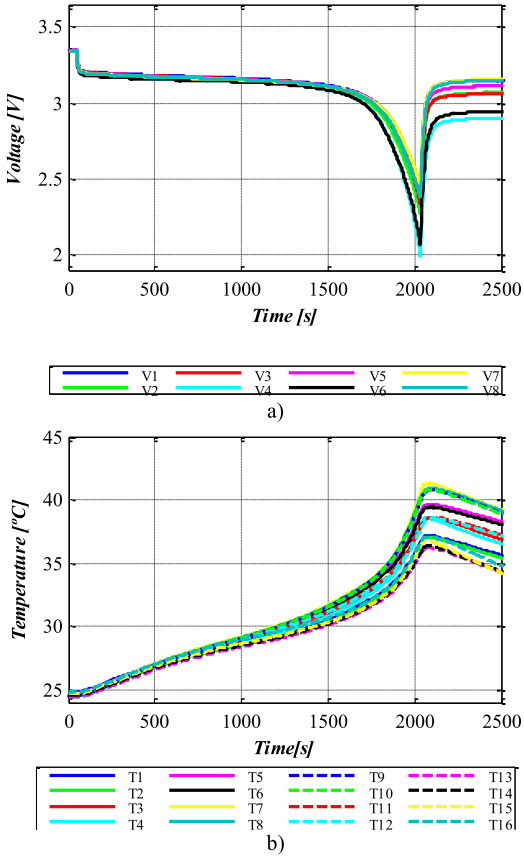

Figure 9. Results for a 2C discharge rate without voltage balancing; a) Voltage distribution; b) Temperature distribution

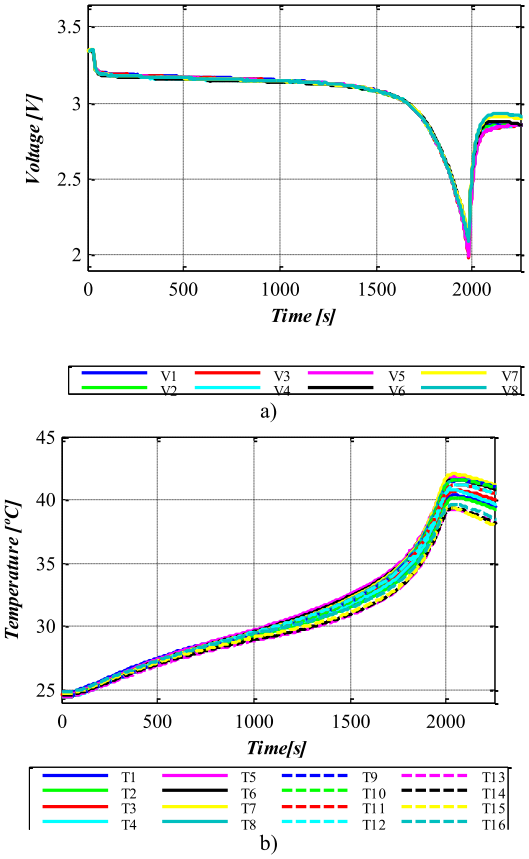

Figure 10. Results for passive balancing 2 (*PB2*) during a 2C complete discharge; a) Voltage distribution; b) Temperature distribution

reached faster and the balancing system works during a shorter period of time.

Without voltage balancing the $(\Delta V)_{max}$ is 0.462 V and the $(\Delta T)_{max}$ is 5.1 ºC; *PB1* obtains intermediate results although it also improves the temperature distribution of the module, with a $(\Delta V)_{max}$ of 0.33 V and a $(\Delta T)_{max}$ of 4.31 ºC. With *PB2* these values are reduced to 0.114 V and 2.78 ºC respectively. Figure 9 and Figure 10 show results for 2C discharge rate without voltage balancing and with *PB2* voltage balancing respectively.

However, passive balancing systems reduce the battery module available energy to balance the voltage; this is the main drawback of this kind of balancing systems. In order to measure the impact of this problem, the evaluated parameter is the energy delivered by the module during each discharge (*E*). In the case without voltage balancing system, the energy delivered by the module (*E*) for 1C discharge rate is 8.88 Ah; for *PB1* this energy is reduced to 8.664 Ah, and for *PB2*, *E* is reduced until 8.447 Ah due to its higher current capability. For 2C rates, without voltage balancing the energy delivered is 9 Ah; for *PB1* this value is again reduced to 8.797 Ah, and for *PB2* is again reduced until 8.694 Ah. In applications without grid connection where the available energy is the most important parameter for the user, this loss of energy can be important. The increase of the energy delivered from 1C rate to 2C rate is considered to be an effect of the improvement of the efficiency due to the higher working temperature for the 2C rate scenario.

B. Active voltage balancing (AB)

In order to improve this parameter the active voltage balancing is proposed; in this voltage balancing system the energy is transferred from the cell with more remaining energy to the weakest cell to balance its voltage. Obviously, there are power losses for this system, but if the current managed is high enough, the discharge process will be longer, improving the amount of energy delivered by the battery module. Figure 9 shows the results of voltage and temperature distribution with 2C discharge rate and with *AB* system. For this voltage balancing system, in the scenario of 1C discharge rate, $(\Delta V)_{max}$ is 0.6 V and the $(\Delta T)_{max}$ is about 3.2 ºC. However, the energy delivered by the module is higher than in the other cases, 9.06 Ah, concretely. For the 2C discharge rate, the $(\Delta V)_{max}$ is 0.58 V and the $(\Delta T)_{max}$ is about 3ºC. In this case, there is no improvement in the energy delivered comparing it with the case without balancing.

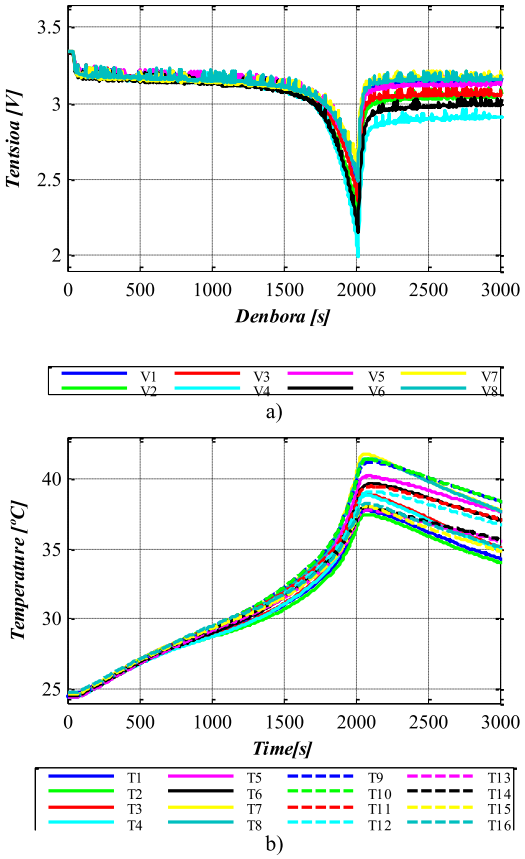

Figure 11. Results for active balancing (*AB*) during a 2C complete discharge; a) Voltage distribution; b) Temperature distribution

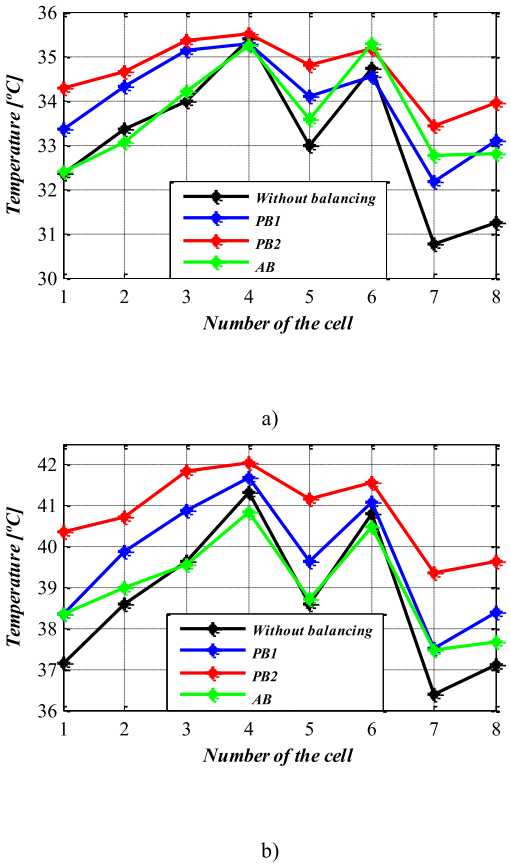

Figure 12. Temperature distribution for the end of discharge moment with different voltage balancing; a) 1C current rate; b) 2C current rate.

In this balancing system the balancing current depends on the voltage differences between cells and the inductors; at the beginning of the discharge the differences are quite low and also the energy transferred between cells. When low *SOC* values are being reached, the voltage differences are higher and the balancing currents increases; however, for 2C discharge rate the end of discharge is reached in a short period of time, thus, the *AC* is not able to improve the delivered energy for this rate.

C. Comparison between passive and active balancing

Both passive and active balancing systems try to reduce the differences between internal heat generations of the cells within the module. Passive balancing systems discharge energy from the cells with higher SOC trying to bring these cells to the SOC of the weakest cell. The consequence is that the internal heat generation of all the cells is more uniform but also higher because the SOC is lower and the internal resistance of all the cells increases.

Active balancing systems try to increase the SOC of the weakest cell transmitting energy from the cells with higher SOC. During the discharge process the cells with higher SOC deliver the energy demanded by the application but also transmit energy to the weakest cell, so the current flowing through their internal resistance is higher and thus their internal heat generation.

The weakest cell delivers the energy of the application but receives the energy of every cell with higher SOC within the module. The resultant current flowing through the weakest cell is reduced and also the internal heat generation of this cell. The difference between these strategies is clearly seen in Figure 12 b.

With PB2 the power losses of the battery module are increased and a higher maximum temperature is reached. However the temperature distribution is more uniform because the internal heat generation mismatch is compensated. AB instead reduces the heat generated by the weakest cell and increases the other heat generations. Thus, the maximum temperature of the module is reduced and also the temperature distribution. Closer results to PB2 can be reached with AB if the inductors of the system are bigger to store more energy with lower voltage differences. Besides, the available energy with AB is similar to the case without balancing but PB reduces the available energy significantly.

TABLE I
SUMMARY OF THE RESULTS FOR THE CONDUCTED TESTS

Balancing system	1C complete discharge			2C complete discharge		
	ΔT_{max} [ºC]	T_{max} [ºC]	E [Ah]	ΔT_{max} [ºC]	T_{max} [ºC]	E [Ah]
No Balancing	4.75	35.2	8.88	5.1	41.3	9
PB1	3.22	35.3	8.664	4.31	41.6	8.797
PB2	2.17	35.5	8.447	2.78	42	8.694
AB	3.2	35.4	9.06	3	40.8	8.99

VI. CONCLUSIONS

Voltage balancing systems are commonly used to avoid *SOC* mismatches between cells within the same module improving their voltage distribution. However, if higher balancing currents are reached for these systems, an important improvement in the temperature distribution can be also obtained in applications where the depth of discharge is high due to the internal heat generation compensation.

PB2 voltage balancing system improves the temperature distribution of a li-ion battery module in a 54% for a 1C rate of discharge since this parameter is improved from 4.75ºC to 2.17ºC. When the current rate is higher, 2C, the improvement is reduced to a 45% (from 5.1ºC to 2.78ºC) because the duration of the discharge is reduced. However, if the balancing current is increased to reach better results with high current rates, the efficiency of the system is reduced. With 1C rate the energy delivered by the module with a *PB2* is reduced in a 5% if it is compared to the case without voltage balancing (from 8.88Ah to 8.45Ah); with 2C rate the available energy is also reduced in a 3.5% (from 9 to 8.7 Ah).

AB mitigates this problem or even improves the available energy for certain working conditions. With a 1C rate scenario the energy is improved in a 2% and when 2C discharge rate is applied the available energy is reduced in a 0.66%. However, the improvement in the temperature distribution is not as notable as with *PB2*. Whit 1C rate an improvement of a 33% is reached (4.75ºC to 3.2ºC); according to 2C rate of discharge the improvement is a 31% (5.1ºC to 3.51ºC).

Comparing both voltage balancing systems it is concluded that passive balancing reaches better temperature distributions but increases the maximum average temperature of the module and reduces the available energy significantly. The active balancing instead reduces the temperature distribution without increasing the average maximum temperature, and also delivers the same energy as the case without voltage balancing.

VII. REFERENCES

[1] M. A. Roscher, O. S. Bohlen, and D. U. Sauer, "Reliable State Estimation of Multicell Lithium-Ion Battery Systems," *IEEE Trans. Energy Convers.*, vol. 26, no. 3, pp. 737–743, 2011.

[2] J. Kim and B. H. Cho, "Pattern Recognition for Temperature-Dependent State-of-Charge/Capacity Estimation of a Li-ion Cell," *IEEE Trans. Energy Convers.*, vol. 28, no. 1, pp. 1–11, 2013.

[3] M. Chen and G. A. Rincon-Mora, "Accurate Electrical Battery Model Capable of Predicting Runtime and I–V Performance," *IEEE Trans. Energy Convers.*, vol. 21, no. 2, pp. 504–511, 2006.

[4] M. Urbain, M. Hinaje, S. Raël, B. Davat, and P. Desprez, "Energetical Modeling of Lithium-Ion Batteries Including Electrode Porosity Effects," *IEEE Trans. Energy Convers.*, vol. 25, no. 3, pp. 862–872, Sep. 2010.

[5] K. Murashko, J. Pyrhonen, and L. Laurila, "Three-Dimensional Thermal Model of a Lithium Ion Battery for Hybrid Mobile Working Machines: Determination of the Model Parameters in a Pouch Cell," *Energy Conversion, IEEE Trans.*, vol. 28, no. 2, pp. 335–343, 2013.

[6] J. Wang, P. Liu, J. Hicks-Garner, E. Sherman, S. Soukiazian, M. Verbrugge, H. Tataria, J. Musser, and P. Finamore, "Cycle-life model for graphite-LiFePO4 cells," *J. Power Sources*, vol. 196, no. 8, pp. 3942–3948, Apr. 2011.

[7] M. Coleman and W. G. Hurley, "An Improved Battery Characterization Method Using a Two-Pulse Load Test," *IEEE Trans. Energy Convers.*, vol. 23, no. 2, pp. 708–713, Jun. 2008.

[8] J. D. Dogger, B. Roossien, and F. D. J. Nieuwenhout, "Characterization of Li-Ion Batteries for Intelligent Management of Distributed Grid-Connected Storage," *IEEE Trans. Energy Convers.*, vol. 26, no. 1, pp. 256–263, Mar. 2011.

[9] C. Zhou, K. Qian, M. Allan, and W. Zhou, "Modeling of the Cost of EV Battery Wear Due to V2G Application in Power Systems," *IEEE Trans. Energy Convers.*, vol. 26, no. 4, pp. 1041–1050, Dec. 2011.

[10] V. Agarwal, K. Uthaichana, R. A. DeCarlo, and L. H. Tsoukalas, "Development and Validation of a Battery Model Useful for Discharging and Charging Power Control and Lifetime Estimation," *Energy Conversion, IEEE Trans.*, vol. 25, no. 3, pp. 821–835, 2010.

[11] A. Pesaran, S. Burch, and M. Keyser, “An approach for designing thermal management systems for electric and hybrid vehicle battery packs,” *Fourth Veh. Therm. Manag. Syst. Conf. Exhib.*, no. January, 1999.

[12] S. Käbitz, J. B. Gerschler, M. Ecker, Y. Yurdagel, B. Emmermacher, D. André, T. Mitsch, and D. U. Sauer, “Cycle and calendar life study of a graphite|LiNi1/3Mn1/3Co1/3O2 Li-ion high energy system. Part A: Full cell characterization,” *J. Power Sources*, vol. 239, pp. 572–583, Oct. 2013.

[13] R. B. Wright, C. G. Motloch, J. R. Belt, J. P. Christophersen, C. D. Ho, R. A. Richardson, I. Bloom, S. A. Jones, V. S. Battaglia, G. L. Henriksen, T. Unkelhaeuser, D. Ingersoll, H. L. Case, S. A. Rogers, and R. A. Sutula, “Calendar- and cycle-life studies of advanced technology development program generation 1 lithium-ion batteries,” *J. Power Sources*, vol. 110, no. 2, pp. 445–470, Aug. 2002.

[14] I. Bloom, B. W. Cole, J. J. Sohn, S. A. Jones, E. G. Polzin, V. S. Battaglia, G. L. Henriksen, C. Motloch, R. Richardson, T. Unkelhaeuser, D. Ingersoll, and H. L. Case, “An accelerated calendar and cycle life study of Li-ion cells,” *J. Power Sources*, vol. 101, no. 2, pp. 238–247, Oct. 2001.

[15] Björn Eberleh, “Thermal Management of battery systems – issues and solutions for the heart of the future drive train,” in *IQPC: 2nd International Conference Thermal Management for EV/HEV*, 2012.

[16] K. Amine, J. Liu, and I. Belharouak, “High-temperature storage and cycling of C-LiFePO4/graphite Li-ion cells,” *Electrochem. commun.*, vol. 7, no. 7, pp. 669–673, Jul. 2005.

[17] B. G. Potter, T. Q. Duong, and I. Bloom, “Performance and cycle life test results of a PEVE first-generation prismatic nickel/metal-hydride battery pack,” *J. Power Sources*, vol. 158, no. 1, pp. 760–764, Jul. 2006.

[18] M. Uno and K. Tanaka, “Single-Switch Cell Voltage Equalizer Using Multistacked Buck-Boost Converters Operating in Discontinuous Conduction Mode for Series-Connected Energy Storage Cells,” *Veh. Technol. IEEE Trans.*, vol. 60, no. 8, pp. 3635–3645, 2011.

VIII. BIOGRAPHIES

Unai Iraola (M'09) was born in Eibar, Spain, on April 25, 1985. He received the B.Sc. and the M.Sc. degree in electrical engineering from the University of Mondragon, Mondragon, Spain, in 2006 and 2009, respectively.

He has been with the Department of Electronics, Faculty of Engineering, University of Mondragon, where he is currently working toward the Ph.D. degree. His research interests include renewable energies, energy storage systems, and modeling and control of power converters.

José María Canales Segade was born in Hengelo, The Netherlands, in 1971. He received the B.Sc. degree in electrical engineering from the University of Mondragon, Mondragon, Spain, in 1993.

In 1993, he joined the Electronics Department, Faculty of Engineering, University of Mondragon, where he is currently an Associate Professor. He teaches courses on power electronics, electric vehicle and energy storage systems. He is responsible of the Medium Voltage Laboratory of the University of Mondragon, and he has experience testing high power converters for medium-voltage applications. His research interests include the modeling control and design of power converters and electrochemical storage systems.

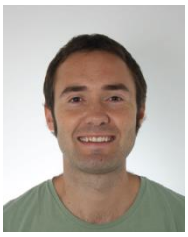

Iosu Aizpuru (M'09) received the B.Sc. and the M.Sc. degree in electrical engineering from the University of Mondragon, Mondragon, Spain, in 2006 and 2009, respectively.

He has been with the Department of Electronics, Faculty of Engineering, University of Mondragon, where he is currently working toward the Ph.D. degree. His current research interests include power electronics modeling and control for energy storage systems. He has participated in various research projects in the fields of traction and stationary systems for railway applications.

Ander Etxeberria Larrazabal works as a professor at the electronics and informatics department in Mondragon University (Spain), in the field of Industrial Automation and Electrical machines. He obtained his PhD at Paul Sabatier University (Tolouse) in 1985, and nowadays he is responsible for subjects related to Industrial Automation and systems control in the Industrial Electronics degree and in the Industrial Engineering master degree. His research activities are focused on mechatronics, directing two PhD works in this field, and on li-ion batteries, directing other PhD works about the estimation of the state of charge, voltage balancing systems and thermal management of batteries.

Lorea Gorrotxategi was born in Oñati, Spain, in 1991. She received the B.Sc. degree in industrial electronics engineering from the University of Mondragon, Mondragon, Spain, in 2013, where she is currently studying for the M.Sc. degree in Energy and Power Electronics.

Since 2013, she has been working as a researcher at the Department of Electronics, Faculty of Engineering, University of Mondragon. Her research interests include power electronics, and integration of power systems for vertical transportation applications.

Iñigo Gil received the B.Sc. degree in electronics and B.Sc. degree in mechanics from the University of Navarra, San Sebastian, Spain, in 2000 and 2004, respectively.

Since 2001, he has been an Engineer at ORONA Elevator Innovation Center. His research interests include energy management and storage, and power electronics in vertical transport applications.

Energy Conversion, IEEE Transactions on 2015. **(SUBMITTED)**

Single Switch Active Balancing Systems for Series Connected Energy Storage Systems

I. Aizpuru
U. Iraola
J.M. Canales
A. Goikoetxea

DOI:

Energy Conversion, IEEE Transactions on 2015. **(SUBMITTED)**

Comparative Study and Evaluation of Passive Balancing Against Single Switch Active Balancing Systems for Energy Storage Systems

I. Aizpuru
U. Iraola
J.M. Canales
A. Goikoetxea

DOI: